



Geneeskundige Stichting Koningin Elisabeth
Fondation Médicale Reine Elisabeth
Königin-Elisabeth-Stiftung für Medizin
Queen Elisabeth Medical Foundation

Verlag – Rapport – Bericht – Report

2021

G.S.K.E. – F.M.R.E. – K.E.S.M. – Q.E.M.F.

www.fmre-gske.be
www.fmre-gske.eu
www.fmre-gske.com

Progress reports of the research projects of young researchers, supported by the Queen Elisabeth Medical Foundation in collaboration with the following professors and doctors (2021)

1. Interuniversity research projects

Prof. dr. Jean-Noël Octave (UCLouvain)	9
Prof. dr. Philippe Gailly (UCLouvain)	9
Prof. dr. Nathalie Pierrot (UCLouvain)	9
Prof. dr. Laurence Ris (UMONS)	9
Prof. dr. Paul Boon (UGent)	9
Robrecht Raedt (UGent)	9
Prof. dr. Sebastiaan Engelborghs (VUB)	21
Prof. dr. Chris Baeken (UGent)	21
Prof. dr. Vincent Van Rompaey (UAntwerpen)	27
Prof. dr. Peter Ponsaerts (UAntwerpen)	27
Prof. dr. Guy Van Camp (UAntwerpen)	27
Prof. Rik Gijssbers (KU Leuven)	27
Prof. dr. An Goris (KU Leuven)	33
Prof. Nathalie Cools (UAntwerpen)	33
Prof. dr. Pascal Kienlen-Campard (UCLouvain)	47
Prof. dr. Loïc Quinton (ULg)	47
Prof. dr. Jan Gettemans (UGent)	47

2. University research projects

Prof. dr. ir. Simon De Meyer	59
Prof. dr. Lieve Moons & Lies De Groef, MSc, PhD	79
Prof. Pierre Vanderhaeghen, MD, PhD (VIB)	89
Prof. dr. Thomas Voets (VIB)	97
Prof. dr. Sarah Weckhuysen, MD, PhD	111

3. Research projects of young researchers

Prof. dr. Evelien Carrette	125
Prof. Riëm El Tahry, MD, PhD	133
Prof. Bernard Hanseeuw, PhD	139
Dr. Lars Emil Larsen, PhD	145
Aya Takeoka, PhD (IMEC)	159
Dr. Valerie Uytterhoeven	171
Dr. Emanuel van den Broeke	185
Eline Wauters, PhD (VIB)	189



Geneeskundige Stichting Koningin Elisabeth
Fondation Médicale Reine Elisabeth
Königin-Elisabeth-Stiftung für Medizin
Queen Elisabeth Medical Foundation

Interuniversitaire onderzoeksprojecten
2020-2022 gefinancierd door de G.S.K.E.

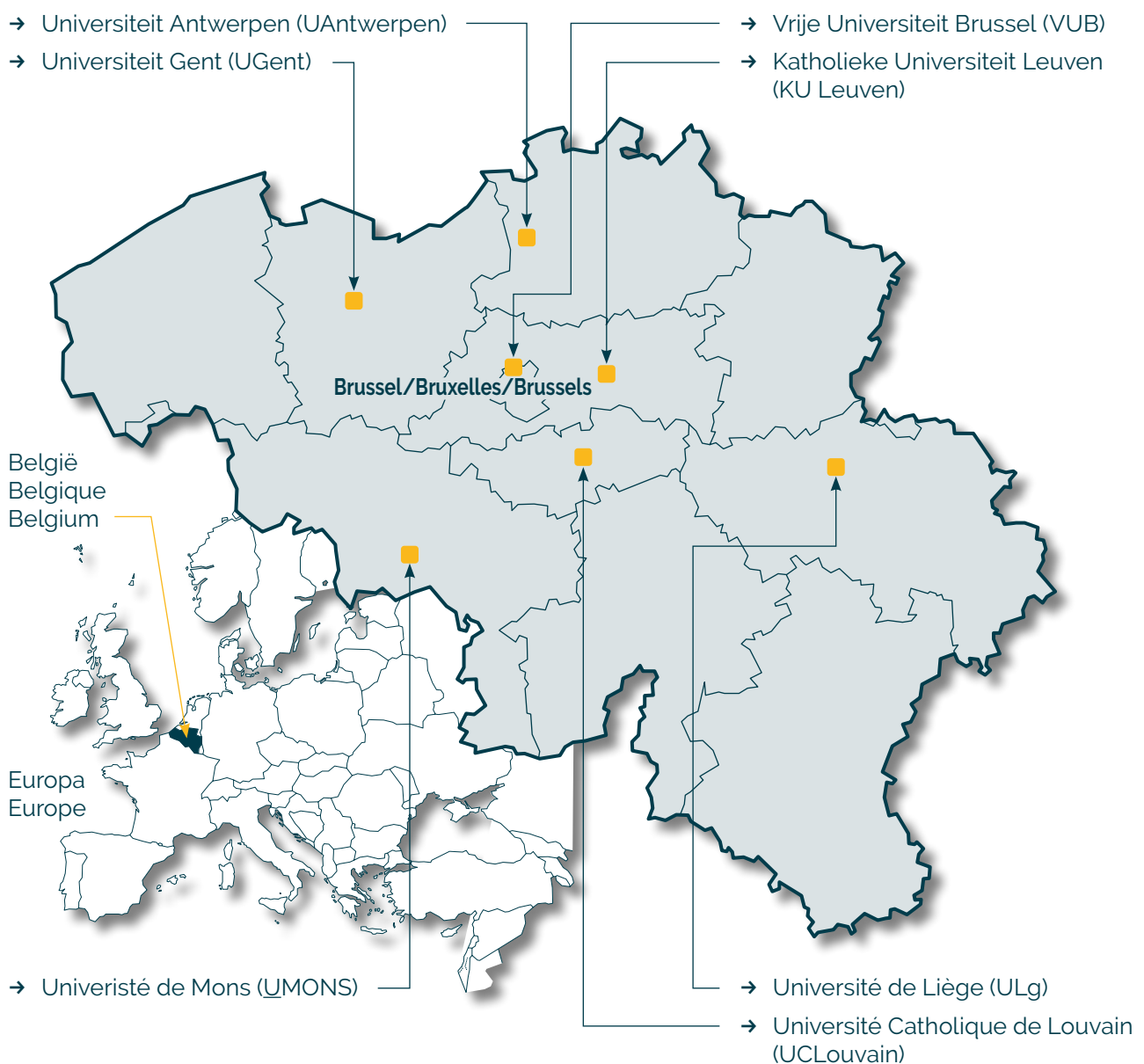
Projets de recherche interuniversitaire
2020-2022 subventionnés par la F.M.R.E.

Interuniversity research projects
2020-2022 funded by the Q.E.M.F.

Universiteiten met onderzoeksprogramma's die gesteund worden door de G.S.K.E.

Universités ayant des programmes de recherche subventionnés par la F.M.R.E.

Universities having research programs supported by the Q.E.M.F.



Interuniversitaire onderzoeksprojecten 2020-2022 gefinancierd door de G.S.K.E.

Projets de recherche interuniversitaire 2020-2022 subventionnés par la F.M.R.E.

Interuniversity research projects 2020-2022 funded by the Q.E.M.F.

Prof. dr. Jean-Noël Octave (UCLouvain)
Prof. dr. Philippe Gailly (UCLouvain)
Prof. dr. Nathalie Pierrot (UCLouvain)
Prof. dr. Laurence Ris (UMONS)
Prof. dr. Paul Boon (UGent)

Involvement of PPAR α activation in the control of synaptic function by APP

Prof. dr. Vincent Van Rompaey (UAntwerpen)
Prof. dr. Peter Ponsaerts (UAntwerpen)
Prof. dr. Guy Van Camp (UAntwerpen)
Prof. Rik Gijssbers (KU Leuven)

Development of allele-specific CRISPR-nuclease gene therapy for late-onset sensorineural hearing impairment in a new humanized DFNA9 mouse model

Prof. dr. Pascal Kienlen-Campard (UCLouvain)
Prof. dr. Loïc Quinton (ULg)
Prof. dr. Jan Gettemans (UGent)

New analytical tools to identify and target pathogenic hexameric A β assemblies in Alzheimer's disease

Prof. dr. Sebastiaan Engelborghs (VUB)
Prof. dr. Chris Baeken (UGent)

Unraveling the link between depression and dementia to improve diagnostic and treatment options

Prof. dr. An Goris (KU Leuven)
Prof. Nathalie Cools (UAntwerpen)

Deep sequencing of myelin-reactive T-cells to elucidate new disease mechanisms and identify correlates for treatment responsiveness



Geneeskundige Stichting Koningin Elisabeth
Fondation Médicale Reine Elisabeth
Königin-Elisabeth-Stiftung für Medizin
Queen Elisabeth Medical Foundation

Progress report of the interuniversity research project of

Prof. dr. Jean-Noël Octave (UCLouvain)

Prof. dr. Philippe Gailly (UCLouvain)

Prof. dr. Nathalie Pierrot (UCLouvain)

Prof. dr. Laurence Ris (UMONS)

Prof. dr. Paul Boon (UGent)

Robrecht Raedt (UGent)

Prof. dr. Jean-Noël Octave (UCLouvain)
Faculty of Pharmacy and Biomedical Sciences
Institute of neuroscience (IONS)
CEMO
Avenue Hippocrate 54/B1.54.10
1200 Woluwe-Saint-Lambert
jean-noel.octave@uclouvain.be

Prof. dr. Philippe Gailly (UCLouvain)
Institute of Neuroscience (IONS)
Laboratory of Cell Physiology (FYCL)
Avenue Mounier, 53 - B1.53.17
1200 Brussels
philippe.gailly@uclouvain.be
Tel. + 32 (0)2 764 55 42

Prof. dr. Nathalie Pierrot (UCLouvain)
Institute of Neuroscience (IONS)
CEMO
Avenue Mounier 53/B1.53.03
1200 Woluwe-Saint-Lambert
nathalie.pierrot@uclouvain.be

Prof dr. Laurence Ris (UMONS)
Lecturer, head of the department of Neuroscience
Faculty of Medicine and Pharmacy
6A, avenue du Champ de Mars 7000 Mons
laurence.ris@umons.ac.be

Prof. dr. Paul Boon (UGent)
Professor and chairman Department of Neurology
Chairman Division of Head, Movement and Senses
Ghent University Hospital - Ghent University
10 Corneel Heymanslaan
9000 Gent
Paul.boon@ugent.be

Robrecht Raedt (UGent)

Involvement of PPAR α activation in the control of synaptic function by APP

1. The context

With a prevalence doubling every 5 years beyond 65, Alzheimer's disease (AD) is a devastating neurodegenerative disorder, which is the most common cause of dementia in the elderly. Together with a progressive loss of cognitive functions, AD is characterized by the existence of extracellular senile plaques containing the amyloid- β (A β) peptide generated from the sequential proteolytic processing of its precursor, the amyloid precursor protein (APP).

Although amyloid deposition occurring in the hippocampus and the cerebral cortex of AD patients potentially explains deficits in memory and cognitive function observed ¹, it remains difficult to influence the course of AD by removing amyloid deposits. Indeed, even if immunotherapy efficiently removes senile plaques from AD brains, clinical trials indicate that cognition is not improved in AD patients. Therefore, a better knowledge of the underlying physiopathological mechanisms involved early in the neurodegenerative process is required. In particular, a considerable bulk of evidence supports that synaptic function is affected at the earliest stages of AD. Indeed, synaptic dysfunction leading to atypical neural synchrony and oscillations observed in AD brain might play an early role in the establishment of pathogenic cascades leading to AD and could contribute to cognitive deficits ^{2,3}.

Synaptic deficits occur very early in AD patients ⁴. Moreover, it was reported that people at risk for AD (e.g. ApoE4 carriers, see below) display increased neuronal excitability without dementia ⁵ and that cognitive and synaptic dysfunctions arise before the formation of plaques in transgenic mouse models of AD ⁶. Using different methodological approaches, including electroencephalography (EEG) ^{7,8}, a lack of functional connectivity between brain areas has been highlighted in AD ^{9,10}.

We previously reported that increase or decrease in APP expression modulates both excitatory and inhibitory neuronal activity in primary rat cortical networks ¹¹⁻¹³. These data suggest an **essential role of APP in the control of both excitatory and inhibitory neurotransmissions, which have to be perfectly balanced to regulate cognitive function.**

In the vast majority of late-onset sporadic AD cases (+/- 99 %), the source of A β accumulation in the brain is still unknown. Nevertheless, it is well established that the epsilon 4 allele of the *apolipoprotein E (ApoE)* gene, encoding the main transporter of cholesterol in the brain, is a genetic risk factor for AD¹⁴. Therefore, a **relationship between AD and lipid metabolism has been established.** We have previously demonstrated that the expression of the neuronal human APP (hAPP) isoform in cortical networks controls cholesterol turnover, needed for neuronal activity ¹⁵, by interacting with the sterol regulatory element binding protein 1 (SREBP1), a transcription factor that regulates expression of sterol- and lipogenic genes ^{16,17}. We reported that **hAPP expression inhibits biosynthesis of both cholesterol and fatty acids (FAs) in cortical cells in culture** ¹⁵.

FAs are the major constituents of brain lipids ¹⁸ and play a critical role in brain development and functioning ¹⁹. Among them, essential brain polyunsaturated FAs (PUFAs) play a critical role in neurogenesis, synaptic function, inflammation, glucose homeostasis, mood and cognition ²⁰. PUFAs are ligands for retinoid X and peroxisome proliferator-activated receptors (RXRs and PPARs, respectively) ²¹, two nuclear receptors forming permissive heterodimers that belong to the

superfamily of ligand-dependent transcription factors²². PPARs act principally as lipid sensors²³ and due to their anti-inflammatory effects, PPARs activation with specific agonists emerged as promising approaches for treating brain pathologies in several mouse models of Parkinson, Huntington and Alzheimer diseases^{24,25}. Recent *in vitro* and *in vivo* evidence point to PPAR α as a promising therapeutic target in AD that we have recently reviewed²⁶. Indeed, it was shown that PPAR α agonists improved amyloid and tau pathologies, decreased neuroinflammation, ameliorated glucose and lipid dyshomeostasis and improved behavior in mouse models of AD²⁷.

We recently reported that **PPAR α expression also plays a crucial role in synaptic function. Activation of PPAR α with a specific agonist improves synaptic plasticity in a transgenic mouse model of AD**²⁸. However, the cellular and molecular mechanisms underlying such effects are poorly understood.

2. The project and first results.

2.1. How does APP modulate excitatory / inhibitory neurotransmission ?

The function of the APP is not fully understood, but its cleavage product A β together with neurofibrillary tangles constitute the hallmarks of AD. Yet, imbalance of excitatory and inhibitory neurotransmission accompanied by loss of synaptic functions, has been reported much earlier and independent of any detectable pathological markers. Recently, soluble APP fragments have been shown to bind to presynaptic GABA $_B$ receptors (GABA $_B$ Rs), subsequently decreasing the probability of neurotransmitter release²⁹. We recently showed that overexpression of wild-type human APP in mice (hAPPwt³⁰) causes early cognitive impairment, neuronal loss, and electrophysiological abnormalities in the absence of amyloid plaques and at very low levels of A. hAPPwt mice exhibited neuronal overexcitation that was evident in EEG and increased long-term potentiation (LTP). Overexpression of hAPPwt did not alter GABAergic/glutamatergic receptor components or GABA production ability. Nonetheless, we detected a decrease of GABA but not glutamate that could be linked to soluble APP fragments, acting on presynaptic GABA $_B$ Rs and subsequently reducing GABA release. By using CGP36216, a specific presynaptic GABA $_B$ R antagonist, we were able to rescue hyperexcitation in hAPPwt animals. Our results provide evidence that APP plays a crucial role in regulating inhibitory neurotransmission (Fig. 1). These results have been published in 2021 (Kreis et al., see reference below and pdf paper attached)

2.2. Regulation of PPAR α by APP affects the pharmacological modulation of synaptic activity.

Among genetic susceptibility loci associated with late-onset Alzheimer disease (LOAD), genetic polymorphisms identified in genes encoding lipid carriers led to the hypothesis that a disruption of lipid metabolism could promote disease progression. We previously reported that APP involved in AD physiopathology impairs lipid synthesis needed for cortical networks' activity and that activation of peroxisome proliferator-activated receptor (PPAR α), a metabolic regulator involved in lipid metabolism, improves synaptic plasticity in an AD mouse model. These observations led us to investigate a possible correlation between PPAR α function and full-length APP expression. Here, we report that PPAR α expression and activation were inversely related to APP expression both in LOAD brains and in early-onset AD (EOAD) cases with a duplication of the APP gene, but not in control human brains. Moreover, human APP expression decreased PPARA expression and its related target genes in transgenic mice and in cultured cortical cells, while opposite results were observed in APP-silenced cortical networks (Fig. 2).

In cultured neurons, APP-mediated decrease or increase in synaptic activity was corrected by a PPAR α -specific agonist and antagonist, respectively. APP-mediated control of synaptic activity

was abolished following PPAR α deficiency, indicating a key function of PPAR α in this process. These results have been published in 2021 (Sáez-Orellana et al., see reference below and pdf paper attached)

2.3. PPAR α activation in hAPPwt animals

In order to confirm the involvement of PPAR α activation in the control of synaptic function by APP we further investigated the effect of a PPAR α agonist in hAPP mice *in vivo*. Therefore, mice were stereotactically implanted with a tripolar recording electrode with electrode tips located in parietal cortex, hippocampal CA1 and dentate gyrus. Spontaneous EEG was recorded in hAPP mice (n = 5) and age-matched non-transgenic littermates (n = 6) and compared upon PPAR α activation with the WY14643 agonist (40 and 80 mg/kg dissolved in saline with 10% Tween-80 and 20% DMSO) and treatment with vehicle. Epileptic spikes were observed on the EEG in hAPPwt animals as described previously (in our paper published in 2021 by Kreis et al.) and were quantified during baseline (one hour before treatment). Treatment with WY14643 (both doses) showed a trend in lowering spikes in hAPPwt animals between 0.5-1.5h and 24-25h after treatment. However, also a trend towards decreased number of epileptic spikes was observed 0.5-1.5h after treatment.

Furthermore, *ex vivo* basal synaptic transmission has been investigated by extracellular recordings on acute hippocampal slices of hAPP and WT mice. The causal effect of PPAR α activity on the observed deficits has been evaluated by treating slices with the WY14643 PPAR α agonist (10 μ M) for 2 h. Basal synaptic transmission has been recorded before and after kainate (2 μ M) application in the presence or absence of PPAR α agonist.

Our results showed a significant reduction of maximal EPSP amplitude in hAPP mice compared to WT ($p < 0.016$). This difference was increased in the presence of PPAR α agonist mainly due to a positive effect of the agonist on WT slices.

Kainate application reduced the fEPSP amplitude both in WT and in hAPP mice but the effect was more severe in hAPP mice where epilepsy was observed. The application of PPAR α agonist reduced this effect.

These results showed that PPAR α has a protective effect against epileptic waves in the hippocampus and against the toxic effect of kainate. Moreover, they showed that hAPP mice are more sensitive to kainate and more susceptible to develop epilepsy (Figure 6).

3. Perspectives.

3.1. Role of KCC2 in neuronal hyperexcitability observed in AD.

Based on *in vitro* results (cells in culture), we hypothesized that hyperexcitability observed in APP-overexpressing neurons could be related to an APP-induced reduction of the expression of KCC2, a K⁺-Cl⁻ transporter responsible for the extrusion of Cl⁻ in mature neurons¹³. However, we did not observe any change in the expression of KCC2 and NKCC1 (the Na⁺, K⁺, Cl⁻ transporter responsible for the influx of Cl⁻ in neurons) *in vivo*, in mice overexpressing hAPPwt, suggesting that the excitatory / inhibitory imbalance was not due to the accumulation of chloride in neurons (Kreis et al, 2021). It is however important to note that APP is not systematically overexpressed in sporadic AD, but that its metabolism and/or function are highly impaired. We previously extended our analysis by examining KCC2 and NKCC1 expression in frontal cortex brain tissues from human control subjects and patients suffering from dementia clinically diagnosed with late onset AD¹³. Interestingly, while NKCC1 expression remained unchanged, we detected a significant decrease in KCC2 expression in the brains of these patients (Fig. 3).

A potential involvement of A β in APP dependent KCC2 regulation cannot be excluded and one could speculate that increased levels of A β combined to an alteration in the physiological function of APP could influence KCC2 expression in AD. We therefore plan to

- i. measure KCC2 expression in AD murine models overexpressing APP.
- ii. investigate spatial reference memory and working memory in vivo as well as LTP on brain slices, in a murine model where KCC2 can be specifically reduced in hippocampal neurons at a specific time point (KCC2^{lox/lox} - CamKII CreERT2 mice) (Collaboration with Thomas Jentsch, Germany). Preliminary results present on Fig. 4 show the feasibility of these experiments, in particular that treatment of these mice by tamoxifen induces an acute decrease of KCC2 expression.

3.2. Role of PPAR α activation in the control of synaptic function by APP in vivo.

We plan to repeat the in vivo WY14643 treatment study in hAPP mice to study the effect on epileptic spikes. Increasing the number of mice will allow to perform repeated measures ANOVA which in order to prove that PPAR agonist treatment reduces epileptiform activity in hAPP overexpressing mice compared to vehicle treatment.

Furthermore, results obtained from WT and hAPP mice will be compared to *App*^{-/-} mice with and without GW6471 PPAR α antagonist (5 μ M, dose used in organotypic slices³¹).

4. Papers published in 2021 (research supported by FMRS-GSKE).

- Kreis A, Desloovere J, Suelves N, Pierrot N, Yerna X, Issa F, Schakman O, Gualdani R, De Clippele M, Tajeddine N, Kienlen-Campard P, Raedt R, Octave JN, Gailly P (2021)
Overexpression of wild-type human amyloid precursor protein alters GABAergic transmission
Scientific reports 11 (1), 1-18
IF : 6.5
Q1
- Sáez-Orellana F, Leroy T, Ribeiro F, Kreis A, Leroy K, Lalloyer F, Baugé E, Staels B, Duyckaerts C, Brion JP, Gailly P, Octave JN, Pierrot N (2021)
Regulation of PPAR α by APP in Alzheimer disease affects the pharmacological modulation of synaptic activity.
Journal of Clinical Investigation Insight 6 (16) JCI : e150099
IF : 8.35
Q1
(not directly related to the project)
- Gualdani R, Yuan JH, Effraim PR, Di Stefano G, Truini A, Cruccu G, Dib-Hajj SD, Gailly P, Waxman SG (2021)
Trigeminal Neuralgia TRPM8 Mutation: Enhanced Activation, Basal [Ca²⁺]_i and Menthol Response
Neurology Genetics 7 (1)
IF = 3.5
Q1

5. Figures

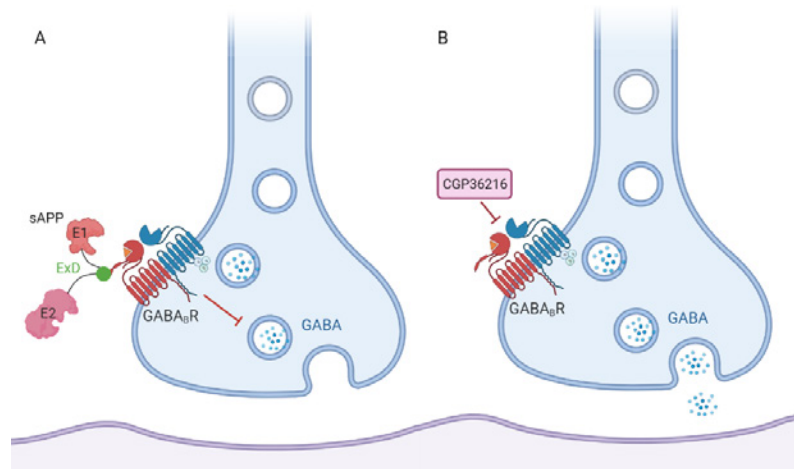


Figure 1: Ligand binding to presynaptic GABA_BRs. A. Soluble APP fragments act as presynaptic GABA_B agonists, by binding to GABA_{B1a} subunits on GABAergic synapses and inhibiting the release of GABA into the synaptic cleft. B. Binding of the antagonist CGP36216 to presynaptic GABA_{B1a} subunits and subsequently allowing the release of GABA. Modified from ref 29.

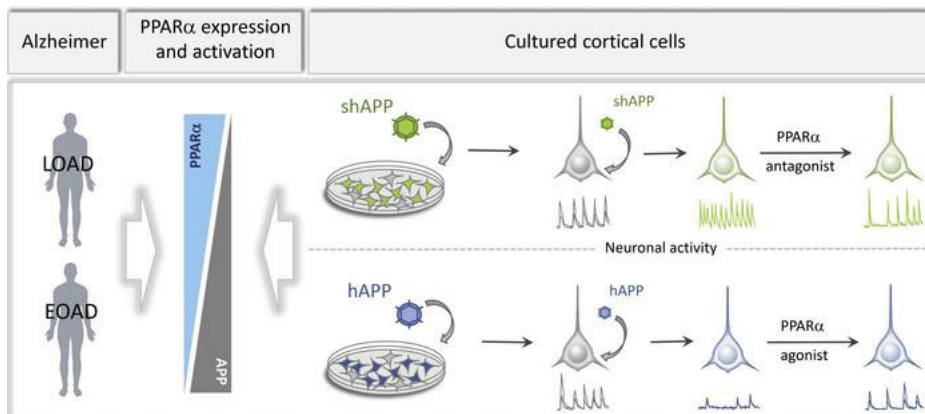


Figure 2: Modulation of APP-induced neuronal activity by PPARα agonists and antagonists.

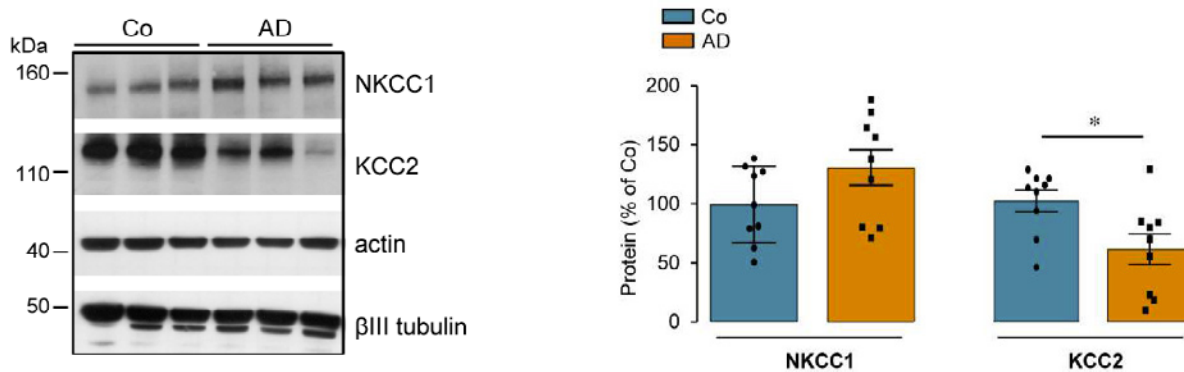


Figure 3: Expression of NKCC1 and KCC2 in late onset AD brains. Representative Western blot of NKCC1 and KCC2 expression in frontal cortex of postmortem human brain tissues from control subjects (Co, n=9) and patients with Alzheimer disease (AD, n=9). Blots were probed using anti-NKCC1, -KCC2, -actin and -III tubulin antibodies. Bottom panel: quantification of NKCC1 / actin and KCC2 / III tubulin ratios. Results were expressed as percentage (mean \pm s.e.m.) of Co, * $P < 0.05$, Student's t-test. From ref 13.

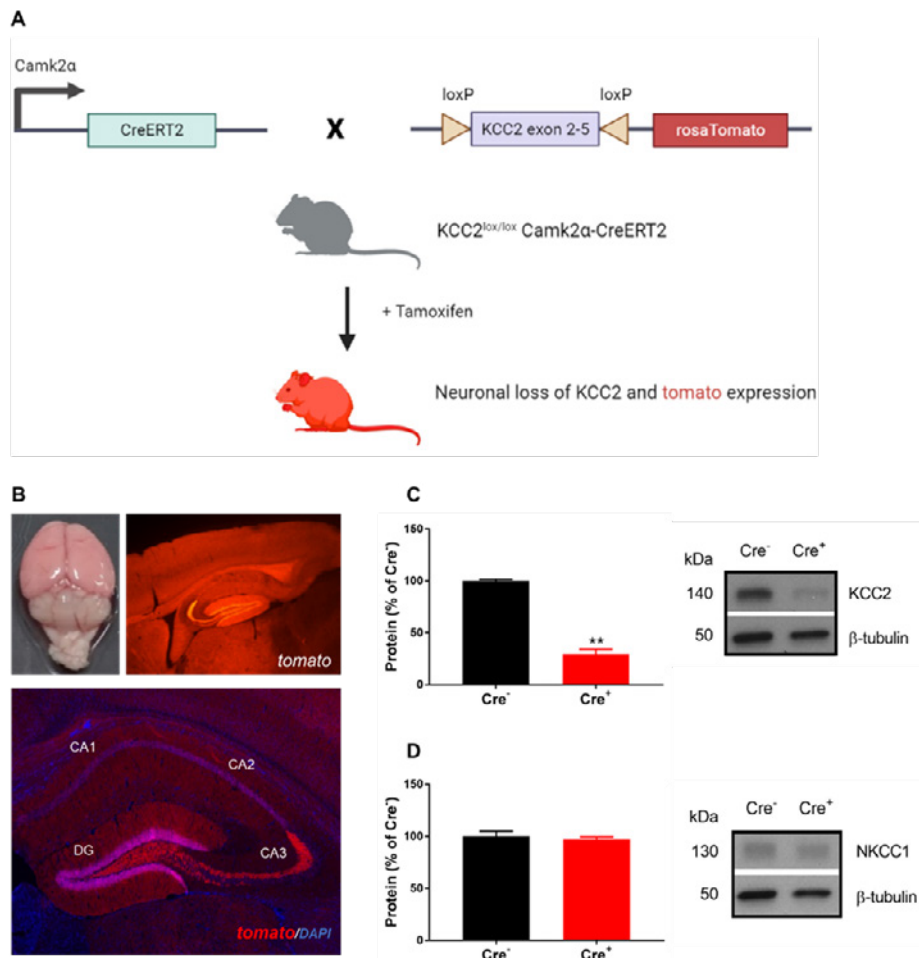


Figure 4: Validation of the KCC2^{lox/lox} CamK2-CreERT2 mouse model. A. Schematic representation of mouse model crossing to obtain mice with floxed KCC2 exons 2-5 and CamK2-CreERT2 expression. Neuronal loss of KCC2 is achieved by tamoxifen injections resulting in rosaTomato expression. B. Neuronal expression of rosaTomato in the cortex and hippocampus after tamoxifen treatment with DAPI counterstaining. Quantification and representative western blots of KCC2 (C) and NKCC1 (D) protein levels of hippocampal tissue lysates of 3 month old Cre⁺ (n=3) and Cre⁻ (n=3) animals. Protein amount was normalized to β-tubulin and expressed as percentage. (Values are means ± SEM; **P ≤ 0.01; unpaired t-test with Welch's correction).

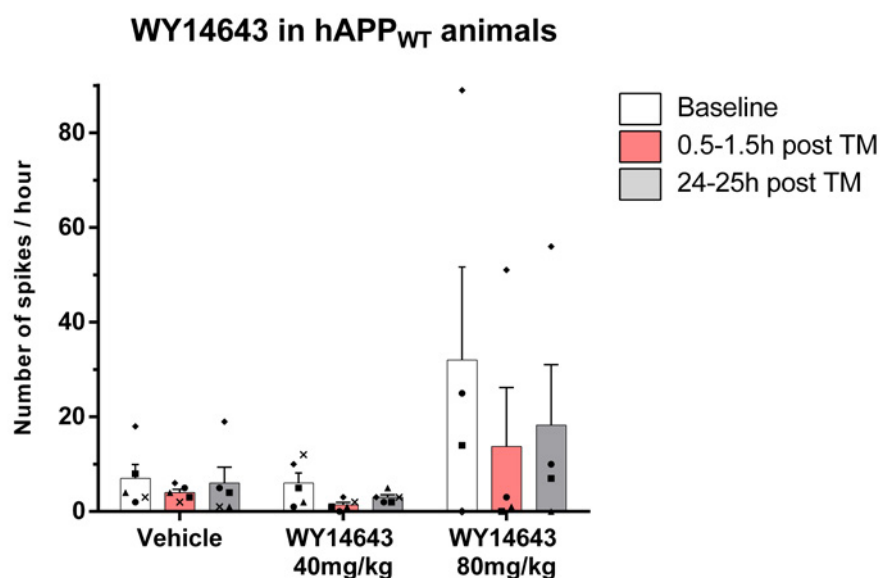


Figure 5: Effect of PPAR α agonist WY14643 on epileptic EEG spikes in hAPPwt animals. Both doses of WY14643 resulted in decrease of epileptic spikes both 0.5-1.5hr and 24-25hr treatment. Also, in the vehicle group lower number of epileptic spikes were seen 0.5-1.5hr after injection. In the coming year the number of animals will be increased and statistical analysis will be performed.

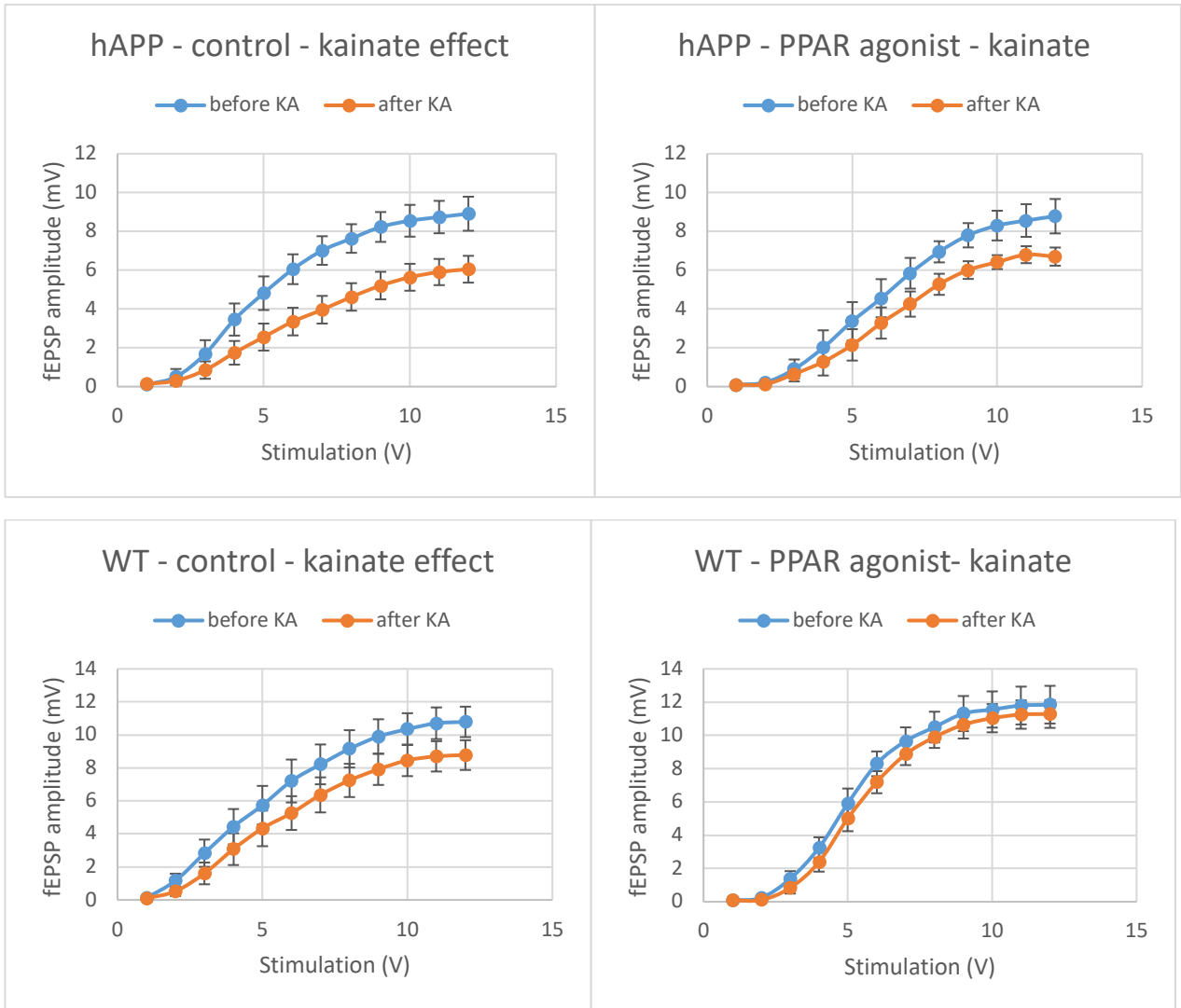


Figure 6: Effect of PPAR α agonist WY14643 on the toxic effect of kainate application on hippocampal slices of hAPP mice and WT mice. Input/output curves obtained from the stimulation of Schaeffer Collaterals with incremental intensity.

6. References

1. Pearson, R.C., Esiri, M.M., Hiorns, R.W., Wilcock, G.K. & Powell, T.P. Anatomical correlates of the distribution of the pathological changes in the neocortex in Alzheimer disease. *Proc. Natl. Acad. Sci. U. S. A* **82**, 4531-4534 (1985).
2. Uhlhaas, P.J. & Singer, W. Neural synchrony in brain disorders: relevance for cognitive dysfunctions and pathophysiology. *Neuron* **52**, 155-68 (2006).
3. Delbeuck, X., Van der Linden, M. & Collette, F. Alzheimer's disease as a disconnection syndrome? *Neuropsychol Rev* **13**, 79-92 (2003).
4. Martin, L.J., Pardo, C.A., Cork, L.C. & Price, D.L. Synaptic pathology and glial responses to neuronal injury precede the formation of senile plaques and amyloid deposits in the aging cerebral cortex. *Am. J. Pathol* **145**, 1358-1381 (1994).
5. Ponomareva, N.V., Korovaitseva, G.I. & Rogaeve, E.I. EEG alterations in non-demented individuals related to apolipoprotein E genotype and to risk of Alzheimer disease. *Neurobiol. Aging* **29**, 819-827 (2008).
6. Sasaguri, H. *et al.* APP mouse models for Alzheimer's disease preclinical studies. *EMBO J* **36**, 2473-2487 (2017).
7. Lustig, C. *et al.* Functional deactivations: change with age and dementia of the Alzheimer type. *Proc. Natl. Acad. Sci. U. S. A* **100**, 14504-14509 (2003).
8. Sperling, R.A. *et al.* Amyloid deposition is associated with impaired default network function in older persons without dementia. *Neuron* **63**, 178-188 (2009).
9. Babiloni, C. *et al.* Brain neural synchronization and functional coupling in Alzheimer's disease as revealed by resting state EEG rhythms. *Int J Psychophysiol* **103**, 88-102 (2016).
10. Bokde, A.L., Ewers, M. & Hampel, H. Assessing neuronal networks: understanding Alzheimer's disease. *Prog Neurobiol* **89**, 125-33 (2009).
11. Santos, S.F. *et al.* Expression of human amyloid precursor protein in rat cortical neurons inhibits calcium oscillations. *J Neurosci* **29**, 4708-18 (2009).
12. Octave, J.N., Pierrot, N., Ferao, S.S., Nalivaeva, N.N. & Turner, A.J. From synaptic spines to nuclear signaling: nuclear and synaptic actions of the amyloid precursor protein. *J. Neurochem* **126**, 183-190 (2013).
13. Doshina, A. *et al.* Cortical cells reveal APP as a new player in the regulation of GABAergic neurotransmission. *Sci Rep* **7**, 370 (2017).
14. Di Battista, A.M., Heinsinger, N.M. & Rebeck, G.W. Alzheimer's Disease Genetic Risk Factor APOE-epsilon4 Also Affects Normal Brain Function. *Curr Alzheimer Res* **13**, 1200-1207 (2016).
15. Pierrot, N. *et al.* Amyloid precursor protein controls cholesterol turnover needed for neuronal activity. *EMBO Mol. Med* **5**, 608-625 (2013).
16. Shimano, H. *et al.* Isoform 1c of sterol regulatory element binding protein is less active than isoform 1a in livers of transgenic mice and in cultured cells. *J. Clin. Invest* **99**, 846-854 (1997).
17. Horton, J.D., Goldstein, J.L. & Brown, M.S. SREBPs: activators of the complete program of cholesterol and fatty acid synthesis in the liver. *J Clin Invest* **109**, 1125-31 (2002).
18. Chang, C.Y., Ke, D.S. & Chen, J.Y. Essential fatty acids and human brain. *Acta Neurol Taiwan* **18**, 231-41 (2009).
19. Luchtman, D.W. & Song, C. Cognitive enhancement by omega-3 fatty acids from child-hood to old age: findings from animal and clinical studies. *Neuropharmacology* **64**, 550-65 (2013).
20. Bazinet, R.P. & Laye, S. Polyunsaturated fatty acids and their metabolites in brain function and disease. *Nat. Rev. Neurosci* **15**, 771-785 (2014).
21. Desvergne, B. RXR: from partnership to leadership in metabolic regulations. *Vitam Horm* **75**, 1-32 (2007).
22. Evans, R.M. & Mangelsdorf, D.J. Nuclear Receptors, RXR, and the Big Bang. *Cell* **157**, 255-266 (2014).
23. Michalik, L. *et al.* International Union of Pharmacology. LXI. Peroxisome proliferator-activated receptors. *Pharmacol. Rev* **58**, 726-741 (2006).
24. Zolezzi, J.M. *et al.* PPARs in the central nervous system: roles in neurodegeneration and neuroinflammation. *Biol. Rev. Camb. Philos. Soc* **92**, 2046-2069 (2017).
25. Moutinho, M. & Landreth, G.E. Therapeutic potential of nuclear receptor agonists in Alzheimer's disease. *J. Lipid Res* **58**, 1937-1949 (2017).
26. Saez-Orellana, F., Octave, J.N. & Pierrot, N. Alzheimer's Disease, a Lipid Story: Involvement of Peroxisome Proliferator-Activated Receptor alpha. *Cells* **9**(2020).
27. D'Orio, B., Fracassi, A., Ceru, M.P. & Moreno, S. Targeting PPARalpha in Alzheimer's Disease. *Curr Alzheimer Res* **15**, 345-354 (2018).
28. Pierrot, N. *et al.* Sex-regulated gene dosage effect of PPARalpha on synaptic plasticity. *Life Sci Alliance* **2**(2019).
29. Rice, H.C. *et al.* Secreted amyloid-beta precursor protein functions as a GABABR1a ligand to modulate synaptic transmission. *Science* **363**(2019).
30. Mucke, L. *et al.* High-level neuronal expression of abeta 1-42 in wild-type human amyloid protein precursor transgenic mice: synaptotoxicity without plaque formation. *J. Neurosci* **20**, 4050-4058 (2000).

31. Johnson, E.C.B. *et al.* Behavioral and neural network abnormalities in human APP transgenic mice resemble those of App knock-in mice and are modulated by familial Alzheimer's disease mutations but not by inhibition of BACE1. *Mol Neurodegener* **15**, 53 (2020).
32. Koch, M. *et al.* Palmitoylethanolamide protects dentate gyrus granule cells via peroxisome proliferator-activated receptor-alpha. *Neurotox Res* **19**, 330-40 (2011).



Geneeskundige Stichting Koningin Elisabeth
Fondation Médicale Reine Elisabeth
Königin-Elisabeth-Stiftung für Medizin
Queen Elisabeth Medical Foundation

Progress report of the
interuniversity research project of

Prof. dr. Sebastiaan Engelborghs (VUB)
Prof. dr. Chris Baeken (UGent)

Prof. dr. Sebastiaan Engelborghs

Vrije Universiteit Brussel (VUB)
Center for Neurosciences (C4N)
Laarbeeklaan 103, 1090 Brussel

Prof. dr. Chris Baeken

Universiteit Gent
Department of Psychiatry & Neuropsychology
C. Heymanslaan 10, 9000 Gent

Unraveling the link between depression and dementia to improve diagnostic and treatment options

1. Publications 2021

Wiels, W. A., Wittens, M. M. J., Zeeuws, D., Baeken, C., & Engelborghs, S. (2021). Neuropsychiatric Symptoms in Mild Cognitive Impairment and Dementia Due to AD: Relation with Disease Stage and Cognitive Deficits. *Frontiers in Psychiatry*, Vol. 12, p. 1322. <https://doi.org/10.3389/fpsyt.2021.707580>

Background: The interaction between neuropsychiatric symptoms, mild cognitive impairment (MCI), and dementia is complex and remains to be elucidated. An additive or multiplicative effect of neuropsychiatric symptoms such as apathy or depression on cognitive decline has been suggested. Unraveling these interactions may allow the development of better prevention and treatment strategies. In the absence of available treatments for neurodegeneration, a timely and adequate identification of neuropsychiatric symptom changes in cognitive decline is highly relevant and can help identify treatment targets.

Methods: An existing memory clinic-based research database of 476 individuals with MCI and 978 individuals with dementia due to Alzheimer's disease (AD) was reanalyzed. Neuropsychiatric symptoms were assessed in a prospective fashion using a battery of neuropsychiatric assessment scales: Middelheim Frontality Score, Behavioral Pathology in Alzheimer's Disease Rating Scale (Behave-AD), Cohen-Mansfield Agitation Inventory, Cornell Scale for Depression in Dementia (CSDD), and Geriatric Depression Scale (30 items). We subtyped subjects suffering from dementia as mild, moderate, or severe according to their Mini-Mental State Examination (MMSE) score and compared neuropsychiatric scores across these groups. A group of 126 subjects suffering from AD with a significant cerebrovascular component was examined separately as well. We compared the prevalence, nature, and severity of neuropsychiatric symptoms between subgroups of patients with MCI and dementia due to AD in a cross-sectional analysis.

Results: Affective and sleep-related symptoms are common in MCI and remain constant in prevalence and severity across dementia groups. Depressive symptoms as assessed by the CSDD further increase in severe dementia. Most other neuropsychiatric symptoms (such as agitation and activity disturbances) progress in parallel with severity of cognitive decline. There are no significant differences in neuropsychiatric symptoms when comparing "pure" AD to AD with a significant vascular component.

Conclusion: Neuropsychiatric symptoms such as frontal lobe symptoms, psychosis, agitation, aggression, and activity disturbances increase as dementia progresses. Affective symptoms such as anxiety and depressive symptoms, however, are more frequent in MCI than mild dementia but otherwise remain stable throughout the cognitive spectrum, except for an increase in CSDD score in severe dementia. There is no difference in neuropsychiatric symptoms when comparing mixed dementia (defined here as AD + significant cerebrovascular disease) to pure AD.

2. Conferences 2021

Dieter Zeeuws (MD, staff psychiatrist UZ Brussel) and Wietse Wiels (MD, neurology resident VUB) are PhD candidates working on this research project. They both attended different conferences that are related to the topic of the project.

Dieter Zeeuws:

- Oral presentation on a virtual symposium about the treatment of therapy resistant depression: "*Behandeling van therapieresistente depressie: bestaande en nieuwe opties anno 2021*" (26/4/21).
- Two-day online course about the psychological vulnerabilities and suicide risk in elderly (18/05/21 and 25/05/21).
- Attended the 29th European congress of Psychiatry (10/4/21-13/4/21)
- Neuroscience Medical Education Forum: Management of depression and escalation strategies: who, when and how? 18/2/2021
- 7de congres ouderen psychiatrie Provinciehuis Leuven 28 okt 2021
- Poster presentation 'Suicidality during neuromodulation in the elderly depressed: study design' has been accepted for the European congress of Psychiatry accepted (may 2022).

Wietse Wiels:

- Attended the 7th congress of the European Academy of neurology (19/6/21-22/6/21).
- Attended the Alzheimer's Association International Conference (26/7/21-30/7/21).

3. Data collection

3.1. WP1: Development of a dementia risk score amongst depressed elderly

Research stay at the University of Maastricht. This stay was originally planned from February until April 2020. However, due to the COVID pandemic this stay ended prematurely. During 2021 PhD candidate Wietse Wiels kept in close contact with the colleagues at the University of Maastricht. Therefore, it was possible to finish the data-collection. A new research stay of Wietse Wiels at University of Maastricht is scheduled for Q1 2022. The data analysis started at the end of 2021 and is expected to be finished in 2022. Subsequently, a research paper will be prepared (2022) that is scheduled to be published in 2023.

3.2. WP2: Validate the dementia risk score in a prospective longitudinal clinical study

The protocol for this study was drafted, reviewed, and finished. It aims to examine the prognostic relevance of depressive symptoms and amyloid status in the elderly, through a prospective evaluation of cognitively healthy controls, depressed patients, and cognitively impaired patients (all groups >65 years of age). All groups will receive serial clinical, imaging, neuropsychological as well as affective/behavioural, and neurochemical assessment. Furthermore, the added value of plasma-based amyloid tests will be evaluated. Recruitment and testing started in 2021 and is ongoing.

3.3. WP3: Evaluate the predictive and clinical effects of non-invasive brain stimulation in the elderly depressed with and without prodromal AD

The protocol for this study was drafted, reviewed, and finished. It will evaluate non-invasive brain stimulation techniques on the elderly depressed, and the impact of this treatment on imaging parameters. FAGG agreement (since it includes medical devices) was obtained. The study is approved by the Ethical committee. Due to the covid-19 pandemic several aspects of this study were delayed. The recruitment and testing are starting in Q1 2022.

4. Budget 2021

A study nurse (Sifra Muller) was hired in 2021 (payroll budget VUB, see attachment). She turned sick in April 2021 and resigned in June 2021.

No expenses were made from the UGent budget (see attachment).

5. Future directions for 2022

WP1: finish data analysis and writing of a research paper that is scheduled to be published in 2023.

WP2: Continue recruitment and data collection.

WP3: Start recruitment and testing.

As from January 2022, Sara De Witte, Ma Psychology and PhD student at UGent, will join the project team as study coordinator. She will initially be paid through the GSKE project budget of UGent.

6. Prolongation of the project

Last, but not least: **given the significant delay with patient recruitment (WP2 and WP3) due to the COVID pandemic, we would like to apply for a budget neutral prolongation of the project with two years (end date: 31 DEC 2024 instead of 31 DEC 2022).**



Geneeskundige Stichting Koningin Elisabeth
Fondation Médicale Reine Elisabeth
Königin-Elisabeth-Stiftung für Medizin
Queen Elisabeth Medical Foundation

Progress report of the interuniversity research project of

Prof. dr. Vincent Van Rompaey (UAntwerpen)
Prof. dr. Peter Ponsaerts (UAntwerpen)
Prof. dr. Guy Van Camp (UAntwerpen)
Prof. Rik Gijsbers (KU Leuven)

Prof. dr. Vincent Van Rompaey (UAntwerpen)

Experimental laboratory of Translational Neurosciences Dept. of Translational Neurosciences
University of Antwerp
Universiteitsplein 1
2610 Antwerp, Belgium
vincent.vanrompaey@uantwerpen.be

Prof. dr. Peter Ponsaerts (UAntwerpen)

Laboratory of Experimental Hematology Vaccine and Infectious Disease Institute University of
Antwerp
Universiteitsplein 1
2610 Antwerp, Belgium
Peter.Ponsaerts@uantwerpen.be

Prof. dr. Guy Van Camp (UAntwerpen)

Human Molecular Genetics laboratory
Center of Medical Genetics, University of Antwerp
Universiteitsplein 1
2610 Antwerp, Belgium
guy.vancamp@uantwerpen.be

Prof. Rik Gijsbers (KU Leuven)

Laboratory of Viral Vector Technology and Gene Therapy Department of Pharmaceutical and
Pharmacological Sciences Faculty of Medicine, KU Leuven
RK-Herestraat 49, box 1023
3000 Leuven, Belgium
Rik.Gijsbers@kuleuven.be

Dr. Erwin Van Wijk

Department of Otorhinolaryngology
Radboud University Nijmegen Medical Center Geert Grooteplein 10
6525 GA Nijmegen, The Netherlands
Erwin.vanWyk@radboudumc.nl

Dr. Erik De Vrieze

Departments of Otorhinolaryngology and Human Genetics Radboud University Medical Centre
Geert Grooteplein Zuid 10
P.O. box 9101, 6500 HB
Nijmegen, The Netherlands

Development of allele-specific CRISPR-nuclease gene therapy for late-onset sensorineural hearing impairment in a new humanized DFNAg mouse model

Work-package 1: the DFNAg^{hWT/mWT} mice arrived at our animal facility in March 2021. These mice are already backcrossed to the C57BL/6 (Cdh23^{753A>G}) mice resulting in the generation of DFNAg^{hWT/hWT} C57BL/6 (Cdh23^{753A>G}) mice where the mutation in the Cdh23 gene, causing early hearing loss in BL6 mice, is corrected. Phenotyping of DFNAg^{hWT/hWT} and DFNAg^{mWT/hWT} mice confirms normal hearing function up to three months. In October 2021, the DFNAg^{hP51S/mWT} mice arrived at our facility. These mice are currently in breeding with our already established DFNAg^{hWT/hWT} C57BL/6 (Cdh23^{753A>G}) mice. Breeding of these mice will result in the generation of DFNAg^{hP51S/hP51S} C57BL/6 (Cdh23^{753A>G}) and DFNAg^{hWT/hP51S} C57BL/6 (Cdh23^{753A>G}) mice in the second generation. We expected to start with the long term assessment of hearing and vestibular function in September 2022 when all mouse models will be available.

We are currently building a set up to measure the Vestibular Ocular Reflex (VOR) which is an objective tool to assess vestibular function in mice. We will use this technique to follow up the vestibular function of our new DFNAg^{hP51S/hWT} mouse model.

Work-package 2: We already injected an AAV2/7 vector, harbouring the luciferase reporter protein next to eGFP, in the inner ear of C57BL/6 (Cdh23^{753A>G}) mice by using the posterior semi-circular canal approach. Injection through the PSC, using the Nanoliter 2020 device, did not induce sensorineural hearing loss (Figure 1A). Bioluminescence imaging (BLI) revealed a bright signal in the region of the left ear 25 days post injection (25 DPI) (Figure 1B). Furthermore, analysis of eGFP expression in the inner ear demonstrate that AAV2/7 can effectively transduce the spiral ligament fibrocytes (Figure 1C).

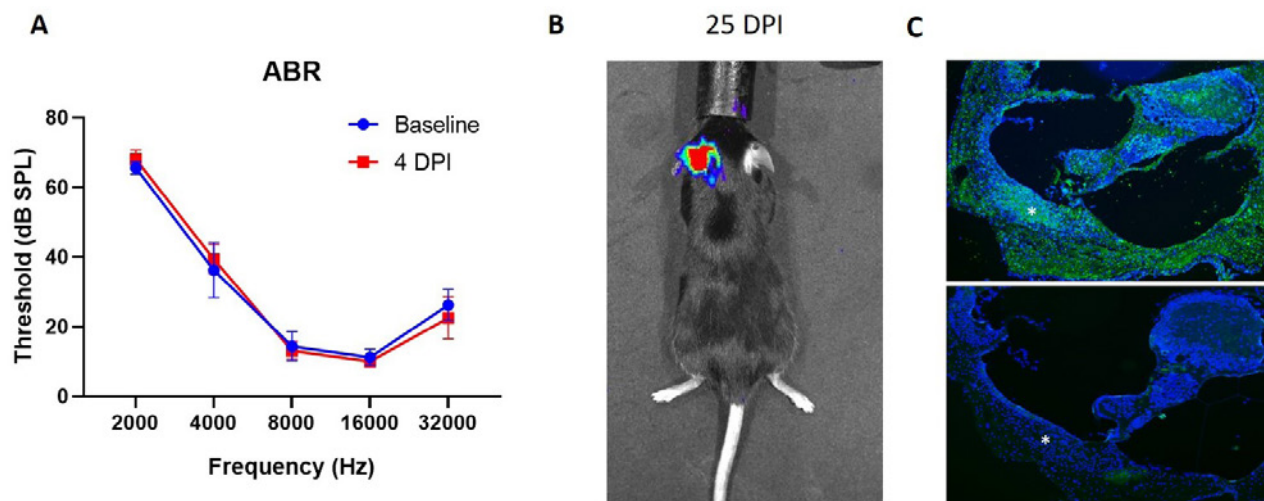


Figure 1. (A) Auditory Brainstem Response (ABR) measurements before and 4 days post Injection (DPI) with AAV2/7. (B) Bioluminescence imaging performed at 25 DPI. (C) eGFP expression in the inner ear at 7 DPI. * indicates the spiral ligament.

A manuscript describing the results of this experiment is currently been prepared and will be submitted to Biomolecules (IF: 4,8) The authors will include a statement in the acknowledge section to thank GSKE for their funding. We will proceed to assess long term safety of rAAV7 injection by evaluating otovestibular function at the age of 3, 6, 9, 12, 15, 18 and 21 months by BLI as well as for hearing and vestibular function.

Work-package 3: The strategy to specifically disrupt the mutant *COCH* allele is designed in collaboration with the H&G lab at the Radboud University of Nijmegen. They already designed allele specific ASOs for the targeting of mutant *COCH* (p.P51S allele) demonstrating that the genomic region of the c.151C>T mutation is amenable allele-specific targeting using a base-pairing approach. We will proceed with the development of a therapeutic strategy that can be delivered as a single dose to treat DFNA9 by the use of CRISPR/Cas9 to disrupt the mutant *COCH* allele. To obtain the highest possible specificity for the c.151C>T mutant *COCH* allele, we will employ spCas9-EQR which has a PAM-site preference of "NGAG". The c.151C>T change creates this PAM site on the complementary strand of the mutant *COCH* gene and allows for allele-specific nuclease activity. The CHOPCHOP webserver (<https://chopchop.cbu.uib.no>) predicts an allele-specific gRNA for SpCas9-EQR with favorable properties (>50% predicted mismatch frequency, no other genomic targets with <2 mismatches). Upon cleavage of the mutant *COCH* allele, the non-homologous end joining (NHEJ) repair pathway will change the gain-of-function allele into a null allele, effectively creating the situation of heterozygous carriers of *COCH* loss-of-function mutations, which we know exhibit normal inner ear function in human and mice. The PhD student working on this project, recently obtained an FWO grant for a research visit to the H&G lab in March 2022. During this visit, she will investigate the molecular efficacy of the spCas9-EQR/gRNA combination in primary fibroblasts derived from DFNA9 patients.

Work-package 4: injections with AAV2/7 encoding the chosen CRISPR nuclease and suitable gRNA sequences (WP3) will be performed in our new DFNA9^{hP51S/hWT} mouse model. This experiment is expected to start in 2024 when WP2 and WP3 are completed. In WP4 we will look at the genome editing efficiency of the different gRNA's in DFNA9^{hP51S/hWT} C57BL/6 (Cdh23^{753A>G}) mice.

Work-package 5: when WP4 is completed we can finally evaluate if the CRISPR nuclease can prevent hearing and vestibular loss in our new DFNA9^{hP51S/hWT} mouse model. We expected to inject our DFNA9^{hP51S/hWT} mouse model with the established CRISPR based gene therapy in the course of 2025.

1. Use of GSKE budget:

The GSKE budget was used for the maintenance, breeding and genotyping of the different mouse models in the animalarium of the University of Antwerp. Furthermore, we used the GSKE budget to purchase material for the AAV injections as well as the cost for the BLI measurements and antibodies to stain inflammatory cells in the inner ear after AAV injection.



Geneeskundige Stichting Koningin Elisabeth
Fondation Médicale Reine Elisabeth
Königin-Elisabeth-Stiftung für Medizin
Queen Elisabeth Medical Foundation

Progress report of the
interuniversity research project of

Prof. dr. An Goris (KU Leuven)
Prof. Nathalie Cools (UAntwerpen)

Prof. dr. An Goris (KU Leuven)
Department of Neurosciences
Laboratory for Neuroimmunology
T +32 16 33 07 72
an.goris@kuleuven.be

Prof. Nathalie Cools (UAntwerpen)
Laboratory for Experimental Hematology
University of Antwerp
nathalie.cools@uza.be

Table of contents

1. Summary and current status of research program
2. Achievements
3. Networking and collaborations
4. Relevance and future perspectives
5. Financial report
6. Publications under GSKE support
7. Team publications
8. References

Deep sequencing of myelin-reactive T-cells to elucidate new disease mechanisms and identify correlates for treatment responsiveness in multiple sclerosis

1. Summary and current status of research program

Multiple sclerosis (MS) is one of the most common neurological disorders in young adults, affecting around 13,500 people in Belgium and 2.8 million worldwide. The disease can lead to important physical as well as cognitive disability at a time that is crucial in the personal and professional development of patients. MS is characterized by three hallmarks: inflammation, demyelination and neuronal loss¹. The exact cause of MS still remains to be elucidated but the past few years have seen exciting progress in the field. Over the last decade, we have – in an international collaborative context as part of the International Multiple Sclerosis Genetics Consortium (IMSGC) – identified >230 genetic risk factors for MS. These include several risk as well as protective variants in the Human Leukocyte Antigen (HLA) region², which in combination with the T- and B-cell receptor likely determine the target of the autoimmune reaction³, and 200 variants throughout the genome, enriched for immunological function and implicating the interplay between B-cells, T-cells, and innate immune cells⁴⁻⁸. Hence, the complex interactions between the identified genetic and environmental factors affect the predominantly immune-mediated underlying mechanisms of the disease.

With previous GSKE support (A. Goris, 2017-2019 and Prize Viscountess Valine de Spoelberch), we focused on the role of B-cells and demonstrated an imbalance between pathogenic and immunoregulatory B-cells in MS that is amenable to treatment⁹⁻¹². Besides, it is currently generally accepted that autoimmunity against antigens expressed in the central nervous system (CNS) is mediated by T-cells. Indeed, CD4⁺ T-cells, in particular Th1 and Th17 cells, directed towards various myelin-derived antigens, including myelin basic protein (MBP), proteolipid protein (PLP), myelin oligodendrocyte glycoprotein (MOG) and B-crystallin have been identified in patients with MS¹³⁻¹⁶, and are shown to migrate between blood and CNS^{17,18}. Nonetheless, these autoreactive T-cells that are thought to be the culprit in MS form a very small subset in the peripheral blood which has hampered their investigation.

Thanks to the previous and current support of GSKE, we were able to implement state-of-the-art genetic methods that allow to analyze DNA and RNA at the level of single B- or T-cells (single-cell sequencing) (manuscript in preparation). This makes it now timely to turn our attention to a detailed understanding of their characteristics that make them pathogenic in MS. The combined expertise of our interuniversity team in immunology and characterization of autoreactive T-cells (N. Cools, U Antwerp) on the one hand and in genetics and single-cell sequencing (A. Goris, KU Leuven) on the other makes it now feasible, timely and innovative to investigate the pathogenic characteristics of autoreactive T-cells in MS. For this, the following three aims have been set forth:

1. What is the TCR repertoire of autoreactive T-cells in MS?
2. What are the transcriptional characteristics of autoreactive T-cells?
3. Can the autoreactive T-cell clonotype repertoire be used as a correlate for therapy responsiveness?

2. Achievements

Achievement 1. TCR repertoire of autoreactive T-cells in MS

1. Summary

T-cells recognize complexes of specific antigenic peptides and autologous HLA molecules through their TCR. In fact, the TCR sequence functions as a unique fingerprint for each T-cell. Hence, analysis of T-cell clonal expansion can allow the identification of T-cells that are assumed to be involved in the disease process. Since autoreactive T-cells may occur naturally in less than 1 in 300 T-cells¹⁹, clonal expansion by activation and proliferation of antigen-specific T-cells can be provoked by *ex vivo* recognition of an antigen.

2. Current status

2.1 Methodology for the identification of relevant TCR:

TCR repertoire sequencing data contain many sequences, originating from naive T-cells, that are unrelated to the underlying immunological condition. Consequently, these sequences do not carry any useful information with regard to the condition under investigation. As a primary method for reducing the enormous search space (often exceeding millions of unique TCRs in one dataset), it is paramount to determine the 'functional' T-cell repertoire. In the T-cell repertoire, many different TCRs will respond to the exact same epitope. We can reduce this redundancy by modeling the repertoire as a network in which the nodes represent the TCRs and edges represent the edit distance (i.e. number of amino acid substitutions, insertions or deletions) between two TCRs. Next, we can determine epitope-specific clusters, based on a similarity criterion linking a group of TCR sequences together. These clusters will subsequently be considered a non-redundant TCR. Next, other filtering strategies will be applied that focus on features derived from the mechanism of V(D)J recombination. One can assume that TCRs that are significantly more common than expected, are under the selective pressure of an immunological driver (e.g. autoantigen in MS). Different models have been developed to estimate the probability for a TCR to be generated. These models are based on the recombination mechanism of the V, D and J gene segments in developing lymphocytes, resulting in a functional TCR chain. The Optimized Likelihood estimate of immunoGlobulin Amino-acid sequences (OLGA) algorithm²⁰ computes generation probabilities (Pgen) from amino acid sequences, whereas the Inference and Generation of Repertoires (IGoR) algorithm²¹ infers Pgen from nucleotide sequences. We can hypothesize that CDR3 sequences that are more abundant than determined by their Pgen are under the selective pressure of an immunological driver, either in the past or present. Consequently, T-cells carrying these sequences hold valuable information and can be analyzed in a specific disease context. The main two parameters that will be tested are (i) frequency of the TCR across all samples and (ii) the Pgen of the TCR (Figure 1). Different cut-offs of these parameters will be evaluated in the context of a classification task where we use the area under the receiver operating characteristic curve (AUROC) as a measure for the classification performance. Different machine learning frameworks can be applied to tackle this classification problem. Different candidate frameworks for which in-house experience is available include:

- Ensemble learning methods: These may include Random Forests (RF) or Gradient Tree Boosting (GTB) algorithms. These ensemble techniques provide flexible, yet very powerful methods to solve a classification task.
- Artificial Neural Networks (ANN): One of the most powerful and diversified machine learning methods to achieve high accuracy in a classification task.
- Conditional Random Fields (CRF): This machine learning method has been derived from Hidden Markov Models and has been used in our group for a number of pattern-recognition applications²²⁻²⁴.

Figure 1 illustrates preliminary results obtained from this procedure on a subset of a well-known TCR repertoire data set by Emerson and colleagues²⁵.

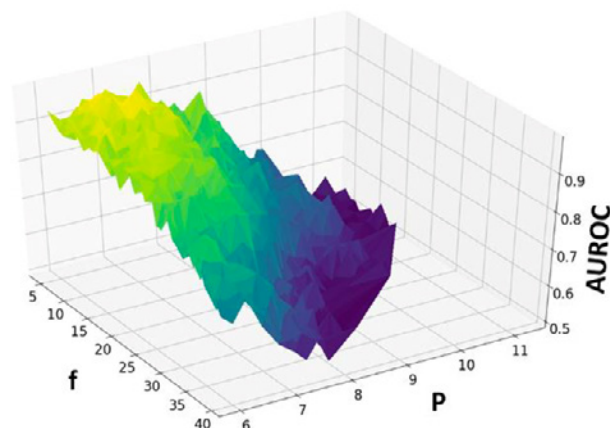


Figure 1. TCR prioritization. Preliminary results of parameter testing in the context of prioritizing relevant TCRs from larger repertoires. A random forest (RF) classifier is trained within a range of cut-offs for f (%) and P. The data originates from a study of CMV in a large cohort. The procedure was performed on a subset to identify highly predictive TCRs for CMV serostatus. Frequency, f; probability of generation, P; area under the receiver operating characteristic, AUROC.

This analysis can be performed on large rep-seq datasets (such as the one by Emerson et al²⁵). The main data sources consist of the immune ACCESS database, NCBI's sequencing read archive (SRA), iReceptor Public Archive and the Pan Immune Repertoire Database (PIRD).

2.2 Characterization of MS epitope reacting TCR:

One of the main objectives of this project is the characterization of T-cells that react to important MS-derived epitopes. Several of these target epitopes have been described for MS²⁶⁻²⁸, but it is still unclear which TCCs are activated by these peptides. To address this question, N. Cools has assembled a unique protocol for enrichment of autoreactive T-cells using a broad antigen panel, and this protocol has been refined in a collaboration between N. Cools and A. Goris so that both sites apply a similar methodology according to (mostly) shared protocols for this project. PBMCs are stimulated *in vitro* in the presence of a selected panel of myelin oligodendrocyte glycoprotein (MOG)-, myelin basic protein (MBP)-, and proteolipid protein (PLP)-derived synthetic peptides that have previously been demonstrated as immunodominant¹³⁻¹⁶ and to act in part independently of HLA-DR^{14,29,30}. Myelin-reactive T-cells are observed using flow cytometric dual detection of CD71 and CD98 (CD4⁺ and CD8⁺) T-cell activation markers following one-week stimulation of T-cells with a pool of myelin-derived peptides (Figure 2). This methodology results in an average of 0.2% of CD4⁺ and CD8⁺ T cells in MS patients being characterized as autoreactive. After multiple and some time-consuming adjustments, the lab of N. Cools and A. Goris have established a consistent and reproducible protocol for the generation of myelin-derived T-cells. In addition, we have corroborated the relevance of our myelin peptide selection, which was previously demonstrated by others through a positive T-cell proliferative response to this peptide mix in 74% of RRMS patients compared to 30% of healthy controls³¹.

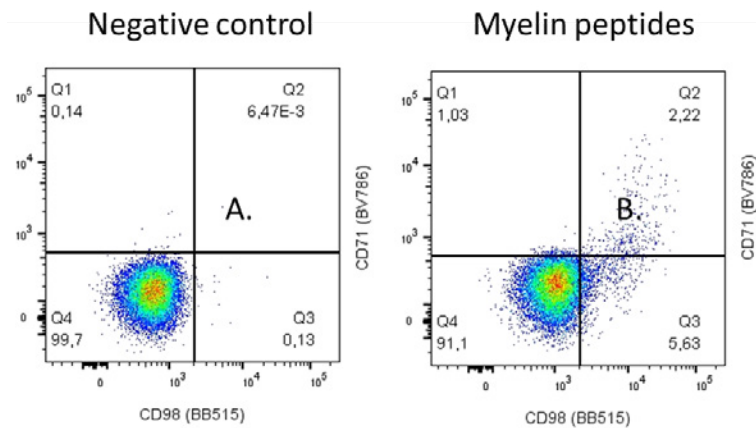


Figure 2. Representative bivariate pseudocolor plots of myelin-reactive CD71- and CD98-positive CD4⁺ T-cells in a patient with MS. (A) indicates dual-activated CD4⁺ T-cells from unstimulated cells in quadrant Q2, while (B) depicts dual-activated CD4⁺ T-cells after myelin-derived peptide stimulation in quadrant Q2.

We will use these sorted autoreactive CD4⁺ and/or CD8⁺ T-cells as input for the Chromium Single Cell V(D)J Solution on the 10x Genomics³² platform available at our institution. We will obtain full-length V(D)J sequences and paired α and β sequences to establish TCR repertoires of autoreactive T-cells on a cell-by-cell basis. For that purpose, we have now implemented the Chromium Single Cell V(D)J Solution on the 10x Genomics³² platform available at KU Leuven and the bio-informatics pipelines necessary to identify clonal expansions based on identical or highly identical immune cell receptors (manuscript in preparation).

Similarly, patient-derived myelin-specific CD4⁺ T-cells are single-cell sorted using FACS, followed by an RT-PCR using 76 TCR-primers, by the Antwerp team. The products are used in a second and third PCR reaction, incorporating individual barcodes into each well. Libraries are purified and sequenced using the Illumina MiSeq platform, after which the resulting paired-end raw sequencing reads are assembled and deconvoluted using barcode identifiers at both ends of each sequence. The resulting sequences are then analyzed using the program MiXCR and the CDR3 nucleotide sequences are extracted and translated. First sequencing results were translated into the full functional sequence of a patient-derived MBP₈₅₋₉₉-specific and MOG₉₇₋₁₀₉-specific TCR and the development of their TCR-encoding constructs. Their expression was tested in two TCR-deficient T cell lines (2D3 and SKW-3) by means of TCR-encoding mRNA electroporation. Our preliminary data show a transgene MBP85-99-TCR expression as high as 90% over the course of 4 days (Figure 3).

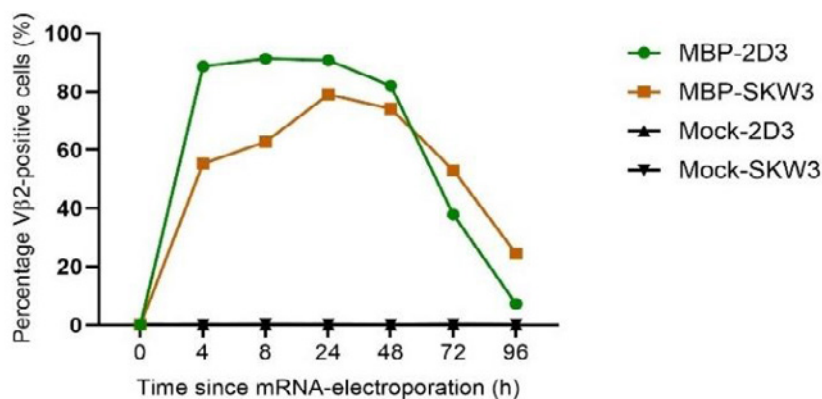


Figure 3. MBP85-99-TCR-encoding mRNA electroporation of TCR-deficient T cell lines. Transgene MBP85-99-TCR expression is visualized using flow cytometry and a fluorochrome-labeled antibody to V2, binding the variable domain of the newly introduced TCR. As a negative control, a MOCK condition is used, to which no mRNA is added.

3. Future plans

An integrated meta-analysis will be performed on publicly available MS datasets, in which MS-associated TCRs will be identified. Five MS datasets are available in the immuneACCESS and SRA databases. All datasets originate from a different source, but all have been sequenced by the same provider (Adaptive Biotechnologies). All datasets will be combined into a uniform format. First, the methodology developed and described in 2.1 will be applied to prioritize MS-associated TCRs. In brief, this method focuses on the identification of non-redundant TCR sequences that appear more often than expected by chance.

In addition, we will investigate peripheral blood T-cells from recently diagnosed and untreated patients with MS according to the revised McDonald criteria³³ (N = 15). To this end, we will extend our single-cell sequencing pipelines from B-cell receptor to T-cell receptor repertoires and superimpose identified clonal T-cell expansions on the peripheral blood and cerebrospinal fluid (CSF) T-cell landscape in patients with MS (achievement 2). Access to patient samples is possible by already existing collaborations of both PIs with University Hospitals Leuven (Prof. B. Dubois) and Antwerp (Dr. B. Willekens), respectively.

Achievement 2. Transcriptional characteristics of autoreactive T-cells.

1. Summary

Autoreactive T-cells in achievement 1 undergo proliferation and activation as part of the enrichment, which may influence their transcriptome but not their TCR repertoire. We can, however, use the TCR “fingerprint” of autoreactive T-cells established in achievement 1 to superimpose these autoreactive clonal T-cells on the peripheral blood CSF T-cell landscape in patients with MS. Based on the distribution of these autoreactive T-cells in the T-cell landscape, we can determine the transcriptional phenotype of these autoreactive T-cells in achievement 2. As TCR is a critical determinant of T-cell fate, we will establish whether autoreactive T-cells have related transcriptional programs as previously demonstrated in mice³⁴.

2. Current status

From PBMCs as collected above, we have sorted (CD4⁺/CD8⁺) T-cells using negative selection magnetic beads (EasySep) as input for the 10x Genomics Chromium Single Cell Solution. We established the required bio-informatics pipelines. Data are processed using Cell Ranger v3.0.2 and further analyzed with Seurat v3.0.0. Bio-informatics. Differentially expressed genes for each cluster are identified and clusters are annotated. A representative example for all T-cells is given in Figure 4. Aside from PBMCs, we have started to collect CSF immune cells from patients with MS (N = 10) and healthy controls (N = 10). At this moment of writing, we have optimized protocols for cryopreservation, thawing and single-cell sequencing of CSF immune cells. The first samples have been sequenced and are ready for bioinformatic analysis.

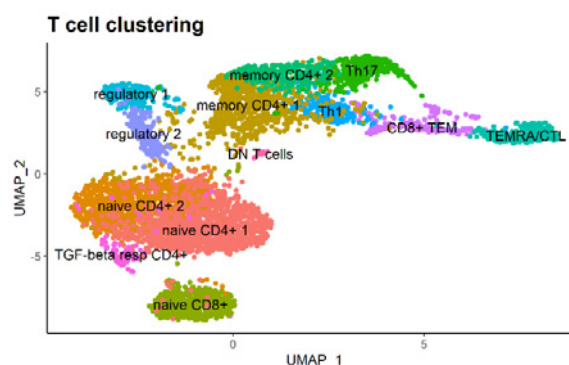


Figure 4. Representative clustering and annotation of single-cell transcriptomics from a T cell sample.

3. Future plans

Based on the single-cell transcriptome and immune cell receptor repertoire data of achievement 1 and achievement 2, we will overlay autoreactive T-cells as determined by their TCR fingerprint. This will indicate whether autoreactive T-cells have related transcriptomes within and across patients, and to characterize differentially expressed genes.

Achievement 3. The autoreactive T-cell clonotype repertoire as a correlate for therapy responsiveness.

1. Summary

Whereas careful patient monitoring is essential in the development path of novel therapies for MS, conventional outcome measures do not correlate well with long-term disability. Alternatively, immunological assays may provide a valuable alternative as measures of the effect of this and other immunotherapies. In this perspective, the sequences of myelinreactive T-cells from blood could be used to track T-cells from the same clone over time.

2. Current status

First, we assessed the kinetics of myelin-specific autoreactive T-cell responses in MS patients. For this, we conducted a prospective cohort study in the MS clinic of the Antwerp University Hospital. PBMC were isolated from 14 MS patients treated with natalizumab at different time points. The mean age of the patients was 41.36 years (SD 10,20, range 24-59). The median EDSS score was 2.0 (range 1-6). Disease duration since first symptoms ranged between 1 year and 20 years (median 8,13 years). Duration of treatment with natalizumab ranged between 6 months and almost 10 years (median 2.25 years). PBMCs were stimulated *in vitro* in the presence of a selected panel of myelin oligodendrocyte glycoprotein (MOG)-, myelin basic protein (MBP)-, and proteolipid protein (PLP)-derived synthetic peptides, as described in WP1. Next, the frequency of myelin-specific autoreactive T cells was determined using IFN-gamma ELISPOT and analysis. We found that T-cell reactivity towards a mixture of myelin-peptides in natalizumab treated MS patients is highly variable. Whereas 80% of patients demonstrate myelin reactivity at baseline, only 30-40% of patients demonstrate myelin-specific autoreactive T cells at every time point that was assessed longitudinally (t=0, t= 8 weeks, t=12 weeks, t= 24 weeks). This underlines that the baseline presence of autoreactive T cells in the peripheral blood of MS patients may be a critical factor when investigating rare cell populations. The observed high intra-patient variability poses some challenges for current project and warrants further investigation.

3. Future plans

To date, no comprehensive framework exists to combine and analyze gene expression data and AIRR-seq data in parallel. Some efforts have been made to unite these two levels of organization in the field of cancer research^{35,36}, but integration remains far from trivial. Using the data from the assay described above, we will develop a comprehensive framework to integrate the immune receptor and transcriptomic data as a means to functionally characterize paired TCR sequences in samples of MS patients. This approach would imply co-clustering of gene expression t-Distributed Stochastic Neighbor Embedding (t-SNE) 60 clusters and TCR clusters (clustered using VDJtools⁴²). Such a framework will provide insight into how a specific functional phenotype (gene expression profile) is associated with the expression of a specific receptor pair. In addition, we will follow the T-cell repertoire fingerprint in MS patients receiving tolDC treatment, as previously described in MS patients treated with stem cell transplantation³⁷. For this, paired PBMCs banked in the context of the clinical trial evaluating the feasibility and safety of the use of tolDC loaded with the selected pool of peptides for the treatment of MS (ClinicalTrials.gov Identifier: NCT02618902), before and after the cell therapy vaccination cycle (N=9x2), will be analyzed as in WP1.

3. Networking and collaborations

Building on expertise gained with GSKE support (A. Goris, 2017-2019 and Prize Viscountess Valine de Spoelberch), the current GSKE project (2020-2022) was set up in collaboration with Prof. Nathalie Cools (U Antwerpen) and was awarded.

Prof. An Goris is coordinator of the International Multiple Sclerosis Genetics Consortium (www.imsgc.org) since 2018, and her research group is a member of the EU Horizon2020 Consortium MultipleMS (www.multiplems.eu) and EXIMIOUS (<https://www.eximious-h2020.eu/>).

Prof. Nathalie Cools is the coordinator of the EU H2020 Restore project https://cordis.europa.eu/project/rcn/213047_en.html, promotor of the EU-EFRO Anicells project (1108, <https://www.vlaio.be/nl/andere-doelgroepen/europees-fonds-voor-regionale-ontwikkeling-efro/ontdek-efro-vlaanderen/overzicht>) and consortium beneficiary of the EU H2020 Marie Curie Training network INSTRuCT, a network of European scientists from academia and industry focused on developing innovative myeloid regulatory cell (MRC)-based immunotherapies.

Over the project duration, members of our research groups attended the online European Conference on the Treatment and Research in Multiple Sclerosis (ECTRIMS) MSVirtual, the online MS Data Alliance Meeting and the online European Charcot Foundation Meeting. Prof. An Goris was invited speaker at ECTRIMS 2021 presenting "Multiple sclerosis genetics: what needs to be done?".

4. Relevance and future perspectives

The relevance of clonal expansions in MS – as recognized in other autoimmune diseases such as rheumatoid arthritis – sprouts, with very recent single-cell sequencing studies demonstrating clonal expansions of both B- and T-cells in MS³⁸⁻⁴⁰. However, characterization of culprit and favorable clonal expansions is sparse, which is where our approach adds novelty. We anticipate that T-cell repertoire sequencing and transcriptomic profiling of autoreactive T cells will become a critical tool in both biomedical discovery and clinical management of patients.

Moreover, recent advances in TCR and chimeric antigen receptor (CAR) engineering may provide prospects for patient-specific treatment strategies with fewer side effects. Indeed, there is a significant and unmet need for safe and effective therapies for MS that are well-tolerated and target the cause of disease to reduce duration and frequency of therapy and to limit side-effects. A better alternative to systemic treatment of inflammation with generalized immunosuppressants would be specific therapies that target only the detrimental and aberrant immune response against the specific disease-associated antigen(s) involved. This approach is known as antigen-specific therapy. While the antigen-specific activation of pathogenic T-cells is considered essential in the initiation and maintenance of MS, leveraging the body's attempt to prevent autoimmunity, i.e. tolerization, focuses on the underlying cause of the disease and could be the key to solving neuro-inflammation.

Finally, the identification of expanded autoreactive TCRs may allow administration of TCR-specific inhibitors in both acute and chronic autoimmune disease, or eventually a new paradigm of targeted T-cell depletion for these disorders.

5. Financial report

As foreseen, GSKE project support has been assigned for consumable costs dedicated to this project. The support of the Prize Viscountess Valine de Spoelberch has been used to attract new staff, thereby ensuring continuity of the research group, and consumable costs. The UA and KU Leuven Financial Departments will provide a detailed report.

The Covid-19 pandemic has resulted in continuing restrictions on the number of researchers that are allowed to work in the lab at the same time throughout most of 2020-2021. Ongoing restrictions and stock breaches at - mainly plastics - suppliers further impacted the wet-lab work. Hence, we have had to alter the project time-planning and moved bio-informatics work to earlier in the project. Our universities provided the necessary structure to efficiently carry out bio-informatics work remotely (remote network access, high-throughput computing cluster, ...). Hence, despite the pandemic, we have been able to make substantial progress towards completion of this three-year project.

6. Publications under GSKE support 2020-2021

* indicates shared first/senior authors and @ indicates corresponding author

- Janssens I@, Campillo-Davo D, Van den Bos J, De Reu H, Berneman ZN, Wens I, Cools N (2022) Engineering of regulatory T cells by means of mRNA electroporation in a GMP-compliant manner. *Cytotherapy*; accepted for publication. [IF 5.414](#)
- Liston A*, Humblet-Baron*, S, Duffy D*, Goris A*@ (2021) Human immune diversity: from evolution to modernity. *Nat Immunol.*; 22:1479-1489. [IF 25.606](#)
- Van Horebeek L, Goris A@ (2020) Transcript-specific regulation in T-cells in multiple sclerosis susceptibility. (Invited Comment) *Eur J Hum Genet*; 28:849-850. [IF 3.65](#)
- Janssens I@, Cools N (2020) Regulating the regulators: Is introduction of an antigen-specific approach in regulatory T cells the next step to treat autoimmunity? *Cell Immunol*; 358:104236. [IF 4.078](#)

7. Team publications 2020-2021

* indicates shared first/senior authors and @ indicates corresponding author

- Derdelinckx J, Cras P, Berneman ZN, Cools N (2021) Antigen-Specific Treatment Modalities in MS: The Past, the Present, and the Future. *Front Immunol*; 12:624685. [IF 7.561](#)
- Willekens B, Wens I, Wouters K, Cras P, Cools N (2021) Safety and immunological proof-of-concept following treatment with tolerance-inducing cell products in patients with autoimmune diseases or receiving organ transplantation: A systematic review and meta-analysis of clinical trials. *Autoimmun Rev*; 20(8):102873. [IF 9.754](#)
- Wens I, Janssens I, Derdelinckx J, Meena M, Willekens B, Cools N (2021) Made to Measure: Patient-Tailored Treatment of Multiple Sclerosis Using Cell-Based Therapies. *Int J Mol Sci*; 22(14):7536. [IF 4.183](#)
- Derdelinckx J, Reynders T, Wens I, Cools N, Willekens B (2021) Cells to the Rescue: Emerging Cell-Based Treatment Approaches for NMOSD and MOGAD. *Int J Mol Sci*; 22(15):7925. [IF 4.183](#)
- Meena M, Van Delen M, De Laere M, Sterkens A, Costas Romero C, Berneman Z, Cools N (2021) Transmigration across a Steady-State Blood-Brain Barrie Induces Activation of Circulating Dendritic Cells Partly Mediated by Actin Cytoskeletal Reorganization. *Membranes (Basel)*; 11(9):700. [IF 4.106](#)
- Withanage K, De Coster I, Cools N, Viviani S, Tourneur J, Chevandier M, Lambiel M, Willems P, Le Vert A, Nicolas F, Van Damme P (2021) Phase 1 randomized, placebo-controlled, dose-escalating study to evaluate OVX836, a nucleoprotein- based influenza vaccine: intramuscular results. *J Infect Dis*; jjab532. [IF 5.226](#)
- Orije MRP, García-Fogeda I, Van Dyck W, Corbière V, Mascart F, Mahieu L, Hens N, Van Damme P, Cools N, Ogunjimi B, Maertens K, Leuridan E (2021) Impact of maternal pertussis antibodies on the infants' cellular immune responses. *Clin Infect Dis*; ciab972. [IF 9.079](#)
- Liston A*, Humblet-Baron*, S, Duffy D*, Goris A*@ (2021) Human immune diversity: from evolution to modernity. *Nat Immunol*; 22:1479-1489. [IF 25.606](#)
- Smets I, Dubois B, Goris A@ (2021) Treatment-Induced BAFF Expression and B Cell Biology in Multiple Sclerosis. *Front Immunol*; 12:676619. [IF 7.561](#)
- Vandebergh M, Dubois B, Goris A@. Genetic Variation in WNT9B Increases Relapse Hazard in Multiple Sclerosis. *Ann Neurol*; 89:884-894. [IF 10.422](#)
- Smets, I*, Goris, A*, Vandebergh, M., Demeestere, J., Sunaert, S., Dupont, P., Dubois, B. (2021). Quantitative MRI phenotypes capture biological heterogeneity in multiple sclerosis patients. *Sci Rep*; 11:1573. [IF 3.998](#)
- Vandebergh, M., Goris, A@ (2020). Smoking and multiple sclerosis risk: a Mendelian randomization study. *J Neurol*; 267:3083-3091. [IF 3.783](#)
- Oldoni, E, Smets, I, Mallants, K, Vandebergh, M, Van Horebeek, L, Poesen, K, Dupont, P, Dubois, B*, Goris, A*@ (2020). CHIT1 at Diagnosis Reflects Long-Term Multiple Sclerosis Disease Activity. *Ann Neurol*; 87:633-645. [IF 9.037](#)
- Van Horebeek L, Goris A@ (2020) Transcript-specific regulation in T-cells in multiple sclerosis susceptibility. (Invited Comment) *Eur J Hum Genet*; 28:849-850. [IF 3.65](#)
- Derdelinckx J@, Nkansah I, Ooms N, Van Bruggen L, Emonds MP, Daniëls L, Reynders T, Willekens B, Cras P, Berneman ZN, Cools N (2020) HLA Class II Genotype Does Not Affect the Myelin Responsiveness of Multiple Sclerosis Patients. *Cells*; 9: 2703. [IF 4.829](#)
- Janssens I@, Cools N (2020) Regulating the regulators: Is introduction of an antigen-specific approach in regulatory T cells the next step to treat autoimmunity? *Cell Immunol*; 358:104236. [IF 4.078](#)

- Joossen C, Baán A, Moreno-Cinos C, Joossens J, [Cools N](#), Lanckacker E, Moons L, Lemmens K, Lambeir AM, Fransen E, Delputte P, Caljon G, Van Der Veken P, Maes L, De Meester I, Kiekens F, Augustyns K, Cos P@. (2020) A novel serine protease inhibitor as potential treatment for dry eye syndrome and ocular inflammation. *Sci Rep*; 10: 17268. [IF 3.998](#)
- Maes E, [Cools N](#), Willems H, Baggerman G@. (2020) FACS-Based Proteomics Enables Profiling of Proteins in Rare Cell Populations. *Int J Mol Sci*; 21: 6557. [IF 4.556](#)

8. References

1. Dendrou, C. A., Fugger, L. & Friese, M. A. Immunopathology of multiple sclerosis. *Nat Rev Immunol* **15**, 545-558 (2015).
2. Moutsianas, L. *et al.* Class II HLA interactions modulate genetic risk for multiple sclerosis. *Nat Genet* **47**, 1107-1113 (2015).
3. Goris, A. & Liston, A. The immunogenetic architecture of autoimmune disease. *Cold Spring Harb Perspect Biol* **4**, a007260 (2012).
4. The International Multiple Sclerosis Genetics Consortium & The Wellcome Trust Case Control Consortium 2. Genetic risk and a primary role for cell-mediated immune mechanisms in multiple sclerosis. *Nature* **476**, 214-219 (2011).
5. The International Multiple Sclerosis Genetics Consortium. Analysis of immune-related loci identifies 48 new susceptibility variants for multiple sclerosis. *Nat Genet* **45**, 1353-1360 (2013).
6. The International Multiple Sclerosis Genetics Consortium. Low-Frequency and Rare-Coding Variation Contributes to Multiple Sclerosis Risk. *Cell* **175**, 1679-1687.e1677 (2018).
7. The International Multiple Sclerosis Genetics Consortium. Multiple sclerosis genomic map implicates peripheral immune cells and microglia in susceptibility. *Science* **365**, eaav7188 (2019).
8. The International Multiple Sclerosis Genetics Consortium. A systems biology approach uncovers cell-specific gene regulatory effects of genetic associations in multiple sclerosis. *Nat. Commun.* **10**, 2236 (2019).
9. Smets, I. *et al.* Multiple sclerosis risk variants alter expression of co-stimulatory genes in B cells. *Brain* **141**, 786-796 (2018).
10. Dooley, J. *et al.* Immunological profiles of multiple sclerosis treatments reveal shared early B cell alterations *Neurol Neuroimmunol Neuroinflamm* **3**, e240 (2016).
11. Lagou, V. *et al.* Genetic Architecture of Adaptive Immune System Identifies Key Immune Regulators. *Cell Rep* **25**, 798-810 e796 (2018).
12. Smets, I. *et al.* Quantitative MRI phenotypes capture biological heterogeneity in multiple sclerosis patients. *Sci Rep* **11**, 1573 (2021).
13. Kerlero de Rosbo, N. *et al.* Predominance of the autoimmune response to myelin oligodendrocyte glycoprotein (MOG) in multiple sclerosis: reactivity to the extracellular domain of MOG is directed against three main regions. *Eur J Immunol* **27**, 3059-3069 (1997).
14. Hellings, N. *et al.* T-cell reactivity to multiple myelin antigens in multiple sclerosis patients and healthy controls. *J. Neurosci. Res.* **63**, 290-302 (2001).
15. Wallstrom, E. *et al.* Increased reactivity to myelin oligodendrocyte glycoprotein peptides and epitope mapping in HLA DR2(15)+ multiple sclerosis. *Eur J Immunol* **28**, 3329-3335 (1998).
16. Jingwu, Z. *et al.* Myelin basic protein-specific T lymphocytes in multiple sclerosis and controls: precursor frequency, fine specificity, and cytotoxicity. *Ann Neurol* **32**, 330-338 (1992).
17. Battistini, L. *et al.* CD8+ T cells from patients with acute multiple sclerosis display selective increase of adhesiveness in brain venules: a critical role for P-selectin glycoprotein ligand-1. *Blood* **101**, 4775-4782 (2003).
18. Ifergan, I. *et al.* Central nervous system recruitment of effector memory CD8+ T lymphocytes during neuroinflammation is dependent on alpha4 integrin. *Brain* **134**, 3560-3577 (2011).
19. Bieganowska, K. D. *et al.* Direct ex vivo analysis of activated, Fas-sensitive autoreactive T cells in human autoimmune disease. *J Exp Med* **185**, 1585-1594 (1997).
20. Sethna, Z., Elhanati, Y., Callan, C. G., Walczak, A. M. & Mora, T. OLGA: fast computation of generation probabilities of B- and T-cell receptor amino acid sequences and motifs. *Bioinformatics* **35**, 2974-2981 (2019).
21. Marcou, Q., Mora, T. & Walczak, A. M. High-throughput immune repertoire analysis with IGoR. *Nature communications* **9**, 561 (2018).
22. Dang, T. H., Van Leemput, K., Verschoren, A. & Laukens, K. Prediction of kinase-specific phosphorylation sites using conditional random fields. *Bioinformatics* **24**, 2857-2864 (2008).

23. Meysman, P. *et al.* Use of structural DNA properties for the prediction of transcription-factor binding sites in *Escherichia coli*. *Nucleic Acids Res* **39**, e6 (2011).
24. Meysman, P. *et al.* Varicella-zoster virus-derived major histocompatibility complex class I-restricted peptide affinity is a determining factor in the HLA risk profile for the development of postherpetic neuralgia. *J Virol* **89**, 962-969 (2015).
25. Emerson, R. O. *et al.* Immunosequencing identifies signatures of cytomegalovirus exposure history and HLA-mediated effects on the T cell repertoire. *Nat Genet* **49**, 659-665 (2017).
26. Zamvil, S. S. *et al.* T-cell epitope of the autoantigen myelin basic protein that induces encephalomyelitis. *Nature* **324**, 258-260 (1986).
27. Kondo, T. *et al.* TCR repertoire to proteolipid protein (PLP) in multiple sclerosis (MS): homologies between PLP-specific T cells and MS-associated T cells in TCR junctional sequences. *Int Immunol* **8**, 123-130 (1996).
28. Haas, J. *et al.* Reduced suppressive effect of CD4⁺CD25^{high} regulatory T cells on the T cell immune response against myelin oligodendrocyte glycoprotein in patients with multiple sclerosis. *Eur J Immunol* **35**, 3343-3352 (2005).
29. Van der Aa, A. *et al.* T cell vaccination in multiple sclerosis patients with autologous CSF-derived activated T cells: results from a pilot study. *Clin Exp Immunol* **131**, 155-168 (2003).
30. Bielekova, B. *et al.* Expansion and functional relevance of high-avidity myelin-specific CD4⁺ T cells in multiple sclerosis. *J Immunol* **172**, 3893-3904 (2004).
31. Grau-Lopez, L. *et al.* Specific T-cell proliferation to myelin peptides in relapsing-remitting multiple sclerosis. *Eur J Neurol* **18**, 1101-1104 (2011).
32. Zheng, G. X. *et al.* Massively parallel digital transcriptional profiling of single cells. *Nature communications* **8**, 14049 (2017).
33. Thompson, A. J. *et al.* Diagnosis of multiple sclerosis: 2017 revisions of the McDonald criteria. *Lancet Neurol* **17**, 162-173 (2018).
34. Zemmour, D. *et al.* Single-cell gene expression reveals a landscape of regulatory T cell phenotypes shaped by the TCR. *Nat Immunol* **19**, 291-301 (2018).
35. Azizi, E. *et al.* Single-Cell Map of Diverse Immune Phenotypes in the Breast Tumor Microenvironment. *Cell* **174**, 1293-1308 e1236 (2018).
36. Li, H. *et al.* Dysfunctional CD8 T Cells Form a Proliferative, Dynamically Regulated Compartment within Human Melanoma. *Cell* **176**, 775-789 e718 (2019).
37. Muraro, P. A. *et al.* T cell repertoire following autologous stem cell transplantation for multiple sclerosis. *J Clin Invest* **124**, 1168-1172 (2014).
38. Pappalardo, J. L. *et al.* Transcriptomic and clonal characterization of T cells in the human central nervous system. *Sci Immunol* **5** (2020).
39. Ramesh, A. *et al.* A pathogenic and clonally expanded B cell transcriptome in active multiple sclerosis. *Proc Natl Acad Sci U S A* **117**, 22932-22943 (2020).
40. Schafflick, D. *et al.* Integrated single cell analysis of blood and cerebrospinal fluid leukocytes in multiple sclerosis. *Nat. Commun.* **11**, 247 (2020).



Geneeskundige Stichting Koningin Elisabeth
Fondation Médicale Reine Elisabeth
Königin-Elisabeth-Stiftung für Medizin
Queen Elisabeth Medical Foundation

Progress report of the
interuniversity research project of

Prof. dr. Pascal Kienlen-Campard (UCLouvain)

Prof. dr. Loïc Quinton (ULg)

Prof. dr. Jan Gettemans (UGent)

Partners of the network

UCLouvain :

Prof. dr. Pascal Kienlen-Campard (PI, spokesperson) – partner 1 (P1)

Institute of Neuroscience

IONS-CEMO, Avenue Mounier 53 bte B1.53.02

B-1200 Brussels

Prof. Bernard Hanseeuw, PhD and **Adrian Ivanoiu** (collaborators) – partner 2 (P2)

Cliniques St Luc, UCLouvain

IoNS- NEUR

ULiège

Prof. dr. Loïc Quinton (PI) – partner 3 (P3)

MS-LAB, UR MolSys

Allée du six Aout 11 - Quartier Agora - Liège Université

B4000 -Liège 1

Ghent University

Prof. dr. Jan Gettemans – partner 4 (P4)

Department of Biomolecular Medicine

Faculty of Medicine & Health Sciences

Campus Ardoyen

Technology Lane 75

B-9052 Ghent

New analytical tools to identify and target pathogenic hexameric A β assemblies in Alzheimer's disease

1. Context

With an estimated 47 million people affected worldwide, dementia is recognized as the 5th leading cause of death (<http://www.who.int>). This number is expected to double within the next 20 years as age is identified as being the biggest risk factor of disease. Alzheimer's disease (AD) is the most common form of dementia and accounts for over 60 per cent of diagnoses, with more than 150.000 cases in Belgium.

A major obstacle in developing a treatment for AD has been the lack of reliable diagnostic markers and straightforward target to block the disease onset and progression. It is therefore imperative to (i) develop a reliable and easy-to-use diagnostic (ii) identify efficient therapeutic targets to treat AD. Several clinical trials have focused on targeting either A β production or its accumulation, an early event in AD pathogenesis. The high potential interest to target pathologic A β forms has for instance been evaluated in passive immunotherapy trials. Unfortunately, they failed so far to improve cognitive function in subjects with mild or moderate AD¹. Indeed, these negative results could stem from two reasons: (i) possibly irrelevant A β targets; (ii) therapies targeting amyloid pathologies might be inefficient if administered in the late phases of the disease.

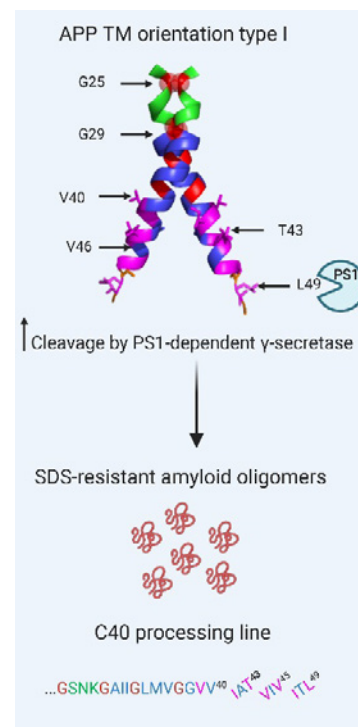
Recent studies including ours indicate that A β neurotoxicity is attributed to oligomers of A^{2,3}. Oligomers are intermediary species formed on the self-assembly pathway of A β from monomers to mature amyloid fibrils. With this in mind, we identify the following points as important research objectives:

1. A better identification of the pathologic A β forms to be targeted. Our work hypothesis is that toxicity is highly attributed to hexameric assemblies of A β found in cellular models.
2. Make available clinical samples to evaluate the relevance of A β oligomers (likely hexamers) we identified in cells to the human AD pathology, possibly at very early stages.
3. The improvement and standardization of analytical approaches as reliable tools to measure A β oligomers, both in biological models and patient samples.
4. The development of a novel approach to efficiently target A β oligomers. We will develop an approach based on nanobodies, which appear much more promising than whole antibodies used so far. Their comparatively low molecular mass leads to a better permeability in tissues and allows them to bind to hidden epitopes that are not accessible to whole antibodies. In addition, they do not show complement system triggered cytotoxicity as they lack an Fc region.

2. Current progress in the different objectives

2.1. Identification of the pathogenic A β oligomers

As stated in the year 2020, with the support of the FMRE, we finalized a first project aimed at identifying the molecular conformations of the Amyloid precursor protein (APP) triggering the production of pathological A β assemblies. We demonstrated that dimeric orientations of amyloidogenic APP C-terminal fragments (C99) regulate the precise cleavage by γ -secretase that releases A. We found that one precise orientation of C99 favored processing to A_{43/40} forms, promoting formation of SDS oligomers, reminiscent of A β peptide oligomers. (See Figure on the right, from Perrin et al., 2020). This work has been published in *iScience*, December 2020 (Perrin et al., 2020). An erratum is associated to clarify the display and calculation in a figure ⁴. **This work involved P1.**



We further investigated the nature and the properties of A β assemblies that we identified in cellular models. The misfolding of A β leads to subsequent amyloid fibril formation by nucleated polymerization. This requires an initial and critical nucleus for self-assembly. We identified and characterized the composition and self-assembly properties of cell-derived hexameric A₄₂ and showed its assembly enhancing properties which are dependent on the A β monomer availability. Identification of nucleating assemblies that contribute to self-assembly in this way may serve as therapeutic targets to prevent the formation of toxic oligomers. **This work involved P1 and P3 and has been published in 2021⁵.** We isolated these hexameric A β assemblies from a cellular model and assessed its effect on primary neuron viability *in vitro*, and its contribution to amyloid deposition *in vivo*. In 5xFAD mice, where human A β species are pre-existing, the hippocampal injection of cell-derived A β hexamers aggravated A β deposition, in agreement with its previously described nucleation properties. Finally, by editing human cell lines, we investigated the respective contribution of Presenilin 1 (PS1) and 2 (PS2)-dependent γ -secretases, which are responsible for the release of monomeric A, to this process. We found experimental evidence suggesting a direct link between PS2-dependent activity and the release of hexameric A β in extracellular vesicles. **This work involved P1, P2 and P3 and has been published in 2021⁶.**

2.2. Patient cohort and clinical samples workflow

P1 together with P2 built up a cohort of around 200 individuals. All patients with clinical symptoms have been genotyped for ApoE4.

2.3. Standardization of analytical approaches

The plasma samples from the UCLouvain/St Luc Hospital cohort is currently formed by AD patients (N=20), age-matched controls (N around 160), non-inflammatory neurological disease (NIND) with dementia (N=16) and non-demented NIND (N=16).

The workflow has been set up to isolate blood exosomes and particularly Neurally-derived blood exosomes (NDBEs) from plasma samples. Standard AD biomarkers are currently evaluated for each patient sample (A β _{42:40} ratio, cognitive assays and amyloid PET imaging when possible). Biomarkers are measured in blood samples through the newly acquired (2021) ultra-sensitive SIMOA[®] immunoassay technology by using multiplex assays. Our next aim (2022) is to establish

the profile of standard AD biomarkers in blood samples (controls and patients). The content of NDBEs is currently under analysis. We expect A β oligomers (hexamers) to be enriched in these fractions. Our aim is to establish to check whether A β hexamers are present in CSF, in case to concentrate them for further analysis by mass spectrometry (**P3**) the A β isoforms composing them. A correlation with other amyloid biomarkers will be estimated (**P2**). This work is mainly conducted by a PhD student (Emilien Boyer, MD. **P1** supervisor, **P2** co-supervisor). He also plans to evaluate the ability of some nanobodies (**P4**) to detect oligomeric A β in biological models (cell lines); in order to test them eventually in human samples.

2.4. Development of nanobodies targeting A β hexamers and other AD related targets.

The team at Ghent university (**P4**) obtained single domain antibodies (nanobodies) against serum amyloid P component or SAP from human or murine origin. SAP interacts with amyloid fibrils and strengthens them. **P4** is keen to understand which proteins interact with SAP and towards this end anti-human SAP nanobodies were derivatized with a C-terminal azido-Phe residue that allows oriented coupling onto alkyne-activated magnetic beads. The beads were used for SAP immunoprecipitation from human plasma and a SAP interactome map has been set up using mass spectrometry together with **P3**. In anticipation of A β hexamers for immunization and nanobody generation, we are developing nanobodies against ApoE4. Two *apoE4* alleles constitute a high risk for developing late onset AD. The protein differs by only one amino acid from its two close isoforms, ApoE3 and ApoE2, but it has a distinct tertiary structure. ApoE4-specific nanobodies could be instrumental in development of a diagnostic test or to understand more about the damaging intracellular effects of this protein. After a first immunization we generated a VHH library and panned this library with ApoE4. The resulting nanobodies were cross-reactive with human ApoE3, but do not cross-react with mouse ApoE. More recently we immunized two animals with a peptide from ApoE4 that was previously used for obtaining ApoE4 conventional antibodies and we aim to identify unique E4 nanobodies from the VHH libraries. Such nanobodies could also be used by **P2**. In addition we have generated nanobodies against RgpA, a bacterial protease believed to be tightly associated with AD, and these are currently being characterized.

3. Dissemination

The restrictions related to the COVID pandemic have again prevented the organization of research meeting/symposia on the topic in 2021 but the network organized remote meetings (Teams) to ensure the exchange of materials and the monitoring of information necessary for the progress of the project.

4. Reference List

1. Salloway S, Sperling R, Fox NC, et al. Two phase 3 trials of bapineuzumab in mild-to-moderate Alzheimer's disease. *N Engl J Med* 2014; **370**(4): 322-33.
2. Decock M, Stanga S, Octave JN, et al. Glycines from the APP GXXXG/GXXXA Transmembrane Motifs Promote Formation of Pathogenic Abeta Oligomers in Cells. *Front Aging Neurosci* 2016; **8**: 107.
3. Marshall KE, Vadukul DM, Dahal L, et al. A critical role for the self-assembly of Amyloid-beta1-42 in neurodegeneration. *Sci Rep* 2016; **6**: 30182.
4. Perrin F, Papadopoulos N, Suelves N, et al. Erratum: Dimeric Transmembrane Orientations of APP/C99 Regulate gamma-Secretase Processing Line Impacting Signaling and Oligomerization. *iScience* 2021; **24**(2): 102057.
5. Vadukul DM, Vrancx C, Burguet P, et al. An evaluation of the self-assembly enhancing properties of cell-derived hexameric amyloid-beta. *Sci Rep* 2021; **11**(1): 11570.
6. Vrancx C, Vadukul DM, Suelves N, et al. Mechanism of Cellular Formation and In Vivo Seeding Effects of Hexameric beta-Amyloid Assemblies. *Mol Neurobiol* 2021; **58**(12): 6647-69.

7. Work published in 2021 acknowledging FMRE

1. Perrin F, Papadopoulos N, Suelves N, et al. Erratum: Dimeric Transmembrane Orientations of APP/C99 Regulate gamma-Secretase Processing Line Impacting Signaling and Oligomerization. *iScience* 2021; 24(2): 102057. (IF 5.08)
2. Vadukul DM, Vrancx C, Burguet P, et al. An evaluation of the self-assembly enhancing properties of cell-derived hexameric amyloid-beta. *Sci Rep* 2021; 11(1): 11570. (IF 4.13)
3. Vrancx C, Vadukul DM, Suelves N, et al. Mechanism of Cellular Formation and In Vivo Seeding Effects of Hexameric beta-Amyloid Assemblies. *Mol Neurobiol* 2021; 58(12): 6647-69. (IF 4.95)
4. Kreis A, Desloovere J, Suelves N, et al. Overexpression of wild-type human amyloid precursor protein alters GABAergic transmission. *Sci Rep* 2021; 11(1): 17600 (IF 4.13)
5. Gettemans J. Site-Specific Fluorescent Labeling, Single-Step Immunocytochemistry and Delivery of Nanobodies into Living Cells. *Method in Molecular Biology* vol 2246. *In press*.



Geneeskundige Stichting Koningin Elisabeth
Fondation Médicale Reine Elisabeth
Königin-Elisabeth-Stiftung für Medizin
Queen Elisabeth Medical Foundation

Universitaire onderzoeksprojecten
2020-2022 gefinancierd door de G.S.K.E.

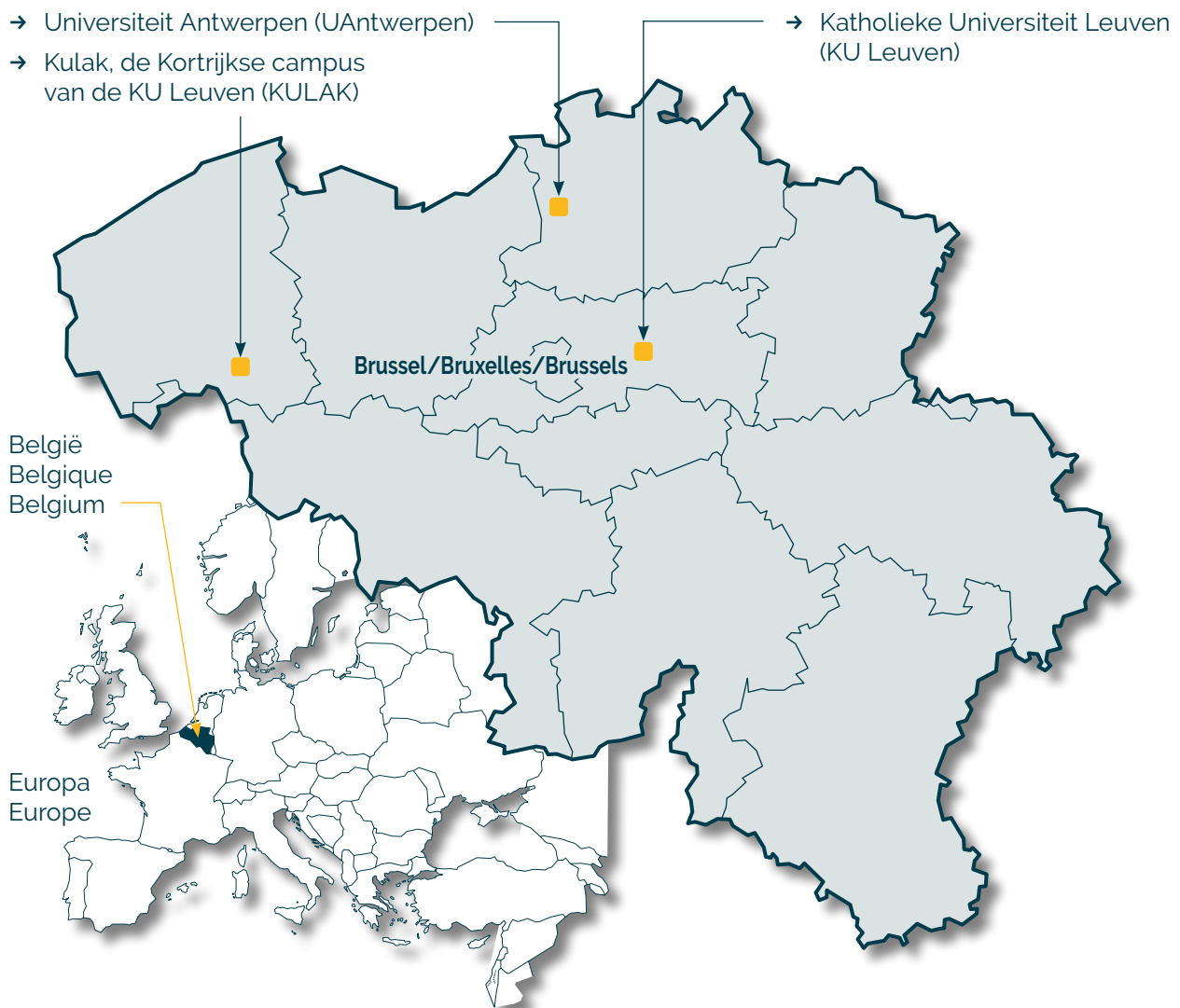
Projets de recherche universitaire
2020-2022 subventionnés par la F.M.R.E.

University research projects
2020-2022 funded by the Q.E.M.F.

Universiteiten met onderzoeksprogramma's die gesteund worden door de G.S.K.E.

Universités ayant des programmes de recherche subventionnés par la F.M.R.E.

Universities having research programs supported by the Q.E.M.F.



Universitaire onderzoeksprojecten 2020-2022 gefinancierd door de G.S.K.E.

Projets de recherche universitaire 2020-2022 subventionnés par la F.M.R.E.

University research projects 2020-2022 funded by the Q.E.M.F.

UAntwerpen



Prof. dr. Sarah Weckhuysen, MD, PhD

Study and targeted treatment development for epileptic encephalopathies using 2D and 3D human induced pluripotent stem cell-derived neuronal cultures

KU Leuven



Prof. Pierre Vanderhaeghen, MD, PhD (VIB)

Deciphering the mechanisms underlying intellectual deficiency and autism spectrum disorders by cellular modelling in human neurons in vivo

Prof. dr. Lieve Moons & dr. Lies De Groef

Oligodendrocytes in Wolfram syndrome: bystanders or partners in crime?

Prof. dr. Thomas Voets (VIB)

Unraveling the cellular and molecular basis of noxious cold sensing

KULAK



Prof. dr. ir. Simon De Meyer

Unravelling the thrombo-inflammatory role of von Willebrand factor in neurodegeneration after ischemic stroke



Geneeskundige Stichting Koningin Elisabeth
Fondation Médicale Reine Elisabeth
Königin-Elisabeth-Stiftung für Medizin
Queen Elisabeth Medical Foundation

Progress report of the
university research project of

Prof. dr. ir. Simon De Meyer
Kulak, de Kortrijkse campus van de
KU Leuven (KULAK)

Prof. dr. ir. Simon De Meyer

Professor, Dept. of Cardiovascular Sciences

Laboratory for Thrombosis Research

KU Leuven Campus Kulak Kortrijk

E. Sabbelaan 53

8500 Kortrijk

Belgium

Tel: +32 56 246232

simon.demeyer@kuleuven.be

www.kuleuven-kulak.be/irf/thrombosis

Unravelling the thrombo-inflammatory role of von Willebrand factor in neurodegeneration after ischemic stroke

1. Summary of the project

Ischemic stroke is one of the leading causes of death and sustained disability worldwide. Blockade of blood flow to the brain by an occlusive thrombus leads to irreversible damage of the associated brain tissue. The enormous clinical, economic and social burden of ischemic stroke is in strong contrast with the limited treatment options that are currently available. In acute ischemic stroke, the mainstay of acute treatment is rapid recanalization of the occluded blood vessel, either via pharmacological thrombolysis or via mechanical thrombectomy.

In recent years, it has become clear that rapid recanalization of the occluded blood vessel is not sufficient to fully salvage the threatened brain tissue. Novel insights show that cerebral ischemia and subsequent reperfusion elicit a thrombo-inflammatory cascade that promotes progressive brain damage in stroke patients.¹ This problem does not only occur after successful thrombolysis but also often complicates stroke outcome after successful mechanical thrombectomy.² This so-called ischemia/reperfusion injury (I/R injury) is a complex process that interrelates thrombosis with inflammation, leading to several pathophysiological effects in the neuro-vascular unit. The exact mechanisms of how cerebral I/R injury accelerates neurodegeneration are still poorly understood. Yet, such insights will be crucial to develop effective strategies to promote neuroprotection in stroke management. One of our major findings in the last decade is our discovery that von Willebrand factor (VWF) plays a crucial role in cerebral I/R injury.^{1,3-6} VWF is a large multimeric plasma glycoprotein that recruits platelets at sites of vascular injury and that promotes both thrombosis and inflammation. Remarkably, we found that initial VWF-mediated platelet adhesion rather than subsequent platelet aggregation contributes to cerebral I/R injury with a prominent role for the interaction between the VWF A1 domain and platelet glycoprotein (GP)Ib.^{4,6-8} At present we do not know exactly how VWF contributes to thrombo-inflammation in the (post-)ischemic brain. Our hypothesis is that VWF, after release by activated (hypoxic) endothelial cells recruits and activates both platelets and leukocytes, leading to obstruction of the microvasculature and local inflammation.

The general objective of this research project was to elucidate the mechanisms by which VWF mediates cerebral I/R injury in ischemic stroke. More specifically, we are aiming at (i) unravelling the inflammatory component of VWF-mediated I/R injury and (ii) at visualizing the molecular and cellular interactions of VWF-mediated thrombo-inflammation in the brain via advanced 3D microscopy.

In order to successfully complete this project, two delineated work packages (WP) were defined:

- WP1: Elucidating the inflammatory component of VWF in cerebral I/R injury
- WP2: Advanced 3D microscopy to map VWF-mediated thrombo-inflammation in the brain

The 2-year progress for each work package is detailed, as well as the planned next steps for the following years.

1.1. WP 1: Elucidating the inflammatory component of VWF in cerebral I/R injury

OBSERVATION 1: VWF-deficiency reduces immune cell recruitment to the brain after ischemic stroke

To examine the cerebral immune cell response mediated by VWF, we performed flow cytometric analysis of single cell suspensions prepared from brain tissue isolated from WT and VWF KO mice subjected to stroke. After stroke, mice were perfused, their brains harvested and subsequently divided into ipsilateral (affected by stroke) and contralateral (unaffected) hemispheres. Interestingly, we observed significantly reduced cerebral infarcts in VWF KO mice, compared to WT mice ($p < 0.01$, Figure 1A). Twenty-four hours after stroke, the ipsilateral hemisphere showed an increased amount of infiltrated white blood cells (WBCs) compared to the contralateral hemisphere in both the WT ($p < 0.005$) and VWF KO mice ($p < 0.05$). However, averaged recruitment of WBC in the ipsilateral hemisphere of VWF KO mice was two-fold lower than in WT mice (5596 ± 1644 vs. 12435 ± 2083 , respectively; $p < 0.05$, Figure 1B). Both the amount of myeloid and lymphoid white blood cells was significantly reduced in the brains of VWF KO mice compared to WT mice ($p < 0.05$, Figure 1C-D).

OBSERVATION 2: VWF deficiency leads to reduced recruitment of inflammatory monocytes, neutrophils and T-cells

To better determine which inflammatory cells were potentially recruited by VWF to the affected brain tissue during stroke, we used two antibody cocktails that allowed discrimination and quantification of recruited inflammatory monocytes, neutrophils, T-cells and CD3^{neg} lymphocytes (B cells and NK cells) (Table 1).

As shown in figure 1E-H, all four subsets of immune cells were significantly increased in the ipsilateral brain of WT mice 24 hours after stroke, compared to the unaffected contralateral hemisphere. However, despite the presence of an infarct core in the affected ipsilateral hemisphere of VWF KO mice, the numbers of neutrophils and T-cells did not increase and remained similar to the baseline values of the contralateral hemisphere (Figure 1E and 1F). Hence, the absolute numbers of recruited neutrophils and T-cells was significantly higher in the ischemic brain of WT mice compared to VWF KO mice (2017 ± 733 vs 512 ± 203 , $p < 0.05$ and 974 ± 184 vs 244 ± 44 , $p < 0.01$ respectively). These results suggest an important role for VWF in recruiting both neutrophils and T-cells to the affected brain tissue during ischemic stroke.

A similar, yet less outspoken, trend was observed for inflammatory monocytes (Figure 1G). In VWF KO mice, the ischemic hemisphere contained significantly more inflammatory monocytes than the unaffected hemisphere, but this was still significantly lower than the number of inflammatory monocytes that were recruited in the ischemic brain of WT mice (2466 ± 955 vs 6760 ± 1414 ; $p < 0.05$).

No differences regarding CD3^{neg} lymphocytes were observed between WT and VWF KO mice as similar numbers were recruited in the ischemic hemisphere of both groups (1162 ± 245 vs 585 ± 188 respectively, $p > 0.05$, Figure 1H). Leukocyte blood counts and circulating platelet-leukocyte complexes were similar between VWF KO and VWF WT mice 24 hours after stroke (data not shown).

Table 1. Antibodies cocktails used to discriminate between different white blood cell subtypes.

	antigen	supplier
Antibody cocktail 1	CD45 APC-Cy7	Biologend
	CD11b PE-Cy7	eBioscience
	Ly6G BV510	Biologend
	Ly6C FITC	Biologend
	CD16/CD32 (Fc-block)	eBioscience
	Live/Death Fixable Violet Dead Cell Stain Kit	ThermoFisher
Antibody cocktail 2	CD45-APC-Cy7	Biologend
	CD11b PE-Cy7	eBioscience
	CD11c PerCp-Cy5	eBioscience
	CD3e FITC	eBioscience
	CD16/CD32 (Fc-block)	eBioscience
	Live/Death Fixable Violet Dead Cell Stain Kit	ThermoFisher

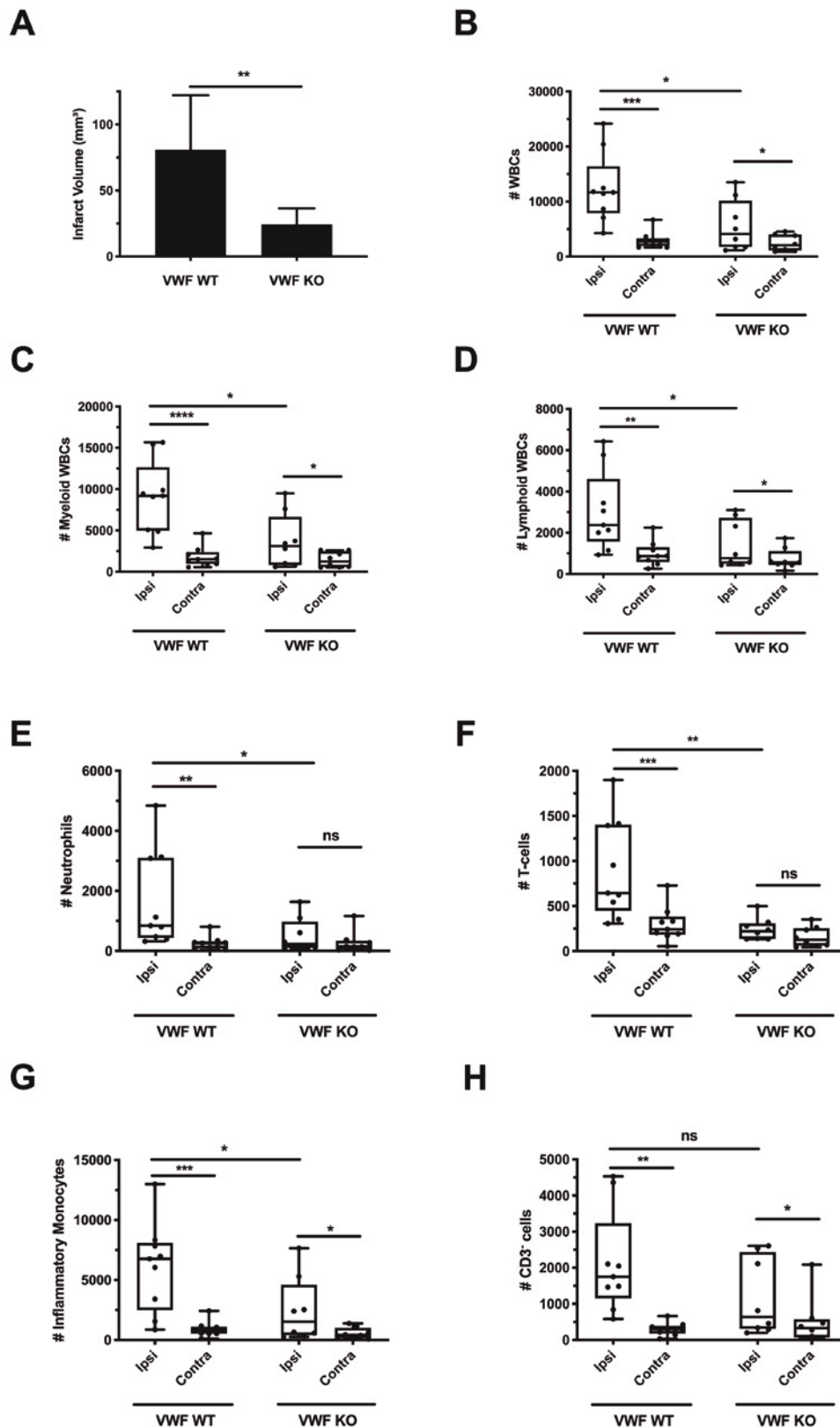


Figure 1 (see next page): VWF deficiency leads to a reduction of the number of monocytes, neutrophils and T-cells to the brain after acute ischemic stroke. Transient focal cerebral ischemia was induced by 60 minutes occlusion of the right middle cerebral artery (tMCAO), followed by 23 hours of reperfusion in WT and VWF KO mice, after which edema-corrected brain infarct volumes were quantified by planimetric analysis (A) and WBC recruitment to each hemisphere was determined by flow cytometry. Total amount of white blood cells (CD45^{high}) was analyzed (B) as well as the myeloid (CD45^{high}; CD11b⁺) (C) and lymphoid white blood cells (CD45^{high}; CD11b⁻; CD11c⁻) (D). More specifically: Neutrophils (CD45^{high}; CD11b⁺; Ly6G⁺) (E); T-cells (CD45^{high}; CD11b⁻; CD11c⁻; CD3e⁺) (F); Inflammatory Monocytes (CD45^{high}; CD11b⁺; Ly6G⁺; Ly6G⁻) (G); CD3^{neg} lymphocytes (CD45^{high}; CD11b⁻; CD11c⁻; CD3e⁻) (H) were quantified. Data are represented as box plots showing all data points and the median value, except for infarct size which is shown as mean \pm standard deviation. * $p < 0.05$; ** $p < 0.01$; *** $p < 0.005$; **** $p < 0.001$. (n = 8-9)

OBSERVATION 3: VWF-mediated thromboinflammation in the ischemic stroke brain via fluorescence microscopy

For visualization of VWF-mediated thromboinflammation, immunofluorescent staining of platelets and leukocytes was performed on brains obtained from VWF WT and KO mice 24 hours after stroke (Figures 2 and 3). In VWF KO mice, very few platelet accumulations were found within the ipsilateral brain (Figure 2A). In contrast, platelet/VWF-rich microthrombi were found frequently throughout the ipsilateral brain of VWF WT mice, underscoring the importance of VWF-mediated platelet adhesion in the ischemic stroke brain (Figure 2B-D). Platelet/VWF-rich microthrombi were absent in the contralateral hemisphere of both WT and VWF KO mice (data not shown).

Next, we visualized immune cell recruitment in VWF WT and KO mice. Since previous studies found no major role for monocytes, but an important detrimental role for both T-cells⁹ and neutrophils¹⁰ in the acute phase of ischemic stroke, we focused on visualizing neutrophils and T-cells in the stroke brain. To stain the vasculature in both VWF WT and KO mice, a sensitive lectin staining of the endothelium was performed (Figure 3). Using a specific histological marker for neutrophils (Ly6G), we observed that neutrophils were more frequently present within the ipsilateral side of the brain of VWF WT mice compared to VWF KO mice (Figure 3A-B). Since the smaller infarct sizes observed in VWF KO mice might bias neutrophil quantification by flow cytometry, we also quantified neutrophil recruitment in the ischemic infarct core in both VWF KO and WT mice by histology. Importantly, analysis of fixed areas of 1 mm² in the infarct core corroborated our flow cytometric data, arguing against a nonspecific effect related to smaller infarct sizes. Quantification of neutrophil recruitment to the infarct core revealed a two-fold reduction of neutrophil density in VWF KO brains compared to WT mice (Figure 3C). Intriguingly, neutrophils were frequently observed within the microcirculation (Figure 3A-B). To investigate this further, intra- and extravascular neutrophils were counted in brain sections of VWF WT mice. On average, 66 ± 4% of neutrophils were found within the vasculature of the ischemic hemisphere, while the remaining neutrophils were already extravasated (Figure 3D). A comparable observation was made when we stained for T-cells, which were also occasionally found within the microvasculature of VWF WT mice (Figure 3E). Due to the low number of T-cells within the ischemic brain, quantification of T-cells was not feasible. Lastly, T-cells were virtually absent in the ipsilateral brain hemisphere of VWF KO mice (Figure 3F), confirming our flow cytometric data.

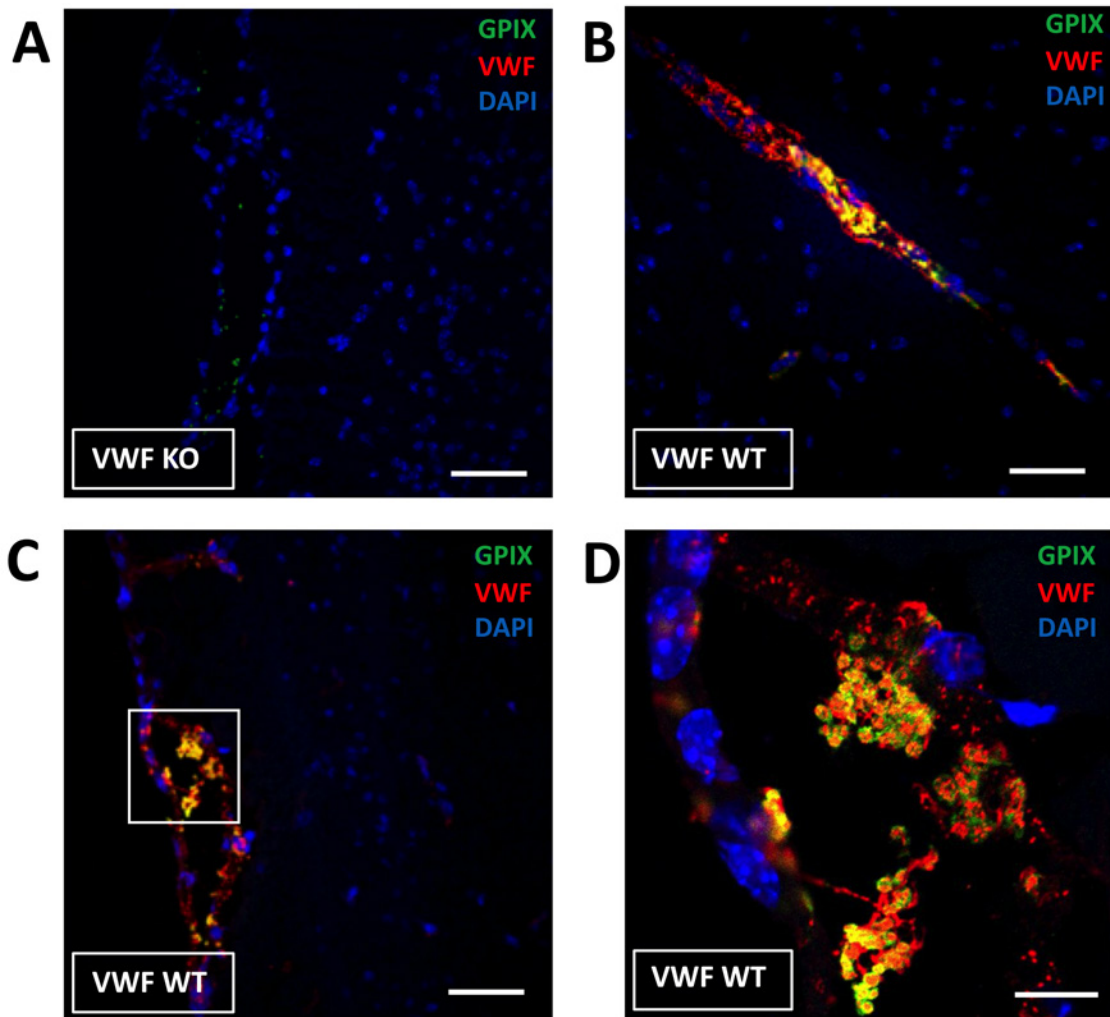


Figure 2: Immunofluorescent visualization of thromboinflammation in the ipsilateral hemisphere of mice 24 hours after ischemic stroke brain injury. Transient focal cerebral ischemia was induced by 60 minutes occlusion of the right middle cerebral artery (MCAO), followed by 23 hours of reperfusion in VWF WT or KO mice, after which, brain-sections were stained for VWF (red), platelets (green) and nuclei (blue). **A.** Only a few platelets are found within the ischemic brain of VWF KO mice. **B-D.** Clumps of VWF together with platelets were frequently found attached to the vessel wall within the ipsilateral hemisphere. Panel D is a magnification of the white box in panel C. Scale bars are 50 μ m except for panel D where the scale bar is 25 μ m. Images are representative for n = 3 per genotype.

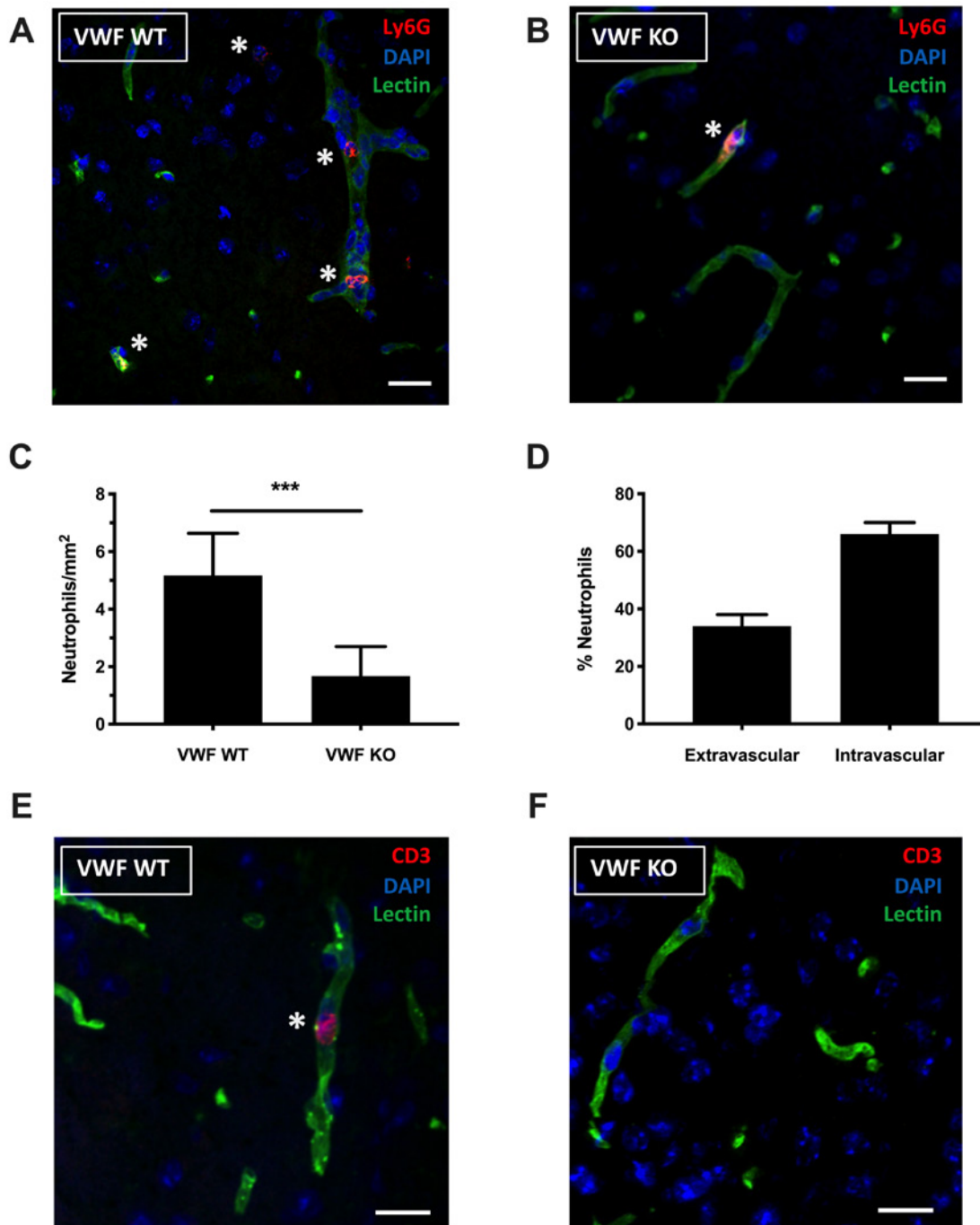


Figure 3: Immunofluorescent visualization of neutrophils and T-cells in the ipsilateral hemisphere of mice 24 hours after ischemic stroke brain injury. Transient focal cerebral ischemia was induced by 60 minutes occlusion of the right middle cerebral artery (tMCAO), followed by 23 hours of reperfusion in VWF WT and KO mice, after which, brain-sections were stained for blood vessels and neutrophils or T-cells. **A-B.** Neutrophils were stained with a marker for Ly6G (red) and blood vessels with a lectin staining (green). Neutrophils are marked with a *. **C.** Quantification of the number of neutrophils/mm² in the infarct core of WT and VWF KO mice. (n = 3) Data is represented as mean ± standard deviation. **D.** The number of neutrophils within and outside the vasculature (n = 3). Data is represented as mean ± standard deviation. **E and F.** T-cells were stained with a marker for CD3 (red) and blood vessels with a lectin staining (green). T-cells are marked with a *. Scale bars are 20µm. Images are representative for n = 3 per genotype.

OBSERVATION 4: Inhibition of the VWF A1 domain limits ischemic stroke brain injury

Given the central role of the VWF A1 domain in cerebral ischemia/reperfusion injury⁴, we next wanted to unravel its potential inflammatory contribution in ischemic stroke. To this end, we used a nanobody (KB-VWF-006bv) that specifically binds the VWF A1 domain, inhibiting its interaction with the platelet receptor GPIIb.¹¹ Intravenous treatment with 10mg/kg of the nanobody was started immediately after establishment of reperfusion. Mean residence time of the nanobody

is 3.5 hours and this allows blocking of the VWF-A1 domain during the acute reperfusion phase. As a control, a nonspecific nanobody (KB-VWF-004bv) was administered. Twenty-four hours after stroke, mice treated with the anti-VWF A1 nanobody KB-VWF-006bv had significantly less ischemic stroke brain damage compared to control-treated mice (Figure 4A and B). This translated in an improved motor score (Figure 4C) and neurological behavior (Figure 4D), although this difference was only statistically significant for the latter. Of note, no intracranial bleedings were observed in any of the mice treated with the VWF A1 nanobody. These data further corroborate the crucial involvement of the VWF-GPIIb axis in cerebral ischemia/reperfusion injury.^{6,7,12,13}

OBSERVATION 5: Inhibition of the VWF A1 domain reduces the recruitment of neutrophils, monocytes and T-cells

Targeting the VWF A1 domain also significantly reduced inflammatory cell recruitment to the ischemic brain (Figure 5). Indeed, similar to our results in VWF KO mice, flow cytometric analysis revealed that inhibition of VWF A1 also leads to a 2-fold reduction of immune cell recruitment in the brains of treated mice compared to control mice (7095 ± 2550 vs 16310 ± 3980 ; $p < 0.005$; Fig. 5A). Both myeloid (5195 ± 2259 vs 11978 ± 3322 ; $p < 0.05$; Fig. 5B) and lymphoid WBCs (1529 ± 269 vs 3017 ± 514 ; $p < 0.05$; Fig. 5C) were reduced in the ipsilateral hemispheres of VWF A1 nanobody treated mice. Specifically, inhibition of the VWF A1 domain reduced the amount of infiltrated inflammatory monocytes (3726 ± 1824 vs 8266 ± 2651 ; $p < 0.05$; Fig. 5D), neutrophils (304 ± 94 vs 1557 ± 317 ; $p < 0.0005$; Fig. 5E) and T-cells (487 ± 93 vs 1111 ± 248 ; $p < 0.05$; Fig. 5F) in the ipsilateral hemisphere of the brain, 24 hours after stroke. These data suggest that the inflammatory effect of VWF in ischemic stroke is mediated through the VWF A1 domain.

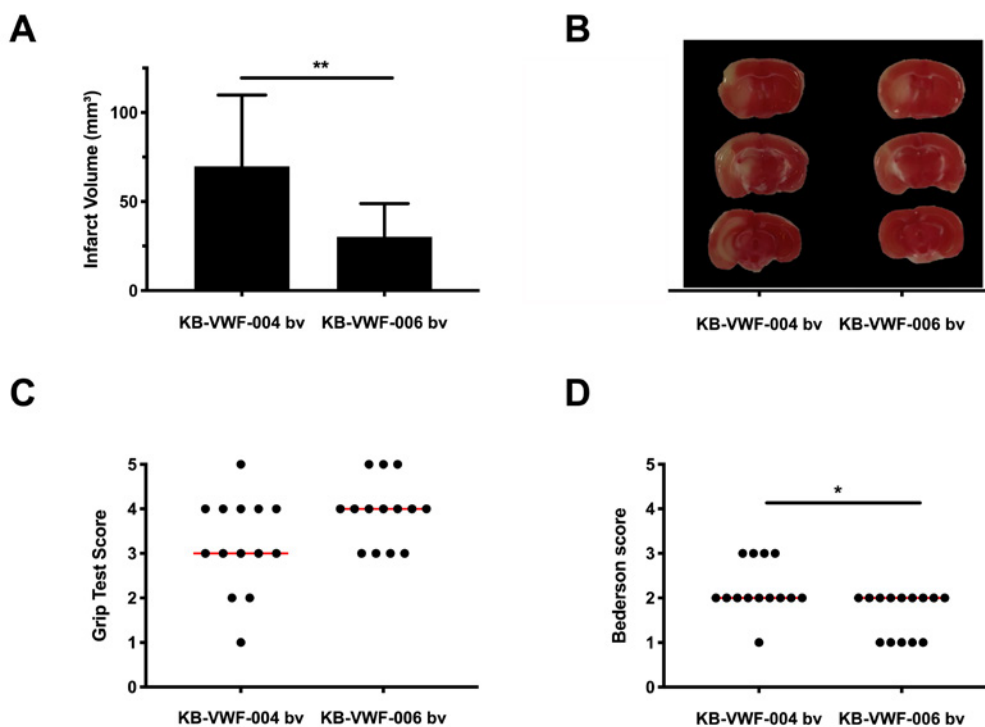


Figure 4: Inhibition of the VWF-A1 domain protects mice from acute ischemic stroke. Transient focal cerebral ischemia was induced by 60 minutes occlusion of the right middle cerebral artery (tMCAO), followed by 23 hours of reperfusion. Immediately at the start of reperfusion, mice were intravenously treated with 10 mg/kg of either control (KB-VWF-004 bv) or inhibitory anti-VWF A1 nanobody (KB-VWF-006 bv). **A.** Edema-corrected brain infarct volumes were quantified by planimetric analysis 24 hours after stroke. **B.** Representative TTC staining of 3 consecutive brain sections. **C.** Motor function was examined using the grip test. **D.** Neurological outcome 24 h after stroke was assessed using the Bederson test. Data are represented as scatter plots showing all data points and the median value, except for infarct size which is shown as mean \pm standard deviation. *, $p < 0.05$; **, $p < 0.01$. ($n = 10-11$)

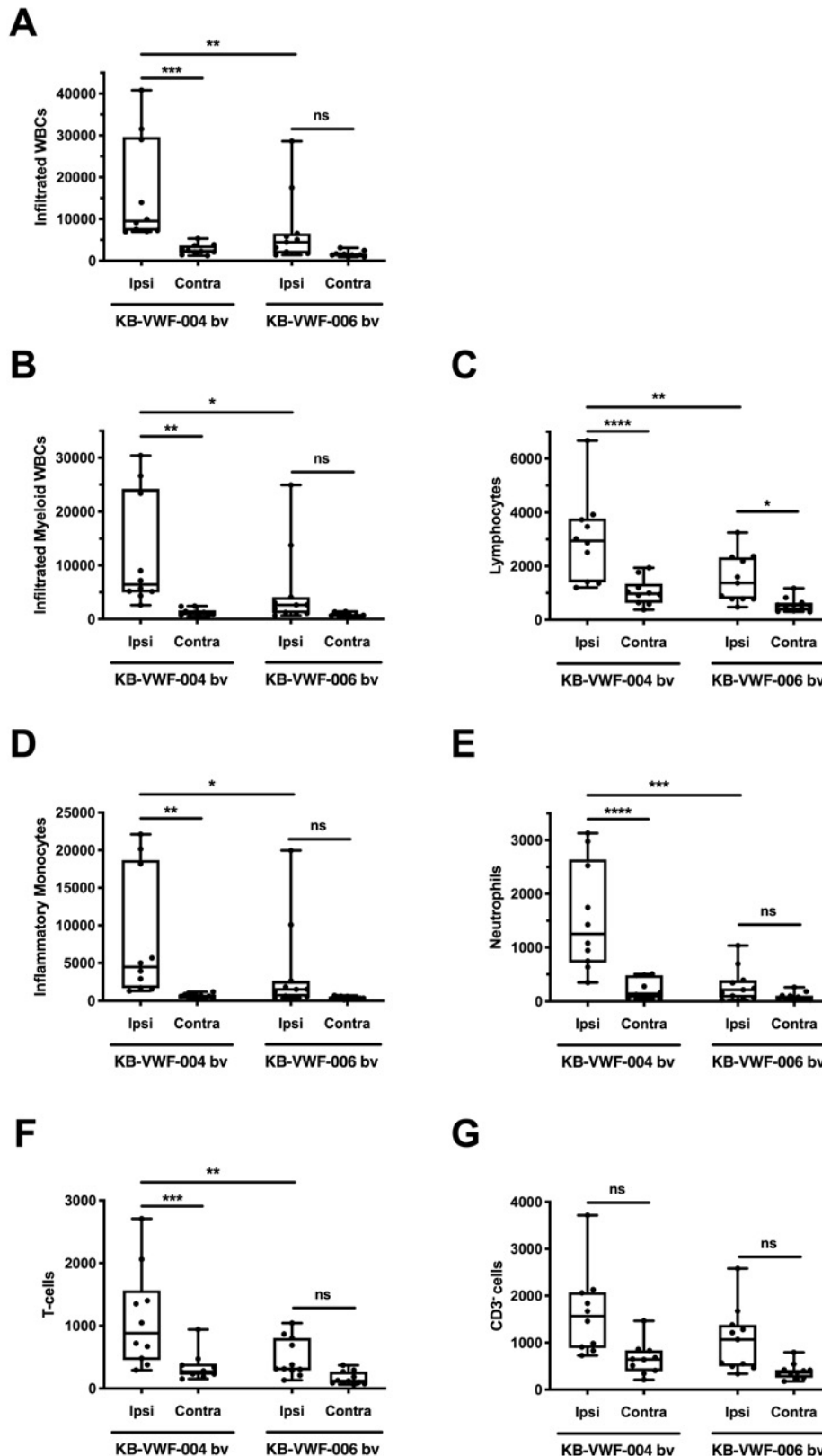


Figure 5: The VWF-A1 domain recruits monocytes, neutrophils and T-cells to the brain after acute ischemic stroke. Transient focal cerebral ischemia was induced by 60 minutes occlusion of the right middle cerebral artery (tMCAO), followed by 23 hours of reperfusion. Immediately at the start of reperfusion, mice were intravenously treated with 10 mg/kg of either control (KB-VWF-004 bv) or inhibitory anti-VWF A1 nanobody (KB-VWF-006 bv). Twenty-four hours after tMCAO, recruitment of specific subsets of WBC to each hemisphere was determined by flow cytometry. **A.** White blood cells (CD45^{high}). **B.** Myeloid white blood cells (CD45^{high}; CD11b⁺). **C.** Lymphoid white blood cells (CD45^{high}; CD11b⁺; CD11c⁺). **D.** Inflammatory Monocytes (CD45^{high}; CD11b⁺; Ly6C⁺; Ly6G⁺). **E.** Neutrophils (CD45^{high}; CD11b⁺; Ly6G⁺). **F.** T-cells (CD45^{high}; CD11b⁺; CD11c⁺; CD3e⁺). **G.** CD3^{neg} lymphocytes (CD45^{high}; CD11b⁺; CD11c⁺; CD3e⁻). * $p < 0.05$; ** $p < 0.01$; *** $p < 0.005$; **** $p < 0.001$. (n = 10-11)

OBSERVATION 6: Neutrophil extracellular traps form during cerebral ischemia/reperfusion injury

To examine the formation of neutrophil extracellular traps (NETs) in cerebral ischemia/reperfusion injury in ischemic stroke, we performed an immunofluorescent staining for neutrophils (Ly6G), citrullinated histones (H3Cit) and DNA (DAPI) on brain slices of WT mice subjected to stroke (Figure 6A). NETs could be identified in the ipsilateral brain hemisphere 24 hours post-ischemia (Figure 6B). To quantify these NETs, tile scans were obtained of three different brain sections per mouse (Figure 6C). NET formation mainly occurred in the ipsilateral (affected by stroke) hemisphere and were virtually absent in the contralateral (unaffected) hemisphere (Figure 6D). Moreover, the number of NETs is correlated with the infarct size (Spearman $r = 0.8322$; $p < 0.01$; Figure 6E).

To study the temporal characteristics of NET formation, NETs were identified at different timepoints post-ischemia (1 hour, 2 hours, 6 hours, 12 hours, 24 hours, 48 hours) in WT mice subjected to stroke using quantitative immunofluorescence microscopy. Interestingly, quantification of NETs at these different timepoints, revealed that no NETs were present at 1 hour and 2 hours post-ischemia in the affected mouse brain. NETs could be detected in the ipsilateral hemisphere at 6 hours, increased at 12 hours, peak around 24 hours and started to disappear again 48 hours after induction of ischemia (Figure 7).

OBSERVATION 7: NETS are predominantly localized intravascularly

To better understand the involvement of neutrophil extracellular DNA traps in the thrombo-inflammatory processes that contribute to progressive stroke brain damage in the reperfused tissue, NETs (Ly6G, H3Cit, DNA) were visualized together with the brain vasculature (lectin), thereby enabling the visualization of intra- or extravascular NETs. Remarkably, NETs were predominantly localized within the brain vasculature at 12 hours, 24 hours and 48 hours post-ischemia and to a lesser extent in the brain parenchyma (Figure 8). These data suggest that NETs might play a role in secondary microthrombotic events leading to an exacerbation of brain tissue damage after ischemic stroke.

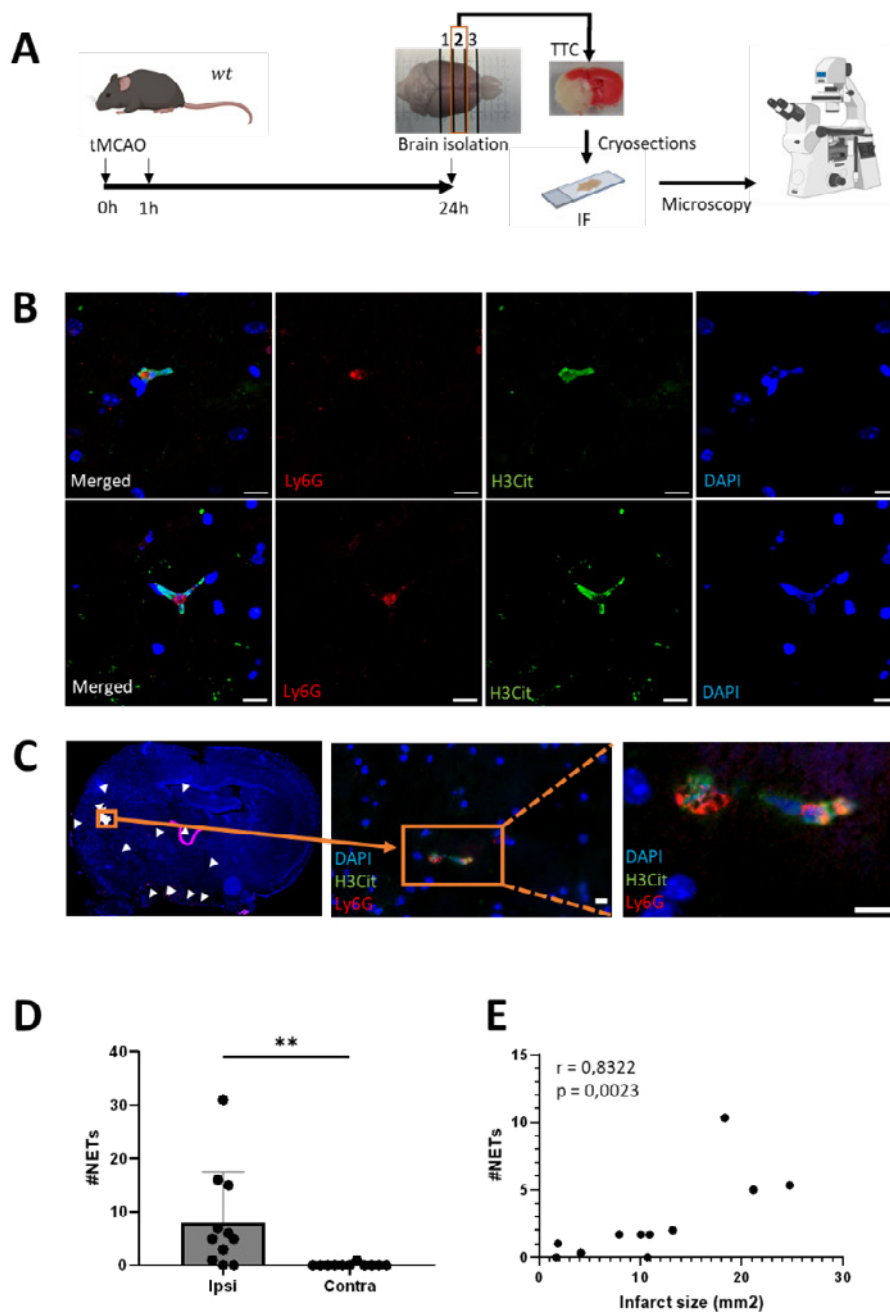


Figure 6: Neutrophil extracellular trap formation in affected mouse brain tissue 24 hours after induction of ischemic stroke. Transient focal cerebral ischemia was induced by 60 minutes occlusion of the right middle cerebral artery (tMCAO) followed by 23 hours of reperfusion in WT mice. Mouse brains were harvested, and infarct volumes were measured. To identify neutrophil extracellular traps (NETs), an immunofluorescent staining for neutrophils, citrullinated histones and DNA was performed on three brain sections per mouse (A). NETs were visualized via 2D fluorescent microscopy in WT mice, 24 hours after induction of ischemia. Neutrophils (Ly6G) are stained in red, citrullinated histones (H3Cit) in green and nuclei (DAPI) are depicted in blue. Scale bars are 10 μ m (B). To quantify these NETs, tile scans of three different brain sections per mouse were made (C). NETs are indicated with white arrows, showing that NETs were found within the affected hemisphere. The orange rectangle depicts an example of a NET. Magnifications are 40x and 100x. Scale bars are 10 μ m (C). NET formation (sum of three sections) predominantly occurred in the ipsilateral hemisphere compared to the contralateral hemisphere. Moreover, the mean number of NETs is related to the infarct size of the mouse brain (D).

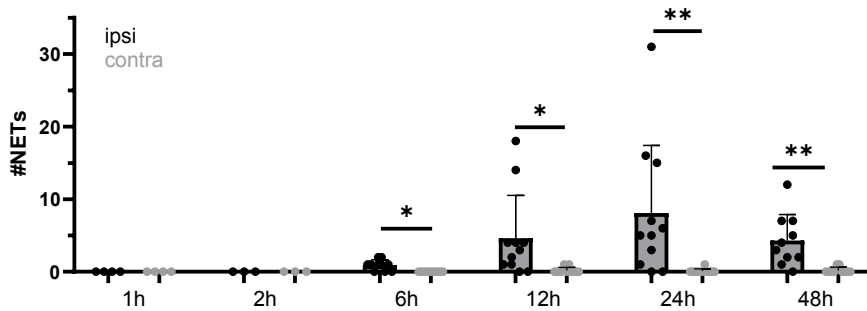


Figure 7: Temporal characteristics of neutrophil extracellular trap formation during ischemic stroke. Transient focal cerebral ischemia was induced in wild-type (WT) mice by 60 minutes occlusion of the right middle cerebral artery (tMCAO), followed by reperfusion. At different timepoints postischemia (1 hour, 2 hours, 6 hours, 12 hours, 24 hours and 48 hours), mice brain sections were stained for neutrophils (Ly6G), citrullinated histones (H3Cit) and DNA (DAPI), after which, neutrophil extracellular traps (NETs) were counted as described above. Data are presented as the sum of NETs on three different brain sections per mouse \pm standard deviation. No NETs are present in the ischemic mouse brain at 1 hour and 2 hours postischemia. NETs were detected in the ipsilateral hemisphere after induction of ischemia, increased at 12 hours, peak around 24 hours and start to decrease again at 48 hours postischemia (*: $p < 0.05$; **: $p < 0.01$).

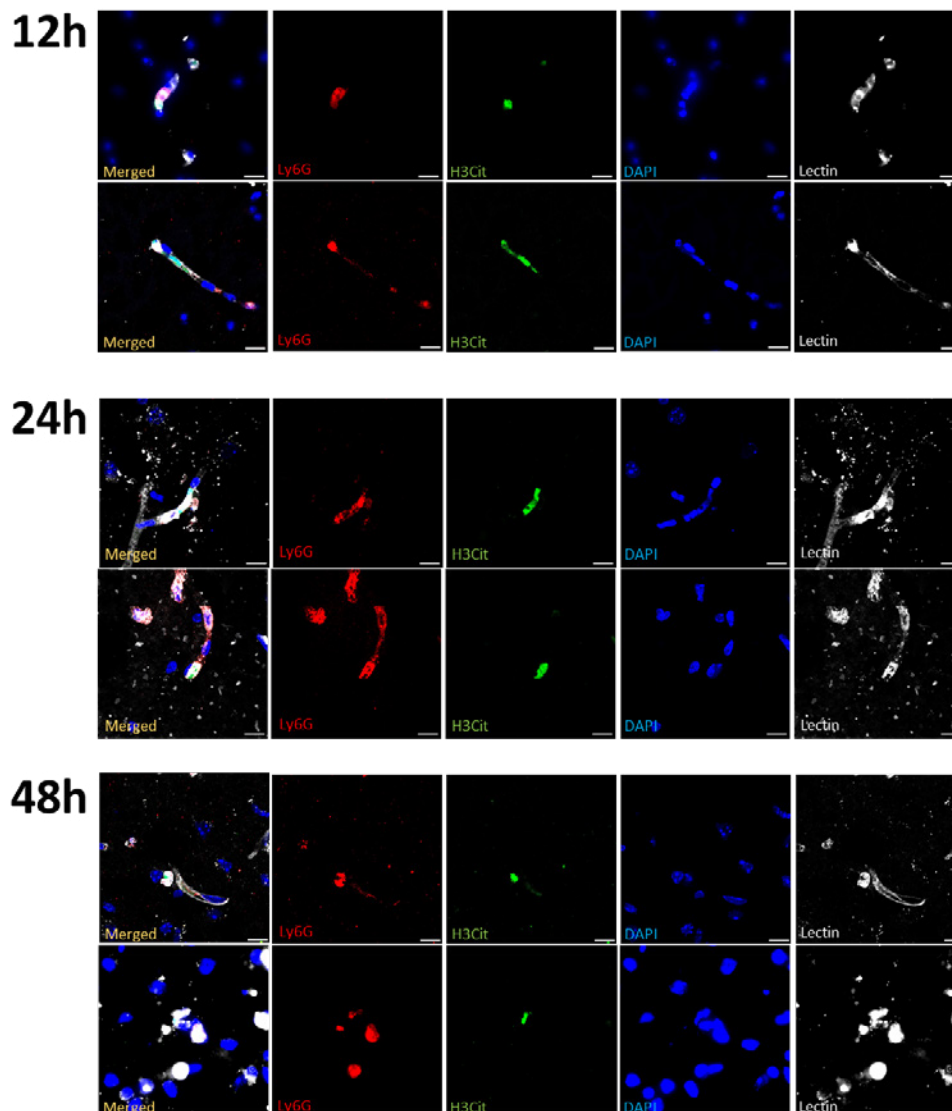


Figure 8: Immunofluorescent visualization of intravascular neutrophil extracellular traps in cerebral ischemia/reperfusion injury in ischemic stroke. Transient focal cerebral ischemia was induced in wild-type (WT) mice by 60 minutes occlusion of the right middle cerebral artery (tMCAO), followed by reperfusion. At different timepoints postischemia (12 hours, 24 hours and 48 hours), mice brain sections were stained for neutrophils (Ly6G, red), citrullinated histones (H3Cit, green), DNA (DAPI, blue) and brain vasculature (lectin, white). Two-dimensional fluorescent images of intravascular neutrophil extracellular traps (NETs) are shown at 12 hours, 24 hours and 48 hours postischemia. Scale bars are 10 μ m.

OBSERVATION 8: Deficiency of VWF is associated with significantly reduced formation of NETs in the ischemic brain

Given the central role of VWF in cerebral ischemia/reperfusion injury in ischemic stroke, further unraveling of the VWF-neutrophil interaction would give more insights into thrombo-inflammatory processes contributing to the aggravation of stroke brain injury. To investigate the potential regulation of NETosis by VWF, brain sections of VWF WT and littermate KO mice subjected to stroke were stained for the presence of NETs (Ly6G, H3Cit, DNA), after which, NETs were quantified in three different brain sections per mouse (Figure 9). A significantly reduced cerebral infarct was observed in VWF KO mice compared to VWF WT mice, 24 hours postischemia ($p < 0.05$, data not shown). NETs were visualized in VWF WT and littermate KO mice 24 hours after induction of ischemia (Figure 9A-B). Strikingly, quantification of these NETs revealed that a significantly lower number of NETs was present in VWF KO mice compared to WT mice 24 hours post-ischemia ($p < 0.001$, figure 9C). To confirm that NET formation was not merely a consequence of the larger infarct sizes observed in VWF WT mice, the number of NETs was normalized for the infarct size of the mouse brain. After normalization, a significant decrease in NET formation was still identified in VWF KO mice compared to WT mice 24 hours post-ischemia ($p < 0.01$, figure 9D). Hence these data suggest that VWF promotes the formation of NETs in the ischemic brain, most likely by recruiting neutrophils to the vascular wall of the ischemic brain.

1.2. WP 2: 3D-microscopy to map VWF-mediated thrombo-inflammation in the brain

A light sheet microscope will be acquired and installed by the summer of 2022. Due to the covid-19 situation, the acquisition of this microscope has been delayed. In the meantime the optical clearing methods have been optimized to start 3D-analysis of the mouse brain after stroke.

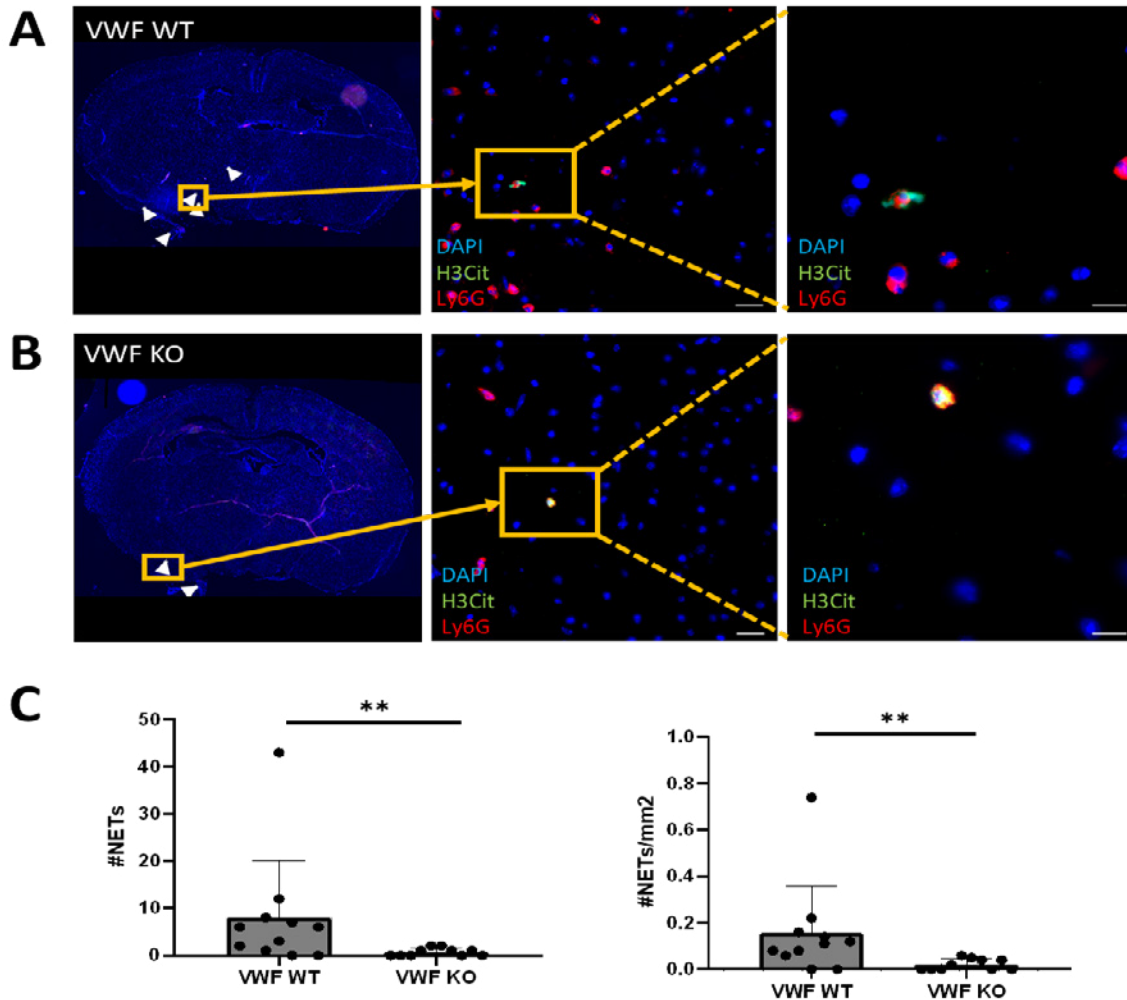


Figure 9: Deficiency of VWF is associated with significantly reduced formation of NETs in the ischemic brain. Transient focal cerebral ischemia was induced in wild-type (WT) and littermate VWF-knockout (KO) mice by 60 minutes occlusion of the right middle cerebral artery (tMCAO), followed by 23 hours of reperfusion. Mice brain sections were stained for neutrophils (Ly6G, red), citrullinated histones (H3Cit, green) and DNA (DAPI, blue). NETs were quantified afterwards in three different brain sections per mouse. A. Representative tile scan of a VWF WT mouse with white arrows pointing towards NETs. Two-dimensional fluorescent pictures (40x, 100x) of a NET found within the infarct core. Scale bars are 20 μ m (40x) and 10 μ m (100x). B. Representative tile scan of a VWF KO mouse with white arrows pointing towards NETs. Two-dimensional fluorescent pictures (40x, 100x) of a NET found within the infarct core. Scale bars are 20 μ m (40x) and 10 μ m (100x). C. A Significant lower number of NETs was observed in VWF KO mice compared to WT mice 24 hours post-ischemia ($p < 0.01$). D. Number of NETs corrected for infarct size was also significantly lower in VWF KO mice compared to VWF WT mice 24 hours after induction of ischemia ($p < 0.01$).

2. Output

2.1. Papers with GSKE acknowledgement (2020-2021):

- De Meyer SF, Langhauser F, Haupteltshofer S, Kleinschnitz C, Casas AI, Thromboinflammation in brain ischemia: recent updates and future perspectives. *STROKE*, under review (invited review) (impact factor 7.91).
- Staessens, S., Francois, O., Brinjikji, W., Doyle, K.M., Vanacker, P., Andersson, T., De Meyer, S.F. (2021). Studying Stroke Thrombus Composition After Thrombectomy What Can We Learn? *STROKE*, 52 (11), 3718-3727. (Impact factor: 7.91)
- Siddiqui, A.H., Waqas, M., Brinjikji, W., De Meyer, S.F., Doyle, K., Fiehler, J., Hacke, W., Hanel, R.A., Jovin, T.G., Liebeskind, D.S., Yoo, A.J., Zaidat, O.O., Andersson, T., Nogueira, R.G. (2021). Embotrap Extraction & Clot Evaluation & Lesion Evaluation for NeuroThrombectomy (EXCELLENT) Registry design and methods. *JOURNAL OF NEUROINTERVENTIONAL SURGERY*. (Impact factor: 5.84)
- Boodt, N., van Schauburg, P.R W S., Hund, H.M., Fereidoonzhad, B., McGarry, J.P., Akyildiz, A.C., van Es, A.C G M., De Meyer, S.F., Dippel, D.W J., Lingsma, H.F., van Beusekom, H.M M., van der Lugt, A., Gijssen, F.J H. (2021). Mechanical Characterization of Thrombi Retrieved With Endovascular Thrombectomy in Patients With Acute Ischemic Stroke. *STROKE*, 52 (8), 2510-2517. (Impact factor: 7.91)
- Denorme, F., Martinod, K., Vandenbulcke, A., Denis, C.V., Lenting, P.J., Deckmyn, H., Vanhoorelbeke, K., De Meyer, S.F. (2021). The von Willebrand factor A1 domain mediates thromboinflammation, aggravating ischemic stroke outcome in mice. *HAEMATOLOGICA*, 106 (3), 819-828. (Impact factor: 9.94)
- Staessens, S., Francois, O., Desender, L., Vanacker, P., Dewaele, T., Sciot, R., Vanhoorelbeke, K., Andersson, T., De Meyer, S.F. (2021). Detailed histological analysis of a thrombectomy-resistant ischemic stroke thrombus: a case report. *THROMBOSIS JOURNAL*, 19 (1), Art.No. ARTN 11 (Impact factor: 5.50)
- Staessens, S., De Meyer, S.F. (2020). Thrombus heterogeneity in ischemic stroke. *PLATELETS*, 32 (3), 331-339. (Impact factor: 3.86)
- Staessens, S., Denorme, F., François, O., Desender, L., Dewaele, T., Vanacker, P., Deckmyn, H., Vanhoorelbeke, K., Andersson, T., De Meyer, S. (2020). Structural analysis of ischemic stroke thrombi: histological indications for therapy resistance. *HAEMATOLOGICA*, 105 (2), 498-507. (Impact factor: 9.94) Staessens S, Fitzgerald S, Andersson T, Clarençon F, Denorme F, Gounis MJ, Hacke W, Liebeskind DS, Szikora I, van Es A, Brinjikji W, Doyle KM, **De Meyer SF**. (2020). Histological stroke clot analysis after thrombectomy: Technical aspects and recommendations. *INTERNATIONAL JOURNAL OF STROKE*, 2020 Jul;15(5):467-476 (Impact factor: 5.27)

3. References

1. De Meyer SF, Denorme F, Langhauser F, et al. Thromboinflammation in Stroke Brain Damage. *Stroke*. 2016;47(4):1165-1172.
2. Mizuma A, You JS, Yenari MA. Targeting Reperfusion Injury in the Age of Mechanical Thrombectomy. *Stroke*. 2018;49(7):1796-1802.
3. De Meyer SF, Stoll G, Wagner DD, Kleinschnitz C. von Willebrand factor: an emerging target in stroke therapy. *Stroke*. 2012;43(2):599-606.
4. Denorme F, De Meyer SF. The VWF-GPIb axis in ischaemic stroke: lessons from animal models. *Thromb. Haemost.* 2016;116(4):597-604.
5. Kleinschnitz C, De Meyer SF, Schwarz T, et al. Deficiency of von Willebrand factor protects mice from ischemic stroke. *Blood*. 2009;113(15):3600-3603.
6. De Meyer SF, Schwarz T, Deckmyn H, et al. Binding of von Willebrand factor to collagen and glycoprotein Ibalpha, but not to glycoprotein IIb/IIIa, contributes to ischemic stroke in mice--brief report. *Arteriosclerosis, Thrombosis, and Vascular Biology*. 2010;30(10):1949-1951.
7. De Meyer SF, Schwarz T, Schatzberg D, Wagner DD. Platelet glycoprotein Ib is an important mediator of ischemic stroke in mice. *Exp Transl Stroke Med*. 2011;3(1):9.
8. Verhenne S, Denorme F, Libbrecht S, et al. Platelet-derived VWF is not essential for normal thrombosis and hemostasis but fosters ischemic stroke injury in mice. *Blood*. 2015;126(14):1715-1722.
9. Kleinschnitz C, Schwab N, Kraft P, et al. Early detrimental T-cell effects in experimental cerebral ischemia are neither related to adaptive immunity nor thrombus formation. *Blood*. 2010;115(18):3835-3842.
10. Jickling GC, Liu D, Ander BP, et al. Targeting neutrophils in ischemic stroke: translational insights from experimental studies. *J. Cereb. Blood Flow Metab*. 2015;35(6):888-901.
11. Aymé G, Adam F, Legendre P, et al. A Novel Single-Domain Antibody Against von Willebrand Factor A1 Domain Resolves Leukocyte Recruitment and Vascular Leakage During Inflammation-Brief Report. *Arteriosclerosis, Thrombosis, and Vascular Biology*. 2017;37(9):1736-1740.

12. Kleinschnitz C, Pozgajova M, Pham M, et al. Targeting platelets in acute experimental stroke: impact of glycoprotein Ib, VI, and IIb/IIIa blockade on infarct size, functional outcome, and intracranial bleeding. *Circulation*. 2007;115(17):2323–2330.
13. Li T-T, Fan M-L, Hou S-X, et al. A novel snake venom-derived GPIb antagonist, anfibatide, protects mice from acute experimental ischaemic stroke and reperfusion injury. *Br. J. Pharmacol.* 2015;172(15):3904–3916.
14. Scully M, Cataland SR, Peyvandi F, et al. Caplacizumab Treatment for Acquired Thrombotic Thrombocytopenic Purpura. *N. Engl. J. Med.* 2019;380(4):335–346.
15. Scully M, Knöbl P, Kentouche K, et al. Recombinant ADAMTS-13: first-in-human pharmacokinetics and safety in congenital thrombotic thrombocytopenic purpura. *Blood*. 2017;130(19):2055–2063.
16. Denorme F, Martinod K, Vandenbulcke A, et al. The von Willebrand Factor A1 domain mediates thromboinflammation, aggravating ischemic stroke outcome in mice. *Haematologica*. 2020;haematologica, 106 (3), 819-828



Geneeskundige Stichting Koningin Elisabeth
Fondation Médicale Reine Elisabeth
Königin-Elisabeth-Stiftung für Medizin
Queen Elisabeth Medical Foundation

Progress report of the
university research project of

Prof. dr. Lieve Moons &
Lies De Groef, MSc, PhD
Katholieke Universiteit Leuven (KU Leuven)

Prof. dr. Lieve Moons

Head Division Animal Physiology and Neurobiology (APN)

Head RU Neural Circuit Development and Regeneration (<http://bio.kuleuven.be/df/LM/>)

Department of Biology, KU Leuven

Zoological Institute, Naamsestraat 61, bus 2464

3000 Leuven

Phone: 32-16-32 39 91

E-mail: lieve.moons@kuleuven.be

Lies De Groef, MSc, PhD

Onderzoeksgroep neurale ontwikkeling en regeneratie premonstreit college

Naamsestraat 61 bus 2464 b-

3000 leuven

lies.degroef@kuleuven.be

Oligodendrocytes in Wolfram syndrome: bystanders or partners in crime?

1. Project aims

Wolfram syndrome is a rare hereditary disease, causing diabetes, blindness, deafness and other neurological problems in infants and young adults, and results in death around the age of 30 years. Wolfram patients carry recessive mutations in the wolframin ER transmembrane glycoprotein (WFS1) gene, resulting in loss of function of the WFS1 protein. Loss of WFS1 has been shown to result in endoplasmic reticulum (ER) stress, dysregulated Ca²⁺ homeostasis and mitochondrial dysfunction. Remarkably, in the brains of Wolfram patients, distinct white matter loss has been observed. Combining this with the observation that myelinating oligodendrocytes are especially sensitive to ER stress, we hypothesize that oligodendrocytes play an important role in the neurodegeneration seen in Wolfram patients. Therefore, in this project, we aim to investigate what the effect of these 'diseased' oligodendrocytes is on the function of 'healthy' neurons, focusing on ER stress, mitochondria and cell metabolism as potential underlying mechanisms. In addition, we plan to further unravel the function of the WFS1 protein by identifying its binding partners in this cellular model system. Finally, we will study the interplay between oligodendrocyte/myelin loss and neurodegeneration in a *Wfs1* knockout (KO) mouse model, and provide seeding evidence that interfering with the studied cellular processes and WFS1 binding partners can rescue the disease phenotype.

The concrete goals of this project are:

- i. To perform a comprehensive study of the WFS1 binding partners.
- ii. To study *in vitro* which cellular processes are affected in induced pluripotent stem cell (iPSC)-derived oligodendroglia from Wolfram patients, thereby focusing on ER stress, mitochondrial function and metabolism; investigating the contributions of the newly identified WFS1 binding partners to these cellular processes; and studying the effect of 'diseased' oligodendroglia on wild-type 'healthy' neurons.
- iii. To study *in vivo* the changes in oligodendrocytes and neurons in a *Wfs1* KO mouse model, to compose a timeline of neuronal *versus* oligodendrocyte pathology.
- iv. To rescue the Wolfram syndrome phenotype in *Wfs1* KO mice by interfering with the newly identified WFS1 binding partners or cellular processes.

2. Progress report

In the first two years of the project –as planned in the original Gantt chart– we have focused on aims (ii) and (iii), thereby performing work package II and the first two (out of three) tasks of work package III. We are now finalizing the *in vitro* study of the effects of WFS1 deficiency in iPSC-derived oligodendroglia (task II.1), and are setting up a continuation of these experiments in neuron-oligodendrocyte co-cultures (task II.2). Furthermore, we have concluded the morphological (task III.1) as well as a functional characterization (task III.2) of the central nervous system integrity in *Wfs1* KO mice, and are preparing a manuscript reporting these data. Experiments related to the study of the WFS1 binding partners (work package I) were postponed and instead more resources were invested into the functional characterization of central nervous system integrity in the *Wfs1* KO mice. We deemed this to be more impactful and more likely to allow us to progress faster to a deeper understanding of the pathological processes underlying Wolfram syndrome.

2.1. Task II.1 *In vitro* study of the effects of WFS1 deficiency in iPSC-derived oligodendroglia

At the start of this project, two Wolfram syndrome patient iPSC lines, one isogenic control line and two commercially available control lines were available in house. Using the protocol published by García-León *et al.*¹ these iPSC lines were differentiated into O4⁺ oligodendrocytes. A first series of experiments with these iPSC-derived oligodendrocytes, however, revealed that differentiation into iPSC is suboptimal. Hence we switched to a newly developed protocol² which can subsequently myelinate neurons, both *in vitro* and *in vivo*. To date, OPCs have been derived from eight different hPSC lines including those derived from patients with spontaneous and familial forms of MS and ALS, respectively. hPSCs, fated for 8 d toward neural progenitors, are transduced with an inducible lentiviral vector encoding for SOX10. The addition of doxycycline for 10 d results in >60% of cells being O4-expressing OPCs, of which 20% co-express the mature OL marker myelin basic protein (MBP that uses genome engineering to deliver SOX10, the 'master' transcriptional regulator of the oligodendrocyte lineage, to iPSCs. We found that iPSC-derived oligodendrocytes from this protocol show a better morphology, survival and tremendously increased oligodendrocyte maturation. Therefore, **three patient and three control isogenic iPSC lines were genome engineered** according to this protocol, using adenine base editing.

These engineered iPSC lines were next differentiated into oligodendrocytes, which were then further characterized to **study *in vitro* the pathological processes that have been linked to Wolfram syndrome**. A first series of experiments using two of the three pairs of iPSC lines shows that patient iPSC-derived oligodendrocytes are more vulnerable to tunicamycin- or thapsigargin-induced ER stress compared to controls, as evident from an X-box binding protein 1 (XBP1) splicing assay (Figure 1A), qPCR for C/EBP homologous protein (CHOP) (Figure 1B), and Western blot for Binding immunoglobulin protein (BiP) (Figure 1C). In addition, we also observed signs of metabolic abnormalities linked to mitochondrial dysfunction in the patient iPSC-derived oligodendrocytes compared to isogenic controls, namely reduced mitochondrial respiration (Figure 1D-E) and mitochondrial membrane depolarization (Figure 1F). Finally, Western blot for Monocarboxylate transporter 1 (MCT1) pointed towards dysfunction of the metabolic coupling of oligodendrocytes with axons in cells derived from Wolfram patients (Figure 1G).

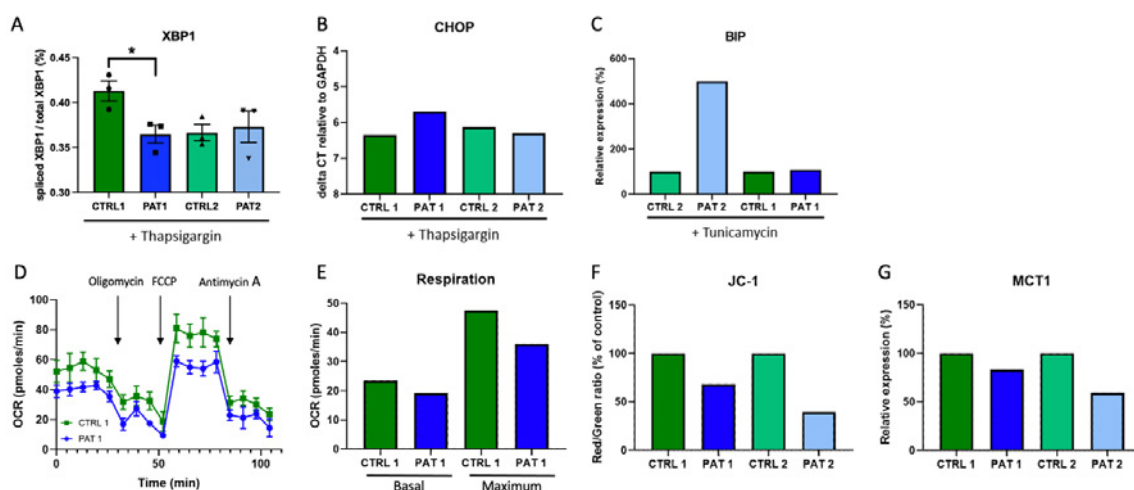


Figure 1. iPSC-derived oligodendrocytes from Wolfram patients are more vulnerable to ER stress, mitochondrial and metabolic dysfunction. (A-C) ER stress assays for different ER stress markers, including an XBP1 splicing assay (A), qPCR for CHOP (B), and Western blot for BiP (C), suggest that iPSC-derived oligodendrocytes from Wolfram patients are more vulnerable to tunicamycin- or thapsigargin-induced ER stress compared to isogenic controls. (D-E) Mitochondrial dysfunction was observed in iPSC-derived oligodendrocytes from Wolfram patients: Seahorse analysis of the oxygen consumption rate in these cells showed reduced mitochondrial respiration (D), and staining with the mitochondrial membrane potential probe JC-1 revealed mitochondrial membrane depolarization in patient iPSC-derived oligodendrocytes compared to isogenic controls (E). (F) Reduced expression of MCT1 by patient iPSC-derived oligodendrocytes, as evident from Western blot analysis, suggests that the metabolic coupling of these cells with axons may be compromised and hence less metabolites can be shuttled from the oligodendrocytes to the axons to support the functioning of the latter. PAT: Wolfram patient-derived cell lines, CTRL: isogenic control cell lines.

Altogether these data suggest that iPSC-derived oligodendrocytes from Wolfram patients may be more vulnerable to ER stress and display signs of mitochondrial dysfunction. This, together with their seemingly reduced capacity to transfer metabolites and thereby support axons, suggests that oligodendrocyte dysfunction may, at least partially, be underlying the neurodegenerative component of Wolfram syndrome. Replicate experiments and additional studies are ongoing to confirm these findings.

2.2. Task II.2. *In vitro* study of WFS1 deficiency in iPSC-derived co-cultures of oligodendroglia and neurons

As our findings point towards a crucial role for non-neuronal cells (*i.e.* oligodendrocytes, but maybe also other glial cells) in the neurodegeneration phenotype of Wolfram syndrome patients (and animal models), we believe that it is essential to elucidate the role of oligodendrocytes *versus* astrocytes *versus* neurons in this disease. Thereto, we are now creating a **3D *in vitro* optic nerve-on-chip model**, using iPSCs from Wolfram syndrome patients and their isogenic control cells, in a microfluidic device (Figure 2). Additional funding to support this task has been secured (FWO SB PhD fellowship to Karan Ahuja; promotor Lieve Moons, co-promotors Lies De Groef & Catherine Verfaillie).

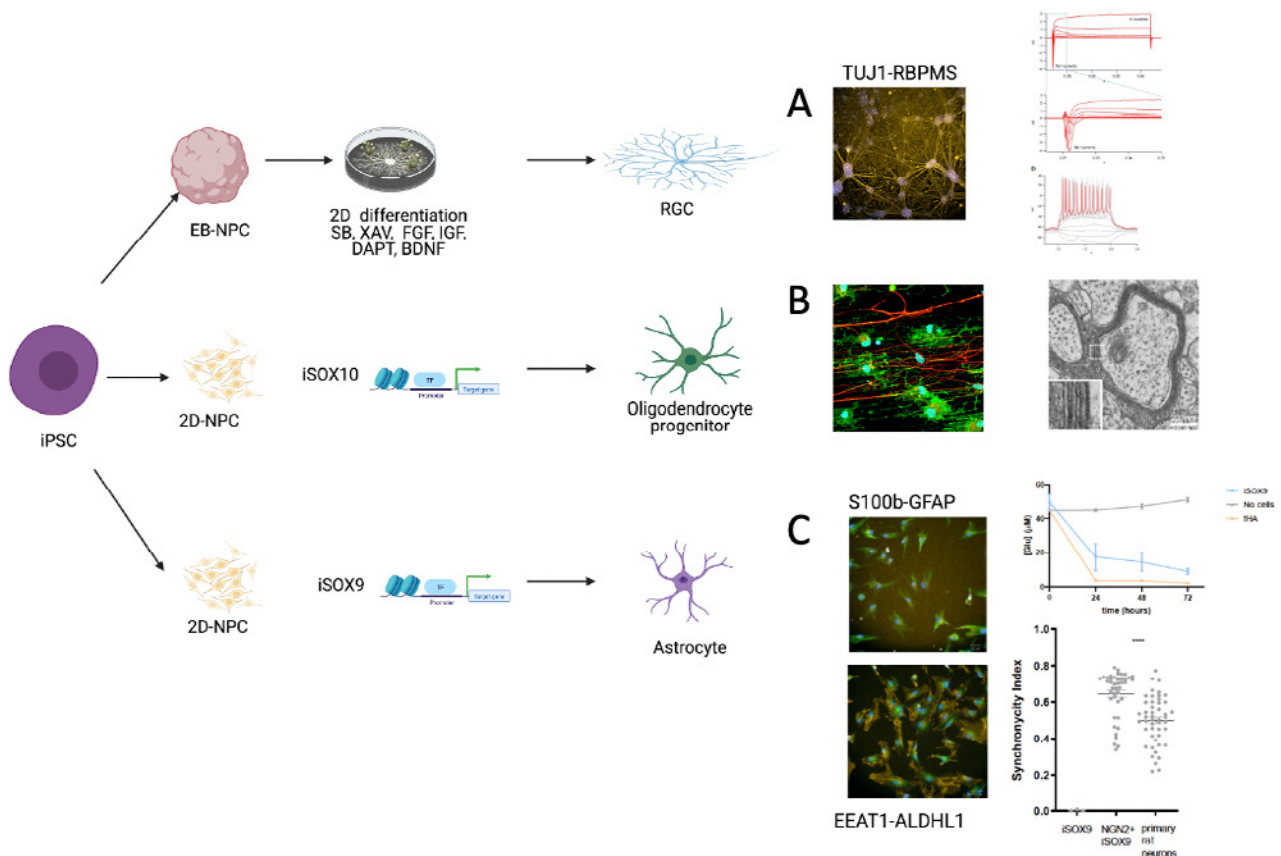


Figure 2. Pilot data showing the first results and feasibility of the *in vitro* triculture optic nerve-on-chip model, using retinal ganglion cells, oligodendrocyte precursor cells and astrocytes from patient-derived iPSCs. The differentiation approaches as well as readouts are shown, including immunostaining and patch-clamp evaluation of retinal ganglion cells (A), immunostaining of oligodendrocyte precursors (green) cocultured with cortical neurons (red), and *in vivo* myelination by oligodendrocyte progenitor cells grafted in immunodeficient Shi-/- mice (B), and immunostaining, glutamate uptake and multi-electrode array-based assessment of astrocyte support of neuronal maturation (C). Data by Karan Ahuja, in collaboration with Prof. Catherine Verfaillie (Stem Cell Institute Leuven, KU Leuven).

2.3. Task III.1 Morphological characterization of CNS integrity in *Wfs1* KO mice & Task III.2 Functional characterization of CNS integrity in *Wfs1* KO mice

The eye, optic nerve and brain phenotype of *Wfs1* KO mice and corresponding WT littermates was studied at 3, 4.5, 6 and 7.5 months of age. Previously, we already reported that *Wfs1* mice display reduced visual acuity, abnormal electrophysiological responses of their retinal ganglion cells and reduced action potential conduction in the optic nerve at 6 to 7.5 months of age. These functional deficits were accompanied by neuroinflammation, as apparent from increased expression levels of glial fibrillary acidic protein (GFAP), S100 calcium-binding protein B (S100B) and Ionized calcium binding adaptor molecule 1 (IBA1).

Since these abnormalities point to optic nerve atrophy, and given the defects seen in oligodendrocytes derived from Wolfram syndrome patients in our *in vitro* work (*cf.* above), we further investigated the optic nerve of *WFS1* KO mice via **transmission electron microscopy** (in collaboration with Prof. E. Wolfs, U Hasselt), **and immunostainings for oligodendrocytes and oligodendrocyte precursor cells**. Transmission electron microscopy analyses of the optic nerve revealed that 6-month-old *Wfs1* KO mice have more axons with a small diameter (Figure 3A) yet there were no overt differences in the G-ratio (*i.e.* myelination status) (Figure 3B-C). However, cell counting of mature oligodendrocytes, all oligodendrocytes and oligodendrocyte precursors (Figure 3D-F) did show a reduced number of oligodendrocyte precursor cells in the optic nerve of 7.5-month-old *Wfs1* KO mice. Together, this suggests a complex interplay of abnormal axonal conduction despite no overt thinning of the myelin sheets, together with a reduction of the oligodendrocyte precursor pool. Additional analyses, including EM studies and cell countings at younger ages, are being conducted to confirm these findings.

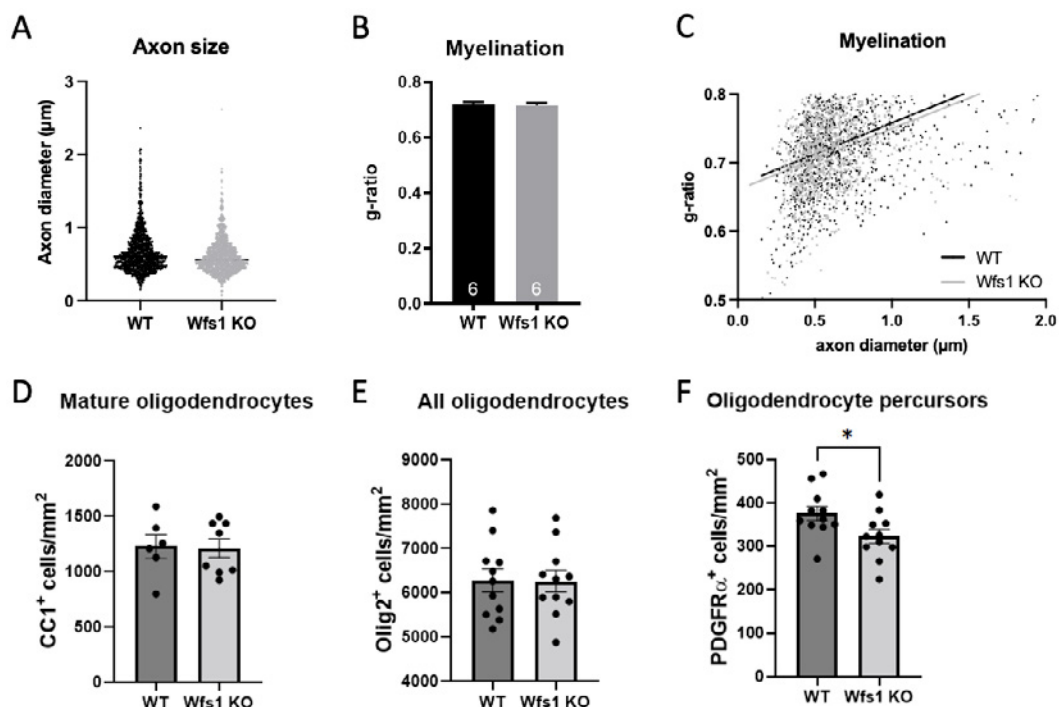


Figure 3. Structural analysis of axonal integrity of the optic nerve, and quantification of oligodendrocyte lineage cells point to oligodendrocyte abnormalities in *Wfs1* KO mice. (A-C) Morphological analyses of electron microscopy images of cross-sections of the optic nerve of 6-month-old wild type versus *Wfs1* KO mice reveal a slightly reduced average axonal diameter in *Wfs1* KO mice (A) but no overt changes in the thickness of the myelin sheet enwrapping the optic nerve axons (B-C). (D-F) Cell countings on immunohistologically stained longitudinal sections of the optic nerve of 7-month-old animals disclosed equal cell numbers for mature (D) and all (E) oligodendrocytes yet a reduced number of oligodendrocyte precursor cells (F) in *Wfs1* KO mice.

Finally, to confirm the above findings, zoom in on the brain phenotype and expand our analysis to other brain regions, we assessed the neurodegeneration phenotype of the *Wfs1* mouse via magnetic resonance imaging (MRI) (in collaboration with Prof. U. Himmelreich, moSAIC,

KU Leuven). Anatomical, T2-weighted and diffusion tensor images, as well as manganese-enhanced MRI images, were collected at 3, 4.5, 6 and 7.5 months of age in *Wfs1* KO and WT mice (Figure 4). Analysis (shown here for 7.5 months of age only) reveals that the volume of several brain regions is reduced, including the cerebellum, total brain, and brainstem (Figure 4A, B, E) – regions also affected in Wolfram patients –, pointing towards neurodegeneration. Furthermore, manganese-enhanced MRI scans show that the diameter of the optic nerve is reduced (Figure 4D) and that the innervated area in the superior colliculus (*i.e.* where the optic nerve axons synapse) is smaller (Figure 4C). Notably, the corpus callosum, which is almost entirely made up by white matter, is also reduced in the *Wfs1* KO mice (Figure 4F). In addition, we also observed changes in the apparent diffusion coefficient in several of these regions (data not shown). Analyses of the fractional anisotropy are currently being performed to elucidate whether these structural changes may reflect changes in myelination.

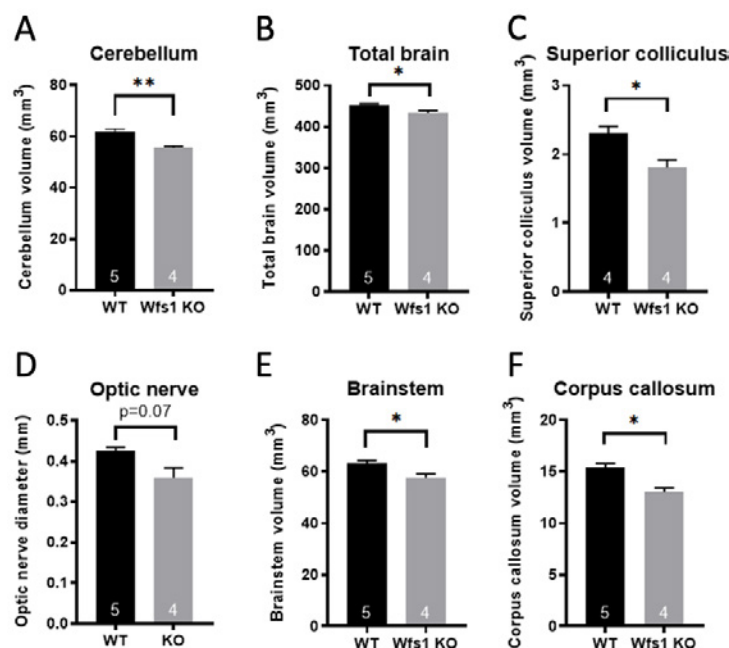


Figure 4. MRI data of 7.5-month-old wild type and *Wfs1* KO mice confirm neurodegeneration in several brain areas that are also affected in Wolfram syndrome patients. (A, B, E, F) The volume of several brain areas, namely the cerebellum (A), total brain (B), brainstem (E) and corpus callosum (F) is smaller in *Wfs1* KO mice. (C-D) Detailed analysis of the optical projection via manganese-enhanced MRI shows a reduced innervation of the primary visual target area, the superior colliculus (C), and a smaller optic nerve diameter (D) in *Wfs1* KO mice.

In conclusion, a pathological phenotype was observed in the retina, optic nerve and brain of *Wfs1* KO mice. This phenotype comprises axonal degeneration, neuronal dysfunction, neuroinflammation and oligodendrocyte abnormalities. These findings are now being prepared for publication. The established phenotype, timeline and read-outs provide us with all things required to next evaluate the effect of a disease-modifying therapy (task III.3).

3. Conclusions and future planning

The data gathered within this project, in Wolfram syndrome patient iPSC-derived oligodendrocytes and a Wolfram syndrome mouse model, point towards a critical role for oligodendrocytes in this neurodegenerative pathology. This supports the central hypothesis of the project, *i.e.* that oligodendrocytes rather than neurons might be the drivers of the disease processes that lead to neurodegeneration in Wolfram syndrome, and confirms that we are on track with the proposed research. Despite some delays due to COVID19, we can state that the work is ongoing according

to the original plans and the goals set for the first two years have largely been reached. As such, everything is in place for the successful completion of the project in the coming year.

4. References

1. García-León, J. A. *et al.* SOX10 Single Transcription Factor-Based Fast and Efficient Generation of Oligodendrocytes from Human Pluripotent Stem Cells. *Stem Cell Reports* **10**, 655–672 (2018).
2. García-León, J. A. *et al.* Generation of oligodendrocytes and establishment of an all-human myelinating platform from human pluripotent stem cells. *Nat. Protoc.* **15**, 3716–3744 (2020).



Geneeskundige Stichting Koningin Elisabeth
Fondation Médicale Reine Elisabeth
Königin-Elisabeth-Stiftung für Medizin
Queen Elisabeth Medical Foundation

Progress report of the
university research project of

Prof. Pierre Vanderhaeghen, MD, PhD (VIB)
Katholieke Universiteit Leuven (KU Leuven)

Prof. Pierre Vanderhaeghen, MD, PhD

Stem Cell and Developmental Neurobiology

Lab VIB-KU Leuven Center for Brain & Disease Research Department of Neurosciences,

Leuven Brain Institute IRIBHM / ULB Neuroscience Institute

pierre.vanderhaeghen@kuleuven.be

Deciphering the mechanisms underlying intellectual deficiency and autism spectrum disorders by cellular modelling in human neurons *in vivo*.

1. State of the art and objectives

Neurodevelopmental disorders (NDDs), including intellectual disability (ID) and autism spectrum disorders (ASD) present a major challenge in clinical genetics and medicine. The advent of novel genomic technologies has led to the identification of many underlying genetic defects ^{1,2}. However, before tailored therapies can be developed, one needs to decipher the exact underlying pathophysiology.

To this aim, most of the studies on NDD have relied on animal models, which has led to substantial progress thanks to the evolutionary conservation of many signaling pathways. However there are also important evolutionary differences in brain development, so that the exact impact of NDD mutations in human neurons remains unknown, as well as the translatability of preclinical findings. This is particularly relevant for ID and ASD, which are mostly linked to alterations of the cerebral neocortex, the most evolutionary divergent structure in the human brain.

Given the the difficulty to study the brain of patients at the cellular level, the advent of human pluripotent stem cell (PSC) has offered new opportunities ³. While *in vitro* PSC-based models have been used successfully to model several NDD, *in vivo* elements are crucially missing from these approaches, which thus display serious limitations to model faithfully all aspects of ID/ASD. For this reason we have started to develop models of xenotransplantation, where PSC-derived human neurons are transplanted into the mouse cortex ^{4,5} Following transplantation in the mouse neonatal cortex, the PSC-derived pyramidal neurons develop like endogenous cortical neurons, and integrate functionally in the host brain, following their species-specific time-line.

In this project we aim to determine the pathophysiological mechanisms of ID/ASD conditions linked to mutations in *SYNGAP1* and *MEF2C*, through the *in vivo* study of human neurons displaying clinically relevant mutations. The project is based on the following objectives:

***Aim1.* Development of fully validated *in vitro* PSC models for *SYNGAP1* and *MEF2C* related disorders.**

***Aim2.* Characterization of *SYNGAP1* and *MEF2C* loss of function in human cortical neurons *in vivo*.**

2. Results

2.1. WP1. Generating human cortical neurons displaying specific NDD mutations.

The first step of the project is to generate isogenic PSC lines displaying specific mutations of *SYNGAP1* and *MEF2C* using directed genomic engineering. We have generated these lines for *SYNGAP1*, including several lines harbouring homozygote or heterozygote mutations, while the generation of *MEF2C* mutants is ongoing. Given the pleiotropic effects of *MEF2* genes on neuronal development, we have also generated inducible gain and loss of function models of *MEF2* function by overexpressing full length or truncated versions fused to repressor or activator domains (*MEF2-En* / *Mef2-VP16*), in order to dissect the precise roles of *MEF2* with optimal temporal and molecular resolution. These approaches were validated *in vitro* (**Figure 1**) and are now used to study *MEF2C* *in vivo*.

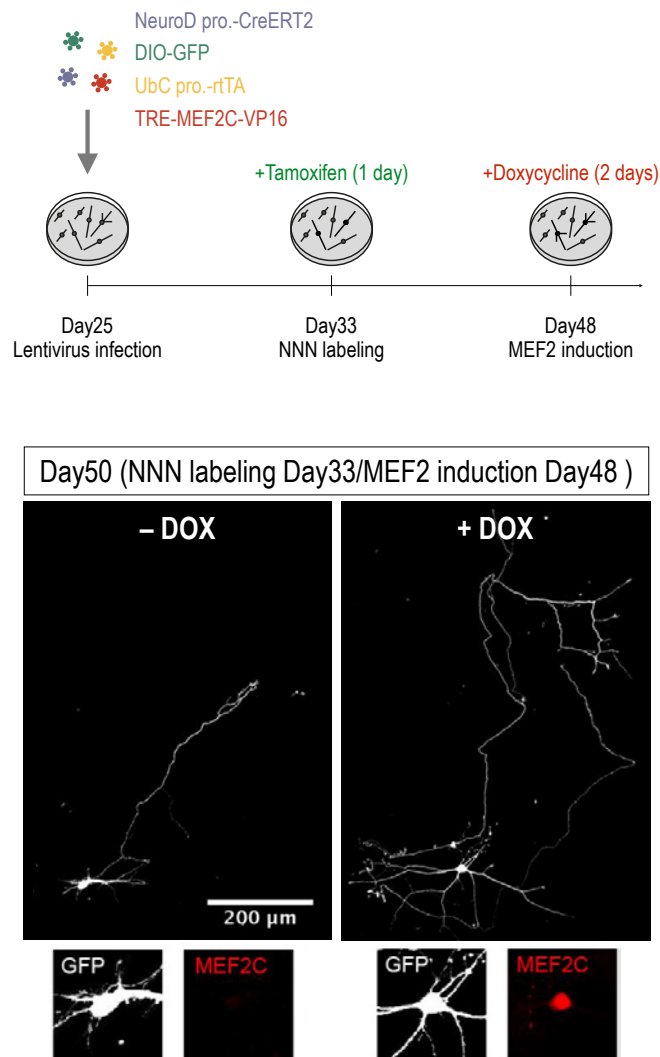


Figure 1. A new model of MEF2 functional analysis in human cortical pyramidal neurons. Using Dox-inducible system in PSC-derived neurons, we have implemented several models to study MEF2 gain and loss of function in a temporal fashion. This approach suggests that MEF2C transient gain of function leads to acceleration of dendritic outgrowth and branching.

2.2. WP2. *In vivo* characterization of SYNGAP1 loss of function in human cortical neurons.

Following *in vitro* validation, human differentiated cortical neurons from mutant and control cell lines are now routinely transplanted into neonatal mice. Specifically we rely on the system that we pioneered, revealing species-specific patterns of development of human cortical pyramidal neurons and their maturation up to physiological functional responses indistinguishable from host mouse neurons.

WP2.1 Synaptic function and plasticity of mutant human cortical neurons *in vivo*.

Control and mutant cortical cells were differentiated *in vitro* and infected by lentiviruses prior to transplantation with fluorescent reporters markers (tdTomato or Venus).

Ex vivo brain slices were prepared from transplanted mice and examined by patchclamp recording focused on GFP-labelled transplanted neurons. The intrinsic electrophysiological properties of grafted neurons were determined, as well as the existence of functional synaptic inputs from host to transplanted neurons.

Remarkably this analysis revealed a striking increase in synaptic activity and maturation in SYNGAP1 heterozygote mutants (**Figure 2**), while intrinsic neuronal properties appear to be normal. This important dataset thus constitutes a first direct evidence that SYNGAP1 haploinsufficiency leads to accelerated synaptogenesis in human neurons.

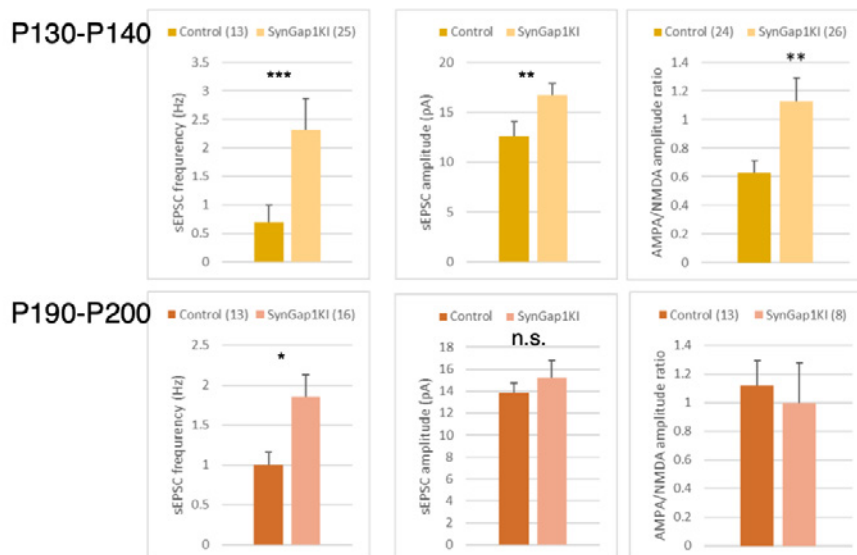


Figure 2: Patch-clamp recordings of human neurons (control and SYNGAP1 heterozygote neurons (KI)) in ex vivo slices from xenotransplanted mice at 130-200 days post-transplantation. SYNGAP1 mutant heterozygote neurons display increased frequency of synaptic activity and increased AMPA/NMDA ratios at P13-P140, while similar levels are found at P190-P200, indicative of greater speed of functional maturation.

WP2.2. Neuronal morphogenesis of mutant human cortical neurons in vivo.

Following recordings, the cells were filled with biocytin to study their detailed morphology using confocal imaging and 3D reconstruction. This analysis revealed increased density of the spines in the mutant neurons, further confirming increased maturation rates in the mutant cells (data not shown).

WP2.3. Live characterization of mutant neurons using in vivo imaging.

Finally, we have started *in vivo* multiphoton imaging to characterize in *live* animals the developmental dynamics and function of human neurons. For developmental dynamics focused on dendritic spines, as a *proxy* of synapse formation, using standard imaging of fluorescently labeled neurons. Briefly, the transplanted animals undergo specific surgery for cranial window at 3MPT or 6MPT, enabling the identification of the human neurons. Then the same neurons are repetitively imaged over a period of up to six weeks, enabling to reveal dendritic spines with high spatial and temporal resolution (**Figure 3**). This has revealed a striking increase of dendritic spine density in both homozygote and heterozygote neurons, together with increased rates of spine formation. For functional analysis, we have started to use GCaMP functional calcium imaging that we have successfully implemented to human neurons transplanted in the mouse visual cortex, enabling to reveal specific functional responses of these neurons following physiological visual stimuli in awake animals. The analysis of the mutant neurons is ongoing but already suggests that, although the basal activity and functional responses of the mutant neurons appear to be normal, they develop at earlier time-points, thus further suggesting that the main defect in SYNGAP1 haploinsufficiency is linked to accelerated neuronal development, in line with the crucial importance of human brain neoteny for the acquisition of normal cognitive function ⁶.

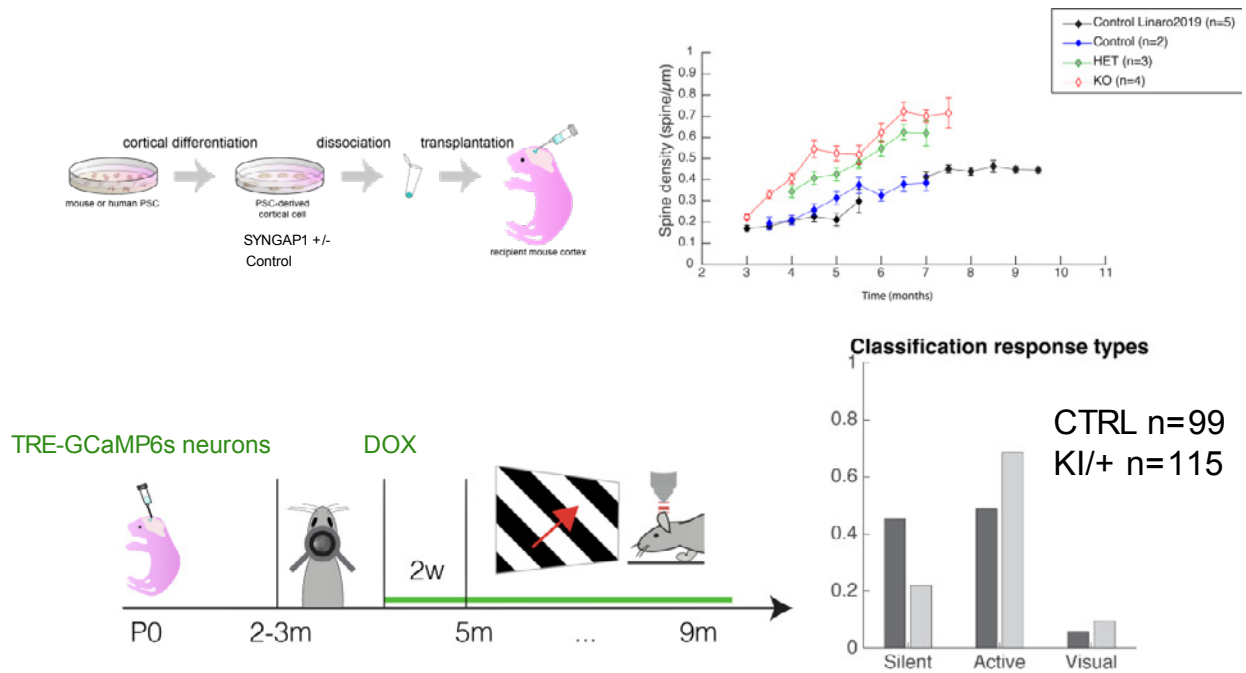


Figure 3: In vivo imaging of dendritic spines in xenotransplanted neurons reveals accelerated rates of dendritic spine outgrowth (upper panels) and precocious acquisition of basal and visually driven activity in SYNGAP1 +/- mutant neuron (lower panels).

Collectively, the experiments that we have performed so far thus enabled us to establish an in vivo neuronal model of SYNGAP1-related neurodevelopmental disorders. Moreover our data obtained so far all converge on a striking acceleration of synaptic maturation in the mutant neurons, thus revealing a first potential physio pathological mechanism of this disease.

We will now pursue these experiments, focusing on function of mutant cells and extending to MEF2C and other pathologies in which we suspect that NDD is caused by disrupted cortical neuronal development, including diseases striking mitochondria, which we recently found to be instructive for human cortical neurogenesis and rates of neuronal maturation ⁷⁸⁹.

3. References

1. Walsh, C. A., Morrow, E. M. & Rubenstein, J. L. Autism and brain development. *Cell* **135**, 396–400 (2008).
2. Zoghbi, H. Y. & Bear, M. F. Synaptic dysfunction in neurodevelopmental disorders associated with autism and intellectual disabilities. *Cold Spring Harb Perspect Biol* **4**, (2012).
3. Brennand, K. J. K. J. *et al.* Creating Patient-Specific Neural Cells for the In Vitro Study of Brain Disorders. *Stem Cell Reports* **5**, 933–945 (2015).
4. Espuny-Camacho, I. *et al.* Pyramidal Neurons Derived from Human Pluripotent Stem Cells Integrate Efficiently into Mouse Brain Circuits In Vivo. *Neuron* **77**, 440–456 (2013).
5. Linaro, D. *et al.* Xenotransplanted Human Cortical Neurons Reveal Species-Specific Development and Functional Integration into Mouse Visual Circuits. *Neuron* **104**, 972–986.e6 (2019).
6. Libé-philippot, B. & Vanderhaeghen, P. Cellular and Molecular Mechanisms Linking Human Cortical Development and Evolution. *Annu. Rev. Genet.* **55**, 1–46 (2021).
7. Iwata, R., Casimir, P. & Vanderhaeghen, P. Mitochondrial dynamics in postmitotic cells regulate neurogenesis. *Science (80-.)*. **862**, 858–862 (2020).
8. Iwata, R. & Vanderhaeghen, P. Regulatory Roles of Mitochondria and Metabolism in Neurogenesis. *Curr. Opin. Neurobiol.* **69**, 231–240 (2021).
9. Iwata, R. *et al.* Species-specific mitochondria dynamics and metabolism regulate the timing of neuronal development. *bioRxiv* <https://doi.org/10.1101/2021.12.27.474246>, (2021).

4. Publications in 2021 in the frame of GSKE

- Species-specific mitochondria dynamics and metabolism regulate the timing of neuronal development. Iwata, R., Casimir, P., Erkol, E., Boubakar, L., Planque, M., Ditkowska, M., Vints, K., Gaspariunaite, V., Bird, M., Corthout, N., Vermeersch, P., Davie, K., Gounko, V., Aerts, S., Ghesquière, B., Fendt, S-M, **Vanderhaeghen P.** *Science, in review. Biorxiv 2021* <https://doi.org/10.1101/2021.12.27.474246>.
- Cellular and molecular mechanisms linking human cortical development and evolution. Libé-Philippot B, **Vanderhaeghen P.** *Annu. Rev. Genetics.* 2021. 55:555-581.
- Regulatory Roles of Mitochondria and Metabolism in Neurogenesis. Iwata R, **Vanderhaeghen P.** *Curr Opin Neurobiol.* 2021; 69:231-240.
- Neuronal fate acquisition and specification: time for a change. Bonnefont J, **Vanderhaeghen P.** *Curr Opin Neurobiol.* 2021;66:195-20.



Geneeskundige Stichting Koningin Elisabeth
Fondation Médicale Reine Elisabeth
Königin-Elisabeth-Stiftung für Medizin
Queen Elisabeth Medical Foundation

Progress report of the
university research project of

Prof. dr. Thomas Voets (VIB)
Katholieke Universiteit Leuven (KU Leuven)

Prof. dr. Thomas Voets

Laboratory of Ion Channel Research
VIB-KU Leuven Center for Brain & Disease Research
KU Leuven, Department of Cellular and Molecular Medicine
Herestraat 49 bus 801
3000 Leuven
Tel: +32 16 33 02 17
Thomas.voets@kuleuven.vib.be

Table of contents

1. Background
2. Scientific objective
3. Results
 - Functional characterization and transcriptome analysis of cold-sensitive sensory neurons
 - Identification of candidate genes underlying cold responses in OCNs
 - Cold-mediated modulation of Asic ion channels
 - The impact of extracellular acidification on OCNs activity
4. Outlook and budget
5. Recent papers (published in 2020-21) mentioning financial support of GSKE
6. References

Unraveling the cellular and molecular basis of noxious cold sensing

1. Background

Noxious cold and noxious heat have detrimental effects on key biological macromolecules, and thus on the integrity of cells, tissues and organisms[1]. Thanks to the action of a subset of somatosensory neurons, mammals can swiftly detect noxiously cold or hot objects or environments. These temperature-sensitive nociceptor neurons become activated when the temperature at their free endings in the skin or mucosae reaches noxious levels, provoking acute pain and initiating avoidance reflexes[2].

In the last two decades, several ion channels of the transient receptor potential (TRP) superfamily have been put forward as key molecular sensors in somatosensory neurons, involved in various aspects of temperature sensing and pain[1-3]. In a recent key paper from our research group, with the support of the Queen Elisabeth Medical Foundation, we uncovered the molecular basis of noxious heat detection, by showing that acute heat-induced pain depends on three TRP channels (TRPV1, TRPM3 and TRPA1), acting as redundant heat sensors in nociceptor neurons[4]. We found that simultaneous elimination of all three TRP channels fully eliminates heat responses in isolated sensory neurons, and completely abolishes heat-induced pain responses in mice[4].

In contrast, the molecular basis of noxious cold sensing remains unresolved[1]. Several studies, including work from our research group, have revealed that TRPM8 and TRPA1 act as molecular cold sensors involved in different aspects of innocuous and noxious cold sensing[5-13]. However, a subset of sensory neurons remains cold sensitive after combined elimination of both channels, and *Trpm8^{-/-}/Trpa1^{-/-}* double knockout mice still exhibit a robust pain response to noxious cold[11, 14]. Thus, the cellular and molecular basis of noxious cold sensing remains essentially unknown[1]. The aim of the proposed research is therefore to unravel the cellular and molecular mechanisms underlying cold-induced pain, by identifying the mechanisms underlying TRPM8- and TRPA1-independent cold sensing.

Elucidating the basis of cold-induced pain not only addresses a fundamental question in sensory neurobiology, but may also have important medical applications. About one in five of adult Europeans suffer from moderate-to-severe chronic pain, and despite the fact that access to adequate pain management is considered a Fundamental Human Right[15], half of these chronic pain sufferers report inadequate pain control with available analgesic treatments[16, 17]. Cold allodynia, the condition where non-noxious cool stimuli evoke pain, is a frequent aspect of chronic pain and represents one of the hallmarks of neuropathic pain following nerve injury or chemotherapy[18]. Unfortunately, there are currently no safe and efficient therapies to treat cold allodynia. We anticipate that novel insights into the mechanisms of cold-induced pain may fuel the development of novel targeted pain therapies.

2. Scientific objective

In earlier work, we and others identified a subset sensory neurons exhibiting robust TRPM8- and TRPA1-independent Ca^{2+} -influx in response to cold[11, 19, 20]. As the origin of their cold sensitivity is unknown, we will name this subset of sensory neurons **Orphan Cold Neurons (OCNs)**. We hypothesize that these OCNs play a central role in cold pain, and express at least one type of cold sensor of unknown molecular identity. We intend to characterize these OCNs and identify the molecular basis of their cold sensitivity.

3. Results

3.1. Functional characterization and transcriptome analysis of cold-sensitive sensory neurons

A number of recent studies have reported RNA-seq-based single-cell transcriptome analyses of mouse DRG neurons, leading to hierarchical clustering of neurons into 11-18 subtypes[21-23]. However, how this transcriptome-based classification relates to the functional properties of sensory neurons is poorly understood. By performing Fura-2-based Ca^{2+} -imaging experiments followed by single-cell sequencing, we generated an approach that combines functional information with the cell's transcriptional fingerprint.

Our published and unpublished results indicate that approximately 8% of DRG neurons can be classified as M8-CNs and approximately 15% as A1-CNs; between 3 and 7% of all DRG neurons are OCNs[11]. In order to properly identify OCNs and exclude TRPA1 and TRPM8-cold mediated responses, we used *TRPA1*^{-/-} knockout mice and excluded all neurons that reacted to the cooling agent menthol (TRPM8 agonist). Therefore, all DRG neurons that responded to cooling but failed to react to menthol (200 μM) stimulation were identified as OCNs. Once we identified by Ca^{2+} -imaging all OCNs, menthol-sensitive neurons and neurons that did not respond to cooling, we individually harvested the neurons of interest. For this, we used microcapillary pipettes connected to a micromanipulator to aspirate single cells under visual control. Individually harvested neurons had their transcriptome profile unraveled by Smart-seq 2 technology. Smart-seq2 is the preferred approach as it provides good coverage of the transcriptome, including rarer transcripts and splice variants [24]. To date, we collected and fully sequenced a total of 46 cells (20 OCNs, 4 menthol sensitive cells and 22 cells that do not respond to cooling). An average of approximately 8.000 genes was identified per cell. The marker genes used to identify cell types were: neurons = *Rbfox3*, endothelial = *Cldn5*, macrophages = *Mrc1*, glia = *Mbp* and fibroblasts = *Mgp*. All the collected samples presented a high expression of the neuronal marker *Rbfox3* (Figure 1A), indicating that we successfully harvested sensory neurons. Some samples showed high expression of the glial cell marker *Mbp* (Figure 1A). DRGs contain a unique type of glial cells, known as satellite glial cells, which form a sheath around the cell body of DRG neurons (generally, one neuron is wrapped by several SGCs), which may explain the high expression of the glial marker in a few neuronal samples (Figure 1A-B).

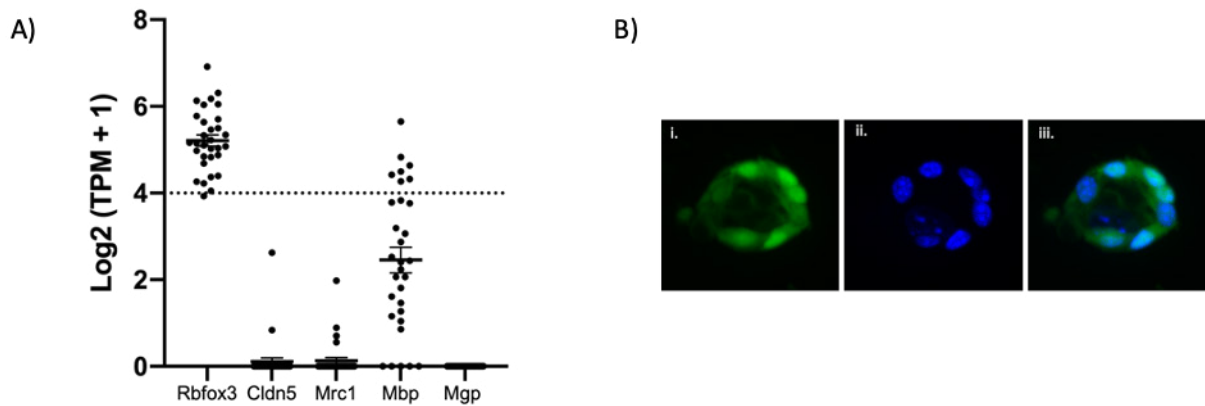


Figure 1: Cell subtype identification in DRG culture. (A) RNA seq data showing DRG cell subtype marker gene expression. Marker genes: *Rbfox3* = neurons, *Cldn5* = endothelial, *Mrc1* = macrophages, *Mbp* = glia and *Mgp* = fibroblasts. (B) Satellite glial cells wrapping DRG neurons in a standard DRG culture. Cells were loaded with the calcium indicator Fluo-4 AM (green) and cell nuclei were stained with Hoechst® 33342 dye (blue). Images were made using a confocal microscope. i. Fluo-4 AM, ii. Hoechst® 33342 and iii. overlay of the two channels.

The functional data obtained by Fura-2-based Ca^{2+} -imaging experiments indicate that an average of 8.5% of the measured sensory neurons (isolated from *TRPA1*^{-/-} knockout mice) are identified as OCNs (Figure 2A). In addition, there is a good correlation between our functional and transcriptome data (Figure 2B-C). The collected neurons that were sensitive to both menthol (TRPM8 agonist) and cooling stimulation turned out to have high expression levels of TRPM8 ion channels (Figure 2B-C). On the other hand, no reads corresponding to TRPM8 transcripts were identified in neurons that did not respond to menthol stimulation (Figure 2B-C).

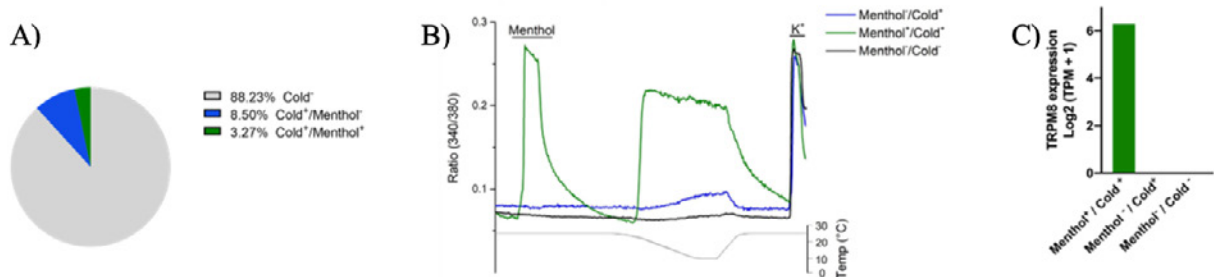


Figure 2: Functional and molecular characterization of DRG neurons. (A) Percentage of neurons that are not sensitive to cold (Cold⁻), neurons that are sensitive to cold and not sensitive to menthol (Cold⁺/Menthol⁻) and neurons that are sensitive to both cold and menthol (Cold⁺/Menthol⁺). (B) Ratiometric measurement of changes in intracellular Ca^{2+} in response to menthol (200 μ M) and cooling stimulation. The traces represent individual responses of 3 distinct neurons. (C) RNA seq data showing TRPM8 transcript expression levels of the cells functionally characterized in panel B. Gene expression is given as $\log_2(TPM+1)$.

3.2. Identification of candidate genes underlying cold responses in OCNs

For further characterization of OCNs and identification of genes that may underlie their cold sensitivity, we compared the transcriptomes of the identified OCNs and those from cells insensitive to cooling stimulation. Our data revealed that 315 genes are differentially expressed between the two groups of cells (Figure 3A). Of these 315 genes, 170 are significantly upregulated in OCNs and thus may contribute to their "orphan" cold sensitivity. Among the upregulated genes found in OCNs, 99 are identified as plasma membrane proteins (Figure 3B). As ion channels and membrane receptors represent prime candidate cold sensors, we will initially focus on genes that encode proteins with at least one transmembrane domain and select either proteins with unknown function or known ion channels. Among the plasma membrane candidates that are upregulated in OCNs, 7 are members of the G-protein coupled receptor family and 11 correspond to ion channels (Figure 3B-C). For example, these possible candidates include ion channels permeable for sodium, potassium and calcium ions (Figure 4).

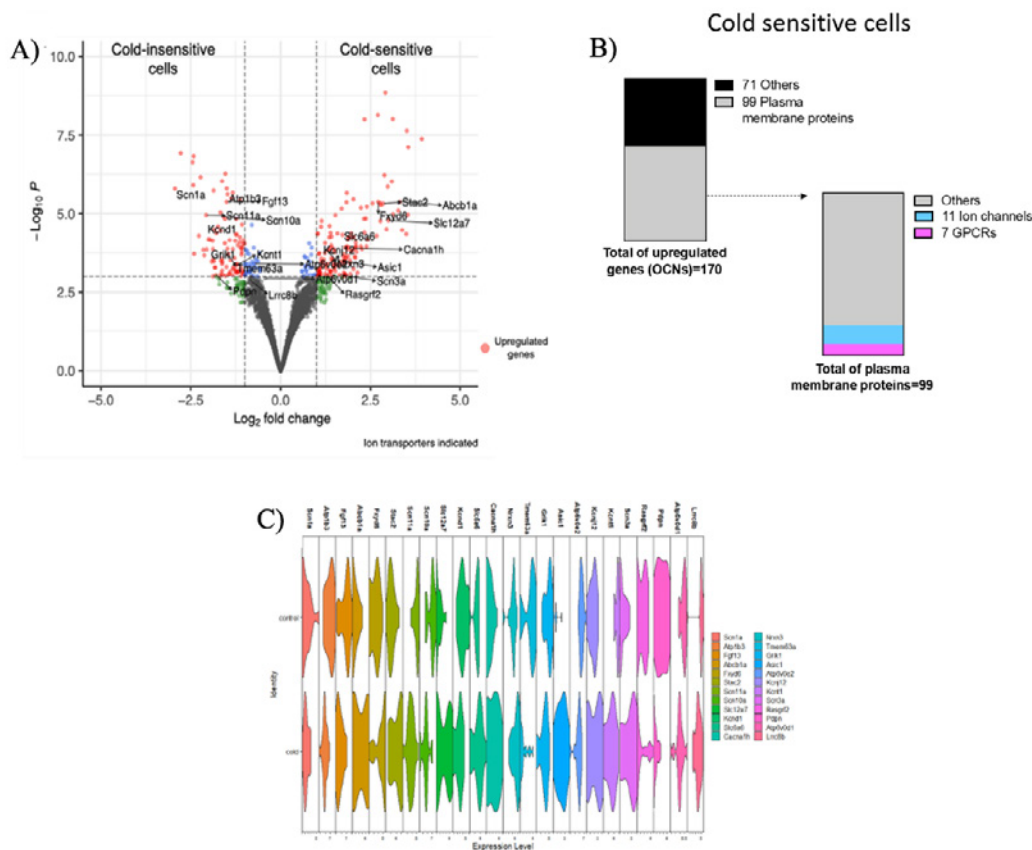


Figure 3: Gene expression analysis of scRNA-seq data. (A) Volcano plot displaying differentially expressed genes of cold-sensitive and insensitive cells. Genes with a P-value smaller than 0.05 and an absolute log (fold change) larger than 1 are considered significant. Upregulated genes in cold-sensitive and insensitive cells are colored in red. Significantly upregulated ion transporters are indicated. (B) General overview of the upregulated genes corresponding to proteins located at the plasma membrane. (C) Summary of the expression levels of ion channel transporters between the 2 groups: Control (cold-insensitive cells) and cold (cold-sensitive cells).

3.3. Cold-mediated modulation of Asic ion channels

Interestingly, our data suggest the acid-sensing ion channel (Asic1) as one of the top candidates for cold sensing in sensory neurons (Figure 4). These channels are members of the epithelial Na⁺ channel (ENaC)/degenerin (Deg) family. Asic channels are proton-gated cation channels widely expressed in the central and peripheral nervous systems. They are modulated by a broad range of pH ranges during physiological and pathological conditions. Asics are trimeric channels and their subunits are encoded by four genes: Asic1, Asic2, Asic3 and Asic4 [25].

We performed whole-cell patch-clamp recordings to investigate the effect of cold temperature on Asic1 channel kinetics. At pH 7.4, cold stimulation could not directly evoke any currents in HEK293T cells expressing Asic1 channels (data not shown). On the other hand, currents induced by low pH were tremendously potentiated at cold temperatures. Cold stimulation not only potentiates current amplitude but also slows channel desensitization (Fig. 5A-B). In order to confirm that the resulting H⁺-gated currents at low temperatures were induced via Asic1 activation, we tested whether the Asic channel inhibitor (amiloride) could impair channel activation. Amiloride could fully inhibit H⁺-gated currents potentiated by cold temperature (Figure 5C).

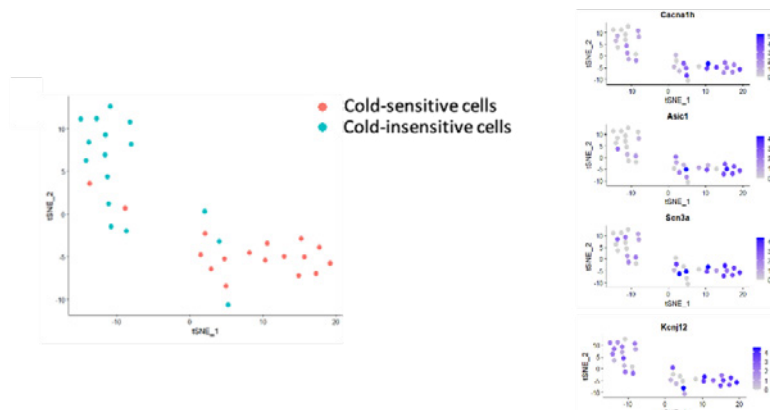


Figure 4: t-SNE plot of the 2 distinct cell clusters: Cold-sensitive and Cold-insensitive cells. In detail: Expression levels of the upregulated calcium (Cacna1h), Asic (Asic1), sodium (Scn3a) and potassium (Kcnj12) ion channels found in OCNs indicated per cell.

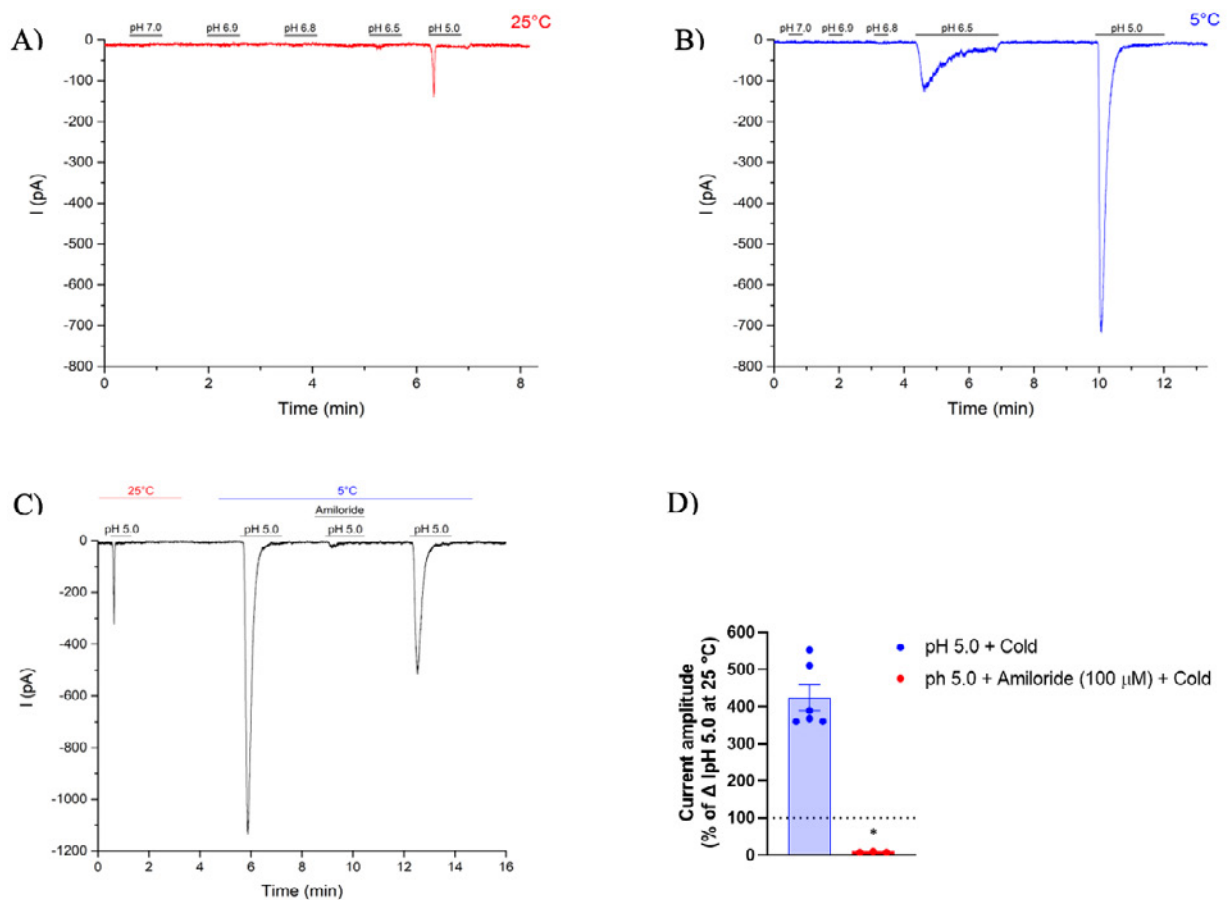


Figure 5: Cold-induced potentiation of H⁺-gated currents of Asic1 channels. Representative currents evoked by stepping from pH 7 to pH 5 solutions recorded from HEK293T expressing Asic1 ion channels at 25 °C (A) and 5 °C (B). Effect of the Asic inhibitor amiloride on potentiated H⁺-gated currents at cold temperature (C-D). (D) Each point represents mean ± S.E.M. from 3-6 cells. *p < 0.05 with Student's two-tailed unpaired t-test.

Since Asic3 is primarily and widely expressed in sensory neurons, we decided to test whether this ion channel is also modulated by cold stimulus [26, 27]. Similar to Asic1, cold temperatures do not directly induce Asic3-mediated currents. However, low temperature potentiates both the outward and inward Asic3 H⁺-gated currents (Figure 6A-B). Additionally, cold stimulus significantly potentiates Asic3 currents at different pH ranges (Figure 6C). The potentiation of Asic H⁺-gated currents by cold has already been described in the literature [28]. However, the gating mechanisms modulated by temperature are not fully understood. Likewise, the impact of temperature on Asic channels in pathological conditions where there is extracellular acidification, for example, during inflammation, has never been explored.

Although amiloride is a well-known Asic inhibitor, it has a paradoxical effect on Asic3 ion channels. This compound blocks the activation of the channel at certain pH ranges. However, amiloride induces a stimulatory effect at a more modest pH fluctuation (such as pH 7). Besides that, at higher concentrations, amiloride induces a sustained current at neutral pH [29]. The way by which amiloride modulates the Asic3 channel has been proven to be quite complex. It has been demonstrated that this compound binds to a non-proton ligand-sensing domain of the channel to induce the observed sustained currents [30, 31]. However, it has been suggested that amiloride may have multiple distinct binding sites that may impact channels gating mechanisms in different ways [29]. Therefore, we wanted to investigate whether cold stimulus would modulate amiloride-induced currents. Our results suggest that cold temperature potentiates the outward amiloride-induced current. Interestingly, holding the cell at negative voltages induced a voltage-dependent component to the amiloride-induced current. The mechanism by which temperature influences Asic activity stimulated by non-proton ligands is yet to be investigated. The impact of that on cell physiology should also be further studied.

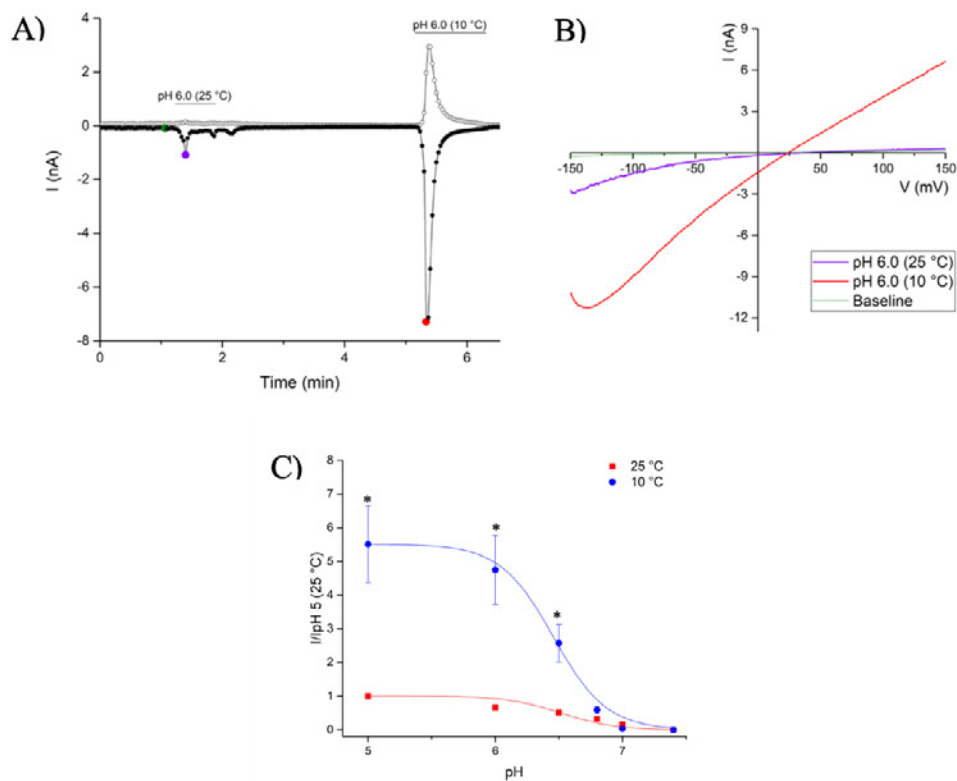


Figure 6: Cold-induced potentiation of H⁺-gated currents of Asic3 channels. (A) Time course of whole-cell patch-clamp recording at holding potentials of +80 mV (open circles) and -80 mV (closed circles) of Asic3 expressed in HEK293T cells during application of pH 6 solution at 25 °C and at 10 °C. (B) Current-voltage relationship (I-V) of time points indicated in panel (A). (C) pH dose-response curves were measured at 25 °C and 10 °C (whole-cell patch-clamp recording at holding potential of -60 mV). Each point represents mean ± S.E.M. from 5-7 cells. Two-way ANOVA with Sidák's multiple comparisons test showing *p < 0.05.

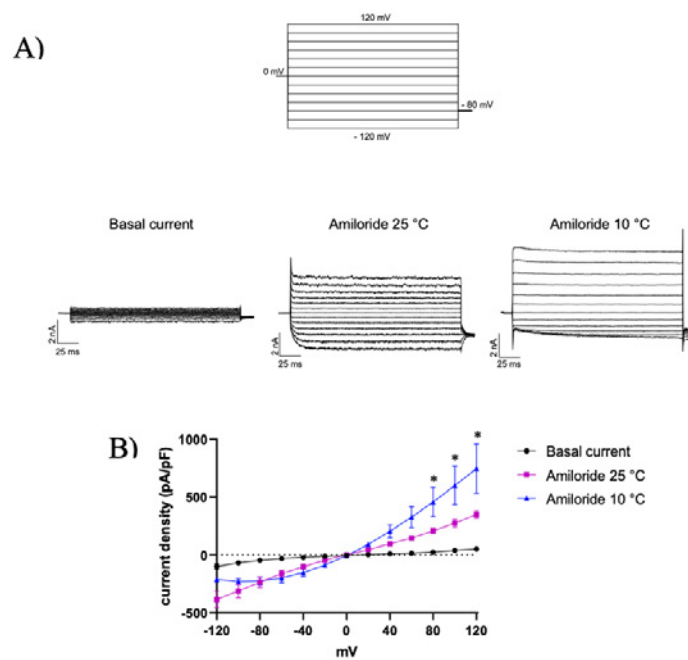


Figure 7: Amiloride-induced currents of Asic3 channels. (A) Representative current traces of HEK293T expressing Asic3 in response to amiloride (100 μ M) at voltage steps measured at 25 $^{\circ}$ C and 10 $^{\circ}$ C. (B) Current-voltage relationship of Asic3 channels in the presence of amiloride (100 μ M) at 25 $^{\circ}$ C and 10 $^{\circ}$ C. Each point represents mean \pm S.E.M. from 2 cells. Two-way ANOVA with Tukey's multiple comparisons showing * $p < 0.05$ for amiloride 25 $^{\circ}$ C vs. amiloride 10 $^{\circ}$ C

3.4. The impact of extracellular acidification on OCNs activity

Protons positively or negatively modulate a significant number of ion channels and receptors. For example, while low pH may stimulate the heat sensor TRPV1, extracellular acidification may suppress currents of the cold sensor TRPM8 [32]. Therefore, modulation of OCNs activity by low pH is an interesting tool to shed light on the functional characteristics of the cold sensors present in these cells. In addition to that, our data suggest that OCNs express proton-gated channels (Asic1) and that temperature greatly influences this ion channel kinetics. Therefore, we tested whether acidification of the extracellular environment would impact OCNs cold-mediated activity. Three different OCN profiles were identified (Figure 8A). Surprisingly, most OCNs (~80%) were inhibited by low pH, around 14% were not modulated by extracellular acidification and only ~7% were stimulated by protons. These data suggest that OCNs comprise a heterogeneous population and that more than one cold sensor may be present in these cells. To further look into OCNs transcriptome information, we have now collected 123 new samples: 11 single cells that respond to menthol and cold stimulation, 48 cold insensitive cells and a total of 64 OCNs. We hope that these additional samples will provide us with better insights into the molecular fingerprint of these poorly understood temperature-sensitive sensory neurons.

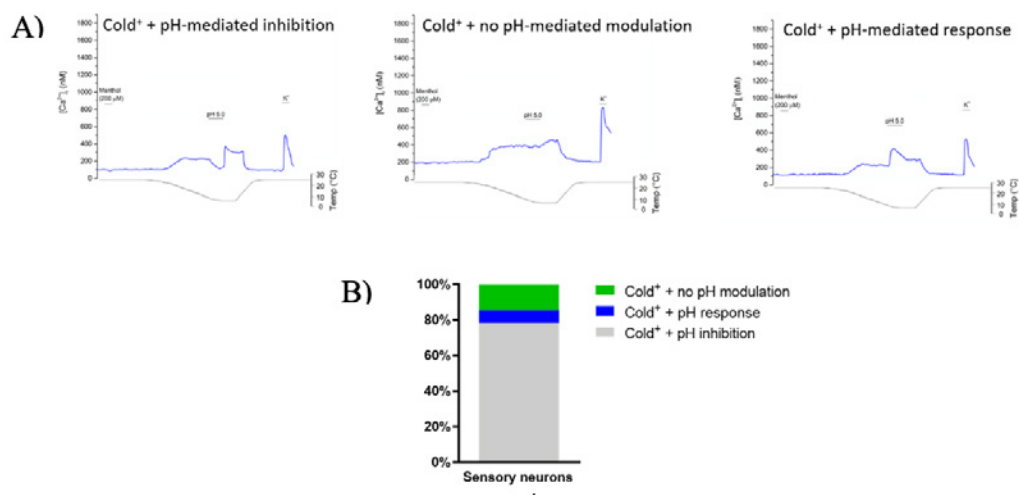


Figure 8: Effect of low pH on cold sensitivity of sensory neurons. (A) Ratiometric measurement of changes in intracellular Ca^{2+} of sensory neurons in response to cooling stimulation and simultaneous application of pH 5.0 solution. (B) Percentage of cold-sensitive neurons corresponding to each profile identified in panel (A).

4. Outlook and budget

With the financial support of the GSKE, we have been able to establish an approach to obtain a detailed transcriptome analysis of functionally characterized sensory neurons and provide part of the salary of a dedicated postdoctoral researcher, Dr. Ana Freitas. This has allowed us to identify a set of candidate genes that may contribute to "orphan" cold responses. We are currently refining the candidate selection based on functional characterization and single-cell sequencing of new samples. Additionally, we are conducting further electrophysiological characterization of OCNs, combining Fura-2-based Ca^{2+} -imaging experiments with whole-cell patch-clamp recordings.

Interestingly, amongst the top candidates is ASIC1, well known as an acid-activated ion channel. Our preliminary data suggest that it may contribute to cold responses in sensory neurons. ASIC1-deficient mice are available commercially (The Jackson Laboratory; strain 013733), so we are currently looking to purchase a breeder pair, which we can cross to TRPA1 and TRPM8 deficient mice that are already available in our team. This will allow us to directly test whether ASIC1 contributes cold-induced pain. The additional cost associated with purchasing and breeding these lines amounts to 20 kEuro.

5. Recent papers (published in 2020-22) mentioning financial support of GSKE

- M. Vanneste, M. Mulier, A.C.N. Freitas, N. Van Ranst, A. Kerstens, **T. Voets**, W. Everaerts. TRPM3 Is Expressed in Afferent Bladder Neurons and Is Upregulated during Bladder Inflammation. *Int J Mol Sci.* (2021)
- A.C.N. Freitas, **T. Voets**. Why the emperor penguin reigns where elephants shiver. *Cell Calcium* 91 (2020) 102263.
- K. Held, V.D. Aloï, A.C.N. Freitas, A. Janssens, A. Segal, J. Przibilla, S.E. Philipp, Y.T. Wang, **T. Voets**, J. Vriens. Pharmacological properties of TRPM3 isoforms are determined by the length of the pore loop. *Br J Pharmacol* (2020).
- B. Kelemen, S. Pinto, N. Kim, E. Lisztes, M. Hanyicska, A. Vladar, A. Olah, Z. Penzes, B. Shu, J. Vriens, T. Biro, T. Rohacs, **T. Voets***, B.I. Toth, The TRPM3 ion channel mediates nociception but not itch evoked by endogenous pruritogenic mediators. *Biochem Pharmacol* 183 (2021) 114310.
- M. Mulier, N. Van Ranst, N. Corthout, S. Munck, P. Vanden Berghe, J. Vriens, **T. Voets***, L. Moilanen, Upregulation of TRPM3 in nociceptors innervating inflamed tissue. *Elife* 9 (2020).
- M. Mulier, I. Vandewauw, J. Vriens, **T. Voets**, Reply to: Heat detection by the TRPM2 ion channel. *Nature* 584(7820) (2020) E13-E15.
- E. Persoons, K. De Clercq, C. Van den Eynde, S. Pinto, K. Luyten, R. Van Bree, C. Tomassetti, **T. Voets**, J. Vriens, Mimicking Sampson's Retrograde Menstrual Theory in Rats: A New Rat Model for Ongoing Endometriosis-Associated Pain. *Int J Mol Sci* 21(7) (2020).
- L. Vangeel, M. Benoit, Y. Miron, P.E. Miller, K. De Clercq, P. Chaltin, C. Verfaillie, J. Vriens, **T. Voets**. Functional expression and pharmacological modulation of TRPM3 in human sensory neurons. *Br J Pharmacol* 177(12) (2020) 2683-2695.
- (*Corresponding and shared last author)

6. References

1. Viana, F. and T. Voets, *Heat Pain and Cold Pain*, in *The Oxford Handbook of the Neurobiology of Pain*, J.N. Wood, Editor. 2019, Oxford University Press: Oxford.
2. Vriens, J., B. Nilius, and T. Voets, *Peripheral thermosensation in mammals*. *Nat Rev Neurosci*, 2014. **15**(9): p. 573-89.
3. Caterina, M.J., et al., *The capsaicin receptor: a heat-activated ion channel in the pain pathway*. *Nature*, 1997. **389**(6653): p. 816-24.
4. Vandewauw, I., et al., *A TRP channel trio mediates acute noxious heat sensing*. *Nature*, 2018. **555**(7698): p. 662-666.
5. McKemy, D.D., W.M. Neuhausser, and D. Julius, *Identification of a cold receptor reveals a general role for TRP channels in thermosensation*. *Nature*, 2002. **416**(6876): p. 52-8.
6. Peier, A.M., et al., *A TRP channel that senses cold stimuli and menthol*. *Cell*, 2002. **108**(5): p. 705-15.
7. Obata, K., et al., *TRPA1 induced in sensory neurons contributes to cold hyperalgesia after inflammation and nerve injury*. *J Clin Invest*, 2005. **115**(9): p. 2393-401.
8. Bautista, D.M., et al., *TRPA1 mediates the inflammatory actions of environmental irritants and proalgesic agents*. *Cell*, 2006. **124**(6): p. 1269-82.
9. Colburn, R.W., et al., *Attenuated cold sensitivity in TRPM8 null mice*. *Neuron*, 2007. **54**(3): p. 379-86.
10. Dhaka, A., et al., *TRPM8 is required for cold sensation in mice*. *Neuron*, 2007. **54**(3): p. 371-8.
11. Karashima, Y., et al., *TRPA1 acts as a cold sensor in vitro and in vivo*. *Proc Natl Acad Sci U S A*, 2009. **106**(4): p. 1273-8.
12. Gentry, C., et al., *The roles of iPLA2, TRPM8 and TRPA1 in chemically induced cold hypersensitivity*. *Mol Pain*, 2010. **6**: p. 4.
13. Uvin, P., et al., *Essential role of transient receptor potential M8 (TRPM8) in a model of acute cold-induced urinary urgency*. *Eur Urol*, 2015. **68**(4): p. 655-61.
14. Knowlton, W.M., et al., *TRPM8, but not TRPA1, is required for neural and behavioral responses to acute noxious cold temperatures and cold-mimetics in vivo*. *Pain*, 2010. **150**(2): p. 340-50.
15. Lohman, D., R. Schleifer, and J.J. Amon, *Access to pain treatment as a human right*. *BMC Med*, 2010. **8**: p. 8.
16. Reid, K.J., et al., *Epidemiology of chronic non-cancer pain in Europe: narrative review of prevalence, pain treatments and pain impact*. *Curr Med Res Opin*, 2011. **27**(2): p. 449-62.
17. Colloca, L., et al., *Neuropathic pain*. *Nat Rev Dis Primers*, 2017. **3**: p. 17002.
18. Jensen, T.S. and N.B. Finnerup, *Allodynia and hyperalgesia in neuropathic pain: clinical manifestations and mechanisms*. *Lancet Neurol*, 2014. **13**(9): p. 924-35.
19. Munns, C., M. AlQatari, and M. Koltzenburg, *Many cold sensitive peripheral neurons of the mouse do not express TRPM8 or TRPA1*. *Cell Calcium*, 2007. **41**(4): p. 331-42.

20. Memon, T., et al., *TRPA1 expression levels and excitability brake by KV channels influence cold sensitivity of TRPA1-expressing neurons*. Neuroscience, 2017. **353**: p. 76-86.
21. Li, C.L., et al., *Somatosensory neuron types identified by high-coverage single-cell RNA-sequencing and functional heterogeneity*. Cell Res, 2016. **26**(8): p. 967.
22. Usoskin, D., et al., *Unbiased classification of sensory neuron types by large-scale single-cell RNA sequencing*. Nat Neurosci, 2015. **18**(1): p. 145-53.
23. Zeisel, A., et al., *Molecular Architecture of the Mouse Nervous System*. Cell, 2018. **174**(4): p. 999-1014 e22.
24. Picelli, S., et al., *Full-length RNA-seq from single cells using Smart-seq2*. Nat Protoc, 2014. **9**(1): p. 171-81.
25. Carattino, M.D. and N. Montalbetti, *Acid-sensing ion channels in sensory signaling*. Am J Physiol Renal Physiol, 2020. **318**(3): p. F531-F543.
26. Babinski, K., K.T. Le, and P. Seguela, *Molecular cloning and regional distribution of a human proton receptor subunit with biphasic functional properties*. J Neurochem, 1999. **72**(1): p. 51-7.
27. Waldmann, R., et al., *Molecular cloning of a non-inactivating proton-gated Na⁺ channel specific for sensory neurons*. J Biol Chem, 1997. **272**(34): p. 20975-8.
28. Askwith, C.C., et al., *DEG/ENaC ion channels involved in sensory transduction are modulated by cold temperature*. Proc Natl Acad Sci U S A, 2001. **98**(11): p. 6459-63.
29. Matasic, D.S., et al., *Paradoxical Potentiation of Acid-Sensing Ion Channel 3 (ASIC3) by Amiloride via Multiple Mechanisms and Sites Within the Channel*. Front Physiol, 2021. **12**: p. 750696.
30. Li, W.G., et al., *Nonproton ligand sensing domain is required for paradoxical stimulation of acid-sensing ion channel 3 (ASIC3) channels by amiloride*. J Biol Chem, 2011. **286**(49): p. 42635-42646.
31. Yu, Y., et al., *A non-proton ligand sensor in the acid-sensing ion channel*. Neuron, 2010. **68**(1): p. 61-72.
32. Behrendt, H.J., et al., *Characterization of the mouse cold-menthol receptor TRPM8 and vanilloid receptor type-1 VR1 using a fluorometric imaging plate reader (FLIPR) assay*. Br J Pharmacol, 2004. **141**(4): p. 737-45.



Geneeskundige Stichting Koningin Elisabeth
Fondation Médicale Reine Elisabeth
Königin-Elisabeth-Stiftung für Medizin
Queen Elisabeth Medical Foundation

Progress report of the
university research project of

Prof. dr. Sarah Weckhuysen, MD, PhD
Universiteit Antwerpen (UAntwerpen)

Prof. dr. Sarah Weckhuysen, MD, PhD

Applied&Translational Neurogenomics Group
VIB-UAntwerp Center for Molecular Neurology
UAntwerp-CDE
Parking P4, Building V
Universiteitsplein 1, 2610 Antwerpen
Belgium
uantwerpen.vib.be

Neurology Department
Antwerp University Hospital
Drie Eikenstraat 655, 2650 Edegem
Belgium
www.uza.be/neurologie

Study and targeted treatment development for epileptic encephalopathies using 2D and 3D human induced pluripotent stem cell-derived neuronal cultures

1. Background

The **developmental and epileptic encephalopathies (DEEs)** are a debilitating subgroup of the epilepsies, characterized by frequent and often treatment resistant seizures with early onset, and developmental delay. The majority of patients have a genetic cause. Current treatments for DEE focus on seizure control using anti-epileptic drugs. However, even though some patients do become seizure free, most patients with genetic DEEs still suffer from severe developmental delay. Many lines of evidence suggest that the developmental and the epileptic features are both, at least partially, an independent result of the underlying genetic defect. There is thus a strong need for new therapies that not only treat seizures, but also target the developmental aspects of DEEs.

The prototype and most common genetic form of neonatal DEE, illustrating many of the characteristics of genetic DEEs, is **KCNQ2 encephalopathy (KCNQ2-E)**. This disorder, described by our group in 2012, is caused by **de novo missense mutations** in the gene *KCNQ2* encoding the Kv7.2 subunit of the tetrameric M channel, a voltage gated potassium channel that is widely expressed throughout the brain, in excitatory and inhibitory neurons at the axon initial segment (AIS), nodes of Ranvier, presynaptic terminals and the soma, as well as in astrocytes. The M-current is responsible for repolarization of the membrane, dampening of repetitive firing and **controlling neuronal excitability**. Both a severe lack and excess of channel function can result in the development of KCNQ-E, due to heterozygous dominant negative or gain of function mutations respectively. Seizures in children with KCNQ-E often respond poorly to anti-epileptic drugs, and more importantly, therapies for the developmental problems are currently unavailable.

With the financial support of the GSKE, we are developing human induced Pluripotent Stem Cell (hiPSC)-derived neuronal cultures starting from patient peripheral blood mononuclear cells, as a model of KCNQ2-E, and perform multimodal characterization of these cultures using electrophysiology and (high-content) microscopy. We are now finalizing the characterization of the model, and in 2022 will use them for drug screenings and to provide proof-of-concept for mutant allele silencing as a treatment strategy for KCNQ2-E, using antisense oligonucleotides as a therapeutic tool.

2. Progress made in 2021

2.1. Generation of an isogenic control of the R201C line

In 2020, we had already generated iPSC lines of 7 patients, a healthy sibling, and one isogenic control. As isogenic controls are preferred because of the identical genetic background, we had asked a service facility to generate one additional isogenic control of another patient line. They however were not successful, so we set up experiments to generate one ourselves, using the novel Crispr prime editing (PE) technology. This technique has shown to have a significant decreased risk of Off Target effects. We inserted the PE construct in the cells using nucleofection, with 60% transfection efficiency. To increase editing efficiency, we isolated the GFP positive population with the MaqSQuant Tyto cell sorter. Sanger sequencing of cell populations with high GFP signal showed a 40% editing efficiency.

The high GFP pool was selected to perform low density seeding for subcloning. Currently, we are expanding the clones for freezing and DNA isolation. The correction will be validated using sanger sequencing, additionally, corrected clones will be subjected to CNV analysis, whole exome sequencing and pluripotency marker expression to verify the absence of abnormalities.

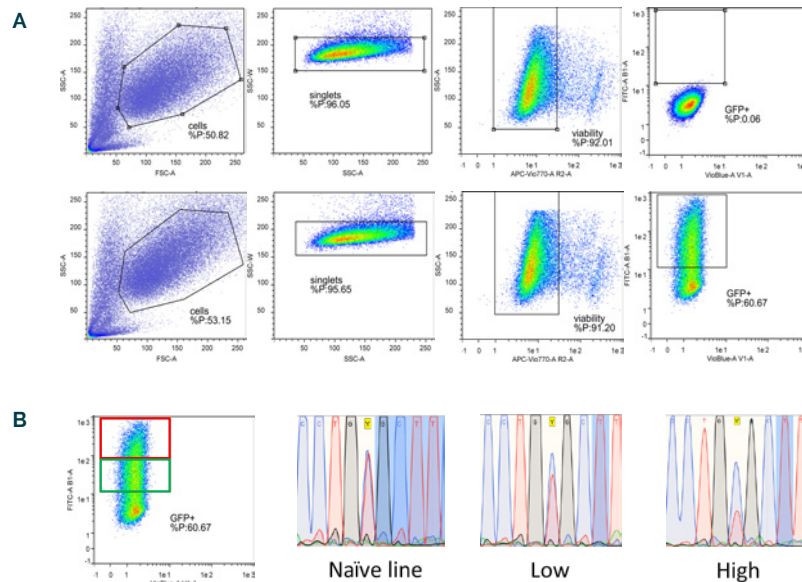


Figure1: Increasing edit efficiency via FACS sorting via GFP positive population. (A) Gating strategy to analyze GFP positive signal in iPSC. Top, negative control without construct shows no GFP signal, bottom, nucleofected iPSCs with the PE2-GFP construct shows ~60% GFP positive cells. **(B)** left, Nucleofected iPSC cells were sorted based on high or low GFP signal. Right, Sanger traces show higher edit efficiency in high GFP+ population compared to low GFP+ population.

2.2. Morphological characterization of iPSC-derived neurons

a. The axonal initial segment

The axonal initial segment (AIS) has the ability to change its length, as well as its distance to the soma as a response to hyperexcitability. To investigate if this is also the case for in our mutant lines, we stained 4 week old cultures using AnkG and MAP2. We optimized a pipeline in ImageJ to detect the AIS and calculate its length automatically. Preliminary analysis of a selection of lines showed an increased AIS length for only one patient line. The analysis to calculate distance between AIS and soma is however still ongoing.

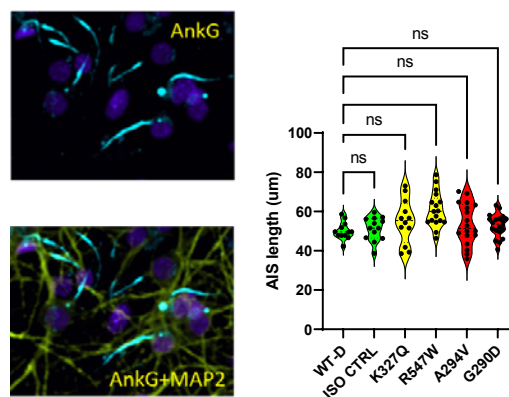


Figure 2: Length measurements of the AIS in iPSC-derived neuronal cultures. Left, Close up of AnkerinG (light blue) and MAP2 (yellow) staining in week 4 neuronal culture. Right, Average length of AIS in healthy and mutant lines.

b. Network morphology

Four week old neuronal cultures were morphologically characterized using a high-throughput microscopy pipeline optimized by the group of Prof. W. De Vos at the University of Antwerp. cultures are immunocytochemically labeled with neuronal specific pre- and post-synaptic markers Bassoon and Homer, and dendrite marker MAP2 (as the mCherry signal faints after PFA fixation). Confocal images are acquired with an automated Opera Phenix High Content Screening System (PerkinElmer) using a 40x water immersion lens (numerical aperture 1.1), enabling the fast generation of high-quality data. The images are processed and analyzed in using the Acapella® software. The strength of this approach lies in the fact that it can account for a number of potential sources of bias. For example, differences in the number of synapses could have many origins such as alterations in cell density, dendrite density or pre- and/or post-synaptic density.

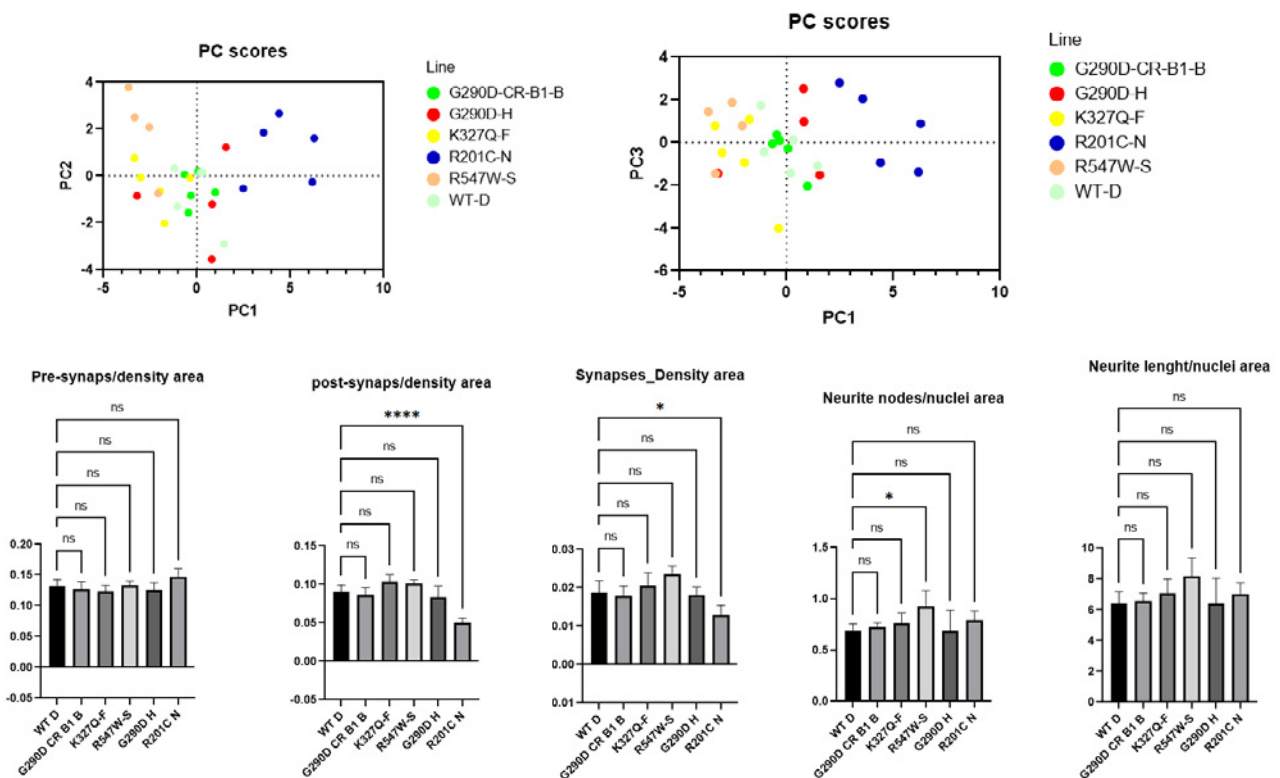


Figure 3: Morphological profile of KCNQ2-E iPSC derived neurons at week 4. Top, Principal component of all parameters corrected for total neuronal area in healthy controls and patient samples. Bottom, A selection of the descriptors for the dendrite network showing significant differences in GOF-R201C line and BFNE-R547W line. The preliminary data shown is from one differentiation only.

Principal component analysis (PCA) demonstrates that the control lines cluster together (WT-D and G290D-CR-B1-B). Furthermore GOF-R201C and BFNE-R547W cluster separate from the control lines. Seeding densities for this experiment were not optimal. More replicates are being performed to evaluate if morphological differences are present and can be used as a read out for the drug screening.

2.3. Electrophysiological characterization of iPSC-derived neurons

a. Microelectrode array (MEA)

Over the last year we have been optimizing the MEA plate preparation and seeding of the neurons. One of the challenges of working with CMOS-MEA systems is the hydrophobicity of the MEA chip where the cultures are seeded on. To have a neuronal culture attach to the surface, the chip needs to undergo several steps to make the surface attractive for neurons to attach on it. The conditions tested in the last year contain;

- Plasma cleaning
- Different concentration of PEI coating
- Different laminins and laminin concentration
- Seeding of astrocytes before neurons vs neurons before astrocytes
- Preconditioning the plate with Tergazyme, complete media or a combination.

Currently, we have found a successful combination, although replicates will have to confirm our observations. With the successful plate, we recorded 6 neuronal cultures (WT, isogenic ctrl, DN-A294V, DN-G290D, GOF-R201C, GOF-R201H) every week for 10 minutes, for 5 weeks long. Figure 3, showing the activity scans of the 6 well at DIV35, demonstrates that the neuronal culture were still attach and active at this timepoint.

Preliminary data also showed unexpected variability between 10 min recordings on the similar day, therefore a 2h recording was performed at week5 (DIV35). This recording showed phasic behavior in most of the lines, explaining non-consistent results during 10 min recordings.

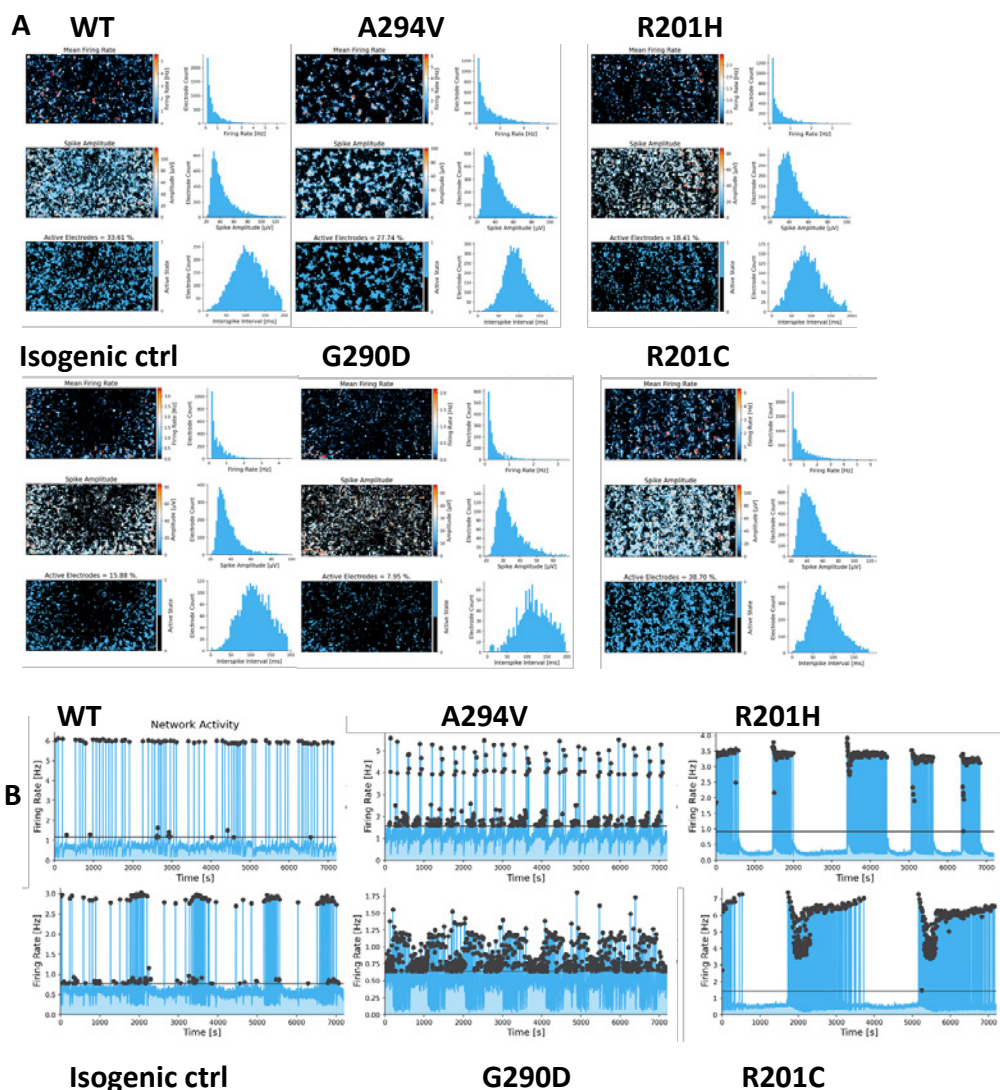


Figure 4: Network activity of 35DIV iPSC-derived neuronal cultures. (A) Activity scan of cMOS-MEA showing localization of the neuronal cultures based on spike amplitude and frequency. Histograms shows the firing rate, spike amplitude and interspike interval of the different lines. (B) 2h long Network scans show phasic behavior in most of the lines.

b. Calcium imaging

Given the initial difficulties with MEA seeding, we also started optimizing fluo4AM calcium imaging experiments as an extra electrophysiological read out. To stimulate neuronal bursting activity we add 10uM of Forskolin, a known compound to increase cAMP in the cell with synchronous bursting of the network as a result. Preliminary data shows significant hyperactive bursting shortly after stimulation in the DN lines vs the control, whereas the BFNE lines do not.

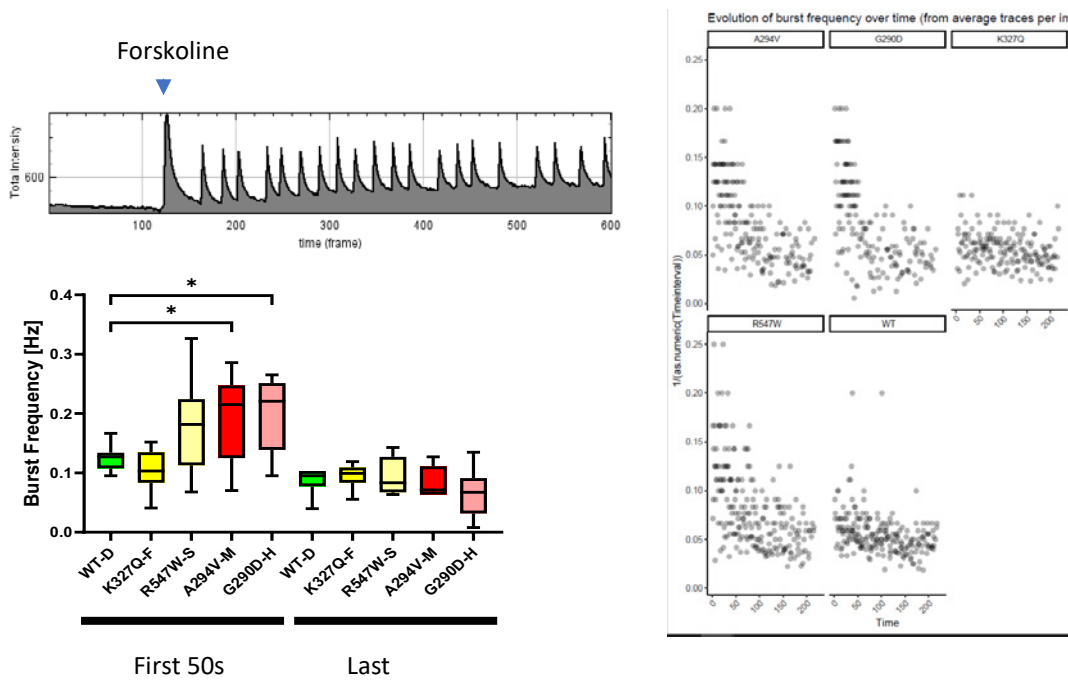


Figure 5: Ca^{2+} -traces of iPSC-derived neuronal cultures. Left top, total fluorescent signal over time shows no network activity before forskolin stimulation, and synchronous, repetitive bursting after stimulation. Right, Overview of burst frequency overtime for all the neuronal cultures. Left bottom, separating burst frequency in early phase and a late phase, demonstrates significant hyperactivity in the early phase for the DN lines vs the control.

3. Additional funding acquired

The GSKE funding allowed us to generate the necessary preliminary data and expertise (as described above) to acquire additional funding for the work on neurodevelopmental and epileptic encephalopathies in our research group. As already mentioned in our previous project report, in 2021 we received funding from the European EJP-RD program to coordinate the international "TreatKCNQ" project. This allowed us among other to recruit a new bright Canadian postdoc (Mark Kaji) who will help us to expand our work with iPSC derived neuronal models. In 2021 we also received project funding from FWO to use iPSC derived neuronal cultures to better understand the mechanisms of KCNQ2 related epilepsies. In addition, in December 2021 we received the good news that we were granted a second FWO project to support our research line that uses advanced genomics techniques to unravel the genetics of the developmental and epileptic encephalopathies. Also in this project, we will use iPSC derived neuronal cultures to validate genetic findings. So also here, the expertise we established with the help of GSKE was instrumental in receiving this funding.

4. Publications mentioning GSKE

Submitted to EBioMedicine: **"KCNQ2 R144 variants cause ID with language impairment and autistic features through a gain-of-function mechanism"** Francesco Miceli, PhD, Charissa Millevert, MD, Maria Virginia Soldovieri, PhD, Ilaria Mosca, PhD, Paolo Ambrosino, PhD, Lidia Carotenuto, MD, PhD, Dewi Schrader, MD, Hyun Kyung Lee, PhD, James Riviello, MD, William Hong, MD, Sarah Risen, MD, Lisa Emrick, MD, Hitha Amin, MD, Dorothée Ville, MD, Patrick Edery, MD, Julitta de Bellescize, MD, Vincent Michaud, MD, Julien Van-Gils, MD, Cyril Goizet, MD, PhD, Marjolein H. Willemsen, MD, PhD, Tjitske Kleefstra, MD, PhD, Rikke S Møller, PhD, Allan Bayat, MD, Orrin Devinsky, MD, Tristan Sands, MD, PhD, G. Christoph Korenke, MD, Gerhard Kluger, MD, Heather C. Mefford, MD, PhD, Eva Brilstra, MD, PhD, Gaetan Lesca, MD, PhD, Mathieu Milh, MD, PhD, Edward C. Cooper, MD, PhD, Maurizio Tagliatela, MD, PhD, Sarah Weckhuysen, MD, PhD



Geneeskundige Stichting Koningin Elisabeth
Fondation Médicale Reine Elisabeth
Königin-Elisabeth-Stiftung für Medizin
Queen Elisabeth Medical Foundation

Projecten jonge onderzoekers
2020-2022 gefinancierd door de G.S.K.E.

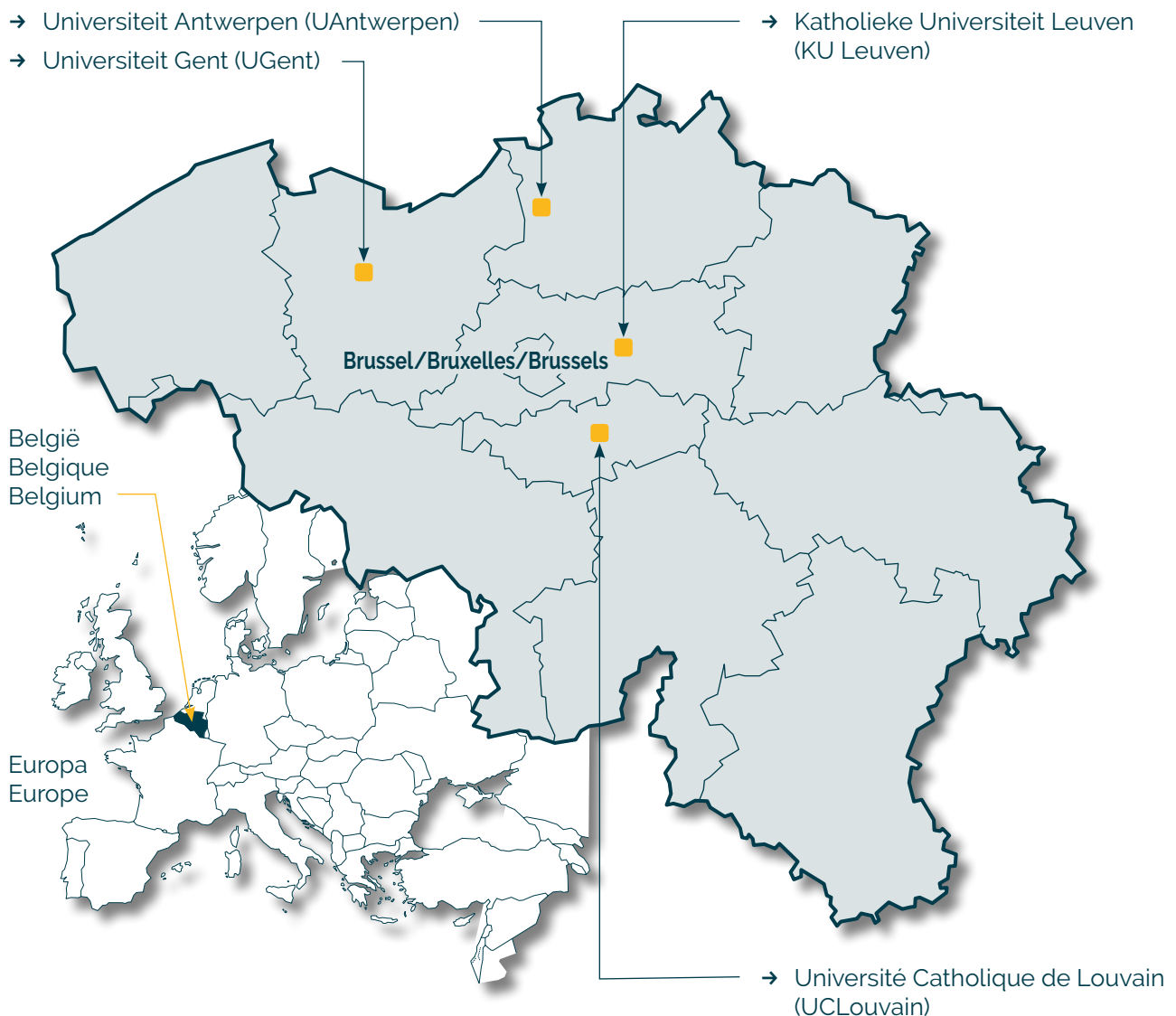
Projets de recherche de jeunes chercheurs
2020-2022 subventionnés par la F.M.R.E.

Research projects of young researchers
2020-2022 funded by the Q.E.M.F.

Universiteiten met onderzoeksprogramma's die gesteund worden door de G.S.K.E.

Universités ayant des programmes de recherche subventionnés par la F.M.R.E.

Universities having research programs supported by the Q.E.M.F.

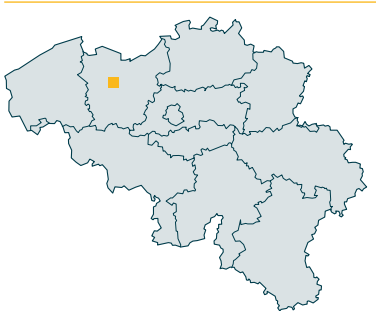


Projecten jonge onderzoekers 2020-2022 gefinancierd door de G.S.K.E.

Projets de recherche de jeunes chercheurs 2020-2022 subventionnés par la F.M.R.E.

Research projects of young researchers 2020-2022 funded by the Q.E.M.F.

UGent



Dr. Lars Emil Larsen, PhD

Closed loop precision therapy for epilepsy using photopharmacology

Prof. dr. Evelien Carrette (UZ Gent)

Novel interventions for patients with drug resistant epilepsy and cognitive decline: neuromodulatory effects of combined transcutaneous vagal nerve stimulation and cognitive therapy

UAntwerpen



Eline Wauters, PhD (VIB)

Onset age variability in GRN-associated frontotemporal lobar degeneration: identification of a functional onset age modifier

KU Leuven



Dr. Valerie Uytterhoeven

Molecular mechanisms and inducers of chaperone mediated Tau autophagy in Alzheimer's Disease

Aya Takeoka, PhD (IMEC)

Learning to walk without the brain: Determining cellular signatures underlying age-dependent spinal cord plasticity

UCLouvain



Prof. Bernard Hanseeuw, PhD

Biochemical mechanisms of regional tau protein aggregation in the human brain

Dr. Emanuel Vandenbroeke

The involvement of top-down facilitatory serotonergic pathways in nocebo- induced pain hypersensitivity

Prof. Riëm El Tahry, MD, PhD

Optimization Vagus nerve stimulation for refractory epilepsy



Geneeskundige Stichting Koningin Elisabeth
Fondation Médicale Reine Elisabeth
Königin-Elisabeth-Stiftung für Medizin
Queen Elisabeth Medical Foundation

Progress report of the research project of the young researcher

Prof. dr. Evelien Carrette
(UZ Gent)

Prof. dr. Evelien Carrette

Beleidsmedewerker

Neurologie | Neuroscience@U(Z)Gent

Universitair Ziekenhuis Gent | C. Heymanslaan 10 | 9000 Gent

T +32 9 332 45 40

evelien.carrette@uzgent.be

Skype eveliencarrette

Ingang 12 | Route 1556 | uzgent.be |

Novel interventions for patients with drug resistant epilepsy and cognitive decline: neuromodulatory effects of combined transcutaneous vagal nerve stimulation and cognitive therapy.

Our goal is to investigate the efficacy and underlying mechanism of action of transcutaneous vagal nerve stimulation (t-VNS), a non-invasive neurostimulation approach for patients with DRE and memory problems at the Reference Center for Refractory Epilepsy at Ghent University Hospital.

We hypothesized that combined tVNS-CT is able to improve the memory performance of these patients better than CT alone by affecting neuronal cortical plasticity networks and aim to demonstrate this by electrophysiological co-registration.

Based on the results of our initial studies that we reported on in our previous progress report, we have slightly adjusted the scope of the research towards further investigation of the mechanism of action and effects of tVNS on epilepsy and cognitive decline using both behavioral and electrophysiological outcome parameters.

1. Achieved results 2021

In the past years we have evaluated the effects of tVNS in depth both in healthy subjects and in patients. We have reported on the results of some of these studies in last years' progress report and have added new results from additional analyses and studies completed in 2021. We have initiated new collaborations to further study the potential of neurostimulation in cognitive decline with both studies in healthy volunteers and in patients.

Studies in healthy volunteers

1.1. investigating the effect of tVNS on verbal memory in young and old healthy volunteers.

We performed a randomized, controlled, crossover study, to investigate the effect of tVNS on verbal memory using a word-recognition paradigm in healthy volunteers (n=48, younger and older group) as a basis for investigating the potential of tVNS to improve cognitive decline. While VNS using an implanted device was previously shown to improve performance on memory paradigms in epilepsy patients, in this study we did not find a significant effect of tVNS, the non-invasive approach to target vagal fibers, on verbal memory performance in a group of young and older healthy participants.

Further research to investigate the potential of targeting vagus nerve fibers noninvasively to improve cognitive function is required. As optimal stimulation parameters have not been elucidated, future research should focus on the effect of different stimulation settings in an individualized way in order to define the most efficient stimulation parameters.

Mertens A, Naert L, Miatton M, Poppa T, Carrette E, Gadeyne S, Raedt R, Boon P, Vonck K. Transcutaneous Vagus Nerve Stimulation Does Not Affect Verbal Memory Performance in Healthy Volunteers. *Front Psychol.* 2020, 15:11:551 (IF 2,9) (attachment 1)

1.2. investigating the effect of tVNS on the cognitive evoked potential in healthy volunteers

The objective of this study was to investigate whether tVNS is able to modulate the P3b component of the P300, a cognitive event related potential (ERP) reflecting noradrenaline (NA) brain activation under control of the Locus Coeruleus (LC) that could serve as a (bio)marker for non-invasive LC activation via tVNS. In this study we demonstrated that targeting vagal nerve fibers via a transcutaneous approach did not alter the P3b in healthy participants. The stimulation parameters used during a relative short period of time may have been insufficient to adequately modulate the LC-NE system. A dysfunctional locus coeruleus - norepinephrine system in patients may be more prone for improvement in contrast to the normal system in healthy volunteers investigated in this study

Gadeyne S, Mertens A, Carrette E, Van den Bossche F, Boon P, Raedt R, Vonck K (2021). Transcutaneous auricular vagus nerve stimulation cannot modulate the P3b event-related potential in healthy volunteers. Clin Neurophysiol. 2021; 29;135:22-29. Epub ahead of print. (IF 3,7) (attachment 2)

1.3. investigating the effect of tVNS on cortical excitability in healthy volunteers

By combining transcranial magnetic stimulation (TMS) with EMG and EEG, we can study the modulation of Motor Evoked Potentials (MEPs) and TMS Evoked Potentials (TEPs). As these MEPs and TEPs are reproducible within subjects, they can be useful to study the effect of neuromodulatory interventions, like tVNS, on cortical excitability. These findings are expected to provide insight in the mechanism of action and help identify more optimal stimulation paradigms to be used in treatment of various neurological disorders such as epilepsy and cognitive decline. We performed a prospective single-blind cross-over study in which 15 healthy male subjects underwent 2 sessions, at least one week apart. During each session, tVNS or sham stimulation was delivered at the maximum tolerated amplitude during one hour. The resting motor threshold, MEPs and TEPs were measured before and after the intervention. For these measurements, 120 single TMS pulses, 120 paired TMS pulses with a short interstimulus interval and 120 paired TMS pulses with a long interstimulus interval, were delivered over the motor hotspot. To assess the effect of tVNS on MEP morphology, we measured the average latency and amplitude of all MEPs for each condition and each pulse type. Intracortical inhibition after paired pulses was assessed by expressing the amplitude of the paired pulse response as a percentage of the amplitude of the single pulse response. MEP latency, amplitude and percentage were then compared at the single subject level before and after each intervention. Statistical analysis was conducted by means of a two-way repeated measures ANOVA. TEP data was preprocessed offline using the TESA toolbox in Matlab. A cluster-based permutation statistical analysis was conducted.

In the overall group of patients, MEP and TEP measurements were not affected by tVNS in this study. We did find an association between tVNS stimulation output current and MEP outcome measures indicating a decrease in cortical excitability in participants who tolerated higher tVNS currents. A subanalysis of participants (n = 8) who tolerated a tVNS current above 2.5 mA showed a significant increase in the resting motor threshold, a decrease in MEP amplitude and modulation of the P60 and P180 TEP components.

In this study it was shown that tVNS did not affect cortical excitability measurements in the overall population in this study. However, tVNS has the potential to modulate specific markers of cortical excitability in participants who tolerate higher stimulation levels. These findings further support the development of appropriate stimulation protocols for future studies investigating the effect of tVNS in epilepsy patients based on the recording of objective outcome parameters.

Mertens A, Carrette S, Klooster D, Lescauwae E, Delbeke J, Wadman WJ, Carrette E, Raedt R, Boon P, Vonck K (2021). Investigating the Effect of Transcutaneous Auricular Vagus Nerve Stimulation on Cortical Excitability in Healthy Males. *Neuromodulation*. 2021 Epub ahead of print. (IF 4,0) (attachment 3)

1.4. investigating tVNS modulation of the heart-evoked potential

In collaboration with our colleagues from the UGent Ghep-lab we investigated the effects of tVNS on the so-called "heart-evoked potential". Accumulating evidence suggests that tVNS influences activity in the brainstem solitary and parabrachial nuclei, the primary relays for the transmission of visceral sensory afferents to the insula. The insula mediates interoception, which concerns the representation and regulation of homeostatic bodily states. Consequently, interoceptive pathways may be relevant to the mechanisms of action of tVNS.

For this study it was hypothesized that tVNS modulates an EEG-derived marker of interoceptive processing known as the heart-evoked potential (HEP) and that tVNS-induced HEP effects would be localizable to the insula.

In a within-subject, sham-controlled study, we recorded EEG and ECG concurrent to tVNS in 43 healthy adults. Using ECG and EEG data, we extracted HEPs. Estimation of the cortical sources of the tVNS-dependent HEP responses observed at the scalp were computed using the Boundary Element Method and weighted Minimum Norm Estimation. Statistics were calculated using cluster-based permutation methods.

We demonstrated that tVNS altered HEP amplitudes at frontocentral and centroparietal electrode sites at various latencies. The tVNS-dependent HEP effect was localized to the insula, operculum, somatosensory cortex, and orbital and ventromedial prefrontal regions.

These results support the hypothesis that tVNS can access the insula as well as functionally and anatomically connected brain regions and that HEPs may serve as an objective, non-invasive outcome parameter for the cortical effects of tVNS.

Poppa T, Benschop L, Horczak P, Vanderhasselt MA, Carrette E, Bechara A, Baeken C, Vonck K. Auricular transcutaneous vagus nerve stimulation modulates the heart-evoked potential. *Brain Stimul*. 2021 Dec 18;15(1):260-269. Epub ahead of print. (IF 8,9) (attachment 4).

In conclusion we found that tVNS is not able to affect verbal memory in healthy volunteers, nor does it affect the cognitive evoked potential. The stimulation parameters used and the relatively short-term delivery of tVNS may have been insufficient to activate vagal fibres and adequately modulate the LC. In the studies in healthy volunteers, normal functioning memory and LC-NA system may simply not be receptive for modulation, in contrast to diseased states in patients with epilepsy, memory problems or depression, in whom a disbalanced LC-NA system may be more prone for improvement.

We did find effects on cortical excitability in a subgroup of patients treated when relatively high output currents were applied, further demonstrating the importance of identifying optimal stimulation parameters to target the vagal nerve fibers in a non-invasive way in individual subjects. We also identified a cortical evoked potential reflective of vagal nerve fiber targeting, the HEP, that may be used in the future as a biomarker in studies investigating tVNS effects on interoceptive pathways.

Studies in patients

1.5. The potential of invasive and non-invasive vagus nerve stimulation to improve verbal memory performance in epilepsy patients

As described higher (study 1), we were unable to confirm the beneficial effects of invasive VNS on verbal memory shown previously in epilepsy patients with non-invasive tVNS in healthy subjects. Therefore we are currently performing a prospective randomized cross-over study in epilepsy patients who received both tVNS and VNS with the implanted device. We aim to replicate the effects shown with invasive VNS in 15 drug-resistant epilepsy patients and in the same patients investigated the effects of non-invasive tVNS.

All patients will conduct a word recognition memory paradigm in 3 conditions: VNS ON, VNS OFF and tVNS (3-period 3-treatment cross-over study design). For each condition, patients memorize 21 highlighted words from text paragraphs. Afterwards, the intervention is delivered for 30 s. Immediate recall and delayed recognition scores are obtained for each condition. This memory paradigm is repeated after 6 weeks of invasive VNS therapy in 2 conditions: VNS ON and VNS OFF (2-period 2-treatment cross-over study design).

We are currently working on the data-analysis and on writing the manuscript and will report on the results in the progress report of 2022.

2. International collaborations and networks

2.1. Scientific Research Network (WOG) on Transcutaneous Vagus Nerve Stimulation

Prof. Evelien Carrette is part of the core group of the Scientific Research Network (WOG) on Transcutaneous Vagus Nerve Stimulation supported by FWO-Flanders. This research network offers the unique opportunity to consolidate and intensify collaborations between internationally renowned research groups, to create a truly multidisciplinary research consortium. The Flemish research groups in the network offer internationally renowned expertise on VNS, both from a clinical standpoint using invasive VNS (UGent) and from a fundamental research standpoint. The non-Flemish research groups of the proposed network have critically contributed to researching the fundamental questions underlying tVNS research, and will provide complementary expertise on psychophysiology, neuro-gastroenterology, (autonomic) neuroscience, anesthesiology, and clinical psychology. While there are already strong collaborations between some of these groups, as attested by several publications and joint symposia, collaborative efforts are currently hampered by the lack of a communicational infrastructure to facilitate communication, data-

and methods sharing, or even shared research projects. Evelien Carrette has organized and moderated international meetings of this consortium. Follow-up meetings are planned during the 4 coming years.

2.2. Guideline on tVNS research

Our 4Brain research group has also been involved in the writing of a guideline in *Frontiers in Human Neuroscience* within the tVNS-Consensus-group. Prof. Kristl Vonck and Dr. Ann Mertens have been listed as authors from 4BRAIN and this work has been published (see below).

2.3. Neuromodulation Task Force for COVID-19

Our 4Brain research group is founding member of the International Neuromodulation Task Force for COVID-19. One of the aims of this consortium is to investigate the potential of tVNS to treat the highly prevalent cognitive problems associated with COVID-19 infections.

3. All publications

- Mertens A, Naert L, Miatton M, Poppa T, Carrette E, Gadeyne S, Raedt R, Boon P, Vonck K. (2020). Transcutaneous Vagus Nerve Stimulation Does Not Affect Verbal Memory Performance in Healthy Volunteers. *Front Psychol.* 2020 Apr 15;11:551. doi: 10.3389/fpsyg.2020.00551. PMID: 32351421; PMCID: PMC7174665 (attachment 1).
- Gadeyne S, Mertens A, Carrette E, Van den Bossche F, Boon P, Raedt R, Vonck K (2021). Transcutaneous auricular vagus nerve stimulation cannot modulate the P3b event-related potential in healthy volunteers. *Clin Neurophysiol.* 2021 Dec 29;135:22-29. doi: 10.1016/j.clinph.2021.11.079. Epub ahead of print. PMID: 35007840 (attachment 2).
- Mertens A, Carrette S, Klooster D, Lescrauwaet E, Delbeke J, Wadman WJ, Carrette E, Raedt R, Boon P, Vonck K (2021). Investigating the Effect of Transcutaneous Auricular Vagus Nerve Stimulation on Cortical Excitability in Healthy Males. *Neuromodulation.* 2021 Jul 20. doi: 10.1111/ner.13488. Epub ahead of print. PMID: 34288274 (attachment 3).
- Poppa T, Benschop L, Horczak P, Vanderhasselt MA, Carrette E, Bechara A, Baeken C, Vonck K. Auricular transcutaneous vagus nerve stimulation modulates the heart-evoked potential. *Brain Stimul.* 2021 Dec 18;15(1):260-269. doi: 10.1016/j.brs.2021.12.004. Epub ahead of print. PMID: 34933143 (attachment 4).
- Farmer AD, et al. International Consensus Based Review and Recommendations for Minimum Reporting Standards in Research on Transcutaneous Vagus Nerve Stimulation (Version 2020). *Front Hum Neurosci.* 2021 Mar 23;14:568051. doi: 10.3389/fnhum.2020.568051. PMID: 33854421; PMCID: PMC8040977 (attachment 5).



Geneeskundige Stichting Koningin Elisabeth
Fondation Médicale Reine Elisabeth
Königin-Elisabeth-Stiftung für Medizin
Queen Elisabeth Medical Foundation

Progress report of the research project of the young researcher

Prof. Riëm El Tahry, MD, PhD
Université Catholique de Louvain (UCLouvain)

Prof. Riëm El Tahry, MD, PhD

Chef de Clinique Adjointe

Neurologie, Centre de référence pour l'épilepsie réfractaire

Tel.: +32 2 764 28 55

Secrétariat:

Tel.: +32 2 764 10 82 / +32 2 764 33 09

Fax: +32 2 764 36 79

Avenue Hippocrate 10

1200 Brussels

Belgium

Tel.: +32 2 764 11 11

www.saintluc.be

Optimization Vagus nerve stimulation for refractory epilepsy

1. Progress report

Dear Pr Jean-Marie Maloteaux, dear President of the Scientific committee,

As requested, we are sending you a report of our scientific activities performed in 2021. In last report we have asked permission to postpone the use of the grant by November 2022 and extend its use until 30 September 2024.

1.1. The following manuscripts were published as last or first author:

1. EEG spectral and connectivity changes induced by acute Vagus Nerve Stimulation Simone Vespa, Youssef Agram, Federico Lucchetti, Susana Ferrao Santos, Antoine Nonclercq, Riëm El Tahry. Accepted in Neurotherapeutics
2. Vagus nerve electroneurogram based seizure detection algorithm in rats Lars Stumpp, Hugo Smets, Simone Vespa, Joaquin Cury, Pascal Doguet, Jean Delbeke, Antoine Nonclercq, Riem El Tahry. International Journal of Neural Systems, 2021, 31(7), 2150024
3. Transcutaneous VNS applied to experimental pain: a paired EEG and behavioral study using thermonociceptive CO₂ laser. Manon Dumoulin, Giulia Liberati, Susana Ferrao Santos, André Mouraux, Riëm El Tahry PLOS ONE, 2021, 16(7 July), e0254480
4. Automated interictal Electrical Source Imaging to characterize insular irritative zone: comparison with concomitant intracranial EEG. Evelina Iachim, Simone Vespa, Amir G. Baroumand, Venethia Danthine, Pascal Vrielynck, Marianne de Tourtchaninoff, Alexane Fierain, Geraldo Ribeiro Vaz, Christian Raftopoulos, Susana Ferrao Susana, Pieter van Mierlo, Riëm El Tahry

The following manuscripts were published as co-author:

Infrared neurostimulation in ex-vivo rat sciatic nerve using 1470 nm wavelength Cury, J., Vande Perre, L., Smets, H., ...Gorza, S.-P., Nonclercq, A. Journal of Neural Engineering, 2021, 18(5), 056018

1.2. Three abstracts will be presented at the International Brain Stim Conference:


1. Effect of Vagus Nerve Stimulation on EEG oscillations and connectivity. Simone Vespa, Youssef Agram, Federico Lucchetti, Susana Ferrao Santos, Antoine Nonclercq, Riëm El Tahry
2. Vagus nerve stimulation-induced laryngeal motor evoked potentials: a biomarker of effective nerve activation. Evelina Iachim, Simone Vespa, Venethia Danthine, Lars Stumpp, Manon Dumoulin, Alexandre Berger, Jean Delbeke, Antoine Nonclercq, Riëm El Tahry
3. Vagus Nerve Electroneurogram-Based Detection of Acute Pentylentetrazol Induced Seizures in Rats, Lars Stumpp, Hugo Smets, Simone Vespa, Joaquin Cury, Pascal Doguet, Jean Delbeke, Antoine Nonclercq, Riem El Tahry.

This last abstract has been accepted as a part of symposium proposal I have submitted entitled : "VNS for refractory epilepsy: new insights and developments & Recent Updates in Vagus Nerve Stimulation Therapy"

In addition, we now have developed our own hand made cuff electrode for vagus nerve implantation in rats, which will allow continuing our research in vagus nerve recording for seizure detection. We are exploring the circadian rhythm of the vagus nerve and aim to better understand its physiological content. We are now actively searching for a new PhD candidate to continue this animal research, as Anton Kavaldzhiev who was previously on the topic decided to leave the project.

On experimental human level, we have elaborated two new research themes that have as a common goal to address the human noradrenergic system with respect to VNS efficacy. To do so, we are now acquiring MRI images of the Locus coeruleus and its reactivity to an oddball paradigm (Alexandre Berger- doctorat en entreprise), as well as measuring pupil reactivity with increasing VNS currents (Simone Vespa, FNRS). In addition, a new PhD student has joined our group (Vénéthia Danthine, FSR) who will study P300 source and EEG connectivity longitudinally prior to and at several time points after implantation.

We would like to thank la Fondation Médicale Reine Elisabeth for its contribution in our research.



Riëm El Tahry



Geneeskundige Stichting Koningin Elisabeth
Fondation Médicale Reine Elisabeth
Königin-Elisabeth-Stiftung für Medizin
Queen Elisabeth Medical Foundation

Progress report of the research project of the young researcher

Prof. Bernard Hanseeuw, PhD
Université Catholique de Louvain (UCLouvain)

Principal Investigator

Prof. Bernard Hanseeuw, PhD

Postdocs

Lisa Quenon

PhD students*Imaging*

- Vincent Malotaux
- Lise Colmant
- Thomas Gérard

Biological analyses (CSF)

- Nathalie Nyalu Ngoie

Main collaborators

Adrian Ivanoiu, MD PhD (Neurology)
Renaud Lhommel, MD (Nuclear Medicine)
Laurence Dricot, Ir PhD (Radiology)
Vincent van Pesch, MD PhD (Neurochemistry)
Yves Sznajder, MD (Neurogenetics)
Didier Vertommen, PhD (Mass Spectrometry)

Website

<https://uclouvain.be/fr/instituts-recherche/ions/neur/the-louvain-aging-brain-lab.html>

Contact

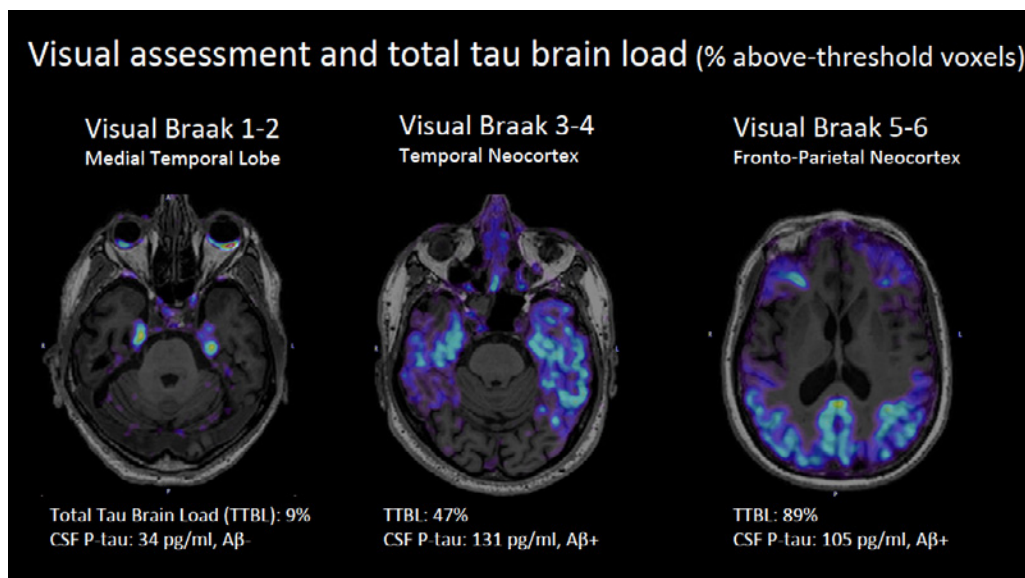
recherche-alzheimer@uclouvain.be
bernard.hanseeuw@uclouvain.be

The Human Tau study

The **Human Tau study** evaluates the manifestations related to pathological aging, such as that caused by Alzheimer's disease (AD) and related disorders, called tauopathies. These disorders all involve biochemical alterations in the tau protein. We relate brain damage disclosed by imaging techniques (MRI, tau-PET using [18F]-MK6240) and biological changes observed in the cerebrospinal fluid (CSF) to cognitive changes measured using neuropsychological testing. Our research targets are patients with mild cognitive impairment who consult the Memory Clinic, normal subjects at family risk for developing Alzheimer's disease and healthy control subjects, young and old.

In 2019, we have acquired the first tau-PET images in French-speaking Belgium. Since then, more than eighty patients benefited from the technique. Three imaging PhD students are funded by the FNRS. We developed a classification of the tau-PET images inspired by the post-mortem neuropathological stages of Heiko Braak (Fig.1). The support of the Queen Elisabeth Medical Foundation has allowed me to expand this research program, and also to hire a biochemical PhD student and cover the high costs of mass spectrometry experiments to characterize the post-translational modifications (PTM) of the tau protein in brain samples and CSF.

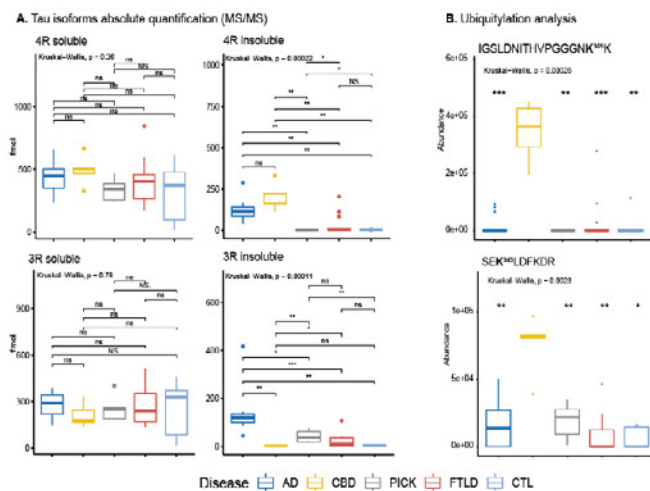
Fig.1 Tau-PET image of patients with various levels of tau pathology: In Braak stage 1 or 2, the pathology is restricted to the medial temporal lobe and CSF is most often normal. In Braak stage 3 or 4, the temporal lobe is strongly affected by tau pathology, but the frontal and occipital lobes are still largely preserved, consistent with the preservation of executive and visuospatial functions observed in patients with mild cognitive impairment. Tau is most often abnormal in the CSF. Braak stage 5 and 6 are mostly observed in patients with AD dementia.



Results accepted for an oral presentation by Thomas Gérard, PhD student at the European Conference on Clinical Neuroimaging in Geneva (March 14-15, 2022).

Nathalie Kyalu Ngoie (3rd year PhD student in 2021-2022) first developed an immuno-precipitating protocol isolating the tau protein from the CSF and brain samples. She then analyzed the protein with mass spectrometry from patients with different tauopathies, such as AD, but also fronto-temporal lobe degeneration (FTLD) or cortico-basal degeneration (CBD). She achieved to identify tau isoforms (3R vs 4R) in tau aggregates and in the soluble fraction of the brain. Whereas tau isoforms followed the expected distribution in the aggregated (4R in CBD, 3R in Pick disease, 3R and 4R in AD), this distribution was not observed in soluble tau, explaining the difficulties

of conducting tau isoform measurements in CSF. We then searched for differences in post-translational modifications (PTMs) in soluble tau and CSF (Fig.2).



In preliminary work (Fig.2), we could demonstrate that differences in tau PTMs were observable in soluble brain fractions, and in post-mortem cerebrospinal fluid (CSF), making these PTMs good candidates to develop *in-vivo* biomarkers distinguishing between tauopathies.

Fig.2: Mass Spectrometry (MS) analyses of (A) tau isoforms and (B) post-translational modifications (PTMs) in soluble and insoluble brain extracts. Tau^{K369} ubiquitination is observed in 4R-tauopathies: CBD and three FTL cases with predominant 4R-tau in the aggregates. This illustrates our ability to conduct biochemical studies, in addition to brain imaging studies. Data presented at EuroTau 2021.

The first imaging publication supported by the Foundation has been submitted earlier in January 2022 to the journal Brain Connectivity. A second imaging publication and a biochemical one are currently in preparation. Vincent Malotau and Nathalie Kyalu will both defend their PhD thesis in 2023.

Finally, the support of the Foundation has allowed me to start collaboration with the lab of Pascal Kienlen-Campard who used CSF that I collected to demonstrate the in-vivo seeding effect of hexameric amyloid assemblies (see first publication below).

Key recent publications

- Vranx C, Vadukul DM, Suelves N, Contino S, D'Auria L, Perrin F, van Pesch V, **Hanseeuw B**, Quinton L, Kienlen-Campard P. (2021). Mechanism of Cellular Formation and In Vivo Seeding Effects of Hexameric -Amyloid Assemblies. **Molecular Neurobiology**.
- **Hanseeuw, B. J.**, Malotau, V., Dricot, L., Quenon, L., Sznajder, Y., Cerman, J., Woodard, J. L., Buckley, C., Farrar, G., Ivanoiu, A., & Lhommel, R. (2021). Defining a Centiloid scale threshold predicting long-term progression to dementia in patients attending the memory clinic : An [18F] flutemetamol amyloid PET study. **European Journal of Nuclear Medicine and Molecular Imaging**.
- Mormont, E., Bier, J.-C., Bruffaerts, R., Cras, P., De Deyn, P., Deryck, O., Engelborghs, S., Petrovic, M., Picard, G., Segers, K., Thiery, E., Versijpt, J., & **Hanseeuw, B.** (2020). Practices and opinions about disclosure of the diagnosis of Alzheimer's disease to patients with MCI or dementia : A survey among Belgian medical experts in the field of dementia. **Acta Neurologica Belgica**.
- **Hanseeuw, B. J.**, Scott, M. R., Sikkes, S. A. M., Properzi, M., Gatchel, J. R., Salmon, E., Marshall, G. A., & Vannini, P. (2020). Evolution of anosognosia in alzheimer's disease and its relationship to amyloid. **Annals of Neurology**, 87(2), 267-280.
- **Hanseeuw, B. J.**, Betensky, R. A., Jacobs, H. I. L., Schultz, A. P., Sepulcre, J., Becker, J. A., Cosio, D. M. O., Farrell, M., Quiroz, Y. T., Mormino, E. C., Buckley, R. F., Papp, K. V., Amariglio, R. A., Dewachter, I., Ivanoiu, A., Huijbers, W., Hedden, T., Marshall, G. A., Chhatwal, J. P., ... Johnson, K. (2019). Association of Amyloid and Tau With Cognition in Preclinical Alzheimer Disease : A Longitudinal Study. **JAMA Neurology**, 76(8), 915.

→ The last publication received the FMRE CBC Prize in 2021.



Geneeskundige Stichting Koningin Elisabeth
Fondation Médicale Reine Elisabeth
Königin-Elisabeth-Stiftung für Medizin
Queen Elisabeth Medical Foundation

Progress report of the research project of the young researcher

Dr. Lars Emil Larsen, PhD
Universiteit Gent (UGent)

Dr. Lars Emil Larsen, PhD

Postdoctoral Researcher

4Brain/MEDISIP

Ghent University

Campus UZ

Corneel Heymanslaan 10,

Entrance 36 - Ground floor

9000 Gent

Belgium

Closed loop precision therapy for epilepsy using photopharmacology

1. Overview of progress

The principal goal of this project is to develop and provide proof of concept for closed loop precision therapy for epilepsy using photopharmacology in a mouse model for temporal lobe epilepsy. In the previous report, I described the identification of DEACM-CPA (cCPA), a coumarin-caged adenosine-1 (A1) receptor agonist, which is uncaged and activated by purple light (405 nm). The cCPA compound gains unique access to the potent seizure suppressing efficacy of the A1 receptor signaling system, without inducing the side effects, such as cardiac and respiratory suppression, that are otherwise associated with systemic activation. I further described how an initial shift towards studying closed-loop photopharmacology at an *in vitro* level, rather than *in vivo* level, was motivated by delays in delivery of crucial electronic equipment (covid-19 related). Finally, a series of preliminary results were presented.

Over the course of 2021, significant progress has been made towards the goal of closed-loop precision therapy. The use of photopharmacology with cCPA has been refined to the point where its utility for closed loop application has been well characterized, with a number of manuscripts in preparation for publication. In the following, I first briefly outline already published work in relation to this grant and secondly, I will provide the outline and status of manuscripts currently in preparation.

Already published work with support of this grant

1. Acharya AR, Larsen LE, Van Lysebettens W, Wadman WJ, Delbeke J, Vonck K, Meurs A, Boon P, Raedt R. Attenuation of hippocampal evoked potentials in-vivo by activation of GtACR2, an optogenetic chloride-channel. *Frontiers in Neuroscience*. 29 March 2021 <https://doi.org/10.3389/fnins.2021.653844>.

Peer Reviewed, Impact factor (2019, most recent) = 3.707, Category: Neurosciences, Rank 96/271, Q2

In this paper, we showed the utility of the GtACR2 opsin, a blue light gated chloride channel, for inhibition of evoked hippocampal activity. Opsins, such as GtACR2 is a powerful alternative to photopharmacology for closed-loop applications.

2. Acharya AR, Vandekerckhove B, Larsen LE, Delbeke J, Wadman WJ, Vonck K, Carette E, Meurs A, Vanfleteren J, Boon P, Missinne J, Raedt R. *In vivo* blue light illumination for optogenetic inhibition: effect on local temperature and excitability of the rat hippocampus. *Journal of Neural Engineering*, 2021 Dec 24;18(6) doi: 10.1088/1741-2552/ac3ef4.

Peer Reviewed, Impact factor (2020, most recent) = 5.379, Category: Engineering, Biomedical, Rank 20/89, Q1

In this paper, effects of blue light on local temperature was explored through modeling and simulations and subsequently validated with experimental recordings from the rat brain. The models constructed and validated in this paper will be of great value in the *in vitro* to *in vivo* translation of our photopharmacology work.

Manuscript in preparation: Characterization of DEACM -CPA (cCPA) as a tool to closed-loop modulation of excitability

In this manuscript, which is the first to be published on the cCPA compound, we will characterize the utility of cCPA in the context of closed loop application. Most of the data for this manuscript has already been obtained and we expect submission to the high-impact journal '*Angewandte Chemie*' towards the end of Q1 2022. Key parts of the manuscript are presented in the following.

An *in vitro* brain slice model was used to study effects of uncaging cCPA with purple light on circuit excitability. In this case, the hippocampal slices were prepared and placed on a 60channel Multi Electrode Array (MEA), which allows both electrical stimulation and acquisition of electrophysiological data. By electrically stimulating afferent fibers of the CA1, the Schaeffer Collaterals, an evoked synaptic response, the field Excitatory Postsynaptic Potential (fEPSP) can be acquired at multiple levels of the CA1 (**Figure 1a**). The amplitude of this response is a proportional measure of the level of neurotransmission. We used this model to study effects of varying light pulse durations on uncaging of a fixed dose concentration of cCPA and effects on CA1 fEPSPs as a result. We observed a light-pulse duration dependent effect on fEPSP amplitude (**Figure 1b-e**).

The A1 receptor is a G-protein couple receptor, which triggers several intracellular signaling mechanisms, ultimately resulting in neuronal inhibition. The dynamics of the A1 receptor signaling system, however, results in a slower response of the receptor than e.g. ion-channels, and the effects last longer. Due to these dynamics, we have refined our vision for the integration of cCPA for closed loop seizure control. Rather than acutely terminating seizures, we hypothesized that we could use cCPA to narrowly control the excitability of neuronal circuits. To demonstrate this concept, we defined a system where the delivery of short light pulses was triggered by fEPSP measurements exceeding a specific predefined threshold, e.g. 50% of the baseline level. Using this approach, we were able to control excitability with an unprecedented level of precision (**Figure 2**).

Beyond the fact that there is no spatial control with conventional antiepileptic drugs, we have no control over the extent of inhibition we induce, often resulting in a large number of side-effects. With this data in mind, we believe we now have a tool to essentially 'normalize' excitability in the epileptic brain, a condition characterized by elevated excitability.

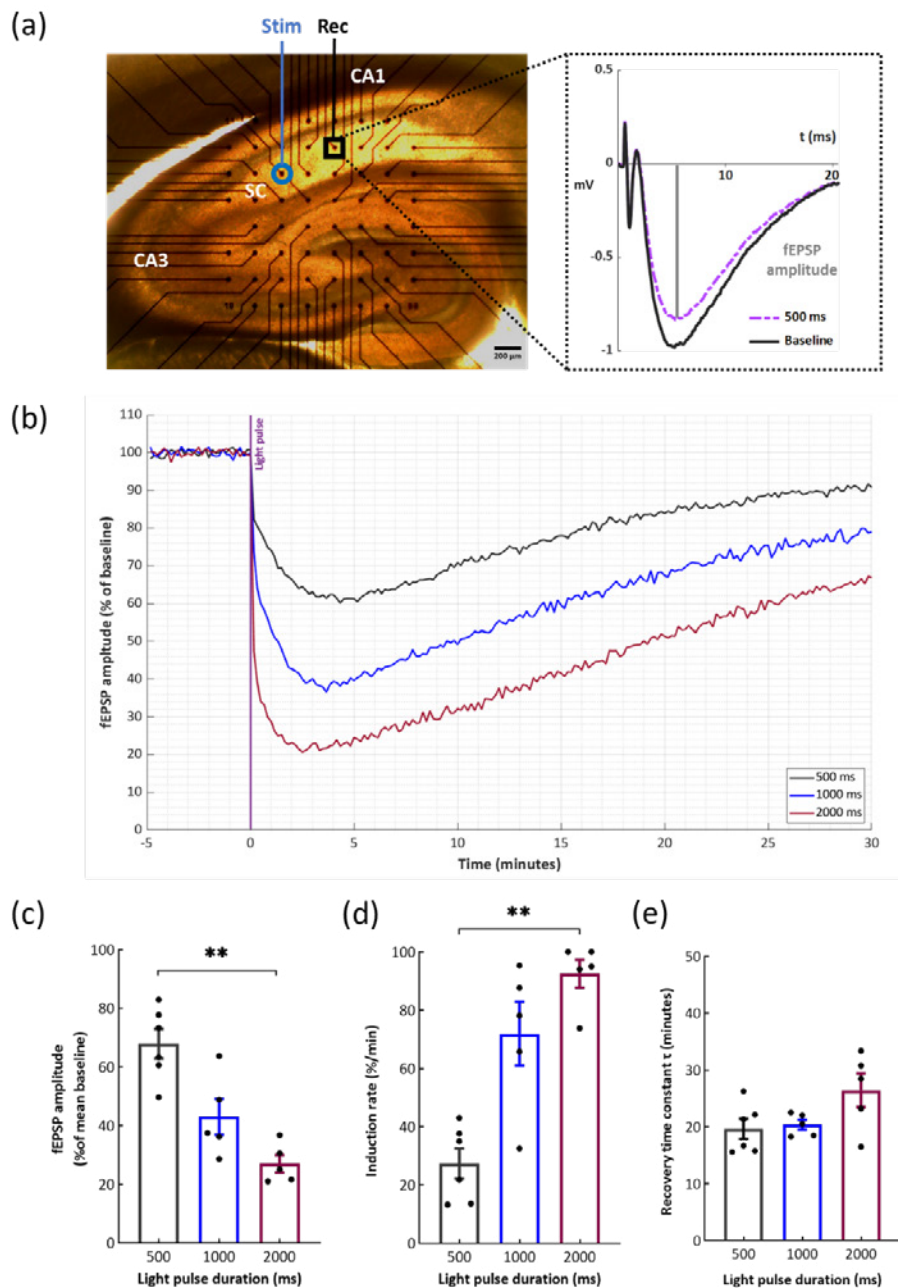


Figure 1: *In vitro* photocontrol of A,R activation with cCPA. (a) Schematic of the recording configuration and example of a hippocampal slice, positioned on a 60 channel MEA. Electrical stimuli are delivered to the Schaeffer Collaterals (SC) with a stimulation electrode (stim). The evoked response is recorded in the CA1 area (rec). Representative fEPSP traces during baseline (grey) and three minutes after a 500 ms light pulse (purple) are shown in the enlarged inset. (b) Time course of effects of uncaging cCPA [3 μ M] on fEPSP amplitude upon exposure to a single 405 nm LED light pulse of variable durations at time point 0 minutes (purple line) in three representative slices. fEPSP amplitude is normalized to mean baseline for each slice individually. (c) Summary of remaining fEPSP amplitude after light exposure, expressed as a percentage relative to mean baseline. Asterisks indicate significance, $p=0.003$, Kruskal Wallis test. (d) Summary of averaged induction rates, fitted with the least-squares method from panel (b) immediately (10 – 30 seconds) after light exposure. Increasing pulse durations resulted in increasing induction rates and subsequent increased fEPSP amplitude reductions. Asterisks indicate significance, $p=0.005$, Kruskal Wallis test. (e) Summary of recovery time constants fitted with a single exponential function from panel (b) 7 – 30 minutes after light exposure. Averaged recovery time constants remained unaltered over all groups. All data represented as mean \pm SEM. Each dot represents an individual slice (500 ms: $n = 6$, 1000 ms: $n = 5$, 2000 ms: $n = 5$).

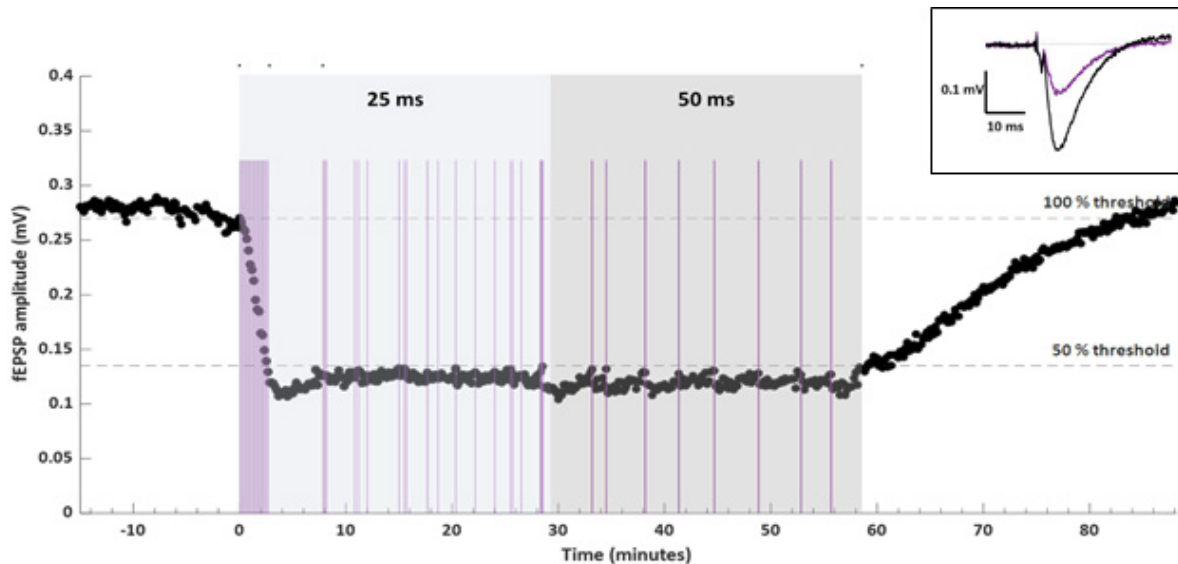


Figure 2: In vitro closed-loop control of the level of synaptic transmission using photopharmacology with cCPA [$3 \mu\text{M}$]. Representative example of the time course of effects of the closed-loop feedback system triggering light exposure using the fEPSP amplitude as control variable. A steady state phase was reached after 8 minutes. fEPSP amplitude remained stable with both 25 and 50 ms light pulses. This has since been reproduced in 8 slices.

Manuscript in preparation: Closed-loop photopharmacology for control of hyperexcitability: *in vitro* proof of concept

In this manuscript, we explore the use of the concept developed in the previous manuscript for control of excitability under hyperexcitable conditions. Preliminary data for this manuscript is encouraging and we are currently in the process of finalizing the data collection. Submission of this manuscript is anticipated for end Q2 or begin Q3, 2022.

The setup for these experiments is similar to the previous manuscript and includes the use of the same type of MEA for *in vitro* slice electrophysiology. Initially, excitability was elevated by exposing slices to elevated potassium-concentrations (8.5 mM), which results in epileptiform bursts. A first part of this manuscript will focus on the characterization of this activity (burst latency, frequency, amplitude and duration) in healthy *ex vivo* brain slice experiments with a main focus on the CA1 area. Similarly, upon exposure to elevated potassium concentrations we observe hyperexcitability reflected by an increase in fEPSP amplitude (**Figure 3a**). In the subsequent experiment we will test the hypothesis that closed loop photopharmacology with cCPA can be used to 'normalize' excitability in a controlled manner by reducing fEPSP to baseline amplitude, and by doing so, preventing the occurrence of epileptiform activity. Preliminary evidence is in support of hypothesis as closed loop photopharmacology can be used to maintain excitability levels at baseline levels even after elevation of potassium levels (**Figure 3b**).

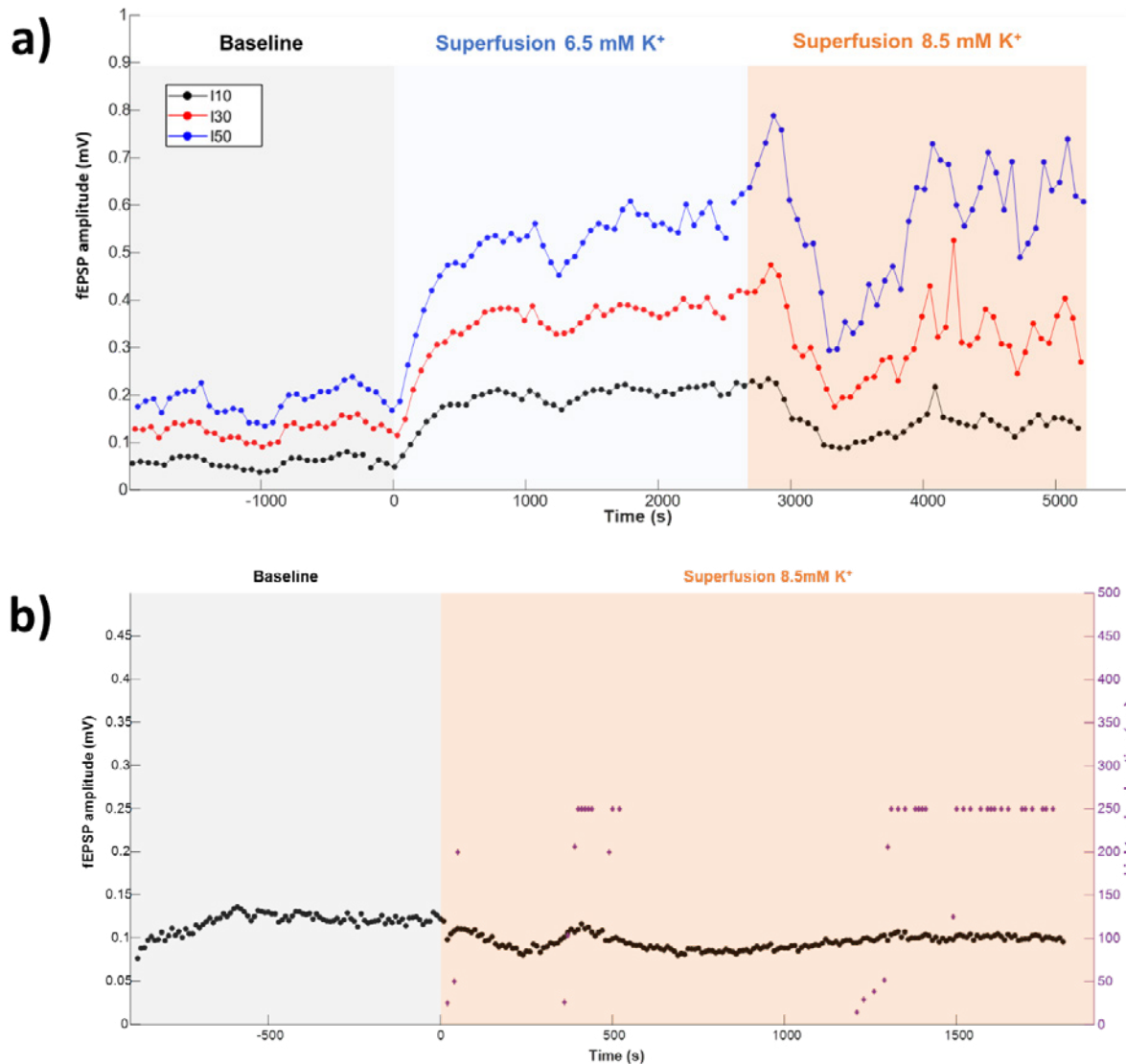


Figure 3: Elevating potassium levels induces hyperexcitability, reflected by an increase in the amplitude of the fEPSP (a). Using closed loop photopharmacology, triggering the uncaging of cCPA by fEPSPs exceeding baseline levels in amplitude, it was possible to 'normalize' excitability even under hyperexcitable conditions.

Manuscript in preparation: Closed-loop photopharmacology in a model for chronic temporal lobe epilepsy, *in vitro*

The previous manuscripts concern the study of cCPA and its utility for closed-loop application in healthy tissue, albeit under conditions of acute hyperexcitability induced with elevated potassium concentrations, as in the previous manuscript. In this manuscript, however, we turn to a commonly used model for chronic temporal lobe epilepsy, the intrahippocampal kainic acid (IHKA) model in mice. In this model, kainic acid is initially injected intrahippocampally to evoke a status epilepticus, resulting in several histopathological changes common to human temporal lobe epilepsy, and the occurrence of spontaneous seizures. We thus aim to adapt the concept of closed-loop photopharmacology with cCPA for control of excitability in this model of chronic temporal lobe epilepsy. This manuscript will still require acquisition of data for its final parts and manuscript finalization is not expected before Q4 2022.

Again, the experimental setup is similar, although in addition to studying the CA1, we here also look at another subregion of the hippocampal formation, the dentate gyrus (DG). Evoked potentials can be studied in the DG by electrically stimulating perforant path afferents originating from the

entorhinal cortex. As a first objective of this manuscript, we describe how excitability is elevated in slices of epileptic mice vs. healthy control mice. In this case we observed that hyperexcitability primarily is observed in the dentate gyrus, where we particularly see an increased prevalence of population spikes in epileptic vs. healthy slices (**Figure 4**).

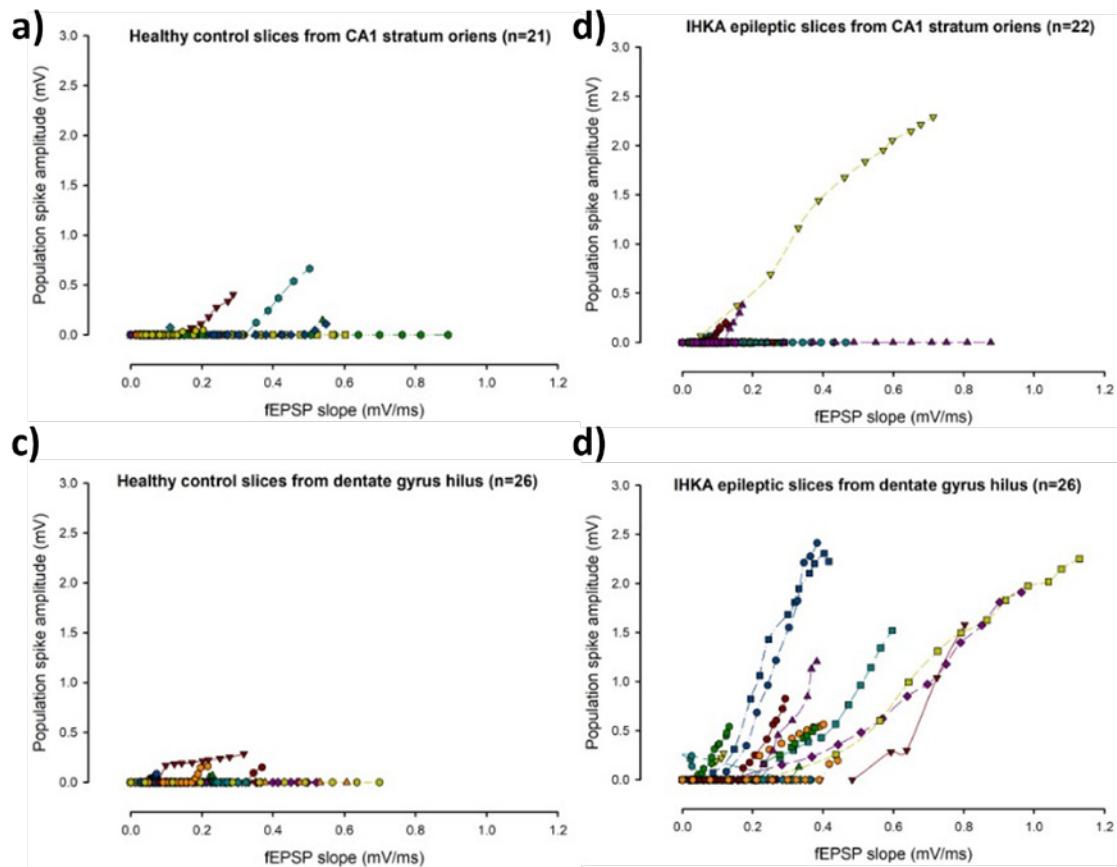


Figure 4: Evoked potentials were recorded in both the CA1 and dentate gyrus (DG) of healthy and epileptic mice. The plots show the population spike amplitude for a given fEPSP slope recorded over a range of varying stimulation intensities and show clear signs of elevated excitability in both the CA1 and DG of epileptic mice.

Statistical analysis of evoked potential parameters showed a significant increase in both fEPSP slope and population spike amplitude in the DG of epileptic mice relative to healthy controls, while no differences were observed for the CA1 (**Figure 5**).

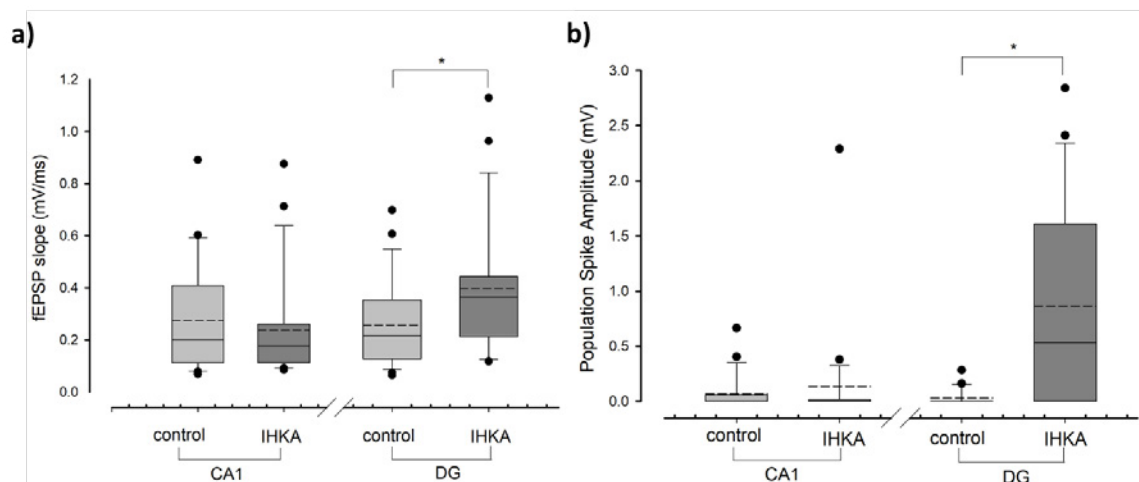


Figure 5: Comparison of fEPSP slope and population spike amplitude of evoked potentials recorded in the CA1 and dentate gyrus (DG) of epileptic and healthy control mice at high stimulation intensities. Elevated fEPSP slope and population spike amplitude is observed in the DG.

Beyond assessing changes in baseline excitability between healthy and epileptic slices, we further wanted to assess any potential changes in the potency of A1 receptor signaling between these conditions as previous reports have indicated compromised adenosine signaling under epileptic conditions. We thus studied effects of varying concentrations of the native CPA on evoked potentials of both the CA1 and DG recorded in slices of both healthy and epileptic mice (**Figure 6**). CPA induced a dose-dependent suppression of fEPSP in both the CA1 and DG. There was a tendency for a stronger suppression of the fEPSP slope in healthy vs. epileptic slices over the concentrations studied. Population spikes were only studied in epileptic slices due to a low prevalence in healthy slices. Although we still need to complete this data, CPA is similarly observed to induce a potent suppression of population spike amplitude. The preliminary data indicates that the doses needed to suppress population spikes are much lower than the concentration needed to suppress the fEPSP component of the evoked potentials.

Apart from collecting additional population spike amplitude data to complete **Figure 7**, we envision to complete this manuscript with an experiment where the closed-loop photopharmacology concept developed in the previous manuscripts will be used to normalize the observed hyperexcitability in this chronic epilepsy model.

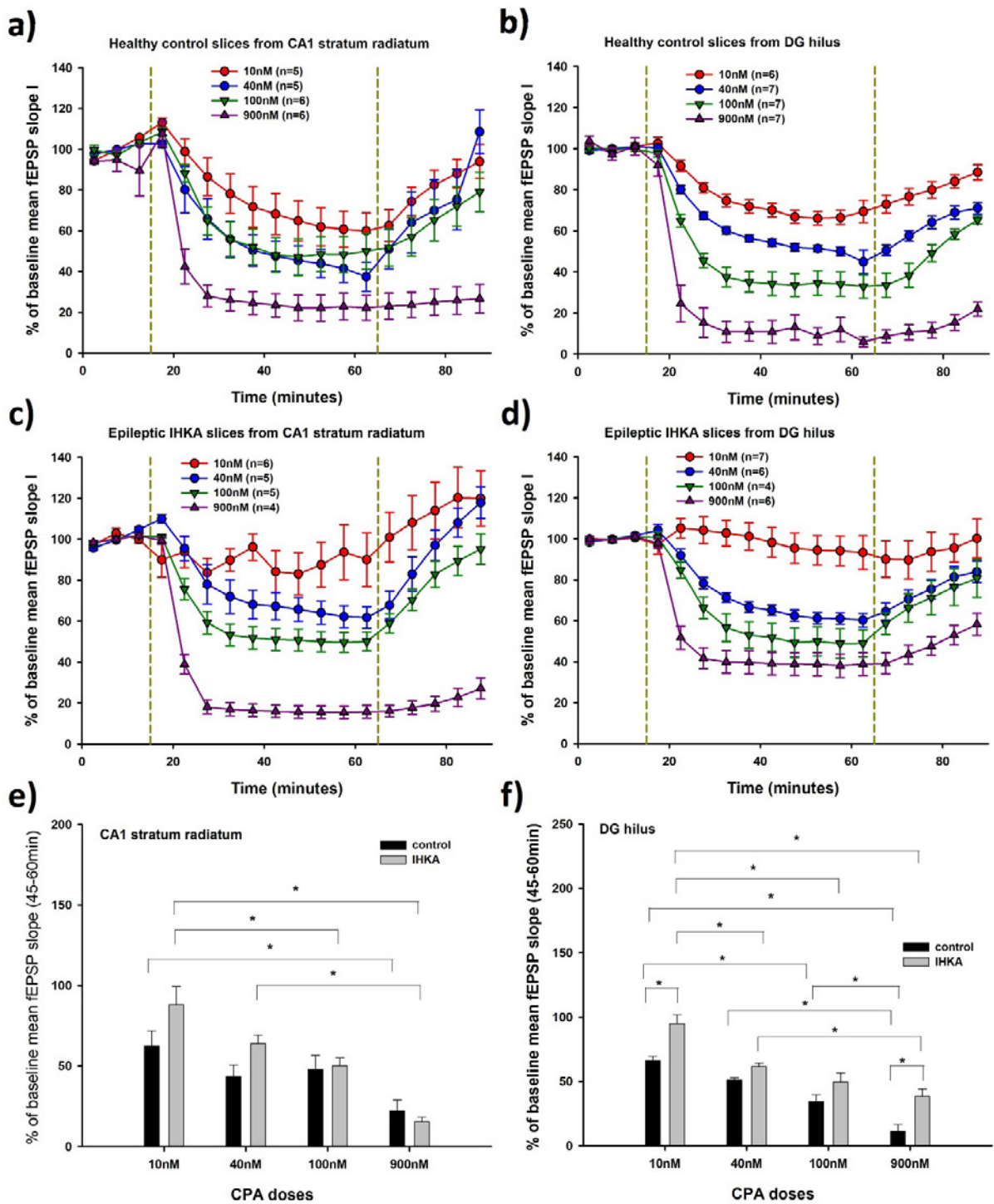


Figure 6: Effects of CPA on the fEPSP slope of evoked potentials recorded in the CA1 and dentate gyrus (DG) in both healthy and epileptic slices. CPA induces an equipotent dose dependent suppression of the fEPSP slope in both the CA1 (a, c, e) and DG (b, d, f) of both healthy and epileptic slices.

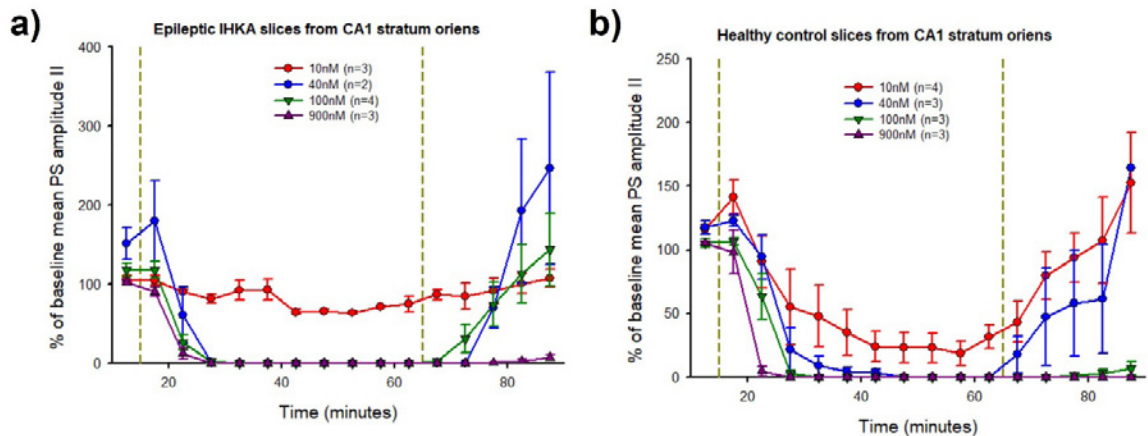


Figure 7: Effects of CPA on population spike amplitude of evoked potentials recorded in the CA1 and DG, respectively.

Manuscript in preparation: Control of circuit-excitability with photopharmacology, *in vivo*

Since our *in-vitro* experiments with both CPA and cCPA provided convincing evidence of being able to both inhibit evoked potentials and epileptiform activity, and control excitability, we have initiated experiments *in vivo* in anesthetized mice. Although the envisioned manuscript is very clear, there are still a number of experiments that will need to be finalized. The manuscript will include the following:

1. Inhibition of DG evoked potentials and spontaneous local field potentials with CPA
2. Inhibition of DG evoked potentials and spontaneous local field potentials with cCPA
3. Closed-loop control of excitability

For the experiments described in the following, mice were anesthetized with isoflurane (5% for induction, 2% for maintenance) and fixed in a stereotactic frame. Stainless steel wire electrodes were implanted in the hilus of the DG for registration of DG evoked potentials. A bipolar stimulation electrode was implanted in the perforant path, the principal afferent input tract to the DG, allowing the acquisition of DG evoked potentials. A Hamilton neurosyringe, was lowered to the level of the lateral ventricle contralateral to the site from which evoked potentials were acquired, which allowed the infusion of either CPA (low dose = 0.25 μg or high dose = 1.25 μg , both dissolved in 5 μL of saline with 2.5% DMSO) or a vehicle solution (control condition). Following administration of CPA, there was a dose dependent suppression of both fEPSP amplitude and the population spike of the DG evoked potentials (**Figure 8**). These observations gave an indication of what we should expect to see with the cCPA if it is working as intended. In the beginning of 2021, we thus took initial steps with the cCPA compound using same experimental setup described above, with the exception of adding a 400 μm optical fiber to the electrode used for evoked potential recordings, which allowed us to deliver light locally in the hippocampus for uncaging of the cCPA compound. We initially had to dedicate a number of exploratory experiments to 1) find suitable light protocols without any direct physiological impact and 2) concentrations of cCPA needed to obtain desired effects.

Light pulses of 50/100/200 ms were tested at a frequency of 0.1/0.5 Hz and at an intensity of 8/10 mW. Illumination protocols with the higher parameters (200 ms pulse durations or 0.5 Hz frequency) were found to often lead to inhibitory effects on evoked potentials in the absence of cCPA, indicating a high sensitivity of our electrophysiological read-out to phototoxic/ photothermal effects of the 405 nm light. The use of 100 ms pulses of 8 mW at 0.1 Hz was deemed as a "safe" illumination protocol as no effects were observed in the absence of cCPA.

Initially, a dose of 2.5 µg pcCPA was administered (equal to the molar quantity of the highest dose of native CPA that was tested in **Figure 8**). Since we could not demonstrate any convincing effect of uncaging with this dose, we increased it tenfold to 25µg pcCPA. At this dose, we occasionally achieved inhibitory effects upon illumination after administration. However, these results were not reproducible with our safe illumination protocol and use of higher intensity illumination made the effects indistinguishable from those caused by light itself. A final increase of the pcCPA dose to 100 µg (using the highest concentration achievable) did lead to reproducible inhibition of both fEPSP slope and population spike amplitude of DG evoked potentials (**Figure 9**), using the safe illumination protocol and thus allowed us to achieve a proof of concept for the uncaging of pcCPA *in vivo*. However, in order to achieve this dose, we had to dissolve the compound in 100% DMSO. At this moment in time, however, we are working intensely with collaborators from the Department of Medicinal Chemistry at Ghent University to optimize the compound through 1) improving water solubility and 2) testing other photocages which are sensitive to light at more favorable wavelengths, i.e. longer wave-lengths which are less absorbed by biological tissue and thus provides better penetrance with less local heating.

Although using 100% DMSO as a solvent is not feasible from a translational point of view beyond terminal *in vivo* experiments, it will be sufficient to bring us towards a demonstration of *in vivo* proof of concept for closed-loop photopharmacology, as already demonstrated *in vitro*. In future experiments, which will conclude this manuscript, we will first and foremost increase the number of animals and include a suitable vehicle condition for the experiment presented in **Figure 8**. We will then move on to adapt the same closed-loop photopharmacology concept, demonstrated *in vitro*, to reduce excitability in a controlled manner in our *in vivo* model. Initially, we will do so under physiological conditions, by reducing the amplitude of our evoked potentials to 50% of baseline. Subsequently, we will do the same under conditions of hyperexcitability, characteristic of the epileptic brain, by elevating concentrations of potassium, as was done *in vitro*. We expect that a majority of this experimental work can be concluded in the course of 2022 and to be ready for publication of this work in the beginning of 2023.

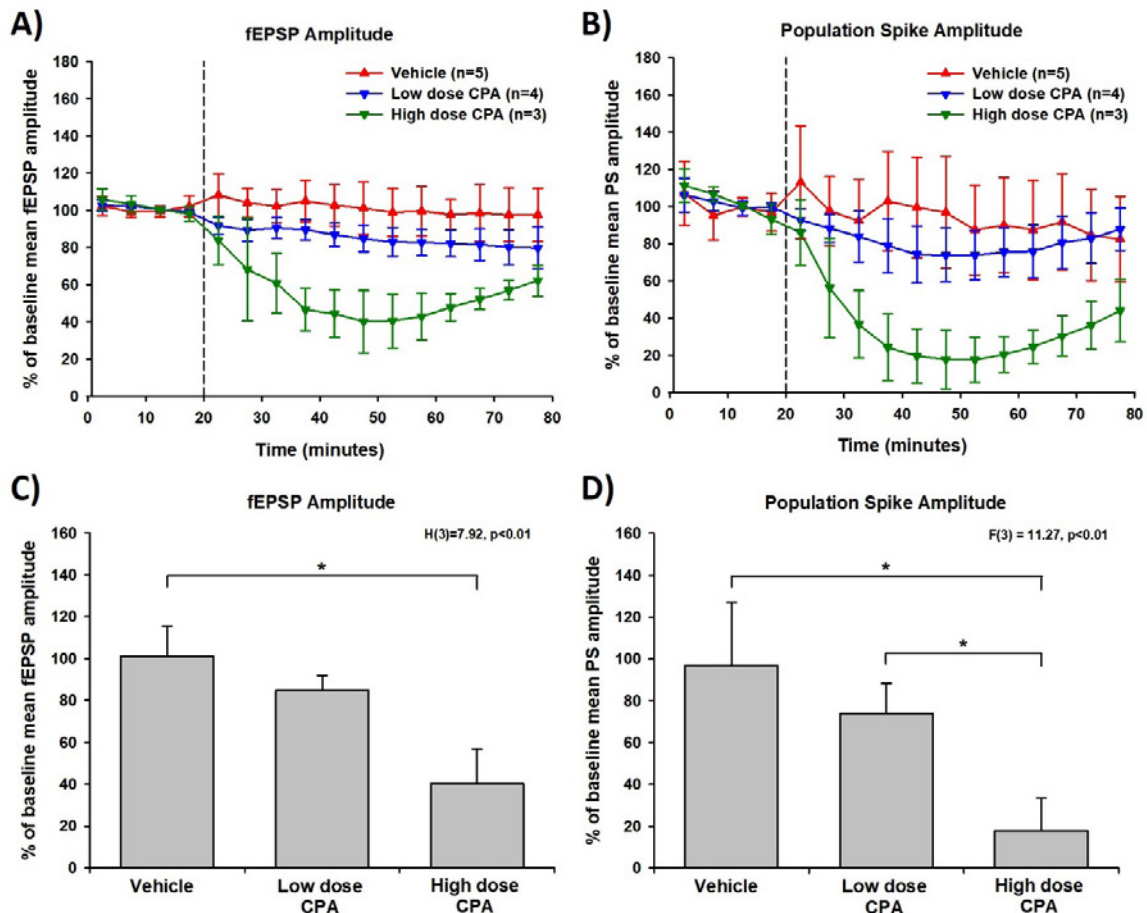


Figure 8: CPA administered intracerebroventricularly induces a dose-dependent inhibition of dentate gyrus EPs, reflected by a gradual reduction in both field excitatory postsynaptic potential (fEPSP) amplitude and population spike amplitude (A and B), which was significant 30 minutes after administration of CPA (C and D).

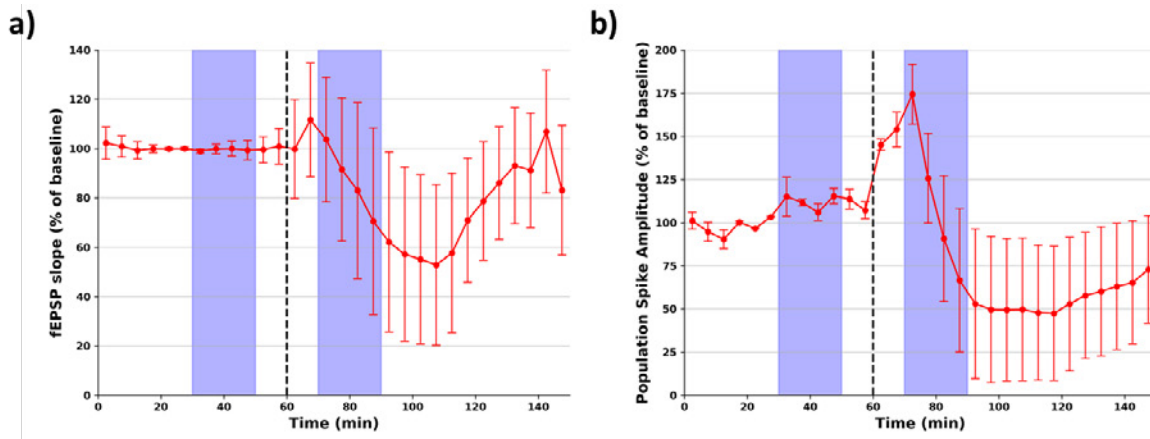


Figure 9: Effects of uncaging cCPA locally in the hippocampus following intracerebroventricular administration on evoked potentials recorded in the dentate gyrus. Light prior to cCPA administration had no effect on fEPSP slope or population spike amplitude (b). Following administration of cCPA, indicated with a dashed vertical line, light induced a strong suppression of both fEPSP slope and population spike amplitude. Data is presented as means \pm SEM (n=3).



Geneeskundige Stichting Koningin Elisabeth
Fondation Médicale Reine Elisabeth
Königin-Elisabeth-Stiftung für Medizin
Queen Elisabeth Medical Foundation

Progress report of the research project of the young researcher

Aya Takeoka, PhD (IMEC)
Katholieke Universiteit Leuven (KU Leuven)

Aya Takeoka PhD

Principal Investigator at NERF, a joint research initiative by imec, VIB and KU Leuven

Assistant Professor, Department of Neuroscience @ KU Leuven

T +32 16 28 31 14

aya.takeoka@nerf.be

www.nerf.be

twitter.com/TakeokaLab

Learning to walk without the brain: Determining cellular signatures underlying age-dependent spinal cord plasticity

1. Aims and summary

Adult rodents with complete spinal cord transection (cSTX) at the thoracic level do not spontaneously regain the capacity to walk. Nevertheless, mice receiving the same injury at an early postnatal period (postnatal day 5, P5) exhibit proficient hindlimb locomotion on a motorized treadmill as adults. This is achieved despite the spinal cord circuits controlling hindlimb movements being functionally isolated from the brain. With support from GSKE/FMRE, **we uncovered the age of injury-dependent divergent synaptic connectivity from interneurons to motor neurons** (Bertels et al., in revision, *Nature Neuroscience*). Adult injury prompts neurotransmitter switching of excitatory interneurons to inhibitory phenotype, promoting inhibition at synapses interfacing motor neurons.

In contrast, neonatal injury causes synaptic sprouting of identical populations to facilitate excitation. Furthermore, genetic manipulation to mimic inhibitory phenotype observed after adult injury by these excitatory interneurons abrogates autonomous locomotor functionality in neonatally injured mice. In comparison, attenuating inhibitory phenotype improves locomotor recovery after adult injury. Together, our study demonstrates that flexible neurotransmitter phenotype of defined excitatory interneurons steers locomotor capacity after injury.

1.1. Finding 1. vGlut2^{ON} interneurons undergo neurotransmitter phenotype switch after adult injury.

Synaptic input from spinal interneurons to MNs is one of the factors regulating the final CNS output that controls muscle contractions. As inhibitory synaptic input to MNs is known to increase after injury, we asked whether the excitatory/inhibitory synaptic input ratio from spinal interneurons to MNs that innervate hindlimb muscles depends on injury age. To visualize excitatory and inhibitory synaptic terminals, we crossed major excitatory or inhibitory NT Cre-driver lines (*vGlut2^{cre}* or *vGAT^{cre}*) with *Tau^{LSL-nlsLacZ-SynGFP}* reporter mice to conditionally express Synaptophysin tagged with GFP (SynGFP^{ON}) in either excitatory or inhibitory spinal interneurons. This approach indelibly labeled presynaptic input derived from either genetically glutamatergic vGlut2^{ON} or inhibitory vGAT^{ON} interneuron populations to choline acetyltransferase^{ON} (ChAT^{ON}) MNs (Fig. 1a). This method shows high fidelity between genetically labeled excitatory or inhibitory terminals to assess protein expression of vGlut2 or vGAT with immuno-labeling (designated as vGlut2+ or vGAT+, as opposed to genetically labeled vGlut2^{ON} or vGAT^{ON}) in intact spinal cords (> 80%; Fig. 1b-d).

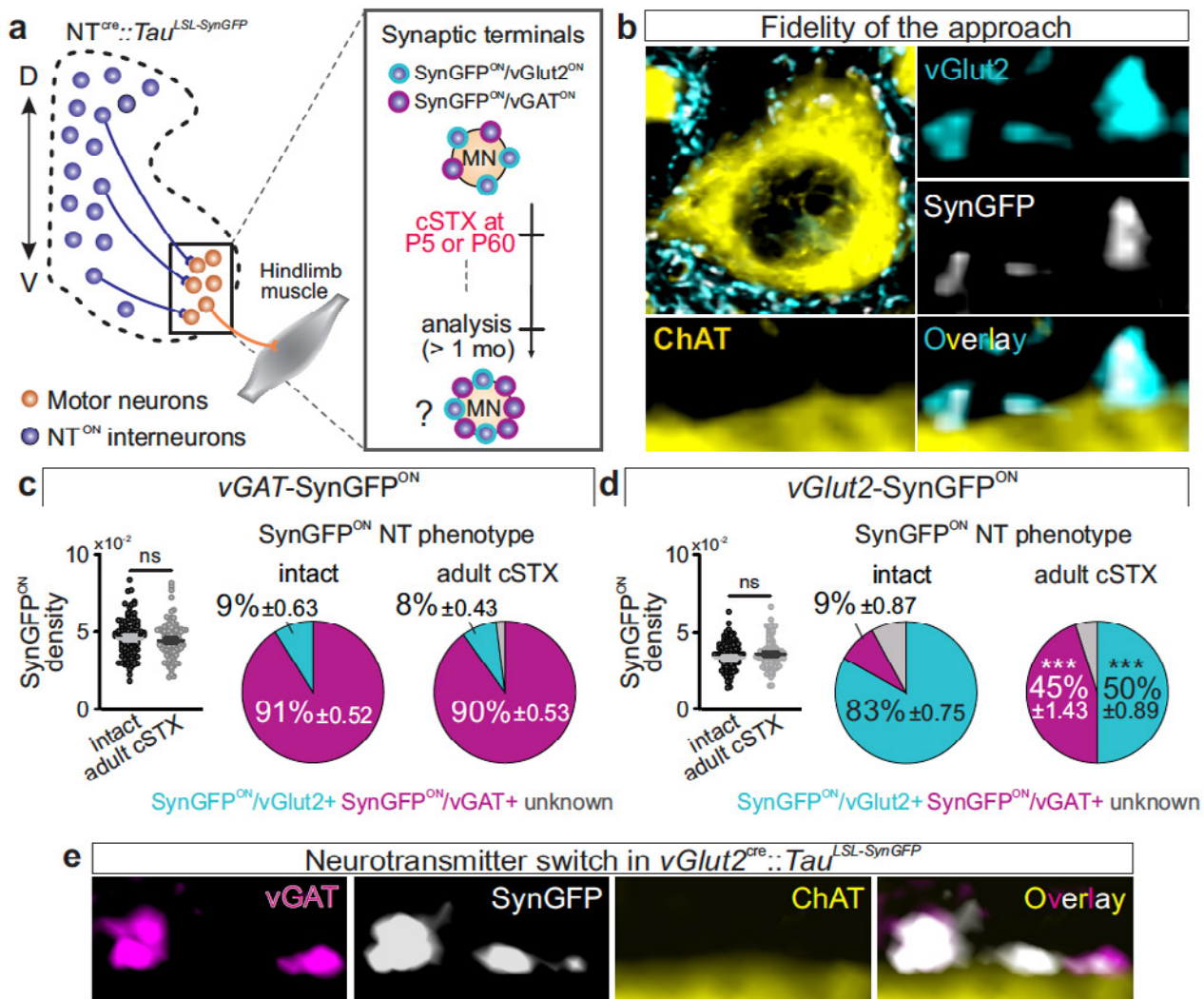


Fig 1. vGlut2^{ON} interneurons undergo neurotransmitter phenotype switch after adult injury.

a. Experimental scheme to visualize and quantify synaptic terminals derived from specific interneurons. **b.** Representative image of synaptic apposition of SynGFP^{ON} terminals to a ChAT^{ON} motor neuron and colocalization of vGlut2 antibody in intact vGlut2^{cre::Tau}LSL-SynGFP spinal cord. **c, d.** Synaptic terminals derived from vGAT^{ON} (**c**) or vGlut2^{ON} (**d**) neurons depicted in the density of SynGFP^{ON} synaptic boutons (μm^2) apposing MNs (left) and % antibody labeling of NT expression (vGlut2+ or vGAT+) with SynGFP^{ON} genetic markings to visualize NT phenotype (right) of intact and adult cSTX spinal cords. Each dot represents one MN. A low level of NT phenotype switch is detected in intact preparation for both intercrosses. **e.** Genetically marked SynGFP^{ON} terminals co-immunolabeled for vGAT protein (vGAT+) in vGlut2^{cre::Tau}LSL-SynGFP spinal cord after adult injury.

Surprisingly, we detected no increase in the number of synaptic terminals derived from genetically marked inhibitory terminals in vGAT^{cre::Tau}LSL-SynGFP spinal cords after adult injury (Fig. 1c). Instead, we detected a five-fold increase of genetically marked excitatory terminals with vGAT+ expression (% SynGFP^{ON}/vGAT+) in vGlut2^{cre::Tau}LSL-SynGFP spinal cords (Fig. 1d, 1e). The number of genetically marked SynGFP^{ON} terminals in the vGlut2^{cre} background remained unchanged after adult injury (SynGFP^{ON} density). In parallel, we found a decrease in % of SynGFP^{ON}/vGlut2+ and, conversely, a strong increase in SynGFP^{ON}/vGAT+ terminals, where almost half of the synaptic terminals derived from vGlut2^{ON} neurons became vGAT+ (Fig. 1d). Supporting this observation, we also found that vGlut2+ or vGAT+ expression at SynGFP^{ON} terminals is mutually exclusive (data not shown).

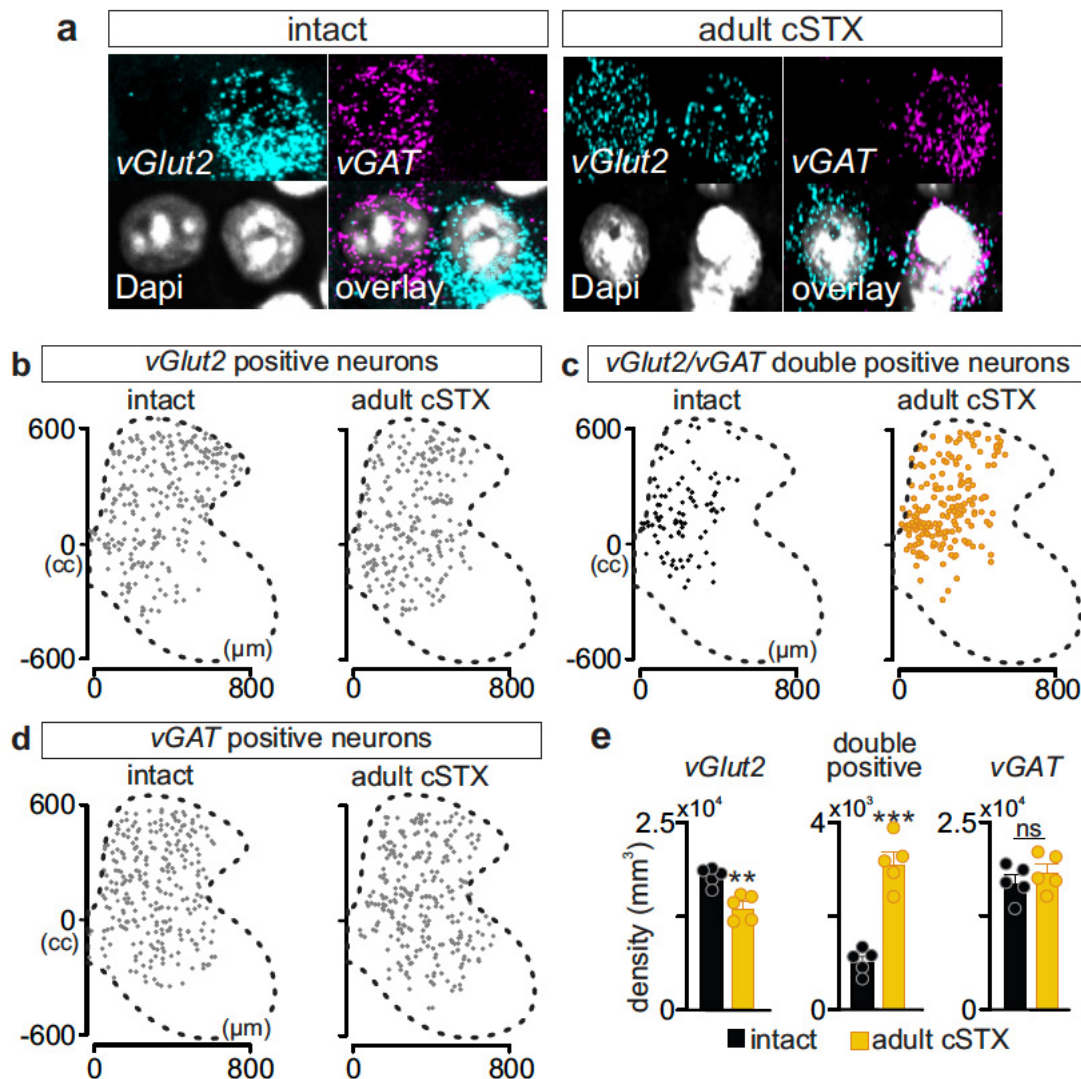


Fig 2. Dorsal and intermediate vGlut2^{ON} interneurons acquire vGAT phenotype after adult injury.

a. Representative *in-situ* hybridization example of the lumbar spinal cord (L4-6) sections with a singular expression of *vGlut2*, *vGAT*, or double-positive (*vGlut2/vGAT*), marked with DAPI.
b-d. Location of neurons with singular *vGlut2*, *vGAT*, or double *vGlut2/vGAT* expression for intact and adult cSTX experimental groups.
e. Density of singular *vGlut2*, double-positive and singular *vGAT* neurons of intact and adult cSTX mice. Each dot represents the mean of individual animals.

A phenomenon of activity-dependent NT phenotype switch in the brain is reported previously. To determine whether this observation at synaptic terminals is the case and, if so, whether the NT phenotype switch occurs uniformly among glutamatergic interneurons, we used *in-situ* hybridization of *vGlut2* and *vGAT* mRNA. In an intact spinal cord, we detected neurons with a singular expression of *vGlut2* or *vGAT* transcripts in equal abundance, with only a minor population of neurons co-expressing *vGlut2* and *vGAT* transcripts distributed sparsely along the dorsoventral axis (Fig. 2a-e). Together with the protein level analysis, we detected a low level of the opposite NT phenotype in genetically marked terminals (Fig. 2c, 2d). This result demonstrates that NT phenotype switch exists in an intact spinal cord. Adult cSTX significantly increased the density of neurons with *vGlut2/vGAT* co-expression in the dorsal and intermediate lamina (Fig. 2a-e). This shift paralleled a decrease in neurons with a singular expression of *vGlut2*, but no change in *vGAT* (Fig. 2e), a finding that suggests a fraction of dorsal and intermediate excitatory interneurons acquires inhibitory NT phenotype at the transcript level after adult injury. Together, our results identified cell type-specific NT phenotype switch as a pathophysiological response to a severe spinal cord injury impacting the mature nervous system.

1.2. Finding 2. vGlut2^{ON} interneurons undergo synaptic sprouting after neonatal injury.

Next, we determined whether a similar NT phenotype switch occurred following neonatal injury. Much in contrast, we found no evidence of NT phenotype switch after neonatal injury. Instead, we observed a significant increase in genetically marked glutamatergic SynGFP^{ON} terminals to MNs in *vGlut2^{cre}::Tau^{LSL-SynGFP}* mice (Fig. 3a, 3b). Together, the two injury models revealed that the age of injury defines two opposing synaptic connectivity profiles of excitatory interneurons to motor neurons. We found genetically marked glutamatergic synaptic sprouting after neonatal injury, in contrast to NT switch after adult injury, which led to high vGAT⁺ synaptic input to MNs (Fig. 3c).

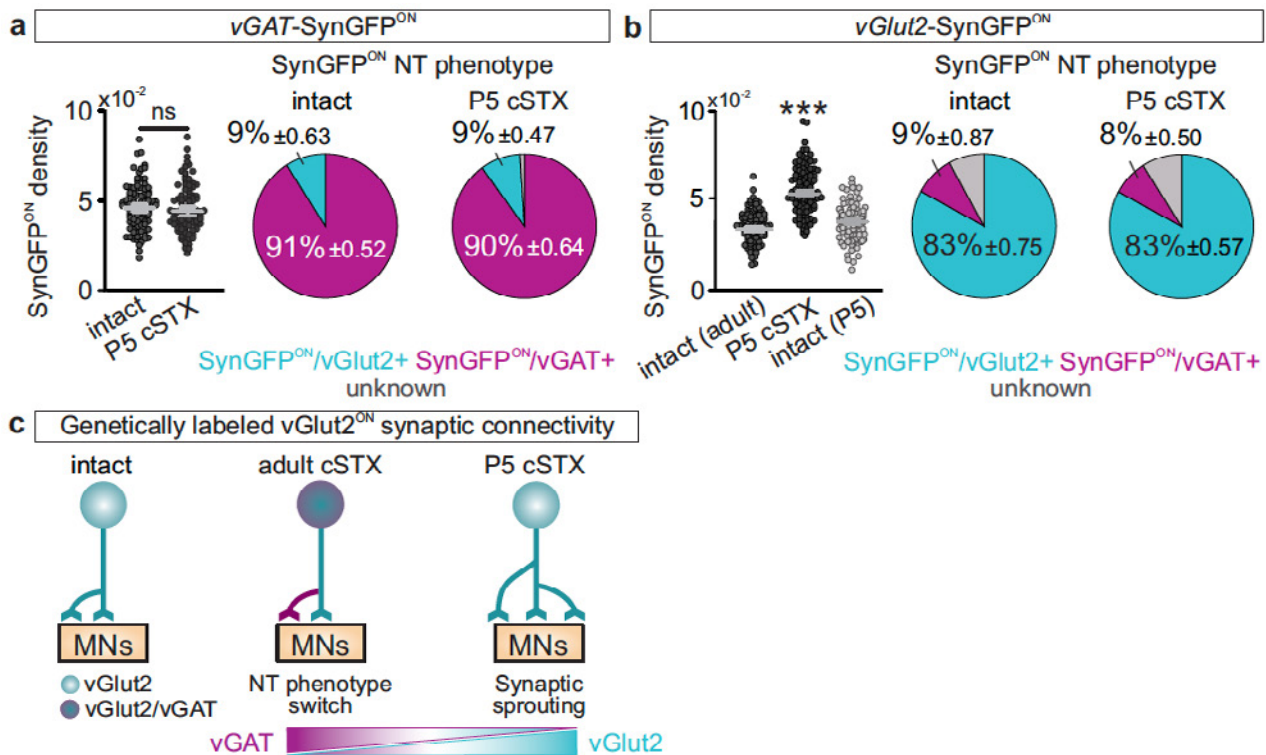


Fig 3. vGlut2^{ON} interneurons undergo synaptic sprouting after neonatal injury.

a, b. Synaptic terminals derived from vGAT^{ON} (**a**) and vGlut2^{ON} (**b**) neurons depicted in density of SynGFP^{ON} synaptic boutons ($/\mu\text{m}^2$) apposing MNs (left) and % antibody labeling of NT expression with SynGFP^{ON} genetic markings to visualize NT phenotype (right). Each dot represents one MN. interneurons. **c.** Summary diagram of NT phenotype switch and synaptic sprouting of genetically labeled vGlut2^{ON} interneurons.

1.3. Finding 3. Age of injur-dependent synaptic input reorganization from glutamatergic interneurons to MNs is subpopulation specific.

Our analysis of *vGlut2* and *vGAT* transcript expression after adult injury reveals that specific vGlut2^{ON} neurons residing in the dorsal and intermediate lamina are driving the process of NT phenotype switch (Fig. 2c). To gain genetic access to different subpopulations of excitatory interneurons residing along distinct dorso-ventral positions in the spinal cord (Fig. 4a), we used stratification by developmental origin. We used three transgenic mouse lines, each expressing Cre-recombinase under the control of a different progenitor domain (PD) specific transcription factor (*PD^{cre}*; Fig. 4b) and intercrossed with the *Tau^{LSL-SynGFP}* reporter line to selectively visualize synaptic output derived from the selected PD population.

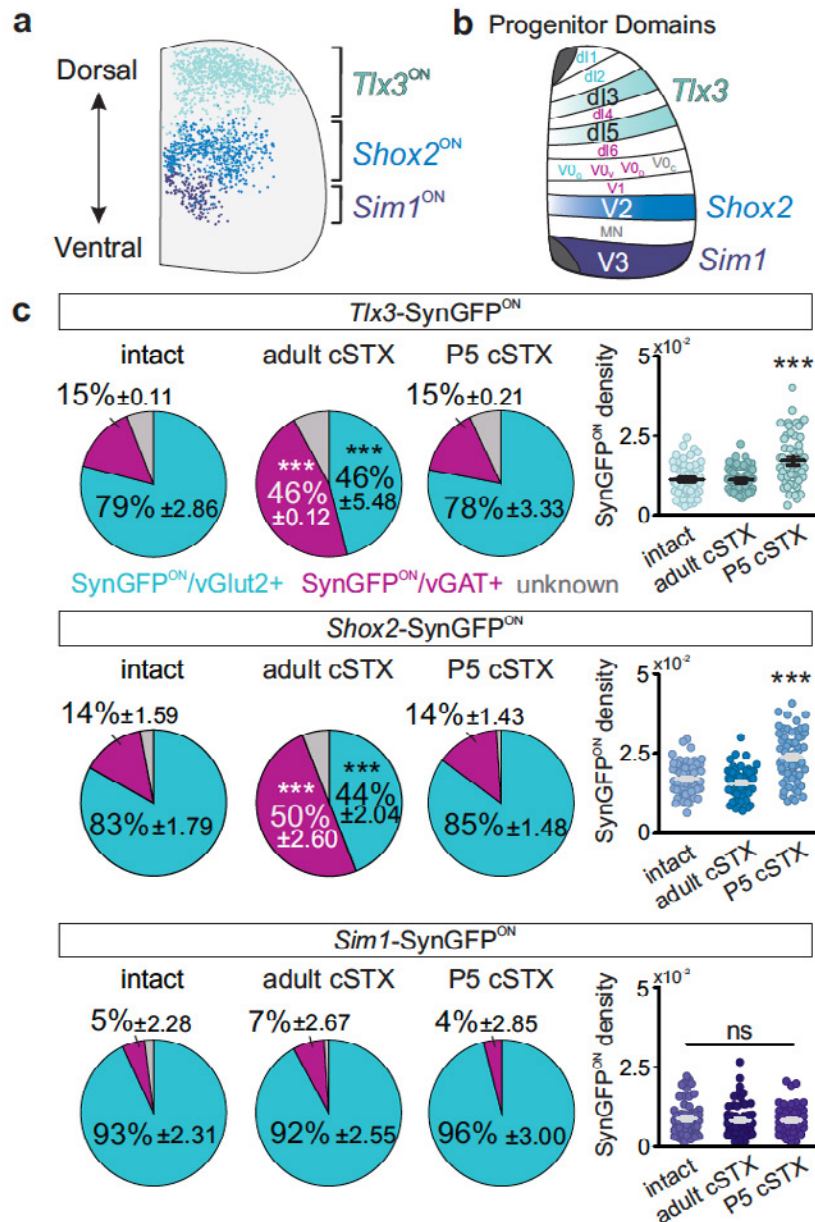


Fig 4. Age of injury-dependent synaptic profile of excitatory interneurons is subpopulation specific.

a, b. Scheme of analyzed excitatory subpopulations and their positions in the mature lumbar spinal cord (**a**) and transcription factor code of spinal cord progenitor domains (PD). PDs that give rise to vGlut2^{ON} interneurons in cyan, cholinergic interneurons, and MN in gray (**b**, PD: dl1-dl6, V0-V3, and MN, examined excitatory subpopulations: light blue *Tlx3*^{ON}, blue *Shox2*^{ON}, and purple *Sim1*^{ON}).

c. Quantification of synaptic terminals derived from *Tlx3*^{ON}, *Shox2*^{ON}, and *Sim1*^{ON} neurons depicted in NT phenotype identity (left: NT+) and density of SynGFP^{ON} synaptic boutons (/ μm^2) apposing MNs (right) in intact, adult cSTX and P5 cSTX spinal cords. Each dot represents one MN.

We found that both PD identity and age of injury determined the NT profile of their synaptic output. After the adult injury, *Tlx3*^{ON} (dl3 and dl5) and *Shox2*^{ON} (V2a), but not *Sim1*^{ON} (V3) interneurons, exhibited increased SynGFP^{ON}/vGAT+ and decreased SynGFP^{ON}/vGlut2+ terminals to MNs (Fig. 4c). After the neonatal injury, all three PD populations maintained their glutamatergic phenotype, consistent with the analysis on pan-vGlut2^{ON} interneurons (Fig. 3b). Interestingly, we found that the neonatal injury-dependent synaptic sprouting was also subpopulation-specific (Fig. 4c). We detected more SynGFP^{ON} boutons from *Tlx3*^{ON} and *Shox2*^{ON}, but not *Sim1*^{ON} interneurons to MNs, in P5 cSTX compared to the intact spinal cord. Together, we unraveled that the age of injury-specific NT identity switches and connectivity rearrangements to MNs occur with remarkable cell type specificity among excitatory interneurons.

1.4. Finding 4. Overexpression of vGAT disrupts walking without the brain after neonatal injury.

Next, we asked whether maintaining the vGlut2^{ON} phenotype is essential for proficient stepping without the brain. We performed an intraspinal injection of LoxP-flanked AAVs in the lumbar spinal cord to express vGAT (AAV-DIO-vGAT-Tag) by excitatory neurons. Broad injection of the virus across lumbar segments led to expression of the Tag at the cell body (data not shown). We then examined the locomotor ability of P5 cSTX mice with AAV-DIO-vGAT-Tag (P5 cSTX+vGAT) or control injection of AAV-DIO-Tag (P5 cSTX+control) at ~P60 (Fig. 5a).

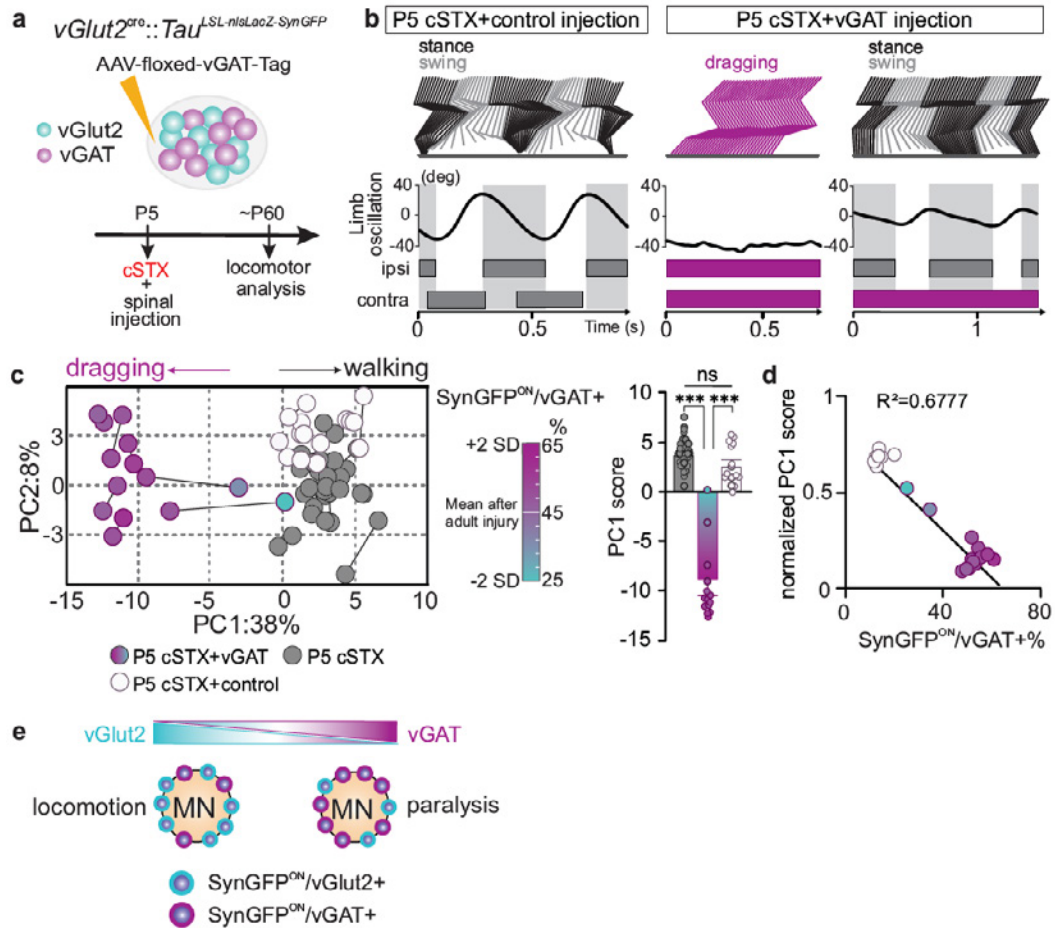


Fig 5. Overexpression of vGAT disrupts the ability to walk without the brain after neonatal injury.

a. Experimental strategy to transduce vGAT expression in vGlut2^{Cre} spinal interneurons and timeline. **b.** Stick decomposition, limb oscillation, and corresponding stance/swing phases of P5 cSTX+control injection and P5 cSTX+vGAT mice. Dark gray horizontal bars indicate stance, and empty spaces correspond to swing. Magenta bars indicate complete dragging of the hindlimbs. **c.** PC analysis was applied on mean values of 94 gait parameters. Each dot represents limb kinematics of either left or right hindlimb of one mouse. Color gradient ranges from 65% to 25% representing the highest (magenta) and the lowest (cyan) % SynGFP^{ON}/vGAT+. PC1 scores of P5 cSTX+vGAT showed a significant difference compared to P5 cSTX and P5 cSTX+control injection. **d.** Linear regression analysis of locomotor capacity and NT composition of SynGFP^{ON} synaptic terminals in P5 cSTX mice with control or AAV-vGAT injections. Individual PC1 values were normalized using z-score and scaled to [0,1].

Virus-mediated expression of vGAT after neonatal injury deteriorated locomotor performance. While P5 cSTX+control mice displayed alternation between left and right limbs, P5 cSTX+vGAT mice largely failed to develop a brain-independent locomotor capacity (Fig. 5b). However, we observed unilateral, non-weight bearing reflexive steps on rare occasions (Fig. 5b, right panel). Therefore, we reconstructed SynGFP^{ON} terminals to MNs and quantified their NT phenotype as a proxy to validate viral transduction efficiency. We applied PC analysis on 94 parameters and then matched the % vGAT phenotype of synaptic terminals to each examined limb. Reconstructed PC space segregated experimental groups primarily based on variability related to dragging-related parameters (Fig. 5c).

Furthermore, limb kinematics during treadmill locomotion broadly matched the extent of viral efficiency among experimental mice, i.e., hindlimbs with low vGAT % synaptic inputs to MNs display ambulatory phenotype and not dragging (Fig. 5d). Therefore, we conclude that acquiring vGAT accompanied by reduction of vGlut2 phenotype by dorsal and intermediate glutamatergic interneurons after neonatal injury deteriorates locomotor ability. Together, our results suggest causality between a NT shift by glutamatergic interneurons in the dorsal and intermediate lamina and locomotor capacity after injury, regardless of whether it is due to spontaneous shift after adult injury or virus-mediated shift after neonatal injury.

1.5. Finding 5. Suppression of vGAT improves locomotor kinematics after adult injury.

Having established that defined subpopulations of vGlut2 interneurons undergo a NT phenotype switch after adult injury and that the vGlut2 neurotransmitter phenotype is critical for proficient locomotion after neonatal injury, we asked whether attenuating NT phenotype switch from vGlut2⁺ to vGAT⁺ facilitates locomotor improvement after adult injury. We devised an approach to conditionally downregulate vGAT expression in vGlut2 interneurons using an intraspinal injection of LoxP-flanked AAVs encoding short-hairpin RNA against vGAT gene expression (*shRNA-vGAT-Tag*; Fig. 6a). We then performed an intraspinal injection of AAV-floxed-*shRNA-vGAT* in *vGlut2^{cre}::Tau^{LSL}-SynGFP* in the lumbar spinal cord followed by a complete transection and assessed stepping capability six weeks after injury (Fig. 6b). All mice with *shRNA-vGAT* injection exhibited a few spontaneous consecutive steps, albeit limited and uncoordinated, compared to almost no steps by untreated mice (Fig 6c, 6d). Although only partially and variably, these data suggest that the treatment influences recovery. Lack of complete recovery is not surprising as a severe injury leads to other circuit changes independent of NT phenotype switch or maintenance. Therefore, we then combined this intervention with weight-supported locomotor training known to ameliorate such maladaptive circuit-wide plasticity.

We subjected subsets of adult cSTX mice with or without *shRNA-vGAT* intervention to daily treadmill training of 20 minutes for four weeks (Fig. 6e). To train mice after adult injury, we used wide-spectrum serotonergic receptor agonists that acutely and temporally enable alternating weight-bearing stepping in rodents with complete spinal cord transection. These agonists elevate the excitability of the spinal cord and allow training without any apparent long-term effects.

After four weeks of training, we quantified spontaneous locomotor capacity based on 102 gait parameters without serotonergic agonists. Like *shRNA* only group, the locomotor ability of the individual mouse was highly variable. Nonetheless, PC1 captured *shRNA-vGAT* effects of both groups with and without training (33% of explained variance), where training further enhanced *shRNA-vGAT* effects (Fig. 6f). Extraction and grouping of parameters highly correlated with PC1 demonstrate that *shRNA-vGAT* combined with daily training significantly reduced the percentage of dragging and improved joint oscillation, measures associated with locomotor recovery (Fig. 6g). While training alone does not improve locomotor ability after an adult injury, a finding that is consistent with previous studies (Fig. 6f, 6g), we found that training alone partially prevented NT phenotype switch, i.e., reduced vGAT phenotype by dorsal and intermediate excitatory interneurons compared to no intervention (data not shown). Furthermore, training facilitated vGlut2^{ON} synaptic sprouting, a circuit reorganization signature we detected after neonatal injury (data not shown), a potential contributing factor to the added recovery observed in the *shRNA+training* group.

Together, our results demonstrate that reducing neurotransmitter phenotype switch alone promotes locomotor pattern expression, and a combination of long-term locomotor training further facilitates distinct aspects of locomotor recovery after adult injury (Fig. 6h).

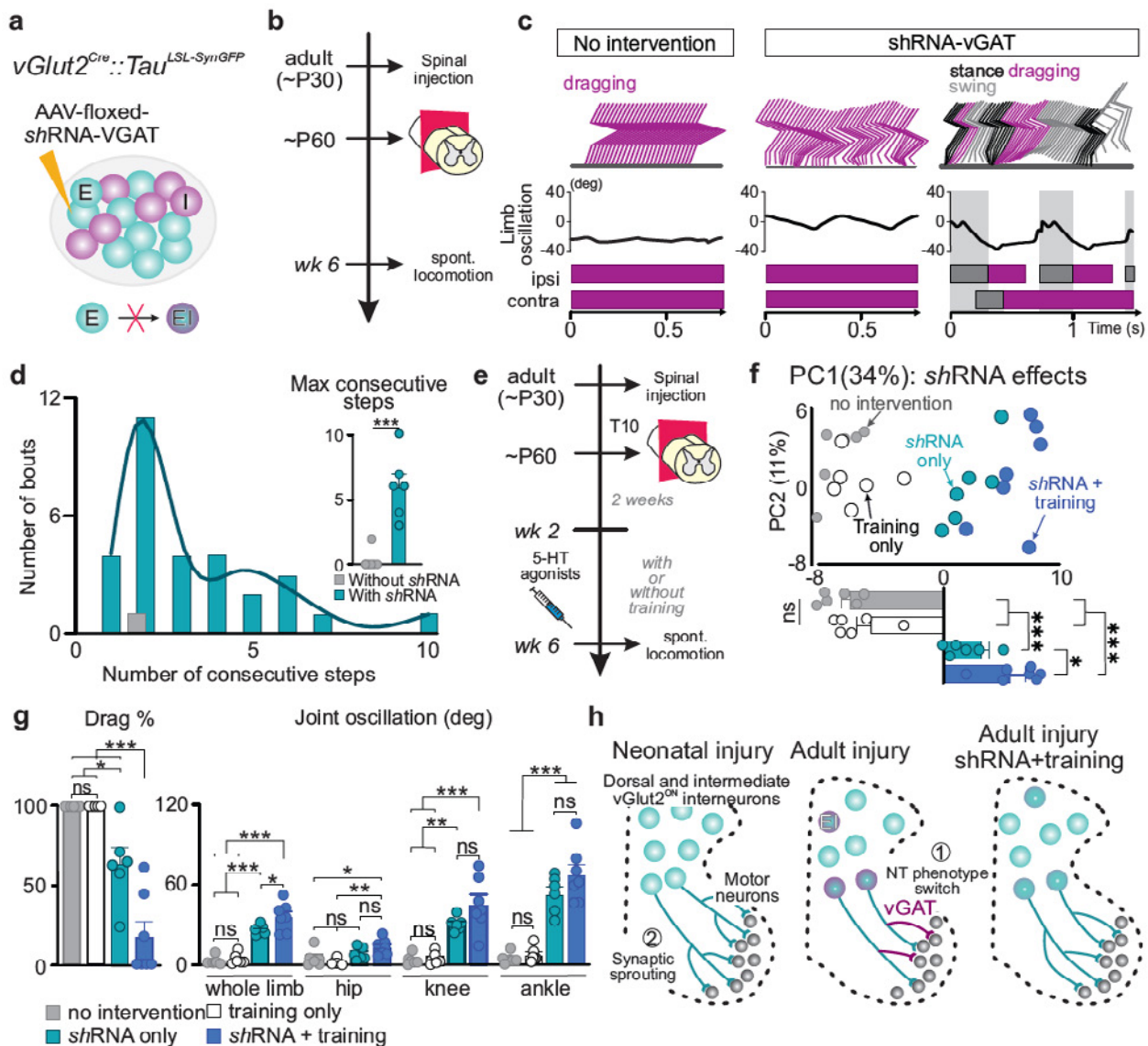


Fig 6. Suppression of vGAT expression by excitatory interneurons combined with locomotor training facilitates locomotor recovery after adult injury.

a, b. Experimental strategy and timeline to attenuate vGAT expression in genetically labeled *vGlut2^{DN}* spinal interneurons after adult injury. **c.** Representative stick decomposition of adult cSTX mice with control (left) and *shRNA-vGAT* (middle and right) injections at week 6. **d.** Frequency plot of stepping bouts and quantification of the maximum number of consecutive steps during a 30-sec recording session. **e.** Timeline to induce stepping after adult injury with or without daily locomotor training and the timeline. **f.** PC analysis of spontaneous stepping at week 6. Each dot represents one mouse. Histogram plots show differences in PC1 scores. **g.** Examples of kinematic parameters with additive effects of daily training combined with *shRNA-vGAT*. **h.** Age of injury-dependent circuit signatures capture decreasing vGlu^{2DN} input due to NT re-specification of dorsal and intermediate excitatory interneurons after adult injury (1) in contrast to increasing vGlu^{2DN} premotor synaptic input derived from the same population to MNs after neonatal injury (2). *shRNA-vGAT* and training interventions respectively minimize NT phenotype switch and facilitate synaptic sprouting, therefore likely contributing to added effects of recovery when combined.

2. Ongoing work and future outlook

We demonstrate that neurotransmitter phenotype of a subpopulation of excitatory interneurons underlies one of the mechanisms that direct locomotor capacity after spinal cord injury. Given these observations, we hypothesized that transcriptomic profiles that define locomotor circuit plasticity are dramatically altered in an age of injury-dependent manner. We are currently working to determine the transcriptomic profiles of adult spinal cord injured as neonate versus adult. Knowledge gained from such experiments will allow us to determine positive/negative regulators beyond neurotransmitter phenotype that are potentially druggable targets. We will further determine the locomotor capacity of mice injured as adults with *in-vivo* manipulation that facilitates novel neural circuit connectivity and locomotor recovery.

3. Manuscript in revision with GSKE/FMRE support

- Bertels H., Ortiz-Vicente G., El Kanbi K., Takeoka A. Flexible neurotransmitter phenotype of spinal excitatory interneurons defines locomotor ability after spinal cord injury. In revision at *Nature Neuroscience*



Geneeskundige Stichting Koningin Elisabeth
Fondation Médicale Reine Elisabeth
Königin-Elisabeth-Stiftung für Medizin
Queen Elisabeth Medical Foundation

Progress report of the research project of the young researcher

Dr. Valerie Uytterhoeven
Katholieke Universiteit Leuven (KU Leuven)

Dr. Valerie Uytterhoeven

Staff Scientist

Center for Brain & Disease Research, VIB-KU Leuven

Laboratory of neuronal communication

Herestraat 49 bus 602

3000 Leuven

Belgium

Tel: +32 16 37 61 03

Molecular mechanisms and inducers of chaperone mediated Tau autophagy in Alzheimer's disease

1. Summary research program

Our lab has shown that Tau mediated neuronal defects are rescued at 9 months with reducing Tau-synaptic vesicle interactions in fruit flies and the TauPS19 mouse models that express human Tau at 9 months, however, Tau continues to accumulate at presynapses in these models. To stop further accumulation of Tau at presynapses, we tested if increasing endosomal microautophagy, as Tau has two endosomal microautophagy recognition motifs, can reduce Tau at fly presynapses. Previously, we have shown that the expression of Hsc70-4 increases endosomal microautophagy in fly presynapses and reduces presynaptic proteins with endosomal microautophagy motifs [1]. We now show that elevated Tau levels at presynapses can be reduced by with the expression of Hsc70-4 rescuing Tau-mediated presynaptic defects and neurodegeneration. However, the Tau^{V337M} mutant which harbors a mutation in the first endosomal microautophagy motif is not rescued with increased endosomal microautophagy. We show with a fluorescent timer attached to Tau that older Tau^{V337M} is present at presynapses compared to Tau^{P301L}, indicating that the turnover of Tau^{V337M} is reduced. Since several Tau mutations result in similar accumulation of Tau at presynapses we hypothesized that different molecular mechanisms result in the accumulation of Tau at presynapses. Using a FRAP assay of Tau-GFP we uncovered that the detachment of Tau from microtubuli in axons is more prominent in Tau^{P301L} mutant presynapses. To further test if both pathways contribute to the accumulation of Tau at presynapses, we generated double P301L and V337M mutants. This resulted in additional accumulation of Tau at presynapses, and neurodegeneration compared to single mutants. Using a fluorescent timer and FRAP assay, we measured that in P301L, V337M double mutants older Tau protein is present at presynapses like Tau^{V337M} mutants, and that Tau detaches from microtubule like Tau^{P301L} mutants. Together in Tau double mutants a defect in turnover and increased detachment from microtubule result in further increased Tau levels at presynapses. Hence, several pathways may contribute to the accumulation of Tau at presynapses.

To further validate our findings in humans, we are characterizing Tau mutant human neurons derived from patients. Using immunohistochemistry and electrophysiological recordings on multielectrode arrays, we will test if Tau also accumulates in human neurons and results in neurotransmission defects as we see tau mutant fruit flies and TauPS19 mouse model [2–4]. Spontaneous activity measurements with the MEA system indicates that Tau^{P301L} mutants have reduced neurotransmission however these results have to be further validated. Further, we will test if lentiviral or compound mediated expression of HSPA8, the human homologue of Hsc70-4, is able to rescue Tau mediated defects including presynaptic Tau accumulation and neurotransmission defects. Thus far, the compound geranylgeranyl acetone (GGA), which increases the expression of HSPA8 via the PKC pathway, reduces overall phosphorylated Tau in human cortical neurons. Since, HSPA8 chaperone has multiple functions, such as refolding proteins via its chaperone function and autophagic turnover via its membrane deformation function, we tested if other proteins with endosomal microautophagy motifs are being degraded with the treatment of GGA. -synuclein, a protein that also harbors endosomal microautophagy motifs, is reduced upon GGA-treatment as quantified after anti -synuclein immunofluorescent labeling in Tau^{P301L} mutant human neurons. Together, the reduction of Tau in Tau^{P301L} mutant human neurons after GGA treatment may be regulated with the increase of endosomal microautophagy but validation experiments are needed.

2. Results

Hsc70-4 has been shown to interact with Tau via a chaperone recognition motif for the degradation of Tau via endosomal microautophagy. However, this has never been shown before at presynapses. Our previous work in fruit flies showed that the expression of Hsc70-4 increases endosomal microautophagy and rejuvenates presynaptic proteins with a chaperone recognition motif [1]. Our very recent and yet unpublished work shows that the accumulation of Tau^{P301L} at presynapses can be reduced with the increase of endosomal microautophagy by the expression of Hsc70-4. In addition, the reduction of Tau^{P301L} at presynapses rescues Tau mediated neurotransmission defects, reduced synaptic vesicle mobility and increased neurodegeneration of aged adult fly brains. However, increasing endosomal microautophagy is not effective in reducing Tau^{V337M} at presynapses. Concomitantly, defects in neurotransmission, synaptic vesicle mobility and neurodegeneration are not rescued in Tau^{V337M} mutant flies when endosomal microautophagy is increased. We suggest that the V337M mutation which lies in the first chaperone recognition motif disrupts the motif so that Tau is not recognized by Hsc70-4 and not degraded via endosomal microautophagy at presynapses. Indeed, when we attach a fluorescent timer, a fluorophore that changes from blue to red over time, we observe increased levels of red Tau protein in presynapses expressing Tau^{V337M} compared to Tau^{P301L} mutant presynapses suggesting that the turnover of Tau^{V337M} is hampered. Since, P301L and V337M Tau accumulate at similar levels in presynapses but the turnover of Tau^{V337M} is different from Tau^{P301L}, we reasoned that the accumulation of Tau^{P301L} at presynapses occurs via a different mechanism. Since, the P301L mutation is located in the microtubule binding domain of Tau, we tested the interaction of the different Tau mutants with microtubuli in the axons. Using a fluorescent recovery after photobleaching assay, we measured that Tau^{P301L} is more mobile in axons compared to Tau^{V337M} suggesting that the detachment from microtubuli contributes to presynaptic accumulation of Tau^{P301L}. Hence, we conclude that in Tau^{V337M} mutants the defect in Tau turnover has a more prominent role in the accumulation of Tau at presynapses and in Tau^{P301L} mutants the detachment of Tau from microtubuli.

We performed additional control experiments that support our conclusion. We generated P301L, V337M Tau double mutant flies to test if a defect in Tau turnover and the detachment from microtubuli can be additive and thus both contribute to the accumulation of Tau at presynapses. Tau immunostainings of Tau^{P301L, V337M} double mutant synapses show increased Tau intensity labeling compared to Tau^{P301L} and Tau^{V337M} single mutants (Figure 4.). In addition, the vacuolar neurodegeneration of 40-day old flies is exacerbated in Tau^{P301L, V337M} mutant flies compared to single mutant flies (Figure 1). Next, we tested if the increased accumulation of Tau in Tau^{P301L, V337M} double mutant presynapses is a result of Tau protein turnover and microtubule attachment defects. With a fluorescent timer attached to the Tau^{P301L, V337M} mutant we measured Tau protein turnover. The red (old protein)/blue (young protein) ratio is increased in the Tau^{P301L, V337M} double mutant compared to the Tau^{P301L} single mutant presynapses and comparable to the Tau^{V337M} single mutant indicating a similar reduction in Tau^{P301L, V337M} protein turnover as the Tau^{V337M} mutant (Figure 3). To test the attachment of Tau to microtubule in axons we attached a GFP to the Tau mutant proteins and performed a fluorescent recovery after photobleaching (FRAP) assay. Tau^{P301L, V337M} has a similar fluorescence recovery time course as Tau^{P301L} and an increased FRAP compared to Tau^{V337M} suggesting increased detachment of Tau from microtubuli in axons (Figure 3). Together, these results show that in Tau^{P301L, V337M} double mutant flies both Tau turnover at presynapses and attachment of Tau to microtubule are affected and that both defects are additive in the accumulation of Tau at presynapses.

An additional control experiment is to assess the health of the endolysosomal system. To test this we measured in different Tau mutant presynapses (P301L, V337M, AA and P301L, V337M double

mutant) the levels of Endophilin A, a presynaptic protein also harboring chaperone recognition-motifs and that we have previously shown to be degraded by endosomal microautophagy [1]. Endophilin A levels at presynapses of flies expressing mutant Tau are comparable to endophilin A levels at presynapses of flies expressing wild type Tau, indicating that endosomal microautophagy at presynapses is still functional when Tau accumulates (Figure 4B). In addition, we measured that the increase of endosomal microautophagy with the expression of Hsc70-4 reduces endophilin A at presynapses compared to presynapses without increased endosomal microautophagy (Figure 4C), indicating that other chaperone recognition-motif containing proteins are still targeted for degradation via endosomal microautophagy. Together, the accumulation of Tau at presynapses does not clog the endosomal microautophagy system and other endosomal microautophagy target proteins are still recognized for turnover.

We obtained patient derived Tau^{P301L} and Tau^{V337M} iPSCs and their isogenic controls from the Celeste Karch lab in Washington University and Neuronal stem cell Institute in New York [5]. I induced them to cortical neuronal progenitor cells and performed immunostainings and QPCR as quality control (Figure 5 A-D). Subsequently, I started the differentiation of the cortical neuronal progenitors into mature neurons tested several markers including, presynaptic, Tau, dendritic markers (Figure 5 E-H) and astrocytic, cortical, glutamatergic, GABAergic markers (not shown). Fruit flies and mice expressing human mutant Tau accumulate Tau at presynapse and have electrophysiological defects [2-4] however, nobody has shown that Tau accumulates at presynapses in Tau mutant human neurons *in vitro*. We performed immunostainings of 65-day old human cortical neurons. We labeled with different anti-Tau antibodies recognizing total Tau or different phosphorylated Tau species, dendrites (MAP2) and different presynaptic markers (synaptogyrin-3, Vglut1). We will perform a compartmental segregation analysis of Tau using the presynaptic and dendritic markers to quantify Tau at presynapses. In addition, electrophysiological recordings on neurons derived from these iPSCs are not published or performed by my knowledge. However, electrophysiological information is available from human neurons derived from triple Tau mutant iPSCs and Tau^{A152T} iPSCs using multielectrode array and patch clamp recording, respectively [6,7]. I used a CMOS multielectrode array (MEA) to analyze if Tau^{P301L} mutant neurons show defective neuronal activity (Figure 6). The MEA has 16000 electrodes at 15µm pitch allowing single cell recordings and spontaneous and evoked responses can be measured. We measured spontaneous activity of cortical neurons at 29 and 36 days old. Tau^{P301L} mutant human neurons show reduced spontaneous activity compared to the isogenic controls at both time points. In addition, at the second time point when neurons could mature 7 days longer, both isogenic control and Tau^{P301L} mutant neurons showed an increase in spontaneous activity, indicating that control and mutant neurons are further maturing (Figure 6). These finding will be further validated using inhibitors and activators of electrical activity and evoked responses will be measured as well at.

In the meantime, we generated lentivirus for the expression of wild type, chaperone defective and endosomal microautophagy defective HSPA8 to modulate endosomal microautophagy levels and we will test if Tau levels are reduced when endosomal microautophagy is increased with WT and chaperone defective HSPA8 but not with endosomal microautophagy defective HSPA8. Besides lentiviral mediated induction also chemical induction of HSPA8 expression is conceived. Geranylgeranyl acetone (GGA) is shown to increase HSPA8 expression by the induction of PKC pathway and is tested nowadays in clinical trials for the treatment of Alzheimer's disease [8-10]. We now tested for the first time GGA treatment in patient derived human neurons. 10 µM GGA is the highest concentration that the neurons stayed healthy over a two-week GGA treatment. The two-week treatment with GGA did not increase HSPA8 levels in the neurons as measured with anti-HSPA8 immunofluorescent labeling (Figure 7C). The same is observed in mice treated

for several days with GGA. Only after acute treatment with GGA an increase in HSPA8 levels was observed [8]. However, despite I did not observe an increase in HSPA8 after a two-week GGA treatment, we analyzed a significant reduction of overall phosphorylated Tau (AT8 and PHF-1, Figure 7D and E) and a trend towards reduction of overall total Tau (HT7, Figure 7F) using immunofluorescent Tau labeling in TauP301L mutant neurons compared to isogenic controls. In addition, -synuclein, another protein harboring a chaperone recognition-motif is reduced in TauP301L mutant neurons compared to isogenic controls after GGA treatment (Figure 7G). However, MAP2, a protein without chaperone recognition motifs is not affected after GGA treatment (Figure 7H). I will further analyze the effect of GGA and lentiviral mediated increase of HSPA8 expression on Tau in different neuronal compartment using immunostainings and overall Tau using western blot. In addition, I will test if GGA and lentiviral mediated induction of HSPA8 rescues electrophysiological defects in TauP301L using a MEA.

3. Future perspectives

3.1. Step 1. Validate presynaptic Tau defects in Tau mutant human neurons.

I differentiated cortical neurons from Tau^{P301L} iPSCs. I will also differentiate cortical neurons from Tau^{V337M} iPSCs. I immunolabeled the differentiated human neurons with dendritic, synaptic and Tau markers and will optimize the analysis of Tau levels in different neuronal compartments. A first experiment on MEA system to record electrophysiological activity shows us that Tau mutant neurons show less spontaneous activity compared to the isogenic control. I will further validate these results using inhibitors and activators of neurotransmission. I will also analyze evoked responses in TauP301L and TauV337M neurons and their respective controls.

3.2. Step 2. Test therapeutic strategies in human neurons

Presynaptic Tau can be reduced with increased endosomal microautophagy by the expression of Hsc70-4. I will test if lentiviral mediated expression of HSPA8, the human homologue of Hsc70-4, rescues Tau mediated phenotypes, such as Tau levels and neurotransmission defects. My preliminary results of the treatment of human neurons with geranylgeranyl acetone (GGA), chemical compound that increases the expression of HSPA8, shows reduction of overall Tau. I will further validate the effect of GGA on Tau levels in different compartments and on neurotransmission. In addition, we will develop in collaboration with a company a molecular glue that brings Tau and Hsc70-4 together.

3.3. Step 3. Validate strategy in chimeric human AD mouse model

The final step is to generate neuronal progenitors that overexpress HSPA8. I will integrate HSPA8 in a safe harbor locus and use these neuronal progenitors for the injection in the APP^{NLGF} AD mouse model and follow the survival and Tau defects in the human neurons overexpressing HSPA8 in the mouse over time.

4. Figures

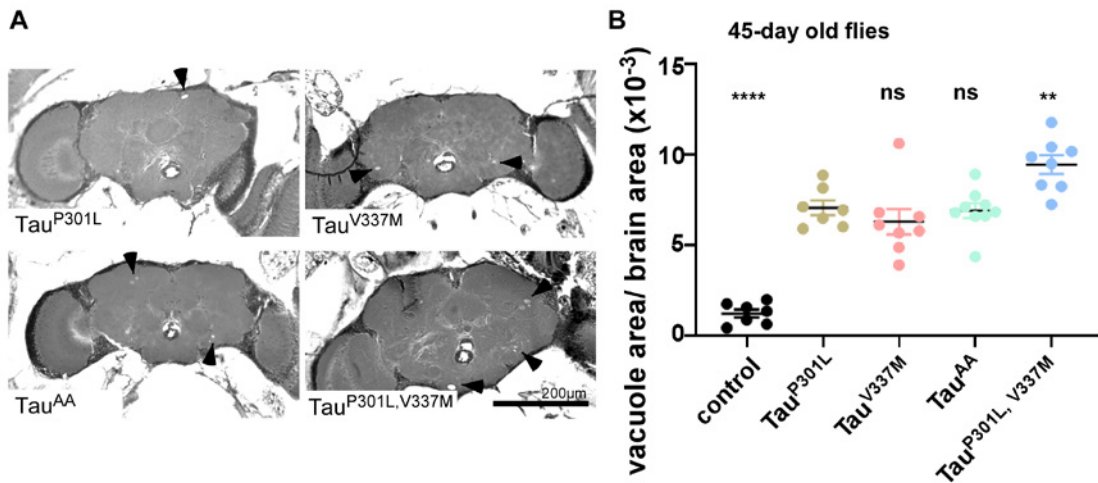


Figure 1. Neurodegeneration in Tau^{P301L, V337M} double mutants is further increased

A) Brain sections of 45-day-old transgenic flies (nSyb-GAL4> Tau^{P301L}; nSyb-GAL4> Tau^{V337M}; nSyb-GAL4> Tau^{AA}; nSyb-GAL4> Tau^{P301L, V337M}) and stained with H&E. **B)** Neurodegeneration was assessed by quantification of vacuole area normalized over brain area. Tau-induced neurodegeneration was further significantly increased in the Tau^{P301L, V337M} double mutants compared to Tau^{P301L} mutant flies. Arrowheads indicate vacuolar degeneration. Data points represent the mean \pm SEM. (number of dots indicate the number of animals (≥ 7)). An ordinary one-way ANOVA with Dunnett's correction for multiple comparison was performed to determine significance levels between all four genotypes; ns, not significant, ** $p < 0.01$, **** $p < 0.0001$. Scale bar: 200 μ m

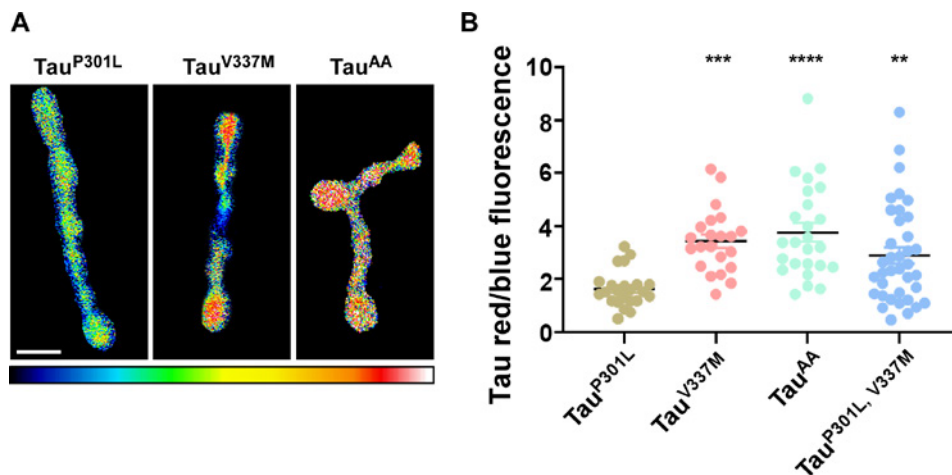


Figure 2. Tau^{P301L, V337M} mutant flies show reduced Tau protein turnover like mutants with tampered chaperone recognition-motifs.

Images **A)** and quantification **B)** of the ratio of red over blue fluorescence intensities of synaptic boutons using the indicated lookup table. The Tau-fluorescent timer was expressed using nSyb-GAL4 in Tau^{P301L}, Tau^{V337M} and Tau^{AA} and Tau^{P301L, V337M} mutants. Scale bar 5 μ m. plotted as individual data points. Graph depicts individual data points and mean \pm SEM. (number of dots is number of synapses imaged from ≥ 8 animals). An ordinary one-way ANOVA with Dunnett's correction for multiple comparisons was performed to determine significance levels between genotypes; ** $p < 0.01$, *** $p < 0.001$, **** $p < 0.0001$.

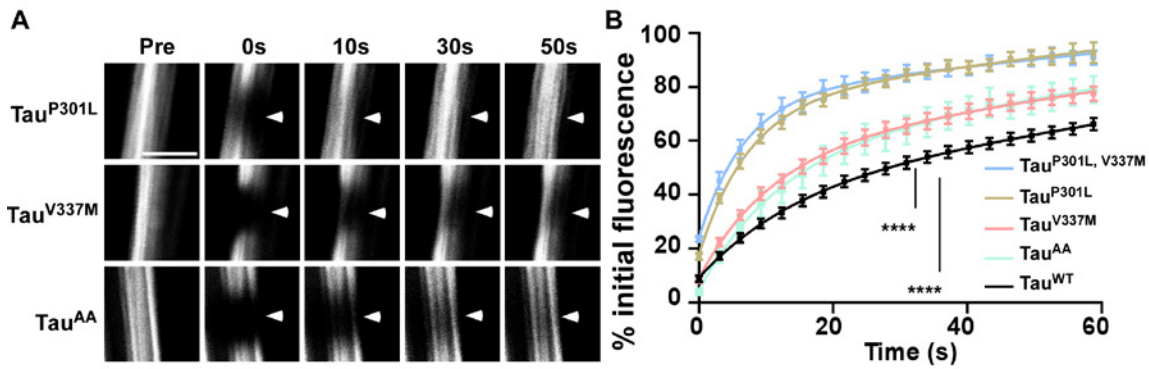


Figure 3. Increased Hsc70-4 mediated endosomal microautophagy rescues TauP301L-induced synaptic vesicle mobility and neurotransmission defects at NMJs

A and B) FRAP assay of Tau mobility within axons. *Drosophila* larvae express Tau-GFP without (WT) or with mutations under the control of the nSyb-Gal4 neuronal driver. **A)** Representative images of Tau-GFP signal before and after photobleaching show fluorescence recovery of a small area (arrowhead) after photobleaching of Tau-GFP fluorescence in presynaptic boutons during a 60 second time frame. Scale bar, 5 μ m. **B)** Plot of Tau-GFP fluorescence recovery over time fit to a double-exponential curve depicting relative Tau mobility in control (black), Tau^{P301L}(brown), Tau^{V337M} (pink), Tau^{AA} (green), and Tau^{P301L.V337M} (blue) larvae. Plots depict mean \pm SEM (axons from \geq 8 animals). A two-way ANOVA with Dunnett's correction for multiple comparisons was performed to determine significance levels between all five genotypes; **** $p < 0.0001$

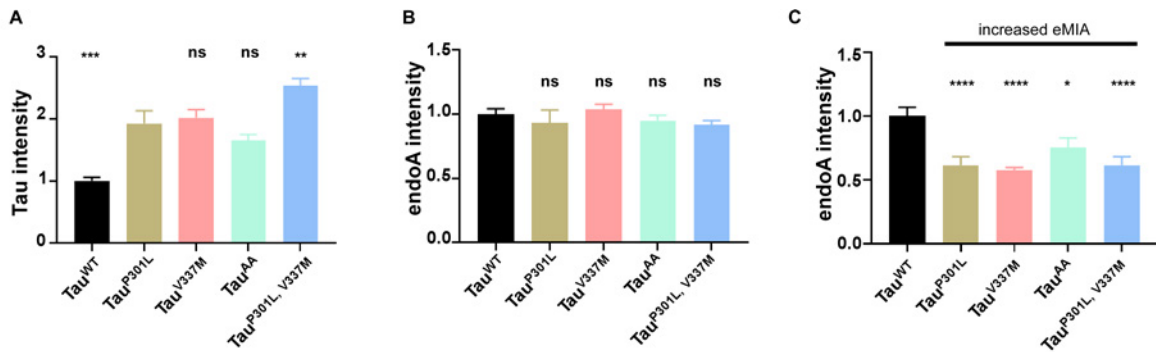


Figure 4. Increased presynaptic Tau in double mutants and functional eMIA system in Tau mutants

A) Quantification of Tau intensities in boutons at neuromuscular junctions expressing human Tau, wild type (nsSyb-GAL4>Tau^{WT}), mutant Tau^{P301L} (nsSyb-GAL4>Tau^{P301L}), Tau^{V337M} (nsSyb-GAL4>Tau^{V337M}), Tau^{AA} (nsSyb-GAL4>Tau^{AA}) or Tau^{P301L.V337M} (nsSyb-GAL4>Tau^{P301L.V337M}). **B)** Quantification of endophilin A (EndoA) immunolabeling intensities in boutons at neuromuscular junctions of the same flies as in **A)**. **C)** Quantification of EndoA immunolabeling intensities in boutons at neuromuscular junction of Tau mutant flies expressing Hsc70^{WT} to increase endosomal microautophagy (nsSyb-GAL4>Tau^{P301L}, Hsc70^{WT} or nsSyb-GAL4>Tau^{V337M}, Hsc70^{WT} or nsSyb-GAL4>Tau^{AA}, Hsc70^{WT} or nsSyb-GAL4>Tau^{P301L.V337M}, Hsc70^{WT}). The flies expressing wild type human Tau (nsSyb-GAL4>Tau^{WT}) do not express Hsc70^{WT} thus endosomal microautophagy is not increased. Bar graphs depict mean \pm SEM. Number of larvae is between 7 or 8 larvae per genotype for **A)** **B)** and **C)**. An ordinary one-way ANOVA with Dunnett's correction for multiple comparisons was performed to determine significance levels between multiple genotypes; ns is not significant, * $p < 0.05$ ** $p < 0.01$, *** $p < 0.001$, **** $p < 0.0001$.

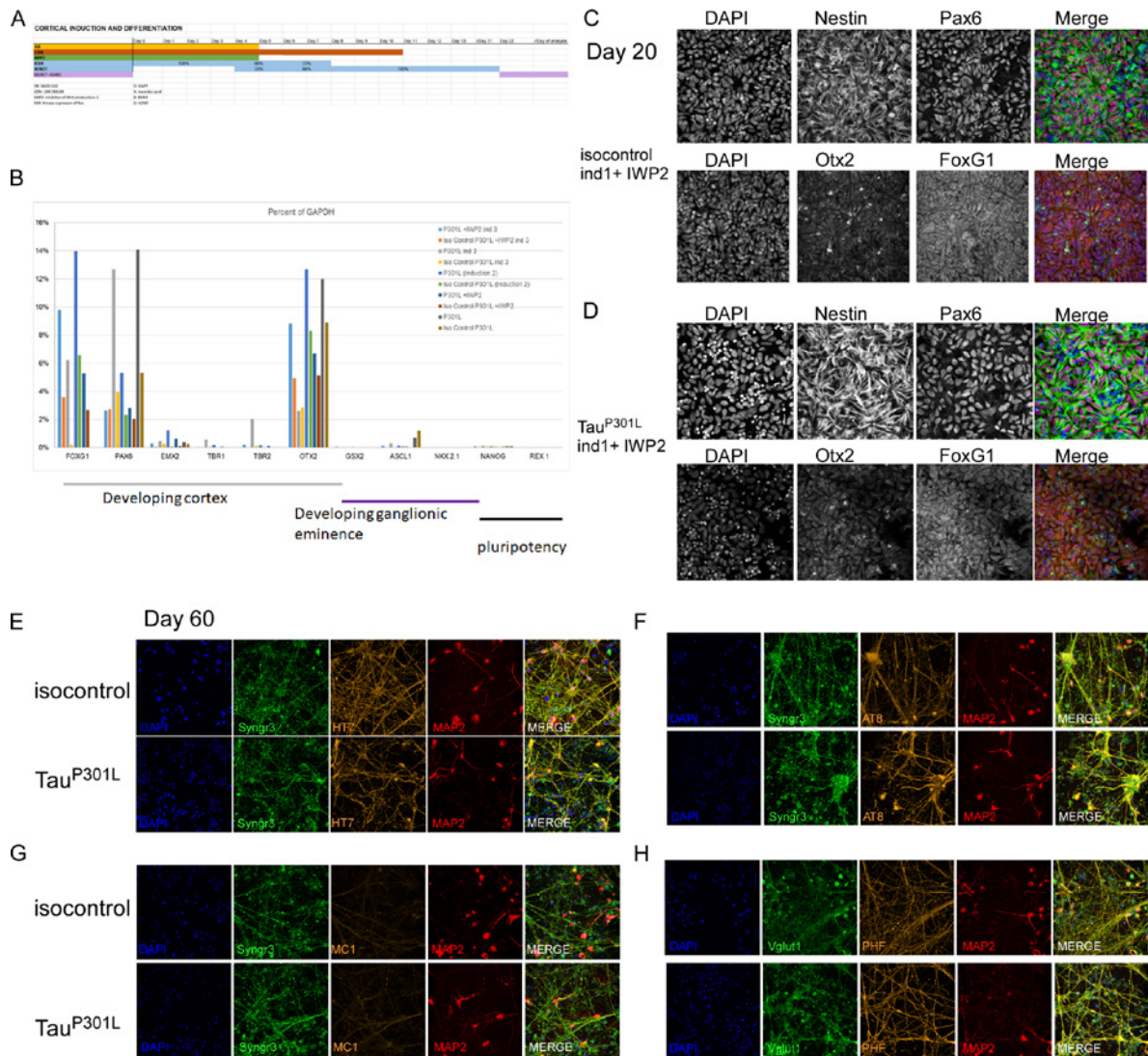


Figure 5. Induction and differentiation of human cortical TauP301L neurons.

A) induction and differentiation scheme of human cortical neurons with or without IWP2. The data shown are cortical neurons induced with IWP2. **B)** QPCR for the quantification of markers of the cortex ganglionic eminence and pluripotency. **C and D)** images of 20-day-old neuronal progenitors labeled for developing cortical markers Nestin, Otx2, Pax6 and FoxG1 in isogenic controls and TauP301L. Percentages shown are percentages from housekeeping gene, GAPDH. **E-H)** images of 60-day-old cortical neurons labeled with presynaptic markers (Synaptogyrin 3 or Vglut1), total Tau (HT7) **E)**, phosphorylated Tau (AT8 and PHF) **F and H)**, conformational changed Tau (MC1) **G)** and dendritic marker (MAP2). Scale bar is 50µm.

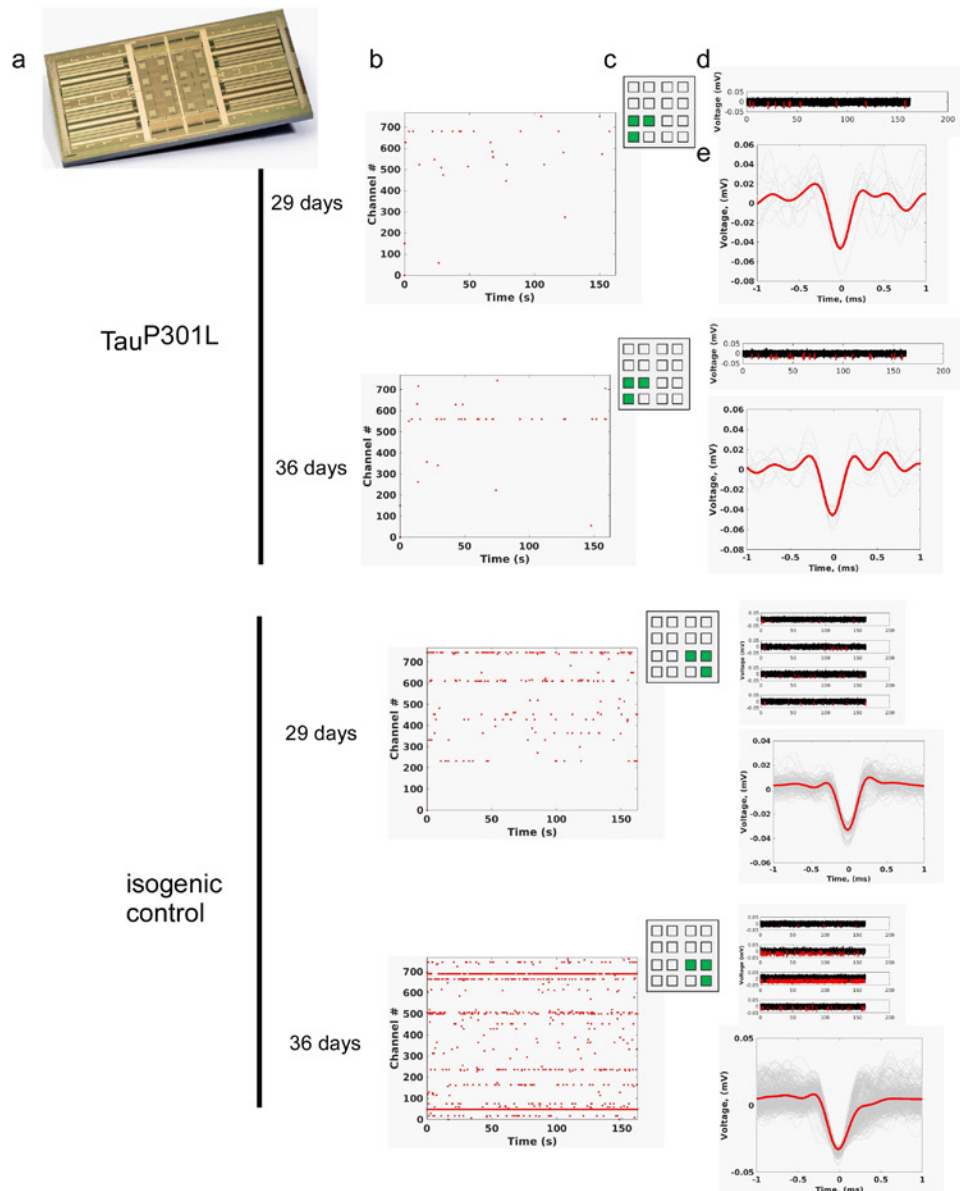


Figure 6. Multielectrode recordings of patient derived TauP301L mutant cortical neurons and their isogenic control. **a)** CMOS chip with 16 active areas each with 1024 electrodes. Electrodes are positioned to allow single cell recordings (15µm pitch). Spontaneous activity recordings in mV from cortical neurons differentiated from patient derived iPSCs harboring the P301L mutation in the MAPT gene and isogenic control and matured for 29 or 36 days as indicated on the figure. **b)** raster plot showing spike density over time. **c)** The data shown are recorded from 3 areas indicated in green. **d)** representative traces in mV over time in one channel for the P301L mutant or multiple channels for the isogenic control. After wave form detection analysis, spontaneous activity peaks are detected. They are indicated in red on the trace. **e)** overlay of the different peaks detected in one of the channels. The red trace is the average of all traces in one channel. Note that the spontaneous activity increased for both genotypes over time. The isogenic controls show more spontaneous activity compared to TauP301L mutant neurons.

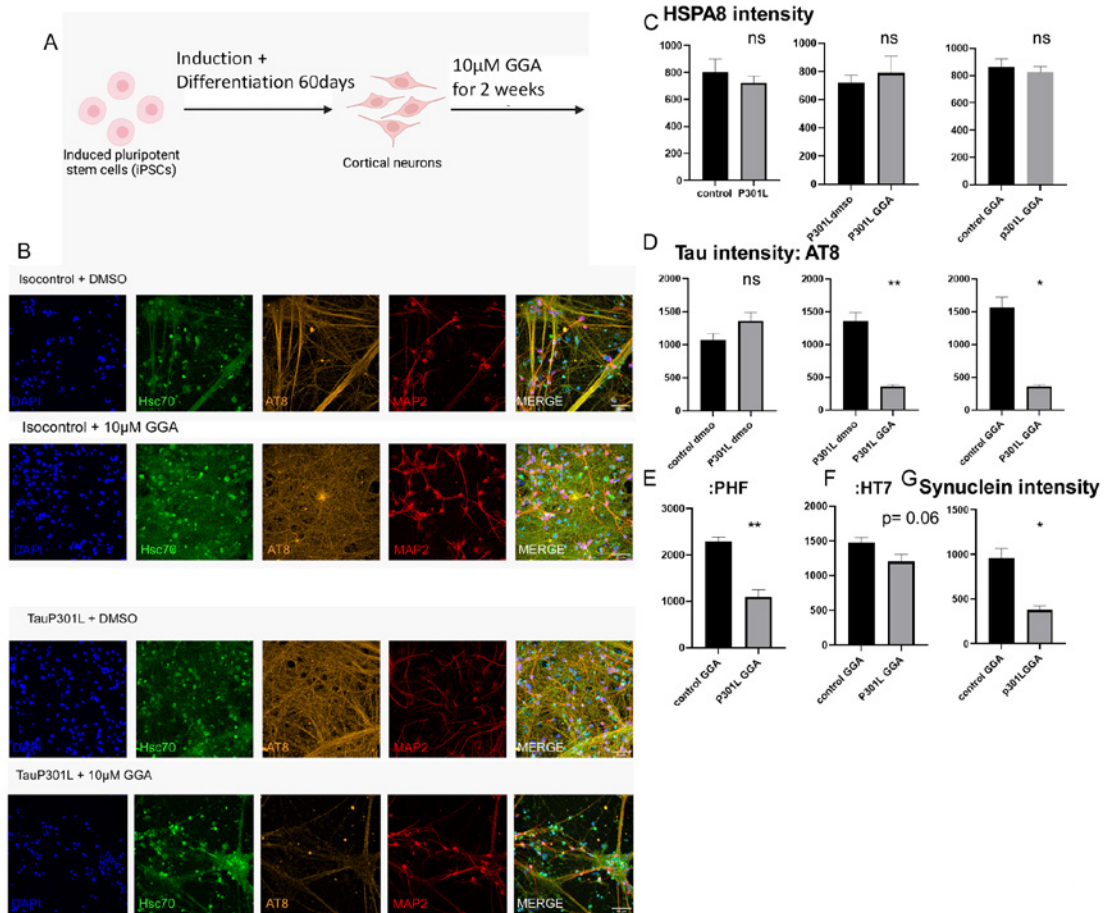


Figure 7. Treatment of TauP301L and isogenic control human cortical neurons with geranylgeranyl acetone compound.

A) 60day old human cortical neurons are treated with 10μM geranylgeranyl acetone (GGA) compound for two weeks. HSPA8, Tau and -synuclein levels are quantified using immunofluorescent labeling. **B)** Representative images of human cortical isogenic and TauP301L mutant neurons treated with DMSO or GGA and labeled with DAPI, HSPA8, phospho-Tau pS396/pS404 (PHF-1), phospho-Tau pSer202/T205 (AT8), total Tau (HT7) and MAP2 antibodies. Scale bars are 50 μm. **C-E)** Quantification of HSPA8 **C)**, Tau **D-F)**, -synuclein **G)** labeling intensity staining. Graph bars depict mean ± SEM. Number of experiment = 1, and ≥3 pictures per condition were analyzed. A student T-test with Welch's correction was performed to determine significance levels between the two genotypes; ns is not significant, *p<0.05 ** p<0.01.

5. Publications GSKE funded

- Increased HSC70-4/HSPA8 regulated autophagy reduces Tau-mediated synaptic dysfunction
Uytterhoeven, V. *et al.* (2021) The pathogenic mutation in Tau defines the route of Tau accumulation at presynapses. *ALZ online*. (conference abstract publication) (<https://alz.confex.com/alz/2021/meetingapp.cgi/Paper/53728>)

6. Publications non GSKE funded

- Gomes LA. , **Uytterhoeven V.**, Lopez-Sanmartin D., O Tomé S., Tousseyn T., Vandenberghe R., Vandebulcke M., von Arnim C.A.F., Verstreken P., Thal DR. (2021). Maturation of neuronal AD-tau pathology involves site-specific phosphorylation of cytoplasmic and synaptic tau preceding conformational change and fibril formation. **Acta Neuropathologica**. Doi: <https://doi.org/10.1007/s00401-020-02251-6>. Impact factor: 17.088 Q:1
- Largo-Barrientos P., Apostolo N., Creemers E., Callaerts-Vegh Z., Swerts J. Davies C., McInnes J., Wierda K., De Strooper B., Spires-Jones T., de Wit J., **Uytterhoeven V.***, Verstreken P. (2021) Lowering Synaptogyrin-3 expression rescues Tau induced memory defects and synaptic loss in the presence of microglial activation. **Neuron** Mar 3;109(5):767-777.e5. * **Co-corresponding author**. Impact factor: 17.173 Q:1

7. References

1. Uytterhoeven, V. *et al.* (2015) Hsc70-4 Deforms Membranes to Promote Synaptic Protein Turnover by Endosomal Microautophagy. *Neuron* 88, 735–748
2. Largo-Barrientos, P. *et al.* (2021) Lowering Synaptogyrin-3 expression rescues Tau-induced memory defects and synaptic loss in the presence of microglial activation. *Neuron* 109, 767-777.e5
3. Zhou, L. *et al.* (2017) Tau association with synaptic vesicles causes presynaptic dysfunction. *Nat. Commun.* 8, 1–29
4. McInnes, J. *et al.* (2018) Synaptogyrin-3 Mediates Presynaptic Dysfunction Induced by Tau. *Neuron* 97, 823–835.e8
5. Karch, C.M. *et al.* (2019) A Comprehensive Resource for Induced Pluripotent Stem Cells from Patients with Primary Tauopathies. *Stem Cell Reports* 13, 939–955
6. Leon, J.A.G. *et al.* (2017) AN ACADEMIC-PRIVATE PARTNERSHIP FOR THE VALIDATION OF NEW MODELS TO UNDERSTAND TAU-RELATED HYPEREXCITABILITY AND AGGREGATION USING HUMAN-INDUCED PLURIPOTENT STEM CELLS. *Alzheimer's Dement. J. Alzheimer's Assoc.* 13, P962–P963
7. Kopach, O. *et al.* (2020) Maturation and phenotype of pathophysiological neuronal excitability of human cells in tau-related dementia. *J. Cell Sci.* 133,
8. Hoshino, T. *et al.* (2013) Suppression of Alzheimer's Disease-Related Phenotypes by Geranylgeranylacetone in Mice. *PLoS One* 8,
9. Yokoyama, S. *et al.* (2019) A Randomized, Double-Blind, Placebo-Controlled Study to Evaluate the Efficacy of Teprenone in Patients with Alzheimer's Disease. *J. Alzheimer's Dis.* 71, 1187–1199
10. Bonam, S.R. *et al.* (2019) HSPA8/HSC70 in Immune Disorders: A Molecular Rheostat that Adjusts Chaperone-Mediated Autophagy Substrates. *Cells* 8,
11. Silva, M.C. *et al.* (2019) Targeted degradation of aberrant tau in frontotemporal dementia patient-derived neuronal cell models. *Elife* 8,



Geneeskundige Stichting Koningin Elisabeth
Fondation Médicale Reine Elisabeth
Königin-Elisabeth-Stiftung für Medizin
Queen Elisabeth Medical Foundation

Progress report of the research project of the young researcher

Dr. Emanuel van den Broeke
Université Catholique de Louvain (UCLouvain)

Dr. Emanuel van den Broeke

Postdoctoral researcher, laboratory Algology (prof. André Mouraux),
Institute of Neuroscience (IONS),
division Systems and Cognition (COSY),
UCLouvain, Brussels
www.nocions.org/emanuel-vandenbroeke

The involvement of top-down facilitatory serotonergic pathways in placebo-induced pain hypersensitivity.

1. Summary of the project

The aim of the project is to assess if serotonergic pathways play a role in the facilitatory effect that negative expectations have on hyperalgesia (increased pain sensitivity). High frequency electrical stimulation will be used to induce hyperalgesia. Before the induction of hyperalgesia, negative expectations about the outcome of HFS (hyperalgesia) will be induced. To investigate the contribution of serotonergic pathways to this expectation-induced hyperalgesia, Odansetron, a 5HT₃ antagonist, will be given to participants before the induction of negative expectations.

2. Status project

Because the set-up of the experiment was changed compared to the original one (see progress rapport 2020-2021) we decided to first run a behavioural experiment, which allows us to estimate better the effect size. We have started the experiment, which is pre-registered (https://osf.io/jzf75/?view_only=2a82941136f742bcada55c10c485abd5), in December and we expect to finish at the end of February (at this moment we have enrolled 10 out of 40 participants). When the results are known, we will plan a new experiment in which we will administer Odansetron or placebo before inducing the placebo.

3. Publications acknowledging the financial support of the FMRE

- **(NEW)** [van den Broeke EN](#), Urđi M, Mouraux A, Biurrun Manresa JA, Torta DME. High-frequency electrical stimulation of cutaneous nociceptors differentially affects pain perception elicited by homotopic and heterotopic electrical stimuli. *J Neurophysiol.* 2021; 126(4): 1038-1044. doi: 10.1152/jn.00289.2021.
- **(NEW)** Torta DM, Meyers E, Polleunis K, De Wolf S, Meulders A, [van den Broeke EN](#). The effect of observational learning on the development of central sensitization. Submitted. Pre-print available on: <https://psyarxiv.com/3hk5j/>.
- van den Broeke EN, Vanmaele T, Mouraux A, Stouffs A, Biurrun-Manresa J. and Torta DM. Perceptual correlates of homosynaptic long-term potentiation in human nociceptive pathways: a replication study *R. Soc. Open. Sci.* 2021; 8200830. <http://doi.org/10.1098/rsos.200830>.

4. Congresses in which the financial support of the FMRE is mentioned

(NEW) I have been selected to organize a topical workshop on the topic placebo and central sensitization at the 12th Pain in Europe Congress in Dublin (April 2022): <https://efic2022.abstractserver.com/program/#/details/sessions/187>. I will present the results of the current experiment.



Geneeskundige Stichting Koningin Elisabeth
Fondation Médicale Reine Elisabeth
Königin-Elisabeth-Stiftung für Medizin
Queen Elisabeth Medical Foundation

Progress report of the research project of the young researcher

Eline Wauters, PhD (VIB)
Universiteit Antwerpen (UAntwerpen)

Eline Wauters, PhD (VIB)

Neurodegenerative Brain Diseases,
VIB Center for Molecular Neurology,
Laboratory of Neurogenetics, I
nstitute Born-Bunge,
University of Antwerp,
Antwerp, Belgium

Onset age variability in *GRN*-associated frontotemporal lobar degeneration: identification of a functional onset age modifier

1. Research Summary

Frontotemporal lobar degeneration (FTLD) is the most common cause of neurodegenerative dementia at young age after Alzheimer's disease (AD). Mutations in the progranulin gene (*GRN*) are a major cause of FTLD, accounting for up to 11.2% of patients. The onset age of *GRN* mutation carriers ranges from 25 to 90 years. This broad onset age range points to the existence of modifiers that affect the onset age of *GRN*-related neurodegeneration. Identifying these factors is of importance as they might represent targets for disease-delaying therapies.

In an extended Belgian founder family, segregating the *GRN* IVS1+5 G>C null mutation, patients present with disease at onset ages ranging from 45 to 80 years. In this family, we have previously identified a quantitative trait locus (QTL) for onset age. The aim of the project is to identify the functional gene and variant underlying the onset age variability, to study the modifier effect in induced pluripotent stem cell (iPSC) derived neurons and microglia, and to extend the findings to international patient cohorts.

2. Progress Report

Please note that due to the COVID-19 measures, the planned execution of this project has been delayed.

2.1. Identification of functional QTL SNPs with a significant effect on onset age

From whole genome (n=23) and exome sequencing data (n=41) of *GRN* founder mutation carriers, I have selected variants located within the onset age QTL (n=635 variants, 620 of which are located in intronic and intergenic regions). To bridge the gap between a genomic locus and mechanisms, I am performing an unbiased high-throughput screen to prioritize functional variants. This technology, REEL-Seq (Regulatory Element Sequencing, (1)), progressed from the SNP-seq technology which I originally envisaged to use (2). I have performed a research stay in the lab of Dr. Li, who introduced both these innovative technologies (University of Pittsburgh (USA), August 2019). REEL-Seq is based on the design of two oligonucleotides for each studied variant – one with the wild-type and one with the alternative allele. This library of oligonucleotides will be incubated with nuclear extract. By performing consecutive cycles of incubation with nuclear extract, gel electrophoresis and PCR amplification, the sequences containing a functional SNP will be enriched in the sequence pool.

I have performed a first REEL-seq experiment in house, using an oligonucleotide library containing QTL variants (Twist Bioscience) and nuclear extract derived from HEK293T cells. The resulting oligonucleotide libraries will be sequenced on the MiSeq platform (Neuromics Support Facility) to quantify the sequences. These data will be analyzed to know which sequences are enriched in the sequence pool and thus contain a functional SNP. Afterwards, I will genotype the identified functional variants in the complete founder family and perform reporter gene assays to determine the effect of the variants on expression.

Fifteen of the 635 variants are located in exons (coding and non-coding). While these are also included in the REEL-seq library, I have moved forward with these variants in a parallel trajectory given the known relevance of variants in this region for protein function or expression.

I have genotyped the 15 exonic variants in members of the *GRN* founder family (n=170 individuals, including 79 *GRN* founder mutation carriers). Genotyping was performed via multiplex PCRs for target enrichment of the regions encompassing the exonic variants (3). The amplicon libraries were sequenced (MiSeq, Illumina). Adapters were trimmed using Fastq-mcf. Reads were aligned to the reference genome hg19 with the Burrows-Wheeler Aligner (4). Variant calling and annotation were performed using GATK (5) and the GenomeComb package (6). For each variant I have estimated the effect on onset age in the *GRN* founder family using Loki (7). This analysis indicated that seven exonic variants have a significant effect on onset age ($p < 0.05$). Six variants are located in 5' or 3' untranslated regions (UTR). One variant is located in a coding exon, leading to a missense mutation. We will evaluate the functional effect of the UTR variants using luciferase reporter assays. To assess the functionality of the missense mutation, we will overexpress the wild-type and mutant protein in a cell model and evaluate effects of the mutation on the known protein function.

For the luciferase reporter assays, the coding sequence of secreted *Nanoluc* luciferase was synthesized (Integrated DNA Technologies, IDT) and cloned into the BamHI and NotI restriction sites of a pGL4 expression vector (Promega) under the TK promoter, thereby substituting the *Gaussia* luciferase coding sequence. Fragments containing the UTR sequences were amplified from cDNA using specific primers and cloned into this plasmid via In-Fusion cloning (Takara Bio). 5' UTR sequences were cloned upstream of the *Nanoluc* luciferase, and 3' UTR sequences downstream of the luciferase. Genetic variants were generated by site-directed *in vitro* mutagenesis. All constructs were validated by Sanger sequencing. HEK293T cells will be co-transfected with the *Nanoluc* luciferase construct and a *Firefly* luciferase plasmid (under the SV40 promoter, Promega). The signal for both luciferases will be generated using the Dual-Luciferase Reporter Assay System (Promega), after which luminescence will be measured.

2.2. Compare gene expression in biomaterials of patients with early and late onset of disease

We have performed transcriptome sequencing on lymphoblast-derived RNA of eight *GRN* founder mutation carriers. To study differential gene expression between early- and late-onset disease, we have compared expression levels between individuals with different genotypes at a QTL variant which has a significant effect on onset age. For this variant, heterozygous (AB) and homozygous (BB) variation carriers developed disease on average 9.0 and 7.9 years later in comparison to homozygous carriers of the wild-type allele ($p < 0.00001$ and $p = 0.0002$, respectively) (**Figure 1**).

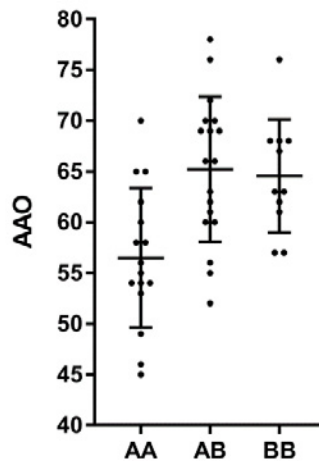


Figure 1: Onset age distributions in the *GRN* founder family for one of the QTL variants with a significant effect on onset age. Patients with known onset age and genotype were included. The mean onset age for each genotype and the standard deviations are visualized. AAO: age at onset. AA/AB/BB: genotypes.

RNA was isolated from lymphoblast cell lines of eight *GRN* founder mutation carriers with different genotypes for the QTL variant. The onset age ranged from 56 to 68 years in six patients. Two additional mutation carriers were selected with current ages of 72 years and 75 years. The coding transcriptome was captured (TruSeq Stranded mRNA Library Prep kit, Illumina) and resulting libraries were sequenced (NextSeq, Illumina). We performed quality control (FastQC, <http://www.bioinformatics.babraham.ac.uk/projects/fastqc/>), adapter removal and low quality read trimming (Trimmomatic, (8)). Reads were mapped to hg38 with Hisat2, using Ensembl v84 gene annotation (9). FeatureCounts was used for transcript quantification (10).

Expression levels were compared between four homozygous carriers of the wild-type allele and four homozygous variation carriers of the QTL variant. Differentially expressed genes were identified with DESeq2 (11). Sequencing batch and gender were included as covariates in the analysis. In total, we found 475 genes that were differentially expressed ($P_{adj} < 0.1$). Enrichment analysis of these genes using GOrilla (12) indicated an important role for endoplasmic reticulum (ER) unfolded protein response and ER stress.

We have expanded our transcriptomics studies and look for converging evidence in transcriptomics data of lymphoblast ($n=58$) and brain material ($n=9$) of *GRN* founder mutation carriers and non-carriers ($n=14$ lymphoblasts, $n=6$ brain) (QuantSeq 3' mRNA sequencing, Lexogen). Analysis of this dataset is ongoing.

2.3. A *GRN*-FTD iPSC model to identify the functional onset age modifier

We have differentiated control iPSCs to cortical neurons following the feeder-free protocol implemented by the Stem Cell Institute Leuven (SCIL) (protocol adapted from (13)), and to macrophages following the protocol described by *Haenseler et al* (14). We have evaluated the RNA expression of *GRN* and of the genes located in the onset age QTL in undifferentiated iPSCs, in cortical neurons (22 days *in vitro*), and in macrophages using SYBR green-based quantitative PCR. This analysis indicated that *GRN* and the onset age QTL genes are indeed expressed in the differentiated cortical neurons and macrophages. We have also investigated the expression of marker genes; the pluripotency marker *Oct4* shows clear expression in the undifferentiated iPSCs, while this is not the case in the neurons and macrophages. Conversely, transcript levels of the cortical marker *Tbr1* were dramatically increased in the cortical neurons, while the expression of microglia/macrophage markers *MERTK*, *GPR34* and *P2RY12* was highly increased in the macrophages in comparison to the iPSCs.

We are using GRN-FTLD iPSC lines that were created by the Stem Cell Institute Leuven (KU Leuven) (15). These lines carry the *GRN* founder mutation. To create isogenic lines, I use CRISPR-Cas9 genome editing to correct the mutation. I am following the same methodology to introduce the *GRN* mutation in control lines from a healthy donor (European Bank for induced pluripotent Stem Cells (EBiSC)). I have identified multiple clones carrying the *GRN* founder mutation in homozygous state. Further optimizations and screenings are ongoing to identify heterozygous clones. In addition, I have created a heterozygous *GRN* knockout line using CRISPR-Cas9 genome editing starting from control iPSCs. In this line, a heterozygous insertion of a "T"-allele in exon 5 causes a frameshift, leading to a decrease in *GRN* expression.

I will use these models to investigate the effect of candidate onset age modifiers on disease-related characteristics such as *GRN* expression, expression of lysosomal proteins, corticogenesis, and TDP-43 accumulation and localization.

2.4. Investigation of the role of the QTL in onset age modification in international patient cohorts

Unrelated FTD patients without GRN mutation

We have evaluated the onset age modifying effect of the QTL in unrelated Belgian frontotemporal dementia (FTD) patients without *GRN* mutations ($n=293$; mean onset age 62.9 ± 10.5 y) by genotyping QTL tagging variants ($n=21$). Homozygous carriers of the top associated SNP developed disease on average 3.7 years later in comparison to patients homozygous for the wild-type allele ($p=0.010$, Mann-Whitney U), indicating that the modifier locus also has an effect in *GRN*-unrelated FTD. To replicate the findings obtained in the Belgian FTD cohort, we will screen international patient cohorts.

Risk factors, such as *TMEM106B* in FTD and *APOE* in AD, are known to affect onset age. It is therefore possible that the onset age QTL variants would affect disease risk. To verify this, I have genotyped the same set of variants in a cohort of Belgian control individuals ($n=684$, age at inclusion range 60 to 98 years). We calculated association with disease (genotypic logistic regression, covariate: gender), and obtained significance for four variants ($p<0.05$).

GRN LOF mutation families

The candidate onset age modifiers were identified in an extended Belgian founder family, segregating the *GRN* IVS1+5 G>C null mutation. To allow evaluation of candidate onset age modifying variants in other families with a *GRN* LOF mutation, we have biomaterials available of 62 other Belgian *GRN* LOF mutation carriers, including 26 index patients. We will genotype the QTL tagging variants in this cohort and evaluate their effect on onset age.

We continuously update this cohort, and recently we identified a novel *GRN* mutation p.E393A in the last codon of exon 10 which was annotated as a missense mutation in the resequencing dataset (*Wauters, Gossye, et al, in preparation*). This mutation has to the best of our knowledge not been reported before and is absent from mutation databases. This alteration in the splice donor sequence leads to aberrant splicing, namely partial intronic read-through into intron 10 and usage of a cryptic intronic splice donor site. This results in a frameshift and nonsense-mediated mRNA decay of the mutant transcript (**Figure 2**). *GRN* protein levels are reduced in serum of the carriers to levels comparable to other known LOF mutations (**Figure 2**). Neuropathological examination of the index patient indicated Alzheimer's dementia pathology and FTLTDP type A pathology, characteristic for *GRN*-related FTLTDP.

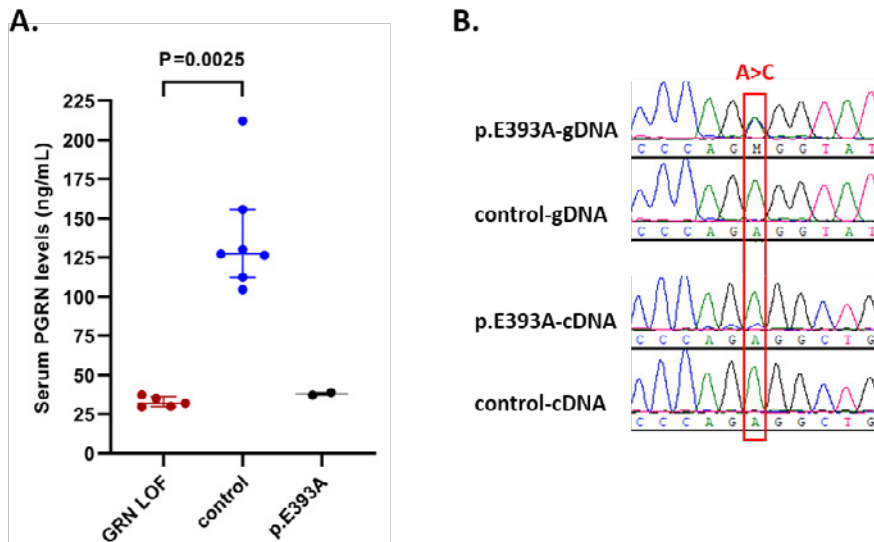


Figure 2: A) Scatterplot for serum PGRN levels measured in carriers of the *GRN* p.E393A mutation (n=2), *GRN* LOF mutations (n=5) and control individuals (n=7). Serum PGRN levels are measured in nanograms per milliliter using ELISA (Adipogen). Horizontal lines are median levels and whiskers indicate the interquartile range. Mann-Whitney U test was performed to compare PGRN levels between *GRN* LOF mutation carriers and control individuals. **B) LCL cDNA Sanger sequencing.** Electropherograms show the results of gDNA and cDNA Sanger sequencing in presence of the mutation. This shows degradation of the mutant transcript. Abbreviations: cDNA: complementary DNA, ELISA: enzyme linked-immunosorbent assay, gDNA: genomic DNA, *GRN*: progranulin gene, LCL: lymphoblastoid cell line, LOF: loss-of-function, PGRN: progranulin protein.

Alzheimer dementia patients

A genetic, clinical, and pathological overlap exists between neurodegenerative disorders such as FTD and AD. It is thus conceivable that QTL variants would affect the onset age of AD patients. To test this hypothesis, we have genotyped the QTL tagging variants in a cohort of unrelated Belgian AD patients (n=559; mean onset age 73.0 ± 9.3 y) and calculated association with onset age (univariate tests, covariates: APOE, gender). This indicated no significant effect (p>0.05).

3. References

1. Zhao et al, Nat Commun, 2020
2. Li et al, Nat Genet, 2018
3. Goossens et al, Hum Mutat, 2009
4. Li and Durbin, Bioinformatics, 2009
5. McKenna et al, Genome Res, 2010
6. Reumers et al, Nat Biotechnol, 2012
7. Heath, Am J Hum Genet, 1997
8. Bolger et al, Bioinformatics, 2014
9. Kim et al, Nat Methods, 2015
10. Liao et al, Bioinformatics, 2014
11. Love et al, Genome Biol, 2014
12. Eden et al, Bioinformatics, 2009
13. Shi et al, Nat Neurosci, 2012
14. Haenseler et al, Stem Cell Rep, 2017
15. Raitano et al, Stem Cell Rep, 2015



Geneeskundige Stichting Koningin Elisabeth
Fondation Médicale Reine Elisabeth
Königin-Elisabeth-Stiftung für Medizin
Queen Elisabeth Medical Foundation

**Geneeskundige Stichting Koningin Elisabeth – G.S.K.E.
Fondation Médicale Reine Elisabeth – F.M.R.E.
Queen Elisabeth Medical Foundation – Q.E.M.F.**

Mailing address:

The scientific director:

Prof. dr. Jean-Marie Maloteaux
3, avenue J.J. Crocq laan
1020 Bruxelles - Brussel
Belgium
Tel.: +32 2 478 35 56
E-mail: jean-marie.maloteaux@uclouvain.be

Secretary:

Mr. Erik Dhondt
3, avenue J.J. Crocq laan
1020 Bruxelles - Brussel
Belgium
Tel.: +32 2 478 35 56
E-mail: fmre.gske@skynet.be
erik.dhondt@skynet.be
e.l.dhondt@skynet.be

www.fmre-gske.be
www.fmre-gske.eu
www.fmre-gske.com